A Dynamic Mechanistic Model and Model-based Analysis of a Continuous Kamyr Digester

Dr. Ing. Thesis

Finn Are Michelsen

Department of Engineering Cybernetics
The Norwegian Institute of Technology
University of Trondheim
1995

Report no. 95-4-W
Department of Engineering Cybernetics
The Norwegian Institute of Technology
N-7034 Trondheim, Norway

Preface

This thesis presents my work for the partial fulfilment of the requirements for the Doktor Ingeniør degree in Engineering Cybernetics at The Norwegian Institute of Technology - NTH, the University of Trondheim, Norway.

The study was funded by the Research Council of Norway (NFR) under grant no. STP 105258/420 running from September 1991 to September 1994. The scholarship was a part of the PROMIA [1] project. Additional funding was provided by M.Peterson & Søn A/S.

I particularly thank my supervisor Professor Bjarne A. Foss for support, advise and many valuable discussions. Special thanks are also expressed to Dr. Peder J. Kleppe and Mr. Per Kirkebak at M.Peterson & Søn AS, Dr. Tor Christensen at Fantoft Prosess AS, and Professor Jens G. Balchen at the Department of Engineering Cybernetics for their constructive contributions to our project group.
During this study I have had valuable discussions with other people as well. I will especially mention Professor Sigurd Skogestad and Professor Per Koch Christensen at the Department of Chemical Engineering, Dr. David Di Ruscio, and Mr. Olav Slupphaug at the Department of Engineering Cybernetics, Dr. Torbjørn Utnes at SINTEF-NHL, Mr. Claes Lysen at Kværner Pulping Technology, Dr. Esko J. Härkönen at United Paper Mills Ltd., Professor Adriaan R.P. van Heiningen at the University of New Brunswick, and Dr. Bruce J. Allison at PAPRICAN, Vancouver. Moreover, thanks are expressed to Mr. Alain Roche at PAPRICAN, Pointe Claire, for organizing my one month visit in Canada, November 1993.
I would like to thank Mr. Stewart Clarke, International Office, The Norwegian Institute of Technology for the final editing work on this thesis.

Trondheim, May 3, 1995

Finn Are Michelsen

[1] Program for Modellering, Instrumentering og Automatisering.

Contents

Summary **9**

List of Tables **11**

List of Figures **13**

Nomenclature **17**

1 Introduction **21**

1.1 Background and the modelling approach 21

1.2 Kraft pulping 22

1.2.1 An introduction 22

1.2.2 The continuous Kamyr digester 24

1.2.3 Pulp quality and the main process variables which affect it 28

1.3 Objective and problem formulation 32

2 A survey of earlier models **33**

2.1 Kinetics 33

2.2 Stoichiometry 36

2.3 Diffusion 36

2.4 Convection 38

2.5 Dispersion 40

2.6 Data driven models 40

2.7 Summary 42

3 Derivation of the proposed model **45**

3.1 Background 45

3.2 Model assumptions, part 1 48

3.2.1 Physical view 50

3.2.2 Transport phenomena 52

3.2.3 Quality measures 60

3.2.4 Other constraints 60

3.3 Definition of basic and derived variables 61

3.3.1 Porosity 61

3.3.2 Volumetric, mass and density variables 63

3.3.3 Pressure variables 70

3.3.4 Velocity variables 72

3.3.5 Temperature variables 73

3.3.6 Some well-established derived variables 73

3.4 Model assumptions, part 2 77

3.4.1 The surface forces and the chip plug movement 77

3.4.2 Compressibility 83

3.5 Mass and component balances 85

3.5.1 The main section 85

3.5.2 The top section 92

3.5.3 The outlet section 95

3.6 Momentum balances 95

3.6.1 The main section 95

3.6.2 The top section 99

3.6.3 The extraction section 100

3.6.4 The outlet section 100

3.7 Energy balances 101

3.7.1 The main section 102

3.7.2 The steam zone 107

3.7.3 The top section 111

3.7.4 The outlet section 112

3.7.5 The liquor circulations 112

3.8 Rescaling of the equations 112

4 Numerical solution **115**

4.1 Introduction 115

4.2 Spatial discretization 116

4.3 Resulting model structure 117

4.4 Some further numerical aspects 119

5 Simulation results **121**

5.1 Dimensional analysis 121

5.2 Steady-state profiles 127

5.3 Dynamic behaviour 134

5.3.1 Sensitivity to manipulated variables; temperature-, alkali-, and residence time changes 135

5.3.2 Sensitivity to some common operational disturbances; changes in feed chip reactivity, -lignin and -air content 151

5.3.3 Short-stop 155

6 Linear analysis **163**

6.1 Tools for linear analysis 163

6.1.1 Linearization 163

6.1.2 Transfer functions and singular value decomposition 164

6.2 The Jacobian matrix 165

6.2.1 The matrix elements 165

6.2.2 The eigenvalues 166

6.2.3 Discussion 168

6.3 Controllability analysis 169

6.3.1 Selection of inputs and outputs 170

6.3.2 About controllability 171

6.3.3 Transfer functions 174

6.3.4 Singular value decomposition 177

6.3.5 Discussion 182

7 Model reduction **185**
7.1 The balance equations . . . 185
7.1.1 Mass balances . . . 185
7.1.2 Momentum balances . . . 189
7.1.3 Energy balances . . . 189
7.1.4 Simulation results . . . 190
7.2 Other structural changes . . . 190
7.2.1 Chip mass movement . . . 192
7.2.2 Step response sub-models . . . 193
7.3 Numerical solution . . . 196

8 Digester control **199**
8.1 The control objectives . . . 199
8.2 Conventional control in general . . . 202
8.3 Conventional residence time control . . . 202
8.4 Improved residence time control . . . 206
8.4.1 Active chip level control . . . 208
8.4.2 Active chip velocity control . . . 210
8.4.3 Active chip level- and chip velocity control . . . 210
8.4.4 Indirect residence time control . . . 211

9 Discussion and conclusions **215**
9.1 The model derivation and the analyses . . . 215
9.2 Model validation . . . 216
9.3 Model weaknesses . . . 217
9.4 Utilization of the model . . . 217

Bibliography **219**

A Porosity **227**

B The multicomponent fluxes **231**

C Formulation of the conservation laws **235**

D Balance equations for a conic vessel **237**

E The yield and pH dependencies for ECCSA **241**

F The compaction of chips in the top section **243**

G Inherent negative feedback **247**

H Local velocity of sound for the chip plug **249**

I Operational conditions **251**

Summary

This thesis contains a variety of topics connected to modelling and control of a continuous Kamyr digester. In the proposed model, emphasis is made on the description of the interaction between the vertical motion of the chip plug, including the chip level, and the chemical reactions in the delignification and degradation of the wood chips. With respect to control of the digester, focus is made on input-output controllability analysis, and residence time control.
The work is formed as a case study, and the object of the study is the digester at Peterson Moss AS in Norway. This is a continuous steam/liquor phase digester which constitutes one part of a two-vessel system for production of liner grades from softwood. Even though some of the conclusions are based on nominal operating conditions for this digester, the results are transmittable to other type of continuous digesters. Hence, the derived model is formulated in general terms.

The thesis is not intended to be a textbook on any of the topics which are treated. However, in Ch. 1 an introduction is given to chemical pulping and the Kamyr digester. Moreover, a brief overview is given for the methodologies and tools which are used in the respective chapters. Literature is cited for more details.

A large part of the thesis concerns model derivation. As an introduction, Ch. 2 summarizes earlier proposed models. The ideas behind some of these are used in the derivation of the proposed model. Based on the first principles method, this is outlined in Ch. 3. A broader treatment is given of the main assumptions behind the model, definition of the model variables, and the main physical mechanisms which are included.
In Ch. 4, some aspects of the numerical solution are discussed. A large part of this concerns the model structure.

Ch. 5 shows the merits of the model in form of simulation results and validation. A dimension analysis indicates which effects are important at steady-state. Typical vertical steady-state profiles, and the model sensitivity to input and disturbance changes are discussed. The ability of the model to predict the conditions during a short-stop is illustrated as well.

In Ch. 6, a linearized version of the model is analysed. Some qualities of the model are revealed by studying the Jacobian matrix and its eigenvalues. As a basis for control structure selection, a controllability analysis is included.

Derived and simplified models, and their qualities are discussed in Ch. 7.

Ch. 8 treats digester control. The main control goals and conventional control structures are discussed. Based upon the proposed model, it is suggested how the control of the residence time for the chips may be improved.

Some main conclusions and a discussion finalises the thesis in Ch. 9.

The appendices contain supplementary material directly related to the main chapters. All calculations are made by use of MATLAB (The MathWorks Inc., 1994).

The main contributions in this thesis are:

- A dynamic mechanistic model, which includes reaction kinetics, thermodynamics and flow dynamics. The modelling of the residence time for the chips and its dependency on the different pulping conditions, the compaction of chips, and the chip level, is the essence in this contribution (Ch. 3).
- Understanding of the background, clarification of the assumptions, and limitations of the proposed model (Ch. 3).
- Explanation of the dynamic and steady-state phenomena which occur in continuous digesters (Ch. 5).
- Improved knowledge about the residence time control in continuous digesters (Ch. 8).

Further, we have made contributions regarding:

- An updated survey of earlier proposed models (Ch. 2).
- A basis for development of improved process control strategies. This is formed by the simulation results and the linear analysis in (Ch. 6).
- Simplified non-linear models where the model reductions are based on physical knowledge (Ch. 7).

Preliminary results from this work are published in Michelsen and Foss (1993), Michelsen and Foss (1994a) and Michelsen and Foss (1994b). More comprehensive articles have been submitted to the two journals Tappi Journal (Michelsen and Foss, 1995b) and Applied Mathematical Modelling (Michelsen and Foss, 1995a).

List of Tables

1.1 Pulp quality tests (from (Smook, 1989)) 29

3.1 Oxygen depletion tests (from Smook (1989)) 75

3.2 Characteristic quantities for the rescaling of the model variables . 113

5.1 Steady-state values of the terms in the wood solid equations 122

5.2 Steady-state values of the terms in the alkali equations 123

5.3 Steady-state values of the terms in the equations for the dissolved solids 124

5.4 Steady-state values of the terms in the compaction equation 124

5.5 Steady-state values of the terms in the momentum equations . . . 125

5.6 Steady-state values of the terms in the viscous friction coefficient . 125

5.7 Steady-state values of the terms in the energy equations 126

I.1 Model parameters 253

I.2 Characteristic quantities 254

I.3 Operational conditions for a steam/liquor phase digester for production of kraft softwood pulp 254

List of Figures

1.1 The Kamyr two-vessel system at Peterson Moss AS, Norway 24
1.2 A typical fibre line in a kraft pulp mill 25
1.3 A Kamyr continuous digester 27

2.1 Classification-tree for earlier proposed models 43

3.1 The extraction section 48
3.2 The top section 49
3.3 The outlet section 49
3.4 The conceptual model of the mass in the digester. 64
3.5 Three different ways of considering the volume distribution of solid material, entrapped liquor, and free liquor inside a wood chip . . . 69
3.6 Two- and three-dimensional plots of the compressibility equation . 71
3.7 An illustration of the chip-chip contact 78
3.8 Schematic classification of flow through porous media (Bear, 1972) 80
3.9 A summary of steady-state non-Newtonian two-parameter models (the Newtonian model is shown for reference) (Bird, Steward and Lightfoot, 1960) 84
3.10 Cause-and-effect diagram for ϵ_c and α_{lig} 90
3.11 Control volume in stratified flow ((Ytrehus, 1987)) 97
3.12 The steam zone 108
3.13 The temperature dependency for the latent heat of vaporization of water. The second order approximation (solid line) and data from thermodynamic tables (dashed line). 109
3.14 The temperature dependency for the partial saturated pressure of steam. The second order approximation (solid line) and data from thermodynamic tables (dashed line). 110

4.1 Staggered control volumes as used in the MAC method 116

5.1 The horizontal axis in the profile plots 122
5.2 -5.13 Steady-state profiles 132-134
5.14 -5.33 Dynamic behaviour without chip level control 136-143
5.34 -5.57 Dynamic behaviour including chip level control 144-151
5.58 -5.67 Dynamic behaviour by disturbances 153-155
5.68 -5.81 Dynamic behaviour during a short-stop 158-161

6.1 Visualization of the sparsity pattern in the Jacobian matrix 165
6.2 The real part of the eigenvalues of the Jacobian at high production rate (solid line), and low production rate (dashed line) 167
6.3 The absolute values of the elements in the eigenvector which correspond to the smallest eigenvalue in the Jacobian matrix at the high production rate 168
6.4 -6.7 Bode plots of transfer functions 175-178
6.8 -6.13 Plots from the singular value decomposition 179-182

7.1 Amount of dissolved carbohydrates versus amount of dissolved lignin, and yield versus Kappa number, according to the model 186
7.2 Amount of dissolved non-lignin versus amount of lignin dissolved in kraft and soda pulping (from Christensen, Albright and Williams (1982)) 187
7.3 -7.6 Simulation results from a reduced model 191-192
7.7 Time response of the chip level from a puls pattern in the blow flow at the high production rate 194
7.8 Comparison between the chip level responses of original (solid line) and the generated model 195
7.9 A conventional chip level control structure 196

8.1 The interactions between the three basic factors with respect to quality (Q) control 200
8.2 A general Kappa number control structure 200
8.3 The principles for chip level controls in two-vessel systems (Granberg and Gustavsson, 1982) 204
8.4 The chip level control strategy for the Peterson digester 205
8.5 A chip level control structure 208
8.6 -8.7 Blow flow, chip level, residence time and the blow flow Kappa number during a 5% increase in the feed chip lignin content when the Kappa number is controlled by the chip level set-point 209

8.8 The closed loop transfer function in the active chip level control structure 210

8.9 Kappa number control by active chip level control including internal feedback from the chip velocity variations 210

8.10 Kappa number control by active chip velocity control 211

8.11 -8.12 Blow flow, chip level, residence time and the blow flow Kappa number during a 5% increase in the feed chip lignin content when the Kappa number is controlled by the blow flow 212

8.13 -8.14 Wash water flow, chip level, residence time and the blow flow Kappa number during a 5% increase in the feed chip lignin content when the Kappa number is controlled by the wash water flow . . . 213

8.15 -8.16 The closed loop transfer function in the indirect residence time control structure where the Kappa number is controlled by respective the blow flow and the wash water flow 214

A.1 Definition of porosity and representative elementary volume (from Bear (1972)) 228

B.1 Schematic diagram showing the approximate relations between fluxes and driving forces in a binary system. From Bird et al. (1960) . . . 232

D.1 A reactor element of length dz and cross section A 237

E.1 ECCSA as a function of pH for spruce wood blocks according to (Hägglund, 1959) 241

E.2 ECCSA as a function of yield for partially digested wood blocks at pH 13.2 according to (Bäckström, 1960) 242

F.1 To volumes of chips with different Kappa numbers. 244

H.1 3D-plot of the equation for the local velocity of sound 250

Nomenclature

This nomenclature list is not complete. To restrict the length of the list, most of the symbols that are used in specific contexts are omitted. These are explained when first introduced. Vector symbols are typeset in bold, like in $\mathbf{x}$. Scaled variables have superscript *.

Latin letters

Symbol	Description	Dimension
A	cross section area of the digester	m^2
A_i	frequency factor, $i = 1, 2$	$(kg/(m^3 s))^{-1}$
b_{lig}	factor of comsumption for lignin	kg EA/kg lig.
b_{carb}	factor of comsumption for carbohydrates	kg EA/kg carb.
c_κ	Kappa number coefficient	$-$
$C_{p,w}$	heat capacity for the wood materials	$J/(kg^oC)$
$C_{p,liq}$	heat cap. for the entr. and the free liquor	$J/(kg^oC)$
D_{EA}	interphase diffusion rate coeff. for alkali	s^{-1}
D_{ds}	interphase diff. rate coeff. for diss. solids	s^{-1}
D_c	dispersion coefficient for the chip plug	m^2/s
D_l	dispersion coefficient for the free liquor	m^2/s
$D_{cond,i}$	mass transfer coeff. for condensation of steam with respect to phase $i = c, l$	s^{-1}
E_c	spesific energy for the chip plug	J/kg
E_l	spesific energy for the free liquor	J/kg
E_i	spesific activation energy, $i = 1, 2$	J/mol
F_Λ	force of viscous interphase friction	N/m^3
F_μ	force of dry friction	N/m^3
g	the constant of gravity	m/s^2
h_c	chip level	m
h_l	free liquor level	m
h_t	distance from dig. bottom to the top section	m
h_s	dist. from the bottom to the top separator	m
$h_i^{'}$	chip/liquor level relative to h_t	m
H_i	spesific enthalpy for phase $i = c, l$	J/kg

Symbol	Description	Dimension
Δh_{lig}	coeff. for heat of lignin reactions	$J/(kg/kg$ ODW)
Δh_{carb}	coeff. for heat of carb. reactions	$J/(kg/kg$ ODW)
Δh_r	coeff. for total heat of chem. reactions	$J/(kg/kg$ ODW)
λ_w	latent heat of condensation	kJ/kg water
$k_{d,ds}$	diffusion coefficient for dissolved solids	$-$
k_{iz}	coeff. for vertical heat of conduction	$J/(ms^oC)$
k_{cl}	coeff. for interphase heat of conduction	$J/(m^3s^oC)$
k_{iw}	coeff. for heat of conduction between phase $i = c, l$ and the side walls	$J/(m^3s^oC)$
k_{is}	coeff. for heat of conduction between phase $i = c, l$ and the steam	$J/(m^3s^oC)$
k_{rpm}	chip meter speed coefficient	$(m^3/s)/rpm$
k_{ts}	empiric coefficient for the top section	m^{-1}
k_i	Arrhenius coefficients $i = 1, 2$	$(skg$ EA/ m^3entr. liq.$)^{-1}$
L/W	liquor-to-wood ratio	m^3/tonne ODW
M_{air}	molar weight of air	$kg/kmol$
M_{water}	molar weight of water	$kg/kmol$
n_{air}	number of mol of air molecules	mol
n_c	number of chips per elementary volume	$[-]$
$p_c^{'}$	chip plug (bed) pressure	Pa
p_c	mean chip plug pressure	Pa
p_l	free liquor pressure	Pa
p_s	steam pressure	Pa
$p_{s,p}$	partial saturated pressure of steam	Pa
p_{air}	partial air pressure	Pa
Q_{cz}	vertical heat of conduction for chips	$J/(m^2s)$
Q_{clw}	sum of interphase heat of conduction and that through the side walls	$J/(m^2s)$
$q_{c,in}$	chip meter speed	rpm
q_{bf}	blow flow	m^3/s
r_{lig}	reaction rate of lignin	$kg/(kg$ ODW$\cdot s)$
r_{carb}	reaction rate of carbohydrates	$kg/(kg$ ODW$\cdot s)$
r	the sum of r_{lig} and r_{carb}	$kg/(kg$ ODW$s)$
R	molar gas constant ≈ 8.314	$J/($mol $K)$
R_1	viscous friction coefficient	$kg/(m^3s)$
R_2	viscous friction coefficient	kg/m^4
RPM	chip meter speed	rpm
t	time coordinate	s
T_i	phase temperature $i = c, l$	^oC
T_s	steam temperature	^oC
T_a	ambient temperature	^oC
U_i	spesific internal energy, $i = c, l$	J/kg
v_i	phase velocity $i = c, l$	m/s
$v_{i,\gamma}$	interphase material velocity $i = c, l$	m/s
V_{outlet}	the volume of the outlet section	m^3
Y	yield	$kg/kgODW$
z	vertical space coordinate	m

Greek letters

Symbol	Description	Dimension
α_{lig}	mass fraction of lignin in a wood chip	$kg/kgODW$
α_{carb}	mass fraction of carb. in a wood chip	$kg/kgODW$
α^0_{carb}	mass fraction of non-reactive carb.	$kg/kgODW$
ϵ_i	volume fraction of phase $i = c, l$	m^3/m^3 mass
$\epsilon_{i,in}$	vol. frac. of phase $i = c, l$ in the feed flow	m^3/m^3 mass
ϵ_{sm}	vol. frac. of solid mat. in the chips	m^3/m^3 ODW
ϵ_{el}	vol. frac. of entr. liq. in the chips	m^3/m^3 ODW
ϵ_{air}	vol. frac. of air in the chips	m^3/m^3 ODW
$\epsilon_{air,atm}$	vol. frac. of air in the chips at atmospheric pressure and temp. 20^oC	m^3/m^3 ODW
ϵ_p	vol. frac. of voids in the chips	m^3/m^3 ODW
∇	divergence operator	m^{-1}
γ	space coordinate for interphase transfer	m
κ_s	absolute humidity for steam	kg water/kg air
κ_i	equiv. abs. humidity for the surface of phase i	kg water/kg air
Φ	specific potential energy	J/kg
κ	Kappa number	-
Λ	viscous friction term	$kg/(m^3 s)$
μ	coefficient for dry friction	$[-]$
η_i	coeff. for viscous eddy diffusion	$kg/(ms)$
ρ_c	mass density of a wood chip	kg/m^3 ODW
ρ_l	mass density of free liquor	kg/m^3 free liq.
$\rho_{c,in}$	mass density of chips in the steam zone	kg/m^3 ODW
$\rho_{dc,in}$	dry solid content in the feed	kg/m^3 ODW
$\rho_{l,in}$	mass density of free liq. in the steam zone	kg/m^3 free liq.
ρ_{sm}	mass density of solid mat. in wood	kg/m^3 ODW
ρ_{el}	mass density of the entr. liq. in wood	kg/m^3 ODW
ρ_{EA}	specific weight of effective alkali	kg/m^3
$\rho_{EA,el}$	mass density of entr. eff. alkali	kg/m^3 ODW
ρ_{lig}	specific weight of lignin	kg/m^3
ρ_{carb}	specific weight of carbohydrates	kg/m^3
ρ_{ds}	specific weight of dissolved solids	kg/m^3
$\rho_{ds,el}$	mass density of the entr. diss. solids	kg/m^3 ODW
ρ_w	specific weight of water	kg/m^3
$\rho_{w,el}$	mass density of water in chips	kg/m^3 ODW
$\rho_{EA,fl}$	mass density of free eff. alkali	kg/m^3 free liq.
$\rho_{ds,fl}$	mass density of free diss. solids	kg/m^3 free liq.
$\rho_{w,fl}$	mass density of water in the free liq.	kg/m^3 free liq.
ρ_{ODW}	mass density of oven dry chips	kg/m^3 ODW
ρ_{air}	mass density of dry air	kg/m^3
ν_s	local velocity of sound	m/s
υ_i	specific volume of phase i	m^3/kg
ω_{180}	the lowest frequency where the phase curve cross -180 degrees	radians/ dim.less time

Chapter 1

Introduction

This chapter explains first the background for the study, and the approach which is used in the modelling of the digester. In Sec. 1.2, an introduction to kraft pulping, and especially the continuous Kamyr digester, is given to readers who are not familiar with the topic. The definition of the quality aspects of the process is included here. Finally, the objective and the problem formulation of this study are stated in Sec. 1.3.

1.1 Background and the modelling approach

This study was initiated in the summer of 1991 when contact was established with the Peterson pulp & paper Mill in Moss, Norway. Our object was to study a dynamic industrial process containing severe non-linearities from a quality control point of view. The objective of any control strategy is of course quality control in some sense. The reason for doing something new in this area is that significant quality variations are still encountered, despite high costs invested in instrumentation and process control equipment. At the same time, new techniques and hardware are available for process modelling and control.
The continuous digester at the Peterson Mill was an excellent case process for my study. Due to its complexity, the influence from different disturbances, and its deficient instrumentation, the quality variations of the pulp from the digester is substantial. An interesting observation from the process measurements is a fairly strong correlation between the pulp quality (the Kappa number) and the chip level in the digester. This lead to certain speculations on an "accordion"-like movement of the mass, and cause-effect relationships between the Kappa number and the chip level. Since no dynamic mechanistic model was avaliable which could help to explain these relationships, a natural starting point was to develop one.

We have pursued the avenue of modelling the digester rigorously to create new understanding which may be used to improve plant operation. This means gaining a physical understanding of how the process behaves. The philosophy is that the

more you know, the better chance you have to improve control. Our approach is a mathematical model with as much first principle input as possible. This has enabled me to study what we regard are the most relevant effects in the digester process. Thus, the model includes all possible effects we believe are important, even though we end up with an inert simulator which is impractical to use in an on-line application. Then, we have a tool by which we can find out which effects are important and which are not. The idea is that this leads to a simpler and faster simulator, which is practical to use for on-line process control and analysis. It should, however, be noted that when modelling such a complex chemical process, the degree of detailing in the model has in theory no limit. The question is where to put the limit in context with the application. This means that it is impossible to model the process purely through first principles. There will always be some data we will need to fit the model to the physical constraints. Hence, "pseudo first principles model" may be the right term to use.
A distributed model like this contains many parameters, and their values have to be based on different tests, approximations and assumptions. In addition, it is impossible to verify the numerous modelled distributed variables by data from the process measurements that most commonly are used. Despite this, provided that the parameters are chosen or estimated properly, the resulting model may be more easily tuned to a real plant, than would be the case with a simpler model. The basic assumptions behind this are that the model incorporates a correct structure of the physical mechanisms in the process, and that the plant data used for identification are not too noisy. It should be noted that the objective of this study first of all is to make a *qualitative model* of the digester. Often, the word "qualitative" is used in the opposite meaning of *quantitative*, i.e. "expressed in figures". Here, however, the meaning is "pertaining to" or "concerned with quality or qualities" (Webster, 1989), even though model parameters are chosen such that the results are expressed in figures. Hence, qualitative description means *predicting trends* in the pulp quality and other essential variables that we focus on in this study. We will do this by elucidating the physical behaviour of the mass inside the digester in a "rough" way, but based on the methods of first principles. Hence, certain simplifications regarding for instance the kinetics can be defended. This means that it is not the intention at this stage to fit the model to a specific plant within a certain accuracy. That is, we do not focus on parameter estimation.

1.2 Kraft pulping

1.2.1 An introduction

Pulping is the process by which wood is reduced to a fibrous mass. This can be accomplished mechanically, thermally, chemically, or by combinations of these treatments. Existing commercial processes are generally classified as mechanical, chemical, semi-chemical (i.e. combined mechanical and chemical) or thermomechanical (i.e. combined mechanical and thermal) (Smook, 1989).
The chemical way of defibering wood is to first remove most of the lignin by chemical reactions. This is denoted delignification. Lignin is one of the two main

groups of solid material in wood, and is a highly complex material acting as a glue for the fibres. The detailed chemical reactions occurring in delignification of wood are not yet fully understood, but the main reactions are well documented (Rydholm, 1967). When saying most of the lignin, this means that not all of it should be removed. This is because the chemicals also react with the wood fibres, i.e. the carbohydrates, which are the other main group of solid material. These are also known as celluloses and hemi-celluloses. The chemicals degrade them, giving reduced pulp yield. Hence, the chemical reactions have to be stopped at a point when the lignin content is low enough for fibre separation, and where an acceptable yield can be achieved. In a complete fibre line, further delignification is achieved by a bleaching processes downstream of the digester. This indicates that the cooking process can be optimized by considering both low lignin content combined with high yield, and the cost of cooking compared to the cost of bleaching. This topic is not discussed further in this thesis.
The delignification stage is performed at high pressures. The second stage of the defibering process is to blow the mass to atmospheric pressure. In this way, the wood fibres are separated. According to the above definition of pulping, the term *pulp* is the fibrous mass, in the form of a suspension in water, resulting from this blow process. This term is, however, commonly used for the discharged mass from the digester as well, i.e. ahead of the blow unit (Smook, 1989). We use this application of the term in this thesis.

This study is about one of the most utilized chemical pulping processes today; kraft pulping in a continuous Kamyr digester. The kraft, or sulphate, process is generally run either as a batch or as a continuous process. Today, $65 - 70\%$ of the world pulp production is sulphate pulp. Approximately one half of this comes from continuous Kamyr digesters. "Kraft" is the Swedish and German word for strength. Hence, the term comes from the high strength of the pulp produced by this process. C.F.Dahl is credited with the development of the sulphate process. The sulphate is chemically reduced to sulphide in a recovery furnace and Dahl found that sulphide greatly accelerated the delignification and produced a much stronger pulp than with the traditional soda process. He obtained a patent for his process in 1884.
When continuous digesters became operational in the late 1950s and early 1960s, a number of advantages were claimed over the batch digester. Factors favouring continuous digesters were: lower steam requirement (less energy), more constant steam demand, more compact equipment, lower capacity of auxiliary components because of constant loading, easier treatment of non-condensibles because of uniform flow, and includes a diffusion wash stage (Kamyr only). Production reliability, operating flexibility and lower maintenance requirements favoured, however, batch digesters. In the beginning, there were serious operational problems with the continuous digesters, but after a while they became easier to operate than the batch digesters (Smook, 1989).
The first commercial installations of the continuous Kamyr digester was made in 1950. Today, approximately 400 units are in operation around the world. The Peterson Moss digester is one of two continuous steam/liquor phase digesters in Norway. The cooking system is a two-vessel unit containing a pre-impregnation

tower ahead of (upstream) the digester, see Fig. 1.1. Steam/liquor phase means that there is high-pressure steam in the digester top where the impregnated chips are rapidly heated when they enter the vessel. This is in contrast to hydraulic digesters where the vessel is totally filled up with liquor. Steam/liquor phase digesters are well suited for chip of nordic spruce and pine, i.e. softwood. Special to the cooking conditions in the Peterson digester, is that the conventional kraft liquor (consisting of caustic soda and sulphide) is modified by the presence of polysulphide (Moxy system) and anthraquinone. These chemicals increase the pulp yield considerably (Kleppe, 1978).

Figure 1.1: The Kamyr two-vessel system at Peterson Moss AS, Norway

Even though the Peterson digester is used as a case study, the derived model and the results apply equally well to other corresponding continuous digesters. Hence, the presentation in the following is made plant independent, and the referred numbers are typical values. Specific conditions for the Peterson digester, such as physical dimensions and nominal operating conditions, are referred in Appendix I, and applied in the analysis and simulations in Ch. 5, 6, 7, and 8. Hence, e.g. adaption to hydraulic digesters is fairly straightforward.

It was mentioned above that after a while, the continuous digesters became easier to operate than the batch digesters. However, because of the process complexity: distributed, non-linear and dynamic, strong interaction between the chemical reactions and the vertical movement of mass, many different and strong disturbances, and deficient instrumentation, it is still hard to produce mass with consistent quality. It has been said that "if somebody had calculated the flows in the Kamyr digester before it was designed, it would never have been built!" This means that the operational gap may be small, and the disturbances may have serious consequences.

1.2.2 The continuous Kamyr digester

This section gives a process description. First, a brief overview of a typical fibre line is given, to show where the digester is located in a pulp mill. Next, the Kamyr

two-vessel system is explained in more detail. This includes a description of the construction and functionality of the steam/liquor phase digester. The material is mainly taken from KAMYR (1970), Smook (1989) and Christensen et al. (1982).

The fibre line in the pulp mill

The continuous digester may be viewed as the heart in the fibre line, or process line through which the wood fibre moves, in a pulp mill. The whole line consists of many sub-processes. Fig. 1.2 shows an example of a fibre line.

Figure 1.2: A typical fibre line in a kraft pulp mill

The continuous two-vessel cooking system is shown on the left hand side of the figure, with the chip feeding and pre-steaming vessel in front. Downstream of the cooking system, the figure shows a diffuser washer which is a second stage for diffusion washing. The first stage is in the lower part of the digester. From the counter-current wash, the residuals from the cooking are extracted. In the double screening stage, oversized particles like knots and uncooked chip fragments are removed from the pulp. The lignin content in the pulp from the digester is not low enough to produce paper grades of high brightness. There are several ways to further delignify the pulp. To reduce the pollution loading, most installations utilize an alkaline oxygen stage as a delignification step prior to the final bleaching with ClO_2 and H_2O_2. The figure does not show the comprehensive recovery system for the unused pulping chemicals. This consists of evaporators, recovering furnace, clarifiers, causticizers etc. In addition, a comprehensive water treatment system also includes in a pulp mill. Modern mills are becoming more and more closed with respect to the loss of energy, water and chemicals.

The Kamyr two-vessel cooking system

To understand the characteristics of the chips which enter the digester, the pre-impregnation stage is first explained, c.f. Fig. 1.1.

The pre-impregnation stage

The wood chips are fed from a surge bin through a volumetric chip meter and a rotary low-pressure feeder into the steaming vessel. A slowly turning screw carries the chips through the horizontal steaming vessel, where flash steam at about $110kPa$ (from the residual liquor) pre-heats the chips at about 120^oC and drives off air and non-condensibles. The chips then fall into a chute connected to the high-pressure feeder. Here, the chips are transferred to the high-pressure system ($600 - 800kPa$). The chips are sluiced away with cooking liquor and carried up to the pre-impregnation vessel inlet. This vessel works at about the same pressure as the digester ($600 - 800kPa$). This high pressure and the pre-steaming facilitates rapid pre-impregnation of the chips and they fall downward by gravity through the liquor-filled space and settle on the chip mass. The chip mass moves downward as a uniform column. The residence time is 20-30 minutes and the temperature is $110-115^oC$. This is assumed to be enough for the chips to be uniformly penetrated by the cooking chemicals. The following phenomena occur here:

- The chemicals diffuse into the interior of the chips to give them more or less uniform concentration.
- The first stage of delignification occurs, in which about 20% of the wood lignin is removed. In addition, almost all the remaining extractives, about 40% of the hemicelluloses and about 10% of the celluloses are dissolved.
- Between $40 - 60\%$ of the caustic (OH-ions) is consumed.

At the bottom of the vessel, the chips are continuously withdrawn by slowly rotating paddles (the bottom scraper) that are mounted on radial arms attached to the hub of the outlet device. In addition, the outflow is helped by the liquor flow from the transport circulation through nozzles both above and below the scraper. The top circulation ensures that the chips are transported to the digester top.

The digester

The digester is designed as a cylindrical vessel of $50 - 60$ metres height and with a diameter of $2 - 3$ metres in the top and $4 - 5$ metres in the bottom. The vessel is then stepwise conic, c.f. Fig. 1.3.

The mass coming from the transport circulation enters through the top separator. Here, most of the liquor is let back in the transport circulation while the chips are exposed to the high pressure steam (typically $700kPa$ and 170^oC) and fall down and settle on top of the chip mass. At the same time, the overflow of liquor also settles on the liquor mass. It is important that the liquor overflow is large enough to keep a sufficient liquor addition to the digester. The chip- and liquor levels are important process variables to keep control of. Ideally, the liquor level should be $1.5 - 2.0$ metres below the chip level. The top 30% of the digester is

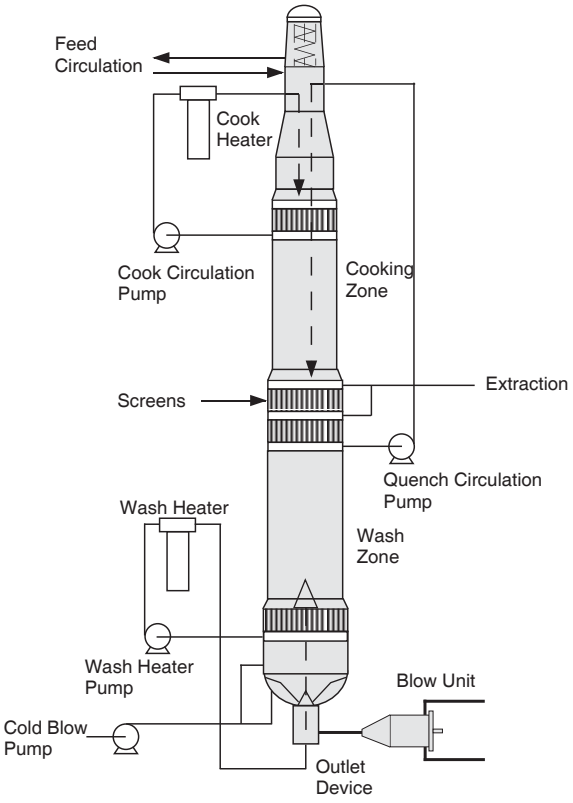

Figure 1.3: A Kamyr continuous digester

referred to as the cooking zone. This ends at the extraction line where the cooking liquor (the black liquor) is withdrawn for the recovery. The temperature in this zone is adjusted by a liquor circulation, called the cooking circulation, to about $160 - 170^oC$. The liquor is sucked through screens in the side walls, pumped through a heat exchanger and fed through a central pipe inside the digester which ends at the same hight as the screens. The chips and the liquor move continuously downwards in the cooking zone. The chip velocity is generally slightly faster than the liquor velocity. This is to avoid socalled external mass transfer limitation which makes the diffusion of chemicals into the chips and the diffusion of dissolved solids out of the chips less efficient. The residence time for the chips in this zone is typically $2 - 4$ hours, depending on the production rate. As the name indicates, it is here most of the delignification occurs. About $90 - 95\%$ of the wood lignin, 60% of the hemicelluloses and $15 - 20\%$ of the celluloses are dissolved by the end of the cooking zone. Due to the exothermic character of the pulping reactions, the maximum temperature is about 4% higher than is provided by the external heating.

The bottom portion of the digester is the cooling and washing section. The pulping reactions are stopped by displacement of the hot residual liquor with dilute

wash liquor from below. The wash water (usually first brown stock filtrate) is injected near the bottom of the vessel through nozzles partly around the side walls and vertically placed in the bottom, and moves counter-current to the chip flow to provide efficient "diffusion washing". The temperature at the nozzles is about 90^oC and the residence time for the chips in the wash zone is $2-6$ hours. The digester is usually provided with sufficient height to allow at least 1.5 hours for the residuals to diffuse out of the chips. The wash water follows the cooking liquor to the recovery process through the extraction screens. There are two of them which alternate by the help of a switching valve. There are two liquor circulations for the wash water. The upper one, also called quench circulation and which has its inlet together with the lower extraction screen, provides radial displacement of the residual cooking liquor and quenches the cooking by the upcoming colder wash liquor. In this way, there is a "temperature wall" between the cooking and wash zones. The quench circulation controls the temperature at this point at about 135^oC. However, this circulation is not strictly necessary as the quenching effect is permitted by the up-flowing colder wash water. Hence, the circulation is often closed. The lower circulation is located just above the digester bottom. It provides both radial displacement and a rise in the temperature of the up-flowing dilute liquor. The temperature here is about 90^oC. The dilute liquor in the bottom cools down the pulp effectively before it leaves the digester. This prevents strength deterioration of the discharged pulp. In the same way as for the pre-impregnation tower, to help the chips out of the vessel, there is a rotating bottom scraper with controllable rotation speed. This makes it possible to control the consistency of the discharged pulp and therefore also the amount of solid materials. The task remains to blow the pulp at a precise rate to atmospheric pressure. This is accomplished by the blow valve.

Perhaps the most difficult operational problem for the digester control is to stabilize the vertical movement of the chips, hereafter referred to as the chip plug. This movement directly determines the residence time for the chips; a critical variable which affects the pulp quality. Two of the main problems related to this are; (1) the chips compact significantly, and (2) direct measurements as a function of delignification and digester elevation. The influence from the different operating conditions on the residence time for the chips is a main topic in this thesis.

1.2.3 Pulp quality and the main process variables which affect it

The preceding discussion indicates that there are many process variables on different levels that interact. There are both rapid and slow dynamics present. As often is the case in industrial processes, the nature of this process and the availability of instrumentation imply that both the number of manipulated variables and the number of measurements are few compared to the complexity of the process. This means that important variables are not measured continuously on-line. This applies first of all to the pulp quality, as this is measured in the final pulp by laboratory tests. However, as already mentioned, this also applies to important variables that affect the pulp quality. In the case of the chip velocity, for instance,

Fundamental properties	*weighted average fibre length *intrinsic fibre strength *fibre coarseness *specific surface *wet compact-ability *chemical analysis of pulp constituents
Empirical tests	*kappa number *CED viscosity *drain-ability *colour and brightness *cleanliness *beater evaluation

Table 1.1: Pulp quality tests (from (Smook, 1989))

it is estimated roughly by the chip meter speed etc. Hence, the operation of a complex process like this in such a way may be complicated.

Quality variables

Quality in process engineering is both a question of *product quality* and *process quality* (here *pulp quality* and *pulping quality*). The former describes the end product for the process, while the latter describes the process itself, that is, consumption of raw materials (wood chips) and level of process manipulations (consumption of steam, liquor flows, alkali charge etc.). High throughput is important as well. As the wood consumption more naturally may be defined as product quality, we include this in that category. As will be clarified in the following discussion, the distinction between these categories may not be clear.

Pulp quality

The pulp quality is a set of derived quantities which are commonly estimated from laboratory tests. A large number of testing methods are in common use to characterise pulps with respect to quality, processability, and suitability for various end uses. A summary of common test methods is given in Table 1.1. The following discussion is inspired by Smook (1989), where a broader discussion on these tests can be found.

Pulp *strength* in terms of tearing resistance (on pulp handsheets), or tear index, is for many products perhaps the most common in use. Other tests are burst, tensile strength, and folding endurance. These indicate the pulp quality as well. These tests should, however, be supplemented by a knowledge of the fundamental

properties to obtain a proper understanding of the pulp qualities. For many applications, however, strength is of secondary importance. In fine papers, for example, *conformability* is more critical.

Since the pulp quality measures above are only available from laboratory tests, there is a need to relate them to process variables that are suited for process control. The most common such control measure is the *Kappa number (κ).* [1] It is commonly measured from laboratory tests, typically with one hour intervals. In some modern mills the Kappa number is measured on-line in the blow line. The measurement is based on reaction with acidic permanganate solution ($KMnO_4$), giving the amount of lignin components in a sample from the pulp. Before the test, the sample is washed. Hence, the lignin components mainly include the solid (i.e. unreacted) materials. In this way, the Kappa number test is a control test for the cooking. Further, the test is used in mill control to indicate the chemical requirement for bleaching. The test is a modified and improved version of the original permanganate number test (commonly called the "P number test" or "K-number test"). Mathematically, the Kappa number, is expressed in Eq. (3.77).

Another process control variable that is closely related to the pulp quality is the *yield (Y).* This measure expresses the total residual content of solid material in the pulp. It is defined simply as the sum of the residual content of lignin and carbohydrates. Hence, high yield means that a large part of the wood remains in the pulp, and the consumption of wood is low. In this way, this is an economic quality measure for pulp. Chemical test methods exist which are empirical but give good indications on the cellulostic portion with respect to average degree of polymerization (CED viscosity tests) and alpha cellulose content.

The wash efficiency in the digester influences the wash effort in the washing stages downstream of the digester. There are two objectives for this. (1) remove residual liquor that would contaminate the pulp during subsequent processing steps, (2) recover the maximum amount of spent chemicals with minimum dilution. In this way, the reaction products and the remaining alkali in the discharged pulp are defined as quality measures. Either chemical analysis of the blow pulp or the black liquor in the extraction line, with respect to alkali and dissolved solids concentrations, are control variables in this context. Note that the measurement in the extraction line is a control measurement for both cooking and washing.

Pulping quality

The amount of process manipulations (consumption of steam, liquor flows, alkali charge etc.) are quality measures in the view of the pulping company.
The concentration of alkali at the end of the cook is a control measure for the consumption of alkali. In the digester this is, however, measured in the cooking circulation. There are two reasons for this: (1) For practical reasons this is a convenient place to measure alkali concentration, as the cooking circulation is already present for energy input. (2) The main part of the delignification is finished at this

[1] For process control, the *H-factor* is still perhaps the most utilized control variable. It is used to estimate the Kappa number, and is further explained in Ch. 2. Because it is a strongly empiric measure, we do not focus on this extensively in this study.

location. The steam temperature and the liquor flows are regarded as manipulated variables in this study. Hence, with respect to process quality, the manipulation of these variables is an optimization problem. This is not focused on in this study.

Real plant digester operation is, however, not only a question of high pulp quality and consumption of raw materials. A high demand for pulp from customers is important for the pulping plant as well. Hence, the production rate, i.e. the product of the blow flow and the mass consistency in the discharged pulp (blow consistency), is also a quality measure. In this study, we regard the blow flow as a manipulated variable. Note that in a higher level control structure, it is possible to optimize the blow flow, and in this way view this as a controllable quality variable. This is not investigated in this study. The control of the blow consistency is the matter of manipulating the bottom scraper speed and the dilution liquor in the bottom. This will not be discussed further in this thesis. Note that constant blow consistency first of all improves the operation of succeeding washing stages.

Variables affecting the pulp quality

The quality of the pulp is influenced essentially by the following four variables.

1. **Temperature**, particularly in the cooking zone where the bulk delignification takes place. It influences the chemical reaction rates for the lignin and the carbohydrates. The temperature and the flow rate of the wash water are also important, as these determine the end of the actual cooking zone.

2. **Concentration of chemicals in the liquor**. This influences the chemical reaction rates for the lignin and carbohydrates as well. Control of the hydroxide concentration in the cooking zone is especially important; a slight excess of NaOH is always needed to prevent lignin re-precipitation.

3. **Residence time for the chips**. A controlled residence time is desired, as the amount of chip degradation is time dependent.

4. **Wood characteristics**. The quality of the uncooked chips changes due to:

    - Various combinations of hardwood, softwood, roundwood, and sawmill chips
    - Changes from hardwood to softwood chips
    - The degree of aging differs erratically for the chips
    - Seasonal variations in frozen chips
    - The chip size, moisture content, and wood-density vary
    - Insufficient pre-steaming and impregnation, leaving some air in the chips

These variations mean uneven cooking conditions for the individual chips due to unequal amount of solid content, weight, or energy. Often, one reason for some of these variations is that the chips are delivered from a number of different saw mills. Hence, the blending of the chips before they enter the fibre line is not always satisfactory.
To maintain a steady operation of the digester, it would be helpful to monitor the chip quality on-line. Then, appropriate adjustments in the cooking temperature, concentration of alkali, and residence time can be made according to the quality variations. In practice, however, they result in process disturbances.

The control of these is treated in Ch. 8.

1.3 Objective and problem formulation

The objective of this work is touched on in Sec. 1.1. This objective can be specified in more detail in the following formulation:

Gain a fundamental physical understanding of what we regard are the most important effects on the mass inside the digester.

Study the dynamical behaviour of the key process variables which affect the pulp quality, as a basis for developing improved control strategies in the effort to improve the pulp quality and minimize the wood costs in this pulping process.

Based on this two-fold objective, the following problem formulation is made:

In order to understand and control the dynamical behaviour of the pulp quality and the key process variables which affect it, a new rigorous mathematical model has to be made, based on first principles methods. This model has to include both mass-, momentum- and energy balances as to describe the inter-connection between the reaction kinetics and the vertical motion of the mass inside the digester. It is of special importance to include the influence of the chip level.

Chapter 2

A survey of earlier models

This chapter gives a review of the main part of earlier proposed models of the kraft digester. As the total amount of the model work in this area is large, no attempt is made to cover it all. However, we believe that the most important contributions, with respect to our model building, is included. The models describe different parts of the process and are of various complexity. Much work is done in describing the kinetics in the chemical reaction processes and the diffusion processes in the transport of chemicals and residuals between the chips and the surrounding liquor. Other models are simple ones that have been found sufficient for identifying certain parameters in the effort to predict a few important process variables.
In this chapter, there is a review of selected works on the kinetics, stoichiometry, diffusion, convection and dispersion phenomena. These are the effects that are considered in the mass and momentum balances in the model which is derived in Ch. 3. In the respective sections, an explanation is given of the physical phenomenon which is treated. Energy balances have been given little attention in the reviewed models, and are therefore only treated briefly here. In Sec. 2.6 some important black-box or data-driven models, that not have been discussed elsewhere in this chapter, are described. As a summary, the models are classified in a tree structure to show their model characteristics in Sec. 2.7.

A conclusion of this survey is that there is no published model today of the dynamical first principles type that includes mass, momentum and energy balances for the chip plug and the liquor, and the chip and liquor levels.
However, to my knowledge, there are on-going industrial modelling activities. Kvaerner Pulping Technology (former Kamyr AB) in Sweden and Weyerhauser Corp. in the USA have developed models for process analysis. These in-house models are not published and therefore are not considered in this review.

2.1 Kinetics

Kinetics in this context is the mass reduction of the lignin and carbohydrate components that are exposed to chemical reactions with the alkali. Rydholm (1967)

probably gives the first important work on the study of the reaction kinetics in pulping processes. This work is referred in most of the later literature on pulping. The delignification process is widely known to be separated into three distinct stages or phases; the *initial-, bulk-*, and the *residual phase*. This was identified by (Kleppe, 1970), (Kleinert, 1966) and (Norden and Teder, 1979). The very rapid lignin removal during the initial phase is characterized as extracted lignin. Removal of the bulk lignin follows a first order reaction. Often, this is expressed as:

$$r = k\rho_A^a \alpha^b \tag{2.1}$$

$$k = Ae^{\frac{-E}{R(T+273.16)}} \tag{2.2}$$

where

r	reaction rate
ρ_A	alkali concentration
α	lignin concentration
a, b	positive real numbers
k	Arrhenius coefficient
A	frequency factor
E	activation energy
R	molar gas constant
T	temperature

Finally, residual delignification occurs at a much slower rate (Smook, 1989).

The first well-known mathematical model which even today is widely used for control purposes is the so-called H-factor. This was developed by Vroom (1957) as a means for expressing the cooking time and temperature as a single variable in batch-reactors. It is defined as:

$$H = \int_{t_0}^{t} k d\tau \ , \ k = e^{43.20 - 16113/(T+273.16)} \tag{2.3}$$

where k is *relative reaction rate of pulping*, i.e. relative to the rate at 100^oC (dimensionless). Note that, at this time, no distinction was made between the reaction rate of lignin versus the reaction rate of carbohydrates. The H-factor is designated as the area under the curve of k vs. time in hours. The factor was developed to predict the temperature or cooking time needed to achieve a given Kappa number. This means that the result is only valid when the relationship between the H-factor and the Kappa number is known, that is, when the other cooking conditions are given (alkali concentration etc.). The results appeared to be quite satisfactory for kraft pulping.
Such models which predict the Kappa number, κ, from the H-factor are called *H-factor models*. A number of different versions have been developed, see Jutila (1979) for a good survey. The general form of these is (Christensen et al., 1982):

$$\kappa = f(\rho_A, H) \tag{2.4}$$

where f is an empirical function of the alkali concentration in the beginning of the cook, ρ_A, and the H-factor. The function contains parameters that have to

be updated due to changes in the cooking conditions. Hence, the H-factor models contains limited information on the kinetics.

Kerr (1970) and Kerr and Uprichard (1976) suggest a first order equation for the delignification of softwood with parameters depending on the effective alkali, sulphidity, chip size, chip moisture and liquor to wood ratio. Clarke (1987) extends Kerr's model to be valid for hardwood, and uses this in H-factor optimization.

A slightly more elaborate model is proposed by Wells, Johns and Chapman (1975) in which the high and low reactive lignin, alkali and sulphidity are modelled dynamically.

Johnsson (1971) also developed one of the earliest dynamic kraft pulping models. He included the reaction of lignin, acetyl groups and sodium hydroxide during the bulk phase, while the carbohydrates and sodium hydrosulphide reactions where omitted. Further, he did not consider the initial phase and the residual phase of reactions, nor the heat of reaction. A similar kinetic model is published by Tyler (1981).

A more comprehensive work on the kinetics in a mathematical model for the conventional kraft process is done by Smith and Williams (1974). This model was later modified by Christensen et al. (1982) (also published in (Christensen, Smith, Albright and Williams, 1983)). The model, often referred to as the Purdue model, has been a basis for several other digester studies (Lee and Datta, 1994), (Wisnewski, 1994). It includes an elaborate description of the main components participating in the cooking process. The wood components are high- and low reactive lignin, cellulose and the hemi-cellulose components galactoglucomannan and araboxylan. These are described by first order equations like Eq. (2.1). Only the initial and bulk stages are considered. The cooking liquor consists of sulphide and effective alkali. Further, dissolved solid material (residuals) are computed. These liquor components are described both in the wood chips (entrapped liquor) and in the free liquor circulating around the chips. An energy balance includes the heat of reaction. Thus, the model consists of mass and energy balances formulated as first order ordinary differential equations that are solved in 50 points (slices) along the digester. A simplified version of this model, but including the compaction of the chips as a model variable, has been commercialized in a product for model predictive control. An implementation of this is reported by Christensen, Ivan, Michaelsen, Lunde and Zetterlund (1994).

Pankonin (1979) developed a kinetic model similar to that by Smith and Williams (1974), accounting for the reaction of lignin, cellulose, glucomannan, xylan, sodium hydroxide and sodium hydrosulphide. He omitted the initial and residual phases of reaction, and the heat of reaction.

Another rigorous model taking the three delignification stages into account has been developed by Gustafson, Sleicher, McKean and Finlayson (1983). It has a slightly different structure than the Purdue model. It is simpler in the way that it

has fewer wood and liquor components. Further, the calculation of carbohydrates is simplified by using a functional relationship between the time derivative of carbohydrates and the time derivative of lignin. However, the equations that describe the three stages of delignification have different structure. A similar delignification model has been developed by Teder and Olm (1981), Johansson, Mjöberg, Sandström and Teder (1984) and Sandström, Lindberg and Teder (1986).

Most of the mathematical modelling works which are done on reaction kinetics studies only cover the influence of alkali and/or sulphide. The influence of anthraquinone (AQ) is, however, also studied. A comprehensive discussion of the effect of this on the lignin reactions can be found in (Poppius, 1985). A rigorous model for the kinetics in the kraft-AQ process is proposed by Burazin (1986). This is also published in (Burazin, 1988). Sequential experimental design (nonlinear regression and model discrimination/parameter estimation) is used to pick the best models and parameters out of 200 model candidates in a 5-dimensional experimental space. The lignin is modelled in four different states; native, residual, dissolved and inert dissolved lignin. Further, three carbohydrate species are considered; celluloses, glucomannan and xylan. These are modelled in native, dissolved and oxidised states. The peeling, stopping and cleavage reaction mechanisms are taken into account. The model objective is to extrapolate beyond current industry practice and explore wide ranges of operating conditions with confidence.

2.2 Stoichiometry

During the chemical reactions, the chemicals are consumed. When the alkali and wood solids concentrations in this way are reduced, the mass of the reaction products has to balance this reduction to keep the total mass balance in equilibrium. This description is called stoichiometry.
Sandström et al. (1986) uses constant consumption rate coefficients. Both Christensen et al. (1982) and Gustafson et al. (1983) specify the rate of consumption of alkali and sulphide as functions of the reaction rates of lignin and non-lignin. Christensen et al. (1982) base their work only on Rydholm (1967), while Gustafson et al. (1983) base their work also on Rekunen, Jutila, Lahteenmaki, Lönneberg and Virkola (1980). There is a discussion of whether the sulphide is consumed during the cook or not. Christensen et al. (1982) refer Sarkanen and Ludwig (1971) and Rydholm (1967) who claim this, while Gustafson et al. (1983) assume that the sulphur content is held constant, provided the initial sulphide concentration is above a value corresponding to about 20% sulphidity. As this matter is not considered in this study, a further discussion is omitted.

2.3 Diffusion

The transport of chemicals and dissolved solids between the chips and the surrounding liquor includes a diffusion process (McKibbins, 1960). Van Heiningen

(1993) defines even penetration as diffusion to low concentration areas in the chip. Experimental results indicate that diffusion in the pores of the chips may sometimes limit the pulping rates in the early stages of the kraft cooks (Christensen et al., 1982). Kinetic studies of the three phases of delignification - initial, bulk and residual, indicate that only the initial period is limited by diffusion because of its low activation energy (Sjöström, 1981). McKibbins (1960) found that the diffusion in the transverse direction (across the fibres) was somewhat slower than in the longitudal direction, and this was expected due to the hindrance offered by the tracheid walls. He also refers to work in which it is suggested that the relationship between longitudal and transversal diffusion is greater for uncooked chips. This is also expected due to the structural changes in the transversal direction after the cook. The critical direction of diffusion is therefore the transversal. Hence, the chip thickness is the most important factor in this context. This is also in agreement with Sjöström (1981). Stone (1957) demonstrated, however, that wood swells considerably between pH 12.0 and 12.9. Further, Talton and Cornell (1987) reports that the diffusion coefficients at pH greater than 12.9 are approximately equal in the three structural directions in an alkaline solution because of swelling of the wood structure. It is also concluded that for wood completely saturated with sodium hydroxide at pH 12.9 or greater, the swelling effect of caustic is assumed to be negligible with respect to diffusion. At lower pH values (< 12.0), diffusion in the longitudinal direction is much greater than in the radial or tangential (transversal) directions.

The usual way to describe non-stationary diffusion in one dimension is by this form of Fick's law of diffusion (c.f. Eq. (B.7):

$$\frac{\partial \rho}{\partial t} = D \frac{\partial^2 \rho}{\partial x^2} \tag{2.5}$$

where ρ is density (concentration), D is the diffusion coefficient, and x is the spatial direction for the transport. Since the diffusion process is a rate phenomenon, (McKibbins, 1960) indicates that the *diffusion coefficient*, $D[m^2/s]$ may be related to the temperature by an Arrhenius like relation:

$$D = A\sqrt{T}e^{(-E/(RT))} \tag{2.6}$$

McKibbins uses these equations to quantify the diffusion of the sodium ion both in longitudal and transverse direction of the wood fibres exposed to conventional kraft cooking operation.
This work is referred to by Christensen et al. (1982) who re-equates this relationship to a *diffusion rate coefficient* with dimension $[s^{-1}]$, and favours this compared to the coefficient which was proposed by Smith and Williams (1974).
Because McKibbins (1960) measured cooked chips, i.e. at a given level of pH and degree of cooking, according to the previous discussion the diffusion coefficient has to be corrected with respect to these variables. This approach is made by Gustafson et al. (1983) who refer to Hartler (1962) on this. The original work on this topic is performed by Hägglund (1959) and Bäckström (1960), see Appendix E.

A similar model is published by Talton and Cornell (1987) who have made experiments of unpulped and pulped wood of 88%, 79% and 67% yields. They found also a linear relationship between the diffusion and the yield at pH greater than 12.9. They believe that this is applicable to the initial or early stages of delignification because it is in this period the delignification is controlled (or limited) by diffusion. Finally, they state that as the cook proceeds, actual alkali diffusion to the reaction sites is much less significant, i.e. not longer rate limiting. However, the temperature range in which they operated was $30-70^oC$, which is significantly lower than both typical pre-impregnation temperature ($115-120^oC$) and cooking temperature ($165-170^oC$).

According to Van Heiningen (1993), because the organic materials have higher molecular weights than the chemicals, they move slower by a factor of 10 in average.
Burazin (1986) accounts for the effect of dissolved solids on the diffusion rate. He refers to Benko (1964) who shows that the diffusion of $NaOH$ is approximately twelve times faster than diffusion of lignin fragments.

The influence of incomplete penetration, as defined by the flow of cooking liquor into the chips under the influence of a pressure gradient, and insufficient diffusion are modelled by Jiménez, Gustafson and McKean (1989). This is a model of the effective alkali and lignin profiles inside the chips as a function of chip depth. The results show that the effect of incomplete penetration before the cook is minimal if the chips are completely penetrated before they reach their maximum pulping temperature, a situation which is likely to happen in two-vessel systems. The results also show that insufficient diffusion is unlikely to occur in chips with thickness less than $5mm$. The modelling of internal profiles in one or three dimensions in the chips is also considered by Johnsson (1971), Pankonin (1979), Gustafson et al. (1983), Jiménez et al. (1989) and Burazin (1986).

A fairly detailed model of counter-current adsorption, including the effects of film resistance and dispersion, particle size, and phase velocities, is developed by Neretnieks (1974a). His results indicate that dispersion has neglible influence in a case of washing cooked wood chips. Some results from a comparison with two industrial digesters are reported in Neretnieks (1974b).

2.4 Convection

Convection is the bulk movement of mass in the spatial directions. In continuous form it is mathematically described by:

$$-\nabla(\rho v) \tag{2.7}$$

i.e. as a function of the gradients of the density and the velocity. This is often the main contribution to the mass movement in distributed processes.

There are in principle two ways of describing a distributed process. The most exact method is to use the conservation laws in differential form, which gives a microscopic model of the process valid in all mathematical points through the solution space, provided the initial conditions are continuous. The model is infinite dimensional and formulated by partial differential equations (PDEs). Then, the accuracy of the solution depends on the numerical algorithm by which the model is solved. The other method is in fact an indirect solution of the PDEs where these are solved in the space direction directly in the model formulation. This gives a finite dimensional, or lumped model, of the process directly. In the limiting case, i.e. when the number of solution points approaches infinity, the two approaches merge. An advantage of the second method is that it can handle discontinuous initial conditions directly. More generally, the difference between the two approaches is a question of approximation; in the first case we make the approximations by means of numerical algorithms and number of discretization points. The second approach is often implemented such that it equals the first approach where the backward Euler algorithm is used in the spatial discretization. In this way, the process is considered as a series of homogeneous volumes (stirred tanks). Hence, by using the two approaches we may end up with the same model.

The first approach is used by Johnsson (1971). A dynamic mechanistic model is derived as a set of mass and energy balances. Both digester coning and profiles inside the chips are included. However, in order to calculate a solution, a steady state version of the model is used.
Takeuchi, Komiyama and Suzuki (1979) have used a so-called stop-and-go method to simulate a model somewhat similar to that used by Johnsson (1971).
A less complex variant of Johnsson's model is exploited in a study by Lundqvist (1975). His model is not expected to be accurate, but to describe the dominating dynamics in the process. The purpose was to optimize changes in the operating points taking the dynamics in the process into account. The model includes the five state variables: concentration of lignin, temperature in the chips, temperature in the liquor, concentration of alkali in the chips, and concentration of alkali in the liquor. Reaction, convection and inter phase mass and heat transfer are included.
Øgård (1980) uses Johnsson's model and estimates residence times in the Peterson digester by the use of correlation analysis.
Recently, Funkquist (1993) has used Lundqvist's model as a basis of what he describes as a "grey box model". This means that parameter identification is performed on a model which includes partial physical information. Certain model parameters are identified according to plant digester data. Steady state profiles of chip compaction, and chip and liquor velocities are also included.

The first mathematical model of the physical motion of the mass inside the digester is published by Härkönen (1984). Some more results are published in Härkönen (1987). This was a fundamental new way of approaching the modelling of the digester. The mass movement is described by flow equations, i.e. including momentum (force) balances, in addition to mass and energy balances. The physical motion of the mass is described as a two-phase flow, where the incompressible free liquor flows through a compressible moving bed of chips forming a column that

can be thought of as an isotropic continuum. This is a steady state model. It does not describe the delignification and degradation reactions specifically. The equations are, however, solved in two spatial directions; axial and radial.
Saltin (1992) uses a simplified one-dimensional version of Härkönen's model together with the component balances from the Purdue model to develop a dynamic model.

As earlier indicated, the second formulation approach is used in the Purdue model. However, only mass and energy balances are considered and, hence, the chip and liquor velocities are assumed to be known.

2.5 Dispersion

Dispersion is a phenomenon which gives rise to nonflat radial velocity profiles. This is due to uneven particle movement, in contrast to the conditions under pure plug flow. Dispersion causes fluctuations in concentration and results from molecular and turbulent (eddy) diffusion caused by both axial and radial mixing (Fogler, 1992). The dispersion term, which is introduced in the mass balances, has the same mathematical form as diffusion, c.f. Eq. (2.5). [1]
As dispersion has to do with turbulent flow, it is connected to the viscosity of the bulk fluid. It is therefore likely that the dispersion coefficient is dependent on the viscosity coefficient.
The phenomenon is considered by Funkquist (1993). However, he describes this only in context to the energy balances. He proposes a dispersion coefficient as the product between the absolute value of the velocity difference between the chips and the liquor, and a coefficient that is estimated from plant data.

2.6 Data driven models

All models are data driven in some sense, even those that we define as pure first principles models. Those are also based on human observations, but these observations are defined as fundamental theory (physics).
Data driven models (also known as statistical, empirical or black-box models) are here categorized as those that are more empirical in nature, in the sense that the model variables and parameters do not have to describe recognizable physical variables. However, they may do so. Classes of such models are known as ARMAX-type models, regression models, principal component models, neural network models, fuzzy logic models etc. The purpose of such models is normally that

[1] This meaning of the term dispersion is analogous with the meaning of the term in other applications. For example, the term is also used to describe the dependency of frequency, or wavelength, on the velocity of propagation of a wave motion. Examples are electromagnetic waves propagating through matter, and surface waves in a liquid. The term is also used to describe refraction of light into a dispersive medium where each component of an incident wave, composed of several frequencies superimposed, will be refracted through a different angle (Alonso and Finn, 1983).

most of the model parameters are to be identified by on-line identification algorithms, that is, the models intend to describe specific real plants. However, this provides that these parameters are identifiable by the existing process measurements. This often requires a very simple model structure.
In this section, some data driven models are treated, which have not been discussed elsewhere in this chapter.

Christensen et al. (1982) refers Stankovic, Majdanac and Draskovic (1976) who have used a first order orthogonal planning technique and regression analysis to investigate the dependence of pulp properties (brightness, lignin content and yield) on cooking conditions (cooking temperature, active alkali concentration and cooking time). The purpose of the model was to investigate if there were any interactions between the independent variables (the cooking conditions), and how important these variables were in determining the pulp properties. For beech wood, it was found that there was no significant interaction between the independent variables, and pulp properties were influenced primary by the cooking temperature. The concentration of active alkali and cooking time were found less critical.

Parameter identification of the heating zone dynamics is considered by Zhong, Bélanger and Gendron (1990). The identification had two purposes. First, it was a first step in the design of an algorithm to control the temperature of the chips leaving the heating zone. Second, it was seen as a possible means of detecting a situation where an agglomeration of chips plug up the digester. The switching action of the screen sets gives rise to periodically time varying dynamics. It is a two-input two-output model where the two switching periods are the inputs and the temperatures in the respective switching periods are the outputs. The process is modelled as an augmented time-invariant linear system. The results were used to design a self-tuning control algorithm.

A time series approach including the Kappa number and the H-factor used in a simple model-based control scheme is proposed by Liao and Wu (1976).

A number of simple models for the relation between two or three process variables have been developed. Hatton (1973) describes an equation for yield based on the H-factor and effective alkali. Masùra (1993) has developed logarithmic straight line equations for the relations between the Kappa number and the H-factor, Kappa number and effective alkali, and the yield and the Kappa number. Vanchinathan and Krishnagopalan (1993) have developed a dynamic model describing the delignification kinetics based on real time liquor data (NaOH and NaSH). Nonlinear statistical analysis is used.

A more advanced approach is reported by Kleppe and Storebråten (1982), where a Kappa number control system is founded on an empirical model for predicting the Kappa number in the blow pulp. The inputs to the algoritm include the production rate, the effective alkali concentration and the temperature in the cooking circulation, the dilution factor, and the temperature in the wash circulations. Adjustments where made according to the polysulphide and anthraquinone charge as

well.

Dayal (1992) applies neural networks for modelling the digester, and a comparison is made to a partial least squares (PLS) regression method. The advantages and limitation of both PLS and neural networks are evaluated and comparisons of PLS and neural network models are made to other semi-empirical modelling approaches. Based on knowledge gained from these models, a multi-loop control strategy is proposed in order to improve the control of the digester. The models provided similar results.

Fuchs and Smith (1971) and Allison, Dumont, Novak and Cheetham (1990) have focused on the modelling and control of the chip level. Fuchs and Smith (1971) has designed a proportional-plus-reset controller by analysis of a simple model where the blow flow is the manipulated variable. Allison et al. (1990) uses an adaptive predictive control technique, based on generalized predictive control (GPC), and model parameter estimation. The blow flow is used as manipulated variable. Both report about significant reductions in chip level and Kappa number variabilities from plant applications. In Allison, Dumont and Novak (1991), an extension of this approach is published, where also the chip meter is used as manipulated variable.

2.7 Summary

The models which are discussed above can be classified through the tree structure in Fig. 2.1.

What characterizes most of the earlier models is that they are either empirical or only partly mechanistic to a degree that we do not find sufficient in the work to reach the objectives which are formulated in Sec. 1.3. Hence, there is room for improvement. Related to the operational problems of the digester, where the chip level control is essential, we find it important to include a rigorous description of the movement of the chip plug. Surprisingly, this topic has been given little interest in the literature.

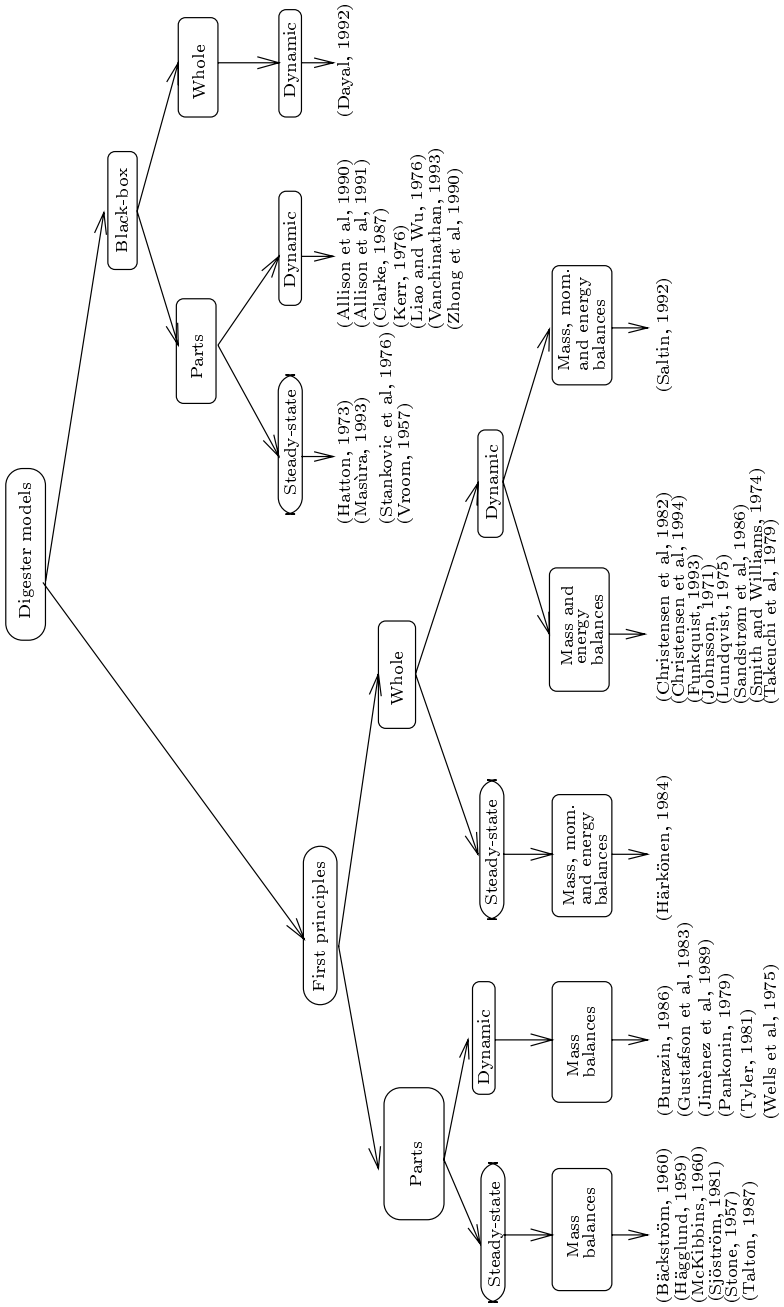

Figure 2.1: Classification-tree for earlier proposed models

Chapter 3

Derivation of the proposed model

In this chapter, the proposed mathematical model is derived. The ideas on which the model is built, are described in Sec. 3.1. The main assumptions behind the model are stated in Sec. 3.2, which includes overall assumptions, and in Sec. 3.4, where a broader discussion about the surface forces and the compressibity assumptions are included. In Sec. 3.3, the definition of basic and derived variables are stated. The model equations are derived in Secs. 3.5, 3.6 and 3.7. Finally, scaling of the equations is described in Sec. 3.8.

3.1 Background

The proposed model is partly based on the ideas behind the earlier model works which are outlined in Ch. 2. Essentially, the digester model consists of balance equations which describe flow dynamics, reaction kinetics, interphase diffusion and thermodynamics. The following sub-sections respectively treat these phenomena.

Flow dynamics

Related to the operational problems of the digester, the chip level control is of greate importance. Hence, the skeleton of the model is a description of the vertical movement of the chip plug. This is a necessary basis for studying the relationship between the Kappa number and the chip level. This also leads us to describe the vertical movement of the liquor, i.e. the free liquor, including the liquor level. By this, it is natural to utilize the ideas of Härkönen (1984) (c.f. Sec. 2.4 and Fig.2.1).

Kinetics

As discussed in the previous chapter, the chemical reactions are thoroughly studied in the literature. Some studies are more detailed than others. It is of course possible to make even more detailed descriptions of the complex reaction mechanisms. In our model, we are only interested in describing the overall kinetics that occur in the digester part of two-vessel systems. Hence, we use the principles behind the referred models, like the Purdue model (Smith and Williams, 1974), (Christensen et al., 1982), or that by Gustafson et al. (1983) or Burazin (1986) (c.f. Fig.2.1). Compared to these, certain simplifications are made. These are mainly:

- The initial delignification stage is omitted because this is completed in the pre-impregnation vessel, i.e. before the chips enter the digester. Hence, the dissolution of the extractives (acetyl groups and resins, such as terpenes) is neither considered.
- The lignin (high and low reactive) and carbohydrate (cellulose and hemicelluloses) components are lumped respectively into one lignin and one carbohydrate group. Regarding the lignin, this simplification is connected to the previous item as the main part of the lignin which is left in the digester of the two-vessel type is the low reactive lignin. Hence, most of the high reactive lignin is dissolved in the pre-impregnation vessel, as it is in the impregnation zone in one-vessel systems (Christensen et al., 1982).
- The kinetics is the same for the bulk and residual phases of delignification. This means that we only consider one mechanism for each component, i.e. for instance the condensation mechanism is not considered. Hence, the kinetic model is mainly valid in the middle Kappa number range $(50 - 150)$.
- The chemicals (i.e. the different species of active ions) are lumped into one group, called *effective alkali*. This is the most common measure for the liquor concentration of chemicals, (Smook, 1989).

The argument for making all these simplifications is that first of all our objective is to find a qualitative description (c.f. Sec. 1.1) of the main mechanisms that we believe are important in the process. Hence, to describe a number of certain reaction mechanisms in detail does not contribute with more qualitative information to the model in our context. Of course, a further refinement of the kinetics may predict the pulp quality more precisely (quantitatively). Such a model will be also be needed e.g. tracing of the sulphide through the process. Anyway, a more detailed model have to include more uncertain parameters (reaction coefficients etc.), even though such have been found with satisfactory results for some data sets from the literature. Christensen et al. (1982) and Burazin (1986) are examples on this. As such, maybe the approach by Burazin (1986) is the most confidential. In his review of earlier models, he says (c.f. the discussion in Sec. 1.1): *"Most pulping studies in the literature have concentrated on pulping conditions close to typical industrial practice. These studies define the behaviour of the process, but typically do not provide enough information to discriminate between sets of reaction equations. For a set of reaction equations to be applicable over a wide range of conditions, the equations should be based on plausible reaction mechanisms, and*

the data used to fit the equation parameters should include experiments specifically designed to place the equations in jeopardy. There can be no confidence in extrapolating reaction equations fitted to data which can be fitted equally well by several different sets of equations." However, model parameters are not unique. Further, to our qualitative model, satisfactory good model parameters are found. This defends our simplifications.

Diffusion

Regarding the diffusion mechanisms, we have found it necessary to modify the diffusion coefficients as proposed by the Purdue workers by including the dependency of the yield (or the degree of delignification) and pH. The reason is that the experiences from the Peterson Mill are that the amount of dissolved solids in the black liquor withdrawn in the extraction line depends heavily on the Kappa number. This may be related to higher diffusion rates at lower Kappa numbers. As discussed in Sec. 2.3, this is a natural model of explanation and hence, it may be generally valid. The results are based on work by (Jiménez et al., 1989), (Hägglund, 1959) and (Bäckström, 1960) (c.f. Fig.2.1).

Thermodynamics

Regarding some of the effects that are included in the energy balances, these are inspired by the model of Härkönen (1984). For the rest, the derivation of the equations is not published in this form as far as continuous digesters are concerned. The heating of the chips, by the high pressure steam in the top, is a special feature in the proposed model.

□

The model building is structured as follows:

1. In Sec. 3.2, 3.3 and 3.4, we specify a *conceptual model* of the mass in the digester. Using the conceptual model approach is one of the most powerful tools in investigating phenomena in complex systems. According to this approach, a complicated physical phenomenon, or system, the mathematical treatment of which is practically impossible, is replaced by some fictitious, simpler system, that *is* amenable to mathematical treatment (Bear, 1972). The assumptions behind the model are stated in Sec. 3.2 and 3.4. Model variables are defined in Sec. 3.3.

2. Derivation of the mathematical model, which includes mass, momentum and energy balances, is described in Sec. 3.5, 3.6, 3.7 and 3.8. The influence of the conic design of the vessel is discussed in Appendix D.

3. Analysis of the model by simulation, and mathematical analysis methods. This is described in Ch. 5 and 6.

4. Verification and validation. This means respectively comparison with both knowledge and understanding by process experts, and real process data. This is included in Ch. 5.

Balance equations are derived from the fundamental conservation laws. The equations are based on the Euler formulation of partial differential equations (PDEs), in which the control volume which cover an elementary volume of mass is fixed in space and the modeller observes the mass flowing through this volume. This is in contrast to the Lagrange formulation where the elementary volume is not fixed in space, but changes in size and position as it follows the motion in the flow. This method is suitable for particle tracing. It is obvious that the Euler formulation has limitations in giving an exact description of the whole mass in the digester. This is due to the fact that the chip/liquor mass does not have constant volume, since the chip and free liquor levels vary with time. This deficiency, however, does not prevent us from solving the problem by this formulation. The whole mass is modelled by separating it into four parts, hereafter denoted as *sections*. The *main section* covers the main part of the mass and is formulated by PDEs. This is separated by the *extraction section*, which covers the area around the extraction screens, see Fig. 3.1. The *top section*, see Fig. 3.2, covers a few metres of the upper part of the mass, i.e. above a certain level from the bottom of the digester, and the *outlet section*, see Fig. 3.3, covers the mass in the outlet device. Thus, these latter sections comprise the boundary conditions for the PDEs. We solve the equations only in the vertical direction, called z.

Figure 3.1: The extraction section

3.2 Model assumptions, part 1

In this section the main assumptions, on which the model is based, are stated and discussed. This means that assumptions that normally are made in the derivation

Figure 3.2: The top section

Figure 3.3: The outlet section

of balance equations, e.g. that heat conduction is expressed by Fourier's law etc., are not considered here.
The assumptions mainly cover the main section. Hence, the assumptions behind the boundary conditions are only briefly treated in Sec. 3.2.4. A further discussion of these is found in the context with the model derivation in Sec. 3.5, 3.6 and 3.7. Regarding the mass balance for the top section, a broader discussion is included in Appendix F. The assumptions behind the choice of model parameters are not discussed. However, the structures of the kinetic model, the interphase diffusion model, the viscous friction model etc. are included here and in Sec. 3.4. Note that the general model which is derived in this chapter is not restricted to these sub-models. There is room for modifications to these as well as for instance the number of lignin, carbohydrate and alkali components. Hence, there is no sharp border between the model assumptions regarding these and model parameters.

The first subsection describes how the mass of chips and liquor is viewed physically, i.e. what it consists of and how it moves. Next, the different transport phenomena are treated. Then, the pulp quality, and some other constraints are discussed. Finally, a broader treatment of the surface forces is made.

3.2.1 Physical view

1. The digester vessel is non-conic, i.e. no cross-sectional area variations.

   Comments: The cross-section area in the main part of a typical digester variates from $13.5 - 14.0m^2$ *in the top to* $16.5 - 17.0m^2$ *in the bottom. This increase is due to the location of the different screens. Further, it helps the vertical downflow of the mass. In the top part where the top separator is located, the area is typically* $5.5 - 6.0m^2$*. It is shown in Appendix D that with respect to the mass flow, the variations only influence the mass balances, and not the momentum balances. The error which results from this assumption is probably not significant (Härkönen, 1994).*

2. The wood chips have no specific shape or size. However, they are assumed to be of equal size, incompressible (inelastic) and the volume of the a chip entering the digester is equal to the volume of an oven-dry wood chip. Further, the density of an oven-dry wood chip is known.

   Comments: Note that the shape or the size (the volume) of the chips does not come into account in the model derivation. However, the volume and mass of an oven-dry wood chip are used as references for the variables that express volume- and mass fractions. Hence, the density of an oven-dry wood chip is needed. One advantage of this convention is that, for instance, the residual content of lignin is related to the mass of the solid content of an uncooked chip and therefore gives a measure of how much the chips have been cooked. The density, $\rho_{ODW} = m_{ODW}/V_{ODW}$*, of an uncooked chip is then a known parameter in the model. In this study, we define oven-dry wood as the dry content in uncooked wood. However, in the literature, oven-dry wood means moisture-free, i.e. generally the dry content in the wood (Smook, 1989). We redefine this term to facilitate the model description.* [1] *This also implies that we assume that the chips do not swell when the pore space is filled with liquor, or are being thermally expanded by the heating. The error is assumed to be of no significance. This assumption simplifies the model. The volume variations of the chips that enter the digester depend on the quality of the chipping. Modern chippers cut chips with even size and shape. Finally, the volume of the individual chips remains practically unchanged throughout the process. This is indicated by the pilot plant experiments by Härkönen (1984) to be a valid assumption.*

3. The size of the chips is very small compared to the size of the digester vessel.

   Comments: Chips that are cooked in real plants satisfy this assumption.

[1] The use of the general meaning of this term results in implicit equations. However, our redefinition does not change the concept.

4. The chip bed is an isotropic porous medium.

   Comments: The porous medium approach means that the chip bed (the collection of individual chips) is regarded as a continuous medium, i.e. a "continuum". This implies that there is no channelling in the mass. Except under extreme operational conditions, this assumption is valid (Christensen et al., 1982). The isotropy assumption is related to assumption 1 and means here that the permeability is equal in every spatial direction.

5. The movement of the mass can be considered as a continuous two-phase flow, where the free liquor (i.e. free to circulate) is regarded as incompressible and flows through a compressible moving chip bed.

   Comments: The two-phase structure, as proposed by Härkönen (1984), is an intuitive way of viewing the pulp inside the digester. The continuity assumption is needed for the use of the continuous Navier Stokes equations. Incompressible free liquor means that no air is present. This may be justified at the pressure levels in question. With respect to the chip plug, it is stated that the chip plug is regarded as a continuous substance in the previous assumption. Simultaneously, when the size of the individual chips is small, c.f. assumption 2, this is an intuitive assumption. Note that no assumptions are made on the movement of the chip plug being a viscous flow. This requires an expression of the viscosity coefficient for the chip plug. This is discussed further in Sec. 3.4.1. The chip plug may be regarded as a non-Newtonian fluid (Bird et al., 1960). The compressibility assumption is discussed further in Sec. 3.4.2.

6. The chips are homogeneous (uniform), i.e. the material distribution is even inside the chips.

   Comments: As discussed in Sec. 2.3, this is valid if the chips are thin enough (typically $\leq 5mm$). This implies that the interphase diffusion of alkali and dissolved solids are not dependent on direction.

7. The chips consist of solid material, entrapped liquor and air. The air does not escape from the chips in the digester.

   Comments: Incomplete penetration, which results in air inside the chips, can be a problem when the process of pre-steaming is insufficient. This is typically due to small capacity in the steaming vessel. The result may be foaming at the top of the chip plug, which causes noise in the chip level measurement. Further, the movement of the chip plug is influenced. We assume that the air cannot escape from the chips inside the digester, as it is entrapped by the solid structure of the wood material. However, it may be the case at normal conditions that the high pressure in the digester compress the air into a volume less than 5% of the chip volume (Van Heiningen, 1993).

8. Air volume variations in the chips only results in exchange of water between the free and the entrapped liquor.

   Comments: This assumption is in principle wrong as the liquor components are mixed in the liquor and hence will also be exchanged between the free and the entrapped liquor. However, if this is to be modelled in more detail,

the model becomes very complex. It may be argued that if the volume variation is small enough, the error will not be significant. This may be true even though the vertical pressure and temperature profiles influence the air volume in the same direction.

9. The entrapped liquor in the chips consists of water, one component of chemicals forming active ions taking part in the chemical reactions, and one component of dissolved solids. The component of chemicals describes the effective alkali concentration.

   Comments: As discussed and justified on page 46, separate species of active ions, i.e. hydroxide, hydrosulphide, anthraquinone, polysulphide ions etc. are lumped together in one single component. This is in accordance with Johnsson (1971). As discussed in Sec. 7.1.1, this gives in practice no freedom to control the yield independently of the Kappa number. The assumption about the dissolved solids is in accordance with earlier proposed models, see e.g. Christensen et al. (1982).

10. The solid material in the chips consists of one component of lignin and one component of carbohydrates.

    Comments: This is discussed and justified on page 46.

11. The carbohydrates contain soluble and insoluble material.

    Comments: According to Christensen et al. (1982) it is likely that about 70% of the celluloses and about 25% of the galactoglucomannan (a hemicellulose component) is unreactive. This means that about 50% of the total amount of solids in the uncooked chips is not dissolved.

12. The free liquor consists of the same components as the entrapped liquor.

    Comments: This means that there are no components in the free liquor which are not able to move into the chips. This is in accordance with earlier proposed models (Christensen et al., 1982), (Johnsson, 1971), (Burazin, 1986).

3.2.2 Transport phenomena

Mass transfer

Convection, dispersion and diffusion

1. There is a certain extent of vertical dispersive transport of both chips and free liquor. The coefficients of dispersion are not location dependent.

   Comments: The dispersion coefficients are assumed to be constant and small enough such that the dispersion terms are small compared to the convective movements at steady-state. As discussed in Sec. 2.5, the coefficients are likely to be dependent on the viscosity coefficients and the vertical velocity difference between the phases.
   The relative velocity dependency is not considered in connection to mass balances in the cited literature. Hence, we have no data that we can rely this dependency on.

Further, although the temperature dependency of the viscosity coefficient for water is considerable in the temperature range in question ($170 - 300 \cdot 10^{-6} kg/(sm)$, *see thermodynamic tables), we omit this dependency because the influence from the dispersion is assumed to be small.*
In Sec. 3.4.1, it is argued that the eddy diffusion, i.e. the viscous normal force, for the liquor is neglible compared to the other forces that are considered. Hence, this is omitted. As dispersion has to do with turbulent flow (eddy diffusion), there are reasons for stating that dispersion has no significant influence for this phase.
Further, as discussed in Sec. 3.4.1, the viscosity coefficient for the chip plug is not know. By intuition, however, the viscosity for the chip plug (a non-Newtonian fluid) may be greater than for the liquor (Newtonian fluid), see Fig. 3.9. Hence, the dispersion coefficient for the chip plug may be greater than for the liquor.
It is notable that as the dispersion terms may have influence when the spatial density gradients are changing considerably (c.f. Eq. (2.5)). Hence, from the numerical solution point of view, we may benefit from including these terms. Further, by including these terms, we have the opportunity to study the dispersive effect in the digester.

2. The cross-sectional distribution of chips (packing) is uniform.

   Comments: This means that the convective and dispersive movements of the chips and the free liquor is vertical (axial), and there are no radial gradients in the packing of chips. The consequence of the assumption is that the flow is irrotational. The assumption of no radial gradients does not hold in certain parts of the digester like near the walls, near the screens and corresponding central piping, and at the bottom. However, these parts of the digester only comprise a small volume compared to the whole digester volume. Note also that because of this assumption, we do not have to assume any cross-sectional geometric form of the digester except for no cross-sectional area variation, c.f. assumption 1 in Sec. 3.2.1. That is, the fact that the digester is a cylindric vessel does not come into account in the description. However, the cross-section area is needed.

3. The diffusion coefficients in the radial direction for the free liquor components are infinitely large.

   Comments: This concerns cross-sectional variations in the concentrations of the alkali and dissolved solids. These variations are neglected (Johnsson, 1971), (Christensen et al., 1982). In the light of the previous assumption and by assuming that the distribution of these components are even over the cross-section initially and in the top of the digester where the feed enters, this assumption will be valid. However, the same restrictions as in the previous assumption are valid here (further comments on this can be found in Christensen et al. (1982).)

4. There is no axial diffusion in the free liquor.

   Comments: It is probable that the vertical convective flow is faster than the diffusive transport (Johnsson, 1971).

5. The Soret effect is neglible with respect to bulk mass diffusion.

   Comments: Despite the temperture gradients in the digester, it is likely that this effect has no significance (c.f. Appendix B).

Chemical reactions

1. There is no reprecipitation of dissolved organic substance on the fibres at any stage in the cook, i.e. the chemical reactions are irreversible.

   Comments: Lignin condensation (reprecipitation) makes the dissolution of the lignin reversible and occurs when the hydroxide concentration is very low (not in excess) (Christensen et al., 1982). During normal digester operation, this assumption is valid (Johnsson, 1971). Further, when anthraquinone is added in the liquor, the condensation reactions are retarded (Dimmel, Shepard and Brown, 1981).

2. The chemical reactions inside the chips are of first order and the structure and the coefficients in the reaction term are known. The reaction rates are respectively described by:

$$r_{lig} = k_1 \rho_{EA,el} \alpha_{lig} \tag{3.1}$$

$$r_{carb} = k_2 \rho_{EA,el} (\alpha_{carb} - \alpha^0_{carb}) \tag{3.2}$$

   where k_i, $i = 1, 2$ are the Arrhenius coefficients:

$$k_i = A_i e^{\frac{-E_i}{R(T+273.16)}} \tag{3.3}$$

   The variables are defined in Sec. 3.3.2. α^0_{carb} is the unreactive part of the carbohydrates (typically 30%) which is formed during the stabilization reactions. The range of validity for these equations covers normal kraft cooking conditions.

   Comments: The structure of these kinetic models is similar to some of the cited models in Ch. 2 (e.g. Christensen et al. (1982) and Burazin (1986)). Our model is, however, simplified compared to these (c.f. the discussion on page 46. Often, an exponent is used in the alkali concentration. From the equations, the reactions for a given type of chips (determining A_i and E_i) is dependent on temperature, alkali and the remaining amount of the solid.

3. The pulping agents do not react with the wood components which are dissolved during the cook. Hence, there is no time delay between the reactions and dissolution of wood components in the entrapped liquor.

   Comments: At present, there is no data available to include this phenomenon. It is even probable that the delay is small for the majority of the molecules compared to the residence time in the digester (Johnsson, 1971). The assumption facilitates the model description by omitting intermediate components (larger molecules of reaction products) needed to fulfill the mass balances if the delay is to be included. Further, it facilitates the calculation of the alkali concentration. Only the end product, denoted dissolved solids (dry content), is needed in the model description. The dissolution is made

by cleavage and oxidation reactions of the reaction products (Christensen et al., 1982). The assumption is in accordance with assumption 9 in Sec. 3.2.1.

4. The pulping agents either remains unchanged in the liquor or are found in the reaction products. The mass fractions of alkali transfered by the reactions (factors of consumption, denoted respectively b_{lig} and b_{carb} for the lignin and carbohydrate reactions) are known.

   Comments: The consumption of alkali by the lignin and carbohydrate reactions is mainly due to the neutralization of acids formed during the chemical reactions (cleaving, peeling reactions etc.). Sodium salts are formed in the case of carbohydrates (Christensen et al., 1982). Hence, the pulping agents are entrapped to both the solid materials and the dissolved solids. We assume that only neutralization of the dissolved solids occur. As argued by Johnsson (1971), this is valid for the main part of the pulping agents.

5. The volume of the dissolved solids is unchanged during the recombination of the solid structures in the dissolution process.

   Comments: This means that the mass and the volume are increased equivalently percentage-wise. The actual volume reduction is neglible compared to the volume of the individual chips. Note, however, that the mass of the dissolved solids is maintained. It is the mass which is important to keep control of, not necessarily the volume. Hence, this assumption is a part of the conceptual model of the mass.

Interphase diffusion

1. The transport of material between the entrapped and the free liquor, i.e interphase mass transfer, is a diffusion process.

   Comments: This is proposed by McKibbins (1960). However, diffusion due to mass density gradients is only one out of several different interphase transport phenomena, including also bulk flow or convection (that is penetration due to pressure gradients etc.), turbulent diffusion (dispersion) due to turbulent flow of liquor across the chip surface, and thermal diffusion (the Soret effect, see Appendix B) due to temperature gradients. In this study, we will not distinguish between all these complex phenomena, and rather collect them in one term, called diffusion. It should, however, be noted that since we operate with separate energy balances for the two phases in our model, it may be a weakness in the model that the thermal diffusion effect is not expressed explisitly. If the chips are large enough and/or the interphase heat of conduction is small, this effect may be considerable.

2. The diffusing components are alkali and dissolved solids.

   Comments: This is in accordance with Christensen et al. (1982), assumption 9 and 12 in Sec. 3.2.1, and is commented further in Sec. 3.3.2 in the discussion about the conceptual model.

3. Diffusion is considered as proportional to the density difference of respective alkali and dissolved solids in the entrapped and free liquor, and a *diffusion*

rate coefficient with dimension $[s^{-1}]$. This coefficient is approximated by using the *diffusion coefficient* with dimension $[m^2/s]$ as proposed by Gustafson et al. (1983). For the alkali, it is described as:

$$D_{EA} = a\sqrt{T_c + 273.16}e^{-b/(T_c+273.16)} \cdot (c\alpha_{lig} + d\rho^e_{EA,el} + f) \tag{3.4}$$

T_c is the chip temperature, α_{lig} is the lignin concentration, $\rho_{EA,el}$ is the effective alkali concentration as defined in Sec. 3.3.2, and a, b, c, d, e and f are parameters. The range of validity for this equation covers normal kraft cooking conditions.

The diffusion coefficient for the dissolved solids is described as:

$$D_{ds} = k_{d,ds} \cdot D_{EA} \tag{3.5}$$

where $k_{d,ds}$ is a constant.

Comments: These assumptions are in accordance with the cited literature which is discussed in Sec. 2.3, and mean that the diffusion coefficients for the two components are different and depend on temperature, yield and pH (c.f. Appendix E).
The results are, however, only valid if the concentration is equal at the surface of the chip and in the surrounding liquor, that is, the transfer of chemicals or dissolved solids in the bulk liquor and through the film at the chip surface is fast compared to the transport inside the chips. This is true only if the two phases move with different velocities. A control objective is to assure that the chips move faster than the liquor. A pre-condition for this is typically that the liquor-to-wood ratio (L/W) is lower than 4.5. Otherwise, external mass transfer limitation occurs, c.f. Sec. 1.2.2. This ratio is described in more detail in Sec. 3.3.6. No published models include this effect, and no studies on this are found in the literature. Hence, it is not included in the model. For proper digester operation, it is a control problem. See also the comments to assumption 6 in Sec. 3.2.1.

Compressibility equation for the chip plug

The compressibility equation (or equation of state) for the chip plug, stating a relationship between the Kappa number, volume fraction of chips and the chip pressure, is given by

$$p_c = 10^4\left(\frac{\epsilon_c - 0.356}{0.831 - 0.139ln(\kappa)}\right)^{1.695} \tag{3.6}$$

as proposed by Härkönen (1987). This is valid at all the cooking conditions which are considered in this thesis.

Comments: The equation is found experimentally by Härkönen in a pilot plant setup and is discussed further in Sec. 3.3.3. It is of course only strictly valid for the cooking conditions which are considered in that study. These include the chip

species which are cooked, the liquor to wood ratio, the Kappa number level etc. However, it is likely that the qualitative behaviour of the model will not change due to variations in these variables within normal cooking conditions. Further, it is only derived for conditions in the cooking zone, but in this study will also be used in the wash zone. An argument for this is that the compaction of chips and the Kappa number do not change dramatically from the bottom of the cooking zone to the wash zone. In Sec. 3.4.2, it is argued that the compressibility is irreversible. Hence, if the chip plug is accelerated downstream, a discontinuous decrease in the chip pressure upstream will occur. This results in channelling of the chip plug. However, since the model is described with continuous equations, these conditions are included in average. A complicating factor in this context may be that the chips change their characteristics during the cook such that they become sticky. Since this gradually occurs in the cooking zone, this effect is implicitly included in the equation.

Momentum transfer

Regarding the assumptions behind viscous and sliding friction forces, these are discussed in a broader treatment of these phenomena in Sec. 3.4.1. A discussion on the pressure variables is included in Sec. 3.3.3. Some main assumptions from these discussions, or assumptions which are not treated there are:

1. All momentum transfer is directed axially in the digester.

   Comments: The consequence of this is that the digester is standing vertically. This is desirable. Hence, the gravity force is not decomposed. However, no radial momentum transfer assumes also that the liquor circulations have no influence on this. As a result, they have no influence on the radial profile of the packing of chips. As commented on assumption 2 in Sec. 3.2.2, this may be a bad assumption at some places in the vessel. Especially under extreme flow conditions, the radial flow at the screens may impede the vertical movement of the chip plug and cause plugging of the screens. This is known as hanging, or hang-up. Another condition which may complicate this is that the position of the outlet of the central pipe may vary in the vertical direction. Inclusion of this effect may require that the radial direction is considered in the way such as proposed by Härkönen (1984). However, the increased complexity by including this is not considered worthwhile in our context. Further, a simple way of including the influence of the liquor circulations on the vertical momentum transfer is to choose larger sliding friction coefficients than normal (or as a function of the liquor circulation flow rate) at the locations where the screens are mounted, c.f. assumption 4 below.
   Even though this assumption may be one of the main deficiencies with the model, it may be defended when used in a qualitative model and under normal flow conditions.
   As a consequence of these assumptions, the assumption of no cross-sectional variations in mass concentrations is valid.

2. There are no shear forces in the liquor or in the chip phase.

Comments: This is one of the reasons for no cross-sectional variations in the mass concentrations. All viscous friction forces are described as interphase volumetric friction forces (Härkönen, 1984).

3. The interphase volumetric friction force is described by the Ergun equation (Ergun, 1952).

   Comments: The same comments as to the assumption about the compressibility equation may be made here. The Ergun equation is further discussed in Sec. 3.4.1.

4. The force of sliding (dry) friction between the chip plug and the digester walls is proportional to the chip pressure.

   Comments: This is discussed further in Sec. 3.4.1.

5. There is no eddy viscous diffusion in the free liquor or in the chip phase.

   Comments: This is discussed further in Sec. 3.4.1, and means that the mass dispersion has no significant effect on the momentum transfer.

6. The chip plug acceleration, and the forces of inertia improve the numerical stability of the model.

   Comments: This may be verified by simulation results, and is discussed further in Sec. 7.3.

Heat transfer

1. The important energy fluxes in this process are *convection* (energy transport by the mass flow), the performance of *work* (pressure works and friction works, i.e. energy transport by the momentum flow), and *conduction* (energy transport by temperature gradients, i.e. thermal energy flow).

   Comments: The first two effects represent the mechanical energy transport, c.f. Appendix B. The energy transport by the dispersive and interphase diffusive mass transport, c.f. the Dufour effect in Appendix B, is typically small in this process. As the dispersive mass transport is already assumed to be of limited importance, the assumption here is valid. Regarding the energy transport by the interphase diffusive mass transport, this is neglible because the net mass interchange between the phases is small compared to the bulk mass. Hence, the interphase energy transport is dominated by heat of conduction. The contribution by the work is determined by the containment of the momentum balances. The heat of conduction also includes vertical heat transfer and the conduction through the digester shell.

2. The mechanical energy is not degraded to thermal energy.

   Comments: Such degradation is only of significance in systems with extreme flow conditions where appreciable temperature change is due to e.g. sudden expansion, compression, or large velocity gradients (Bird et al., 1960). In this context, the digester process is reversible. Thus, the final form of the energy balance equations only includes thermal energy.

3. There is no thermic expansion of the chips or the liquor.

   Comments: Regarding the chips, this corresponds to the results reported by Härkönen (1984), and hence together with assumption 2 in Sec. 3.2.1, the chips retain their volume throughout the process. It is likely that this effect has no significance with respect to the liquor either.

4. The coefficient for heat of reaction is the same for lignin and carbohydrates.

   Comments: There has not been found any data from the literature to separate these effects.

5. The coefficients for heat conduction within the chips and in the radial direction in the bulk mass are infinitely large.

   Comments: Together with assumption 6 in Sec. 3.2.1 and assumption 2 and 3 about convective, dispersive and diffusive mass transfer, this simplifies the modelling by only regarding axial variations in all the model variables.
   Regarding the heat conduction within the chips, this assumption is valid when we assume that the chips are relatively small (and thin) and the vertical velocity is low. Then, the heat has enough time to be conducted through the chips. Hence, no internal profiles inside the chips are modelled.
   Except for the temperatures and in general the other variables in certain parts of the digester (c.f. assumption 2 about convective, dispersive and diffusive mass transfer), the results from Härkönen (1984) indicate that the assumptions about no cross-sectional variations are valid. Especially for digesters that are outdoors, the temperature at the shell will be considerably lower than at the centre of the digester in the winter time. However, it is common to mount the digester in-house in areas that have cold winters. The operational problems due to inappropriate radial displacement, caused by the liquor circulations, are commonly more serious. Results by Horng, Mackie and Ticky (1987) indicate that deficient performance in continuous digesters (defined as the ratio of the tear index at a selected tensile breaking length of mill pulp to that of laboratory pulp) is mainly a consequence of low liquor recirculation flow rate. This results in non-uniform pulping. In our model, the energy flow from the liquor circulations is a function of the circulation flow rate. Hence, such non-uniform pulping may be predicted.

6. The interphase heat of conduction and that through the digester shell can be expressed by a constant coefficient times respectively the temperature difference between the phases, and between the respective phase and the ambient temperature.

   Comments: This is a common way to express such conduction terms, see e.g. Bird et al. (1960). The heat transfer coefficients are dependent on temperature. Especially the temperature dependency of the heat conduction coefficient for the liquor is known, see e.g. Ineropera and De Witt (1990). However, our simulation results indicate that this heat of conduction term is small compared to the convection term which is dominant for the energy balances, see Sec. 5.1. Hence, this dependency will not be considered. Such data for the other parameters are not found in the literature. Hence, we assume these as being constant.

7. The screen switching does not influence the mass temperature.

   Comments: Zhong et al. (1990) indicates that cyclic oscillations in the cooking temperature may be an effect from screen switching. However, this may be regarded as a heat exchanger control problem (possibly by using a periodic heat exchanger temperature at steady-state).

3.2.3 Quality measures

The pulp quality is described by the Kappa number, the concentration of entrapped dissolved solids in the blow pulp, and the concentration of effective alkali in the black liquor (the extraction flow). These variables are defined in Sec. 3.3.2.

Comments: In Sec. 1.2.3, an explanation is given why these are quality measures. Note that the actual pulp quality variables, which are discussed in Sec. 1.2.3, require information about how they can be described mathematically, and their dependencies of the basic pulping variables (like temperature, alkali etc.). As an example, Nelson and Irvine (1992) report results on a study of the dependency between the tearing resistance and pulp yield where this varies only with effective alkali. This is an empiric description of these relations. As we have not found any more detailed mathematical description of these measures in the literature, and as this is not a study about pulp quality as such, we do not discuss this further.

3.2.4 Other constraints

1. The model error caused by the boundary conditions for the PDEs does not aggravate the accuracy of the solution too much.

   Comments: These are further described in the respective subsections, and includes valve characteristics, bottom scraper model and ODEs for chip and liquor densities, -velocities and -levels. See also Appendix F. It is likely that these descriptions only affect the gains (preferentially with right signs) in the model. Dependent on the use of the model, this may be defended.

2. The process manipulators have no dynamics.

   Comments: Typically, e.g. valves and electrical actuators are fast compared to the most dominating dynamics in the process. Hence, this assumption is valid.

3. The chosen numerical methods, discretization errors, and numerical fitting at the boundaries give a stable solution with proper accuracy.

   Comments: Established numerical methods are used in the solution, see Ch. 4. Even though the resulting system of differential and algebraic equations is a nonlinear DAE (see Sec. 4.3), the system is "kind", that is, there are probably no bifurcation points etc. that do not make the solution unique.

3.3 Definition of basic and derived variables

In this section, the basic volumetric, mass, density, pressure, velocity and temperature variables, as well as some well-established derived variables, are defined and stated. These are used in the model development. As a fundament, the concept of *porosity* in this context is first discussed.

3.3.1 Porosity

This study concerns flow through a porous medium. Porosity is a fundamental concept encountered in many branches of engineering and science, e.g. ground water hydrology, reservoir engineering, soil mechanics and chemical engineering as in this study. A thorough discussion of this topic can be found in Bear (1972), and based of this work, it is reasonable to state some definitions and characteristics of porous media.

Characteristics of a porous medium:

1. *A portion of a space is occupied by a heterogeneous (or multiphase) matter. At least one of the phases comprising this matter is not solid. They may be gaseous and/or liquid phases. The solid phase is called the* **solid matrix**. *That space within the porous medium domain that is not part of the solid matrix is referred to as* **void space** *(or* **pore space***).*
2. *The solid phase should be distributed throughout the porous medium within the domain occupied by a porous medium; solid must be present inside each representative elementary volume (c.f. Appendix A). An essential characteristic is that the specific surface (the total interstitial surface area of the pores per unit bulk volume of the porous medium) of the solid matrix is relatively high. In many aspects, this characteristic dictates the behaviour of fluids in porous media. Another basic feature is that the various openings comprising the void space are relatively narrow.*
3. *At least some of the pores comprising the void space should be interconnected. The interconnected pore space is termed effective pore space. As far as flow through porous media is concerned, unconnected pores may be considered as part of the solid matrix. Certain portions of the interconnected pore space may also be ineffective as far as flow through porous media is concerned. For example, pores may be dead-end pores or blind pores.*

In the digester, the chips comprise the solid matrix, while the void space is filled with the free liquor. It is normally hard or hopeless to define the geometry of the solid surfaces, which act as boundaries to the flow in the void space. This is because the size of the chips, their geometry, and their inter-constellation vary unpredictably. However, there are no practical reasons for determining this geometry. Hence, the *continuum approach* is used as a tool for handling phenomena in porous media. The continuum approach is an averaging procedure where the porous medium (or the *bulk medium*) is viewed at a macroscopic level.

In Appendix A, a definition of volumetric porosity is given. The definition is based on this averaging procedure and states that the porosity, ϵ, is a continuous characteristic around a mathematical point given by the relation between the volume of the void space, V_{void}, and a *representative elementary volume (REV)* around this point, V_{REV} (bulk volume), i.e. volume fraction of void space:

$$\epsilon = V_{void}/V_{REV} \tag{3.7}$$

Porosity is, in a sense, equivalent to *density* (mass per unit volume). When considering the volume fraction of chips, this can be visualized as the *bulk density of chips*, and expresses how much the chips *are* compressed absolutely. Thus, based on the continuum approach, the chips inside the digester are assumed to be even distributed such that they are all in contact, i.e. no chip is flowing freely. This means no channelling. Further, because they are not physically inter-connected, no dead-end pores and unconnected pores exist, i.e. all the void space is free for liquor flow.
Thus, by introducing the concept of porosity and the definition of REV, the digester mass is replaced by a fictitious continuum in which we may assign values of any property to any mathematical point in it.

In the model derivation, we use the fact that area porosity equals volume porosity (see Appendix A). According to assumption 4 in Sec. 3.2.1, we assume that the chip bed (the collection of individual chips) is regarded as a continuous medium. We denote this as the *distributed volume model*. Note that the sum of the surfaces of the individual chips is much greater than the area fraction of chips of the outer surface of a volume occupied by the porous medium. We denote this as the *collected volume model*. However, we use friction forces that are experimentally found for a representative portion of chips. Hence, the geometric dependency is implicitly included in these terms. The distributed volume model is used in the density descriptions, while the collected volume model is used in the application of Gauss' theorem in the derivation of the balance equations. In the application of this theorem (also called the divergence theorem), see e.g. Edwards and Penny (1986), a *closed* piecewise smooth surface bounding the space region in question (e.g. an REV) is assumed. However, the definition of the area porosity, as given in Appendix A, is related to a plane through the mathematical point P, whose normal is in any direction, i.e. an *open* surface. The following illustration shows how this definition is adapted to our collected volume model that require a closed surface in Gauss' theorem.

Given an REV, having the shape of a cube (for simplicity of this illustration). The REV has a mathematical point P as the centre, porosity $n(P)$, and outer closed surface with area $A_{REV,closed}$. The void space has an **open** *outer surface with area $A_{v,open}$ as a part of the outer closed surface of the REV. Consider a plane with area A_j through P, whose normal is in the direction of the unit vector* $\mathbf{1j}$*. Then, by Eq. (A.4), $(n_A)_j(P) = n(P)$. Since $n(P)$ is independent of direction (see Appendix A), this is valid on any of the six outer (open) surfaces of the REV, i.e.*

$$A_{v,i} = n(P) \cdot A_{REV,i}, \quad i = 1, .., 6$$

where $\sum_{i=1}^{6} A_{REV,i} = A_{REV,closed}$. *This gives:*

$$A_{v,open} = \sum_{i=1}^{6} n(P) \cdot A_{REV,i} = n(P) A_{REV,closed} \tag{3.8}$$

Now, assume that the void space is collected in a bounded volume inside the REV, having a **closed** *outer surface with area* $A_{v,closed} = A_{v,open}$. *This is our collected volume model, and we have:*

$$A_{v,closed} = n(P) A_{REV,closed} \tag{3.9}$$

Of course, this is valid for any shape of the REV. Further, the same line of arguments is valid for the solid material as porosity is the same as volume fraction, and volume fraction of solids $= 1-$ *volume fraction of void space.*
□

Hence, there is no conflict between these "models". This corresponds well to the fact that no assumptions are made about the individual chip surface.

What makes the digester mass special, compared to other applications of porous media, is that the solid matrix is a moving bed rather than a stationary one (like in oil reservoirs).

3.3.2 Volumetric, mass and density variables

Inside the digester (see Fig. 3.4), chips have volume fraction related to a representative elementary volume of mass given by:

$$\epsilon_c = V_c / V_{REV} \tag{3.10}$$

The interstitial void space between the chips is filled with steam above the liquor level, and free liquor, below. The volume fraction of this liquor related to the mass is given by:

$$\epsilon_l = V_{fl} / V_{REV} \tag{3.11}$$

i.e. the porosity of the mass. Hence, we have the relation:

$$\epsilon_c + \epsilon_l = 1 \tag{3.12}$$

A wood chip consists of solid materials (soluble and insoluble) with volume V_{sm}, and due to its porosity, entrapped liquor and air with volume V_p. Before the chips enter the high pressure system, the natural moisture content comprises the entrapped liquor, and the air content is considerable. When the chips come in contact with the liquor in the entrance to the high pressure system, some (or all) of the air space is replaced by cooking liquor. The volume fractions of solid material and pore space in a wood chip are defined by:

$$\epsilon_{sm} = V_{sm} / V_{ODW} \tag{3.13}$$

$$\epsilon_p = V_p / V_{ODW} \tag{3.14}$$

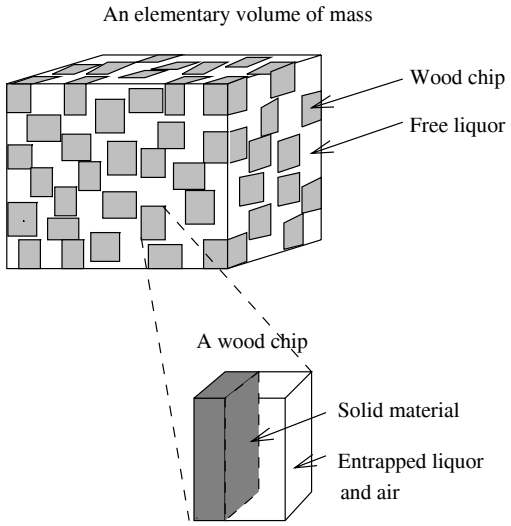

Figure 3.4: The conceptual model of the mass in the digester.

where V_{ODW} is the volume of one single oven-dry wood (ODW) chip, c.f. assumption 2 in Sec. 3.2.1. The consequence of this assumption gives the following relation for the total volume of chips in an elementary volume of mass:

$$V_c = n_c \cdot V_{ODW} \tag{3.15}$$

where n_c is the number of chips in the volume. Since $V_{sm} + V_p = V_{ODW}$, we have:

$$\epsilon_{sm} + \epsilon_p = 1 \tag{3.16}$$

The pore space consists of entrapped liquor and air. We define their volume fractions relative to the chip volume as:

$$\epsilon_{el} = \frac{V_{el}}{V_{ODW}} \tag{3.17}$$

$$\epsilon_{air} = \frac{V_{air}}{V_{ODW}} \tag{3.18}$$

such that:

$$\epsilon_{el} + \epsilon_{air} = \epsilon_p \tag{3.19}$$

Penetration of liquor into the chips is defined as the fraction of the pore space, V_p, which is filled with entrapped liquor:

$$P = \frac{V_{el}}{V_p} = \frac{\epsilon_{el}}{\epsilon_p} \tag{3.20}$$

Total penetration means $P = 1$. In this study we assume that $0 \leq P \leq 1$. $P < 1$ means that the penetration is incomplete, i.e. air is remained in the chips.

As "density (or concentration) variables" for the lignin and the carbohydrates, we use mass fractions. They are defined as:

$$\alpha_{lig} = m_{lig}/m_{ODW} \tag{3.21}$$
$$\alpha_{carb} = m_{carb}/m_{ODW} \tag{3.22}$$

where m_{lig} is the mass of lignin and m_{carb} is the mass of carbohydrates in one single chip. m_{ODW} is the mass of the solid content in an uncooked chip (c.f. assumption 2 in Sec. 3.2.1). This is a convention which is often used as density description of mass components in solutions (Johnsson, 1971), (Smith and Williams, 1974).

The volume fractions of lignin and carbohydrates related to the chip volume are:

$$\epsilon_{lig} = V_{lig}/V_{ODW} \tag{3.23}$$
$$\epsilon_{carb} = V_{carb}/V_{ODW} \tag{3.24}$$

which gives:

$$\epsilon_{lig} + \epsilon_{carb} = \frac{V_{sm}}{V_{ODW}} = \epsilon_{sm} \tag{3.25}$$

By this, the densities of lignin and carbohydrates in a wood chip are expressed as:

$$\rho_{lig,chip} = \frac{m_{lig}}{V_{ODW}} = \frac{V_{lig}}{V_{ODW}}\frac{m_{lig}}{V_{lig}} = \epsilon_{lig}\rho_{lig} \tag{3.26}$$
$$\rho_{carb,chip} = \frac{m_{carb}}{V_{ODW}} = \frac{V_{carb}}{V_{ODW}}\frac{m_{carb}}{V_{carb}} = \epsilon_{carb}\rho_{carb} \tag{3.27}$$

ρ_{lig} and ρ_{carb} are the *specific weights* of lignin and carbohydrates. Further, we have:

$$\rho_{lig,chip} = \frac{m_{lig}}{V_{ODW}} = \frac{m_{lig}}{m_{ODW}}\frac{m_{ODW}}{V_{ODW}} = \alpha_{lig}\rho_{ODW} \tag{3.28}$$
$$\rho_{carb,chip} = \frac{m_{carb}}{V_{ODW}} = \frac{m_{carb}}{m_{ODW}}\frac{m_{ODW}}{V_{ODW}} = \alpha_{carb}\rho_{ODW} \tag{3.29}$$

Eqs. (3.26)-(3.29) give:

$$\epsilon_{lig} + \epsilon_{carb} = (\frac{\alpha_{lig}}{\rho_{lig}} + \frac{\alpha_{carb}}{\rho_{carb}})\rho_{ODW} \tag{3.30}$$

i.e by Eqs. (3.16) and (3.25)

$$\epsilon_p = 1 - (\frac{\alpha_{lig}}{\rho_{lig}} + \frac{\alpha_{carb}}{\rho_{carb}})\rho_{ODW} \tag{3.31}$$

As density variables for the entrapped alkali, dissolved solids and water, we define (see e.g. Smith and Williams (1974)): [2]

$$\rho_{EA,el} = \frac{m_{EA,el}}{V_{ODW}} \tag{3.32}$$

[2] It may be more natural to relate the densities of the entrapped liquor components to the volume of entrapped liquor since this is the volume which covers these components. However, if this is to be modelled in more detail, the model becomes fairly complex as we consider a time variating volume which depends on both the chemical reactions and the temperature explicitly.

$$\rho_{ds,el} = \frac{m_{ds,el}}{V_{ODW}} \tag{3.33}$$

$$\rho_{w,el} = \frac{m_{w,el}}{V_{ODW}} \tag{3.34}$$

These are hereafter referred to as *concentrations*, in contradiction to *density* which is used to describe e.g. the "density of a chip", i.e. the weight of a chip divided by its volume, V_{ODW}.
The volume fractions of alkali, dissolved solids and water relative to the chip volume are defined as:

$$\epsilon_{EA,el} = \frac{V_{EA,el}}{V_{ODW}} \tag{3.35}$$

$$\epsilon_{ds,el} = \frac{V_{ds,el}}{V_{ODW}} \tag{3.36}$$

$$\epsilon_{w,el} = \frac{V_{w,el}}{V_{ODW}} \tag{3.37}$$

Further, we have that $\rho_{EA,el} = (V_{EA,el}/V_{ODW})(m_{EA,el}/V_{EA,el}) = \epsilon_{EA,el}\rho_{EA} =$ where $\rho_{EA} = m_{EA,el}/V_{EA,el}$ is the specific weight of effective alkali. This gives:

$$\epsilon_{EA,el} = \frac{\rho_{EA,el}}{\rho_{EA}} \tag{3.38}$$

Equivalently, $\rho_{ds,el} = \epsilon_{ds,el}\rho_{ds}$ where $\rho_{ds} = m_{ds,el}/V_{ds,el}$ is the specific weight of dissolved solids. This gives:

$$\epsilon_{ds,el} = \frac{\rho_{ds,el}}{\rho_{ds}} \tag{3.39}$$

V_{air} is the part of the entrapped air which is dry. This means that when the entrapped air is humid, we only consider the dry part as air, and regard the moisture as a part of the entrapped liquor.
At atmospheric pressure $p_{atm} = 1.01325 \cdot 10^5 Pa$ and temperature $T_{atm} = 20^oC = 293.16K$, we define the volume fraction of air relative to the chip volume as:

$$\epsilon_{air,atm} = \frac{V_{air,atm}}{V_{ODW}} \tag{3.40}$$

As we consider the dry air as an ideal gas, we have the equation of state:

$$n_{air} = p_{atm}V_{air,atm}/(RT_{atm}) = 41.57V_{ODW}\epsilon_{air,atm}[mol] \tag{3.41}$$

In the digester, $V_{air} = n_{air}R(T_c + 273.2)/p_l$ such that:

$$\begin{aligned} \epsilon_{air} = \frac{V_{air}}{V_{ODW}} &= 41.57\epsilon_{air,atm}R(T_c + 273.2)/p_l \\ &= 345.63\epsilon_{air,atm}(T_c + 273.2)/p_l \end{aligned} \tag{3.42}$$

Further, the concentration of air relative to the chip volume is constant, as we assume that no air escapes from the chips in the digester (assumption 7 in Sec. 3.2.1):

$$\rho_{air} = \frac{m_{air}}{V_{ODW}} = \frac{n_{air}M_{air}}{V_{ODW}} = 1.2\epsilon_{air,atm} \tag{3.43}$$

where M_{air} is the molar weight of air. By using the equivalence:

$$\epsilon_{EA,el} + \epsilon_{ds,el} + \epsilon_{w,el} + \epsilon_{air} = \epsilon_p \tag{3.44}$$

and (c.f. Eqs. (3.38) and (3.39)):

$$\rho_{w,el} = \rho_w \epsilon_{w,el} \tag{3.45}$$

where $\rho_w = m_{w,el}/V_{w,el}$ is the specific weight of water, we have according to assumption 8 in Sec. 3.2.1:

$$\rho_{w,el} = \rho_w[\epsilon_p - \frac{\rho_{EA,el}}{\rho_{EA}} - \frac{\rho_{ds,el}}{\rho_{ds}} - 345.63\epsilon_{air,atm}(T_c + 273.2)/p_l] \tag{3.46}$$

Equivalently as for the entrapped liquor, we define for the free liquor: [3]

$$\rho_{EA,fl} = \frac{m_{EA,fl}}{V_{fl}} \tag{3.47}$$

$$\rho_{ds,fl} = \frac{m_{ds,fl}}{V_{fl}} \tag{3.48}$$

$$\rho_{w,fl} = \frac{m_{w,fl}}{V_{fl}} \tag{3.49}$$

By using:

$$\epsilon_{EA,fl} = \frac{V_{EA,fl}}{V_{fl}} = \frac{\rho_{EA,fl}}{\rho_{EA}} \tag{3.50}$$

$$\epsilon_{ds,fl} = \frac{V_{ds,fl}}{V_{fl}} = \frac{\rho_{ds,fl}}{\rho_{ds}} \tag{3.51}$$

$$\epsilon_{w,fl} = \frac{V_{w,fl}}{V_{fl}} = \frac{\rho_{w,fl}}{\rho_w} \tag{3.52}$$

and the equivalence:

$$\epsilon_{EA,fl} + \epsilon_{ds,fl} + \epsilon_{w,fl} = 1 \tag{3.53}$$

we derive similar to Eq. (3.46):

$$\rho_{w,fl} = \rho_w \epsilon_{w,fl} = \rho_w(1 - \frac{\rho_{EA,fl}}{\rho_{EA}} - \frac{\rho_{ds,fl}}{\rho_{ds}}) \tag{3.54}$$

Based on these relationships, the concentrations (related to an elementary volume of mass) of lignin, carbohydrates, entrapped alkali, -dissolved solids, -water and -air, free alkali, -dissolved solids and -water, can be expressed as:

$$\rho_{lig,mass} = n_c \frac{m_{lig}}{V_{REV}} = \frac{m_{lig}}{m_{ODW}} \frac{m_{ODW}}{V_{ODW}} \frac{V_{ODW}}{V_{REV}} n_c = \alpha_{lig} \rho_{ODW} \epsilon_c \tag{3.55}$$

[3] Note that these density variables express mass related to a time variating volume, V_{fl}. However, as we show in Sec. 3.5.1, the dynamics in the component balances and the dynamics related to this volume variation can be separated. Hence, this variation have no influence on these concentrations.

$$\rho_{carb,mass} = n_c \frac{m_{carb}}{V_{REV}} = \frac{m_{carb}}{m_{ODW}} \frac{m_{ODW}}{V_{ODW}} \frac{V_{ODW}}{V_{REV}} n_c = \alpha_{carb} \rho_{ODW} \epsilon_c \quad (3.56)$$

$$\rho_{EA,el,mass} = n_c \frac{m_{EA,el}}{V_{REV}} = \frac{m_{EA,el}}{V_{ODW}} \frac{V_{ODW}}{V_{REV}} n_c = \rho_{EA,el} \epsilon_c \quad (3.57)$$

$$\rho_{ds,el,mass} = n_c \frac{m_{ds,el}}{V_{REV}} = \frac{m_{ds,el}}{V_{ODW}} \frac{V_{ODW}}{V_{REV}} n_c = \rho_{ds,el} \epsilon_c \quad (3.58)$$

$$\rho_{w,chip,mass} = n_c \frac{m_{w,el}}{V_{REV}} = \frac{m_{w,el}}{V_{ODW}} \frac{V_{ODW}}{V_{REV}} n_c = \rho_{w,el} \epsilon_c \quad (3.59)$$

$$\rho_{air,c,mass} = n_c \frac{m_{air}}{V_{REV}} = \frac{m_{air}}{V_{ODW}} \frac{V_{ODW}}{V_{REV}} n_c = \rho_{air} \epsilon_c \quad (3.60)$$

$$\rho_{EA,fl,mass} = \frac{m_{EA,fl}}{V_{REV}} = \frac{m_{EA,fl}}{V_{fl}} \frac{V_{fl}}{V_{REV}} = \rho_{EA,fl} \epsilon_l \quad (3.61)$$

$$\rho_{ds,fl,mass} = \frac{m_{ds,fl}}{V_{REV}} = \frac{m_{ds,fl}}{V_{fl}} \frac{V_{fl}}{V_{REV}} = \rho_{ds,fl} \epsilon_l \quad (3.62)$$

$$\rho_{w,fl,mass} = \frac{m_{w,fl}}{V_{REV}} = \frac{m_{w,fl}}{V_{fl}} \frac{V_{fl}}{V_{REV}} = \rho_{w,fl} \epsilon_l \quad (3.63)$$

The density of a wood chip is:

$$\rho_c = m_{chip}/V_{ODW} = (\alpha_{lig} + \alpha_{carb})\rho_{ODW} + \rho_{EA,el} + \rho_{ds,el} + \rho_{w,el} + \rho_{air} \quad (3.64)$$

the density of the free liquor is:

$$\rho_l = m_{liq}/V_{fl} = \rho_{EA,fl} + \rho_{ds,fl} + \rho_{w,fl} \quad (3.65)$$

and the density of the bulk mass is: [4]

$$\rho_{mass} = n \cdot m_{chip}/V_{REV} + m_{liq}/V_{REV} = \rho_c \epsilon_c + \rho_l \epsilon_l \quad (3.66)$$

A remark about the conceptual model

We have made four assumptions as to assure that no mass disappears in the derivation of the model.

- During the chemical reactions V_{sm} is reduced and V_{el} is increased equivalently to maintain a constant chip volume according to our conceptual model of a wood chip (c.f. assumption 2 in Sec. 3.2.1). Then, α_{lig} and α_{carb} are reduced.
- As commented to assumption 4 about chemical reactions in Sec. 3.2.2, the alkali reacts with the resulting acids from both the lignin and the carbohydrates, and thus are eventually entrapped to both the solid material and the dissolved solids. For simplicity, we assumed that only the neutralization of the dissolved solids occur. Thus, the consumption of alkali results in mass increase in the dissolved solids. Moreover, $\rho_{EA,el}$ is reduced due to the consumption of the alkali.

[4] Note that when the volume of a wood chip in the feed to the digester (uncooked chip) differs from that of an oven-dry wood chip V_{ODW}, ρ_{ODW} has to be replaced by $\alpha_c \rho_{uc}$ where $\alpha_c = m_{ODW}/m_{uc}$, $\rho_{uc} = m_{uc}/V_{uc}$. m_{uc} and V_{uc} are respective the mass and the volume of a representative uncooked chip, c.f. assumption 2 in Sec. 3.2.1.

- The volume reduction of the dissolved solids because of the recombination of the solid structures in the dissolution process, is omitted (assumption 5 about chemical reactions in Sec. 3.2.2). This means that $m_{ds,el}$ and $V_{ds,el}$ are increased equivalently in a percentage. Thus, $\rho_{ds,el}$ is increased both because of the mass reduction in the solids and because of the mass reduction in the alkali during the neutralization process. As argued, even though this mechanism actually reduces $V_{ds,el}$, the mass of the dissolved solids is maintained. If this volume reduction is to be included in the mass balance of the dissolved solids, this also has to be included in the mass balance of the other components in the entrapped and free liquor, to keep the chip volume constant. We simplify by omitting this mechanism.

- In the mass transfer process between the entrapped and the free liquor, the alkali, dissolved solids and air are replaced by an equal volume amount of water, also to maintain a constant chip volume in our conceptual model of a wood chip (c.f. Eqs. (3.46) and (3.54) and assumption 8 in Sec. 3.2.1).

Fig. 3.5 shows three different ways of considering the volume distribution inside a wood chip where b) is the one which is used in this study. Case c) corresponds to the second item above. Case a) is used in the Purdue-models (Smith and Williams, 1974), (Christensen et al., 1982), and is a simplification which is convenient to use when the water balance is not considered. In our model, the density of the chips and the free liquor are computed. Hence, we have to compute the water content. Even though this influences the main driving force for the chip plug, which is the gravity, simplifications may be defended. This is further discussed in Ch. 7.

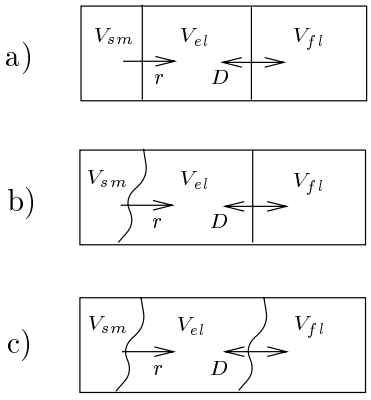

Figure 3.5: Three different ways of considering the volume distribution of solid material, entrapped liquor, and free liquor inside a wood chip. a) is what is used in the Purdue-models, b) is what is used in this study, and c) is the case where the chip volume varies due to the diffusion process. r denotes the chemical reactions, and D denotes the interphase diffusion.

3.3.3 Pressure variables

Liquor pressure, p_l

This is defined simply as the hydrostatic pressure in the free liquor. Physically, it is a statistical concept that is only valid when a large number of molecules is involved. It is defined as the average of the forces between the liquor molecules, F_l, over a reference area, divided by that area (see e.g. Alonso and Finn (1983)). This area, A_l, covers only the space occupied by the liquor (pore space). It is a plane whose normal is in the direction of the force F_l (area porosity). In this way, $p_l = F_l/A_l$. This pressure is defined as *pore pressure*. [5] In this study, it is simply referred to as pressure.
Because the liquor is assumed to be incompressible, no equation of state (giving the liquor density as a function of the pressure) is defined for this phase.

Chip pressure, p_c

Similar as the definition of the liquor pressure, the chip pressure (or chip bed pressure) is defined as the mean value of the contact forces between the chips over a reference area, divided by that area (Härkönen, 1984). The contact forces between the chips are usually referred to as *inter-particle stresses* (or here *inter-chip stresses*) in the porous matrix (Bear, 1972). This is discussed further in Sec. 3.4.1.
However, unlike in the case of the liquor pressure, the reference area is chosen as a representative reference area (REA), c.f. Sec. 3.4.1, i.e. an area occupied by the both phases. This has two reasons. First, the chip pressure acts only between the chips, and not on the surrounding liquor. The counter force from the chips on the liquor is of course equal to the hydrostatic liquor force. Generally, the liquor pressure deviates from the chip pressure. In this context, we regard the chip bed as a collection of individual chips. This leads us to the nature of the *compressibility* of the chip bed, and is discussed in the Sec. 3.4.2.
The second reason is that we use the results by Härkönen (1987), where the volume fraction of liquor has been measured as a function of the chip pressure (defined evenly distributed over the REA), and the Kappa number:

$$\epsilon_l = 0.644 + (\frac{p_c}{10^4})^{0.59}(-0.831 + 0.139ln(\kappa)) \tag{3.67}$$

Härkönen found this from regression analysis of experimental laboratory data. However, in this study, this equation is solved for the chip pressure, Eq. (3.6):

$$p_c = 10^4(\frac{\epsilon_c - 0.356}{0.831 - 0.139ln(\kappa)})^{1.695}$$

This is the compressibility equation, or equation of state, for the chip plug. It is shown in two- and three-dimensional plots in Fig. 3.6.

[5] The term *pore pressure* is sometimes referred to the averaging over an REV of the medium, with the argument "as only such average pressure is measurable. This means that measuring pressure in the medium, the instrument should be large enough to "see" the volume over which such an average is taken" (Bear, 1972). Note that it is actually the force, F_l, which is given by the pressure, p_l, times the area, A_l, as it is the pressure which is the basic variable. Hence, the definitions express the same.

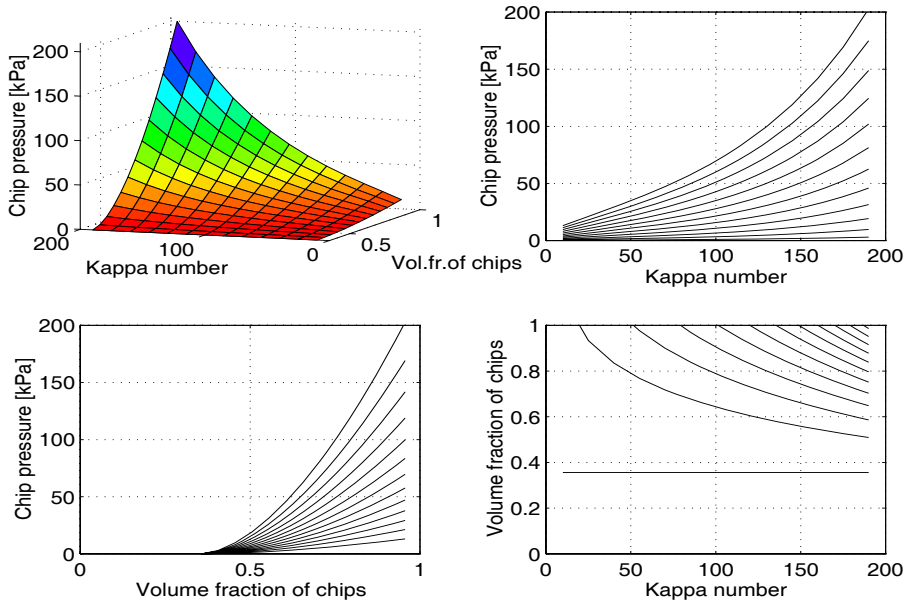

Figure 3.6: Two- and three-dimensional plots of the compressibility equation

It appears from the figure that at reduced Kappa numbers:

- the compaction increases at the same chip pressure
- the chip pressure decreases at the same compaction

The combined effect of the Kappa number and the compaction on the chip pressure is discussed in Secs. 5.2 and 5.3. Note that this equation is only valid for $\epsilon_c \in [0.356, 1.0]$, which means that for lower chip volume amount than 35.6%, the chips do not make any force against each other that will contribute to their movement. In this case, the pieces of chips will freely float in the liquor. This corresponds to the percentage of chips "in a bucket", i.e. free uncompressed volume fraction of chips, and is therefore also used as a basis for calculating the volume fraction of chips in the top section of the digester (see Eq. (3.145)). It should be noted that the value 0.356 is specific to the laboratory test conditions where this result was found, c.f. the comments at page 56. Härkönen made several tests, and the results in Härkönen (1987) differ from those in Härkönen (1984). In this earlier work, the lower limit is found to be 0.347. The different results are probably partly due to different test arrangements, and partly because of different chip qualities (Härkönen, 1994). However, Härkönen's results indicate that the factor seems to be in the range $0.35 - 0.36$ independent of the chip quality (Härkönen, 1994).
Note further that the equation relates the compaction to the chip pressure at different degrees of cooking, i.e. the Kappa number. The physical interpretation of this is that the chips become softer during the cook due to increased porosity inside them. Then they change their shape, rather than their volume (c.f. assumption 2 in Sec. 3.2.1). Thus, the chips conform more, and they are packed more tightly. The softening mechanism is described by reduced chip pressure. This is further

discussed in Sec. 3.5.1. In Appendix H, the *local velocity of sound* for the chip plug is discussed.

3.3.4 Velocity variables

The following definitions are based on established terms, see e.g. Bird et al. (1960). The chips form a continuous structure known as the chip plug. Even though the shape of either the chip plug or the free liquor is clearly defined, their convective velocities may be defined simply as the mean velocity of the respective phase at a mathematical point. The assumption of no cross sectional variations, gives mean values for the velocities over the cross section. The *phase velocity* for the free liquor in this study is defined as what is often called *interstitial velocity*, which is the average flow velocity in the cross section available for flow of liquor; v_l. Equivalently, the phase velocity for the chip plug is defined as the average flow velocity in the cross section available for flow (or better movement) of chips; v_c.

The mass flow of chips and liquor (kg/s) is stated by Dupuit's assumption (Dupuit, 1863):

$$q_i^m = \rho_i \epsilon_i A v_i \tag{3.68}$$

$i = c, l$. Here, $\epsilon_i A$ is the part of the total cross section available for flow of phase i. Hence, the volume flow of chips and liquor (m^3/s) is defined as:

$$q_i = \epsilon_i A v_i \tag{3.69}$$

This is often written as:

$$q_i = A v_{0,i} \tag{3.70}$$

where $v_{0,i} = \epsilon_i v_i$ is referred to as *superficial velocity*, and is the average linear velocity the phase would have in the column if the other phase were not present, i.e. referred to the total cross-section area.

In a distributed flow system, the average velocity is generally given by:

$$v = \frac{1}{\rho} \sum_i \rho_i v_i \tag{3.71}$$

where the summation covers all the components in the bulk flow. ρ_i is the density of the different components and ρ is the bulk mass density such that $\sum_i \rho_i = \rho$. v_i are the velocities of the separate components, and we can write:

$$\rho_i v_i = \rho_i v + j_i \tag{3.72}$$

where j_i is mass flux of diffusion for component i. Hence, j_i is the deviation from the average velocity. In this study, we define:

$$\rho_i \epsilon_i v_{i,j} = \rho_i \epsilon_i v_i + j_j \tag{3.73}$$

where j_j is composed of one vertical directed (z), and one interphase diffusive (γ) term; $j_j = j_z + j_\gamma$. The former gives the dispersive term (c.f. Fick's law for diffusion in Appendix B):

$$\begin{aligned} j_z &= -D_i \frac{\partial(\rho_i \epsilon_i)}{\partial z} \\ &\Downarrow \\ \frac{\partial j_z}{\partial z} &= -D_i \frac{\partial^2(\rho_i \epsilon_i)}{\partial z^2} \end{aligned} \tag{3.74}$$

when D_c is not a function of z (assumption 1 on page 52). The second term gives the interphase diffusion:

$$j_\gamma = \epsilon_i \rho_i v_{i,\gamma} \tag{3.75}$$

where we define:

$$\begin{aligned} \frac{\partial j_\gamma}{\partial \gamma} &\triangleq D_{EA}(\rho_{EA,el} - \rho_{EA,fl}) + D_{ds}(\rho_{ds,el} - \rho_{ds,fl}) \\ &= \Delta(D\rho) \end{aligned} \tag{3.76}$$

which expresses the net mass transfer from the chips to the free liquor.

3.3.5 Temperature variables

The phase temperatures, which are explicit expressions for the respective energies, are defined in a similar way as for the velocity variables.

3.3.6 Some well-established derived variables

Kappa number and yield

The Kappa number is related to the foregoing definitions by:

$$\kappa = (\%(\alpha_{lig}/(\alpha_{lig} + \alpha_{carb})))/c_\kappa \tag{3.77}$$

It is defined in Rydholm (1967). The factor c_κ varies in the literature. According to Christensen et al. (1982) it is 0.153, according to Koch Christensen (1991) it is $1/7 \approx 0.14$, and Smith and Williams (1974) who refers Rydholm (1967) uses the factor 0.13. [6] The yield is expressed as:

$$Y = \%(\alpha_{lig} + \alpha_{carb}) \tag{3.78}$$

[6] This factor is somewhat higher for sulphite pulp.

Compaction

The compaction (or packing) of chips is normally defined as the relationship between the weight of dry wood per m^3 in the digester and in the feed (KAMYR, 1971):

$$p = \frac{\epsilon_c \rho_{ODW}(\alpha_{lig} + \alpha_{carb})}{\epsilon_{c,feed}\rho_{ODW}(\alpha_{lig,feed} + \alpha_{carb,feed})} \tag{3.79}$$

We may also define compaction as an expression of how much the chips inside the digester *have been* compressed relative to the feed (c.f. the discussion about the bulk density of chips, ϵ_c, in Sec. 3.3.1). Hence, we may use this simpler definition:

$$p = \epsilon_c / \epsilon_{c,feed} \tag{3.80}$$

We use this expression in the calculations in this thesis. However, as $\epsilon_{c,feed}$ may be regarded as being constant (or an input variable), we see that ϵ_c itself is a measure of compaction.

Consistency

Consistency is defined as the relation between the weight of dry solid wood (i.e. the weight of unsolved lignin and carbohydrates) and the total weight of mass (SCAN, 1964):

$$\begin{aligned} c &= \frac{n_c \cdot m_{lig} + n_c \cdot m_{carb}}{m_{mass}} = n_c \frac{m_{lig}}{m_{ODW}} \frac{m_{ODW}}{m_{mass}} + n_c \frac{m_{carb}}{m_{ODW}} \frac{m_{ODW}}{m_{mass}} \\ &= (\alpha_{lig} + \alpha_{carb}) n_c \frac{m_{ODW}}{V_{ODW}} \frac{V_{ODW}}{V_{REV}} \\ &= \frac{\alpha_{lig} + \alpha_{carb}}{\rho_{mass}} \rho_{ODW} \epsilon_c \end{aligned} \tag{3.81}$$

with dimension kg fibre per kg mass. We may also define a consistency measure based on volume (*volume consistency*), i.e. the relation between the volume of dry solid wood and the total volume of mass:

$$\begin{aligned} c' &= \frac{n_c \cdot V_{lig} + n_c \cdot V_{carb}}{V_{REV}} = n_c \frac{V_{sm}}{V_{ODW}} \frac{V_{ODW}}{V_{REV}} = \epsilon_{sm} \epsilon_c \\ &= (\frac{\alpha_{lig}}{\rho_{lig}} + \frac{\alpha_{carb}}{\rho_{carb}}) \rho_{ODW} \epsilon_c \end{aligned} \tag{3.82}$$

with dimension m^3 fibre per m^3 mass.

Chemical oxygen demand (COD)

The oxygen demand of the final pulp is often used as a measurement of the residual content of dissolved solids in the pulp. It is a direct measure of the wash efficiency. The residual content should be as low as possible, as it is desirable to remove most of the reaction products.
The test is one out of several oxygen depletion tests for measurement of pollution. Table 3.1 shows some of them.

Table 3.1: Oxygen depletion tests (from Smook (1989))

Chip meter speed

The wood chips are fed from a surge bin through a volumetric chip meter into the cooking system. Thus, the chip feed is measured as the rotation speed of the chip meter. Hence, it is convenient to calculate the feed flow to the digester in terms of this as well, although there is a time delay (and other dynamics) between the actuator and the inlet to the digester that we do not model in this study.
The calculation is based on empiric knowledge about the volume fraction of chips in the chip meter (the filling factor), and the relation between the rotation speed and the volume flow through the chip meter. According to Eq. (3.69) we have:

$$\begin{aligned} q_{c,in} &= \epsilon_{c,in} A v_{c,in} [m^3/s] \\ &= k_{rpm} \epsilon_{c,in} A v_{c,in} [rpm] \\ &= RPM \end{aligned} \tag{3.83}$$

where RPM is the chip meter speed. It should be noted that this linear relationship is only valid in the normal operating range. For higher RPM values, the filling factor decreases and hence, the relationship is nonlinear.

Liquor-to-wood ratio

External mass transfer limitation may occur when the liquor-to-wood ratio (L/W) is lower than 4.5 (assumption 3, page 56). This ratio is defined as m^3 liquor per tonne dry-content of chips (Smook, 1989). $L/W = 4.5$ is approximately the value in batch digesters and indicates the ratio between the liquor and wood content

when the pore space between the chips is totally filled with liquor. Hence, if the chip and liquor levels in a continuous digester are controlled at this L/W value, the two phases move approximately with the same velocities. If L/W is lower than 4.5, the chips move faster than the liquor. This is a desired operational condition. Related to the digester operation, the liquor-to-wood ratio is a manipulated variable for the liquor feed. Hence, according to our definitions of basic variables, we define:

$$\begin{aligned} L/W &= \frac{A(1-\epsilon_{c,in})v_{l,in}[m^3/s]}{A\epsilon_{c,in}v_{c,in}\rho_{dc,in}[kg/s]}10^3\frac{kg}{ton} \\ &= 10^3\frac{q_{l,in}}{q_{c,in}\rho_{dc,in}} \end{aligned} \tag{3.84}$$

where $\rho_{dc,in} = (\alpha_{lig,in} + \alpha_{carb,in})\rho_{ODW}$ is the dry solid content of mass in the feed to the digester, and $q_{c,in}$ has dimension $[m^3/s]$.

Dilution factor

The dilution factor is a measure of the wash water applied in excess to the amount required for total displacement, expressed as kg water per kg bone-dry pulp (BDP), (Smook, 1989). [7] Hence, this is a direct measure of the water amount being added to the liquor system, i.e to the wash zone. According to our definitions, this factor can be expressed as:

$$DF = (q^m_{fl,wash} - q^m_{el,wash})/q^m_{BDP} \tag{3.85}$$

where:

$$\begin{aligned} q^m_{fl,wash} &= \epsilon_{l,wash}v_{l,wash}A\rho_{l,wash} \\ q^m_{el,wash} &= \epsilon_{c,wash}\epsilon_{el,wash}v_{c,wash}A\rho_{el,wash} \\ q^m_{BDP} &= (\alpha_{lig} + \alpha_{carb})\rho_{ODW}\epsilon_{c,wash}v_{c,wash}A \end{aligned}$$

These are mass flows with dimension kg liquor per second. $\rho_{l,wash} = \rho_{EA,fl,wash} + \rho_{ds,fl,wash} + \rho_{w,fl,wash}$ and $\rho_{el,wash} = \rho_{EA,el,wash} + \rho_{ds,el,wash} + \rho_{w,el,wash}$.

As these variables cannot be measured in real plants, DF is often estimated as:

$$DF = (q_{C9,s} + q_{C9,b} - (q_{bf} - k_n q_{c,in})/(k_d q_{c,in}) \tag{3.86}$$

where $q_{C9,s}$ and $q_{C9,b}$ are the wash water flows through the side- and bottom nozzles, q_{bf} is total pulp outlet flow (i.e. the blow flow), $q_{c,in}$ is the chip meter speed, and k_n, k_d are empiric coefficients (Pedersen, 1983).

The term *dilution* or *excess water*, with dimension m^3 per hour, is used as well (see e.g. (Koch Christensen, 1991)). This can be expressed as:

$$\begin{aligned} EW &= q_{fl,wash} - q_{el,wash} \\ &= 3600A(\epsilon_{l,wash}v_{l,wash} - \epsilon_{c,wash}\epsilon_{el,wash}v_{c,wash}) \end{aligned} \tag{3.87}$$

[7] Bone-dry pulp (BDP) means moisture-free and is another word for oven-dry wood (ODW) in the sense dry content of the wood in general. This is not to be confused with the dry content of uncooked chips as used in this study (c.f. assumption 2 in Sec. 3.2.1.)

3.4 Model assumptions, part 2

3.4.1 The surface forces and the chip plug movement

Here, the viscous and sliding friction forces, and the pressure forces are discussed. This discussion gives a fundament to understand the background for the respective terms that are included in the momentum balances. Finally, there is a discussion of the characteristics of the movement of the chip plug.

Surface forces

The surface forces, that are the forces acting on the surface of the phases, cover pressure forces and friction forces (viscous- and sliding-, or dry, friction).

The surface forces are described by the generalized *stress tensor* $\sigma = \{\sigma_{i,j}\}$, which is a 2nd order, three-dimensional symmetrical tensor containing the *normal stresses* on the diagonal, and the *share stresses* in the off-diagonal elements. Its elements can also be written as the sum:

$$\sigma_{i,j} = -p\delta_{i,j} + P_{i,j} \tag{3.88}$$

where p is the static stress (pressure), $\delta_{i,j}$ is Kronecker δ, and $P_{i,j}$ are the elements in the viscous stress tensor. The Kronecker symbol is used because the pressure in the pore space is isotropic. The minus sign results from the fact that in general, negative normal stresses occur in a fluid, i.e. a positive stress component means tension (Bear, 1972).

In this study, we define the viscous stress tensor as the sum of the viscous friction force between the two phases and the sliding friction force against the side walls as off-diagonal elements (Ytrehus, 1987). The latter one is, however, treated as a dry friction force. Generally, the viscous normal stress (i.e. viscous eddy diffusion $\eta\frac{\partial^2 v}{\partial z^2}$) comprises the diagonal elements in this tensor, but as argued in the sequel, this effect is neglected. Note that the eddy viscous diffusion can also be regarded as a part of the convective term, or as a part of the molecular momentum transfer.

The pressure forces

The static stress in the liquor phase is the liquor pressure, p_l, (i.e. hydrostatic pressure), while for the chip plug it is the sum of the liquor pressure and the chip pressure, p_c (c.f. the discussion about the compressibility in Sec. 3.4.2). This can be illustrated by the following discussion inspired by Bear (1972):

Fig. 3.7 shows a typical vertical slice of the mass in the digester at time t. According to Terzaghi (1943), Terzaghi (1960), the total load of chips and liquor (and actually also that resulting from the steam pressure) above a given horizontal plane passing through the mass, is balanced by inter-chip stresses in the porous matrix

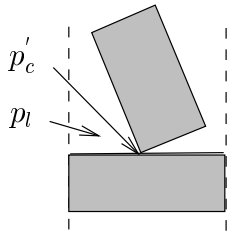

Figure 3.7: An illustration of the chip-chip contact

(i.e. the chip bed) and by the liquor pressure. Taking into account the contact areas of chips and of liquor intersected by the horizontal plane, we may write:

$$\sigma_c^{'} = p_c^{'} + p_l \tag{3.89}$$

where $\sigma_c^{'}$ is the total stress on the chip plug over the chip area, A_c. When A is the total cross-section area, $A_c = A\epsilon_c$ is the area of chip-chip contact (i.e. the area occupied by the chips, c.f. area porosity equals volume porosity in Appendix A), and $A_l = A\epsilon_l$ is the area of liquor-chip contact (i.e. the area occupied by the liquor (pore space)). $p_c^{'}$ is the stress in the chip plug (i.e. chip force, F_c, per unit chip area, A_c). F_c is the mean value of the contact forces between the chips over the chip area. p_l is the liquor pressure acting on the chip area (i.e. liquor force, $F_{l,c}$, per unit chip area, A_c, and equals liquor force, F_l, per unit liquor area, A_l (c.f. Sec. 3.3.3)). $F_{l,c}$ is the force excited by the liquor on the chips, while F_l is the force excited by the liquor on the liquor. Then we may write:

$$\begin{aligned} \sigma_c &= p_c^{'}\epsilon_c + p_l\epsilon_c \\ &= p_c + p_l\epsilon_c \end{aligned} \tag{3.90}$$

where σ_c is the total stress on the chip plug over the total area, A. Terzaghi called the product $p_c^{'}\epsilon_c = p_c$ the effective stress of the solid matrix. This is what we have defined as the chip pressure in Sec. 3.3.3.

Equivalently, the total stress, σ_l, on the liquor over the total area, A is:

$$\sigma_l = p_l\epsilon_l \tag{3.91}$$

Then, the total stress (load), σ, on the chips and liquor over the total area is:

$$\begin{aligned} \sigma &= \sigma_l + \sigma_c \\ &= p_c + p_l \end{aligned} \tag{3.92}$$

This equation, first introduced by Terzaghi (1943), Terzaghi (1960), is fundamental in soil mechanics. The idea leading to it is called the effective stress concept.

Viscous friction

The flow resistance acts against the flow relative to the medium through which the flow goes. The corresponding viscous friction force is often associated with the results of the experiments by Darcy (1856). Henry Darcy investigated the flow of water in vertical homogeneous sand filters in connection with the fountains of the city of Dijon, France. The experimentally derived form of *Darcy's law* (for a homogeneous incompressible fluid) was limited to one-dimensional flow. For three-dimensional flow, the generalization of Darcy's law is:

$$\mathbf{v_0} = -K\nabla\phi \tag{3.93}$$

where $\mathbf{v_0}$ is the vector of relative superficial velocities (also called *specific flux vector* or *specific discharge*), c.f. Sec. 3.3.4, in the three spatial directions, $\nabla\phi$ is *hydraulic gradient* vector, and $K = \{K_{ij}(x, y, z)\}$ is a symmetric three-dimensional second order tensor of *hydraulic conductivities* in each direction. This is generally valid for *inhomogeneous*, *anisotropic* media (dependency of both position and direction within the medium). As, in this study, the medium is assumed to be inhomogeneous, isotropic and only the vertical direction, z, is considered, K reduces to a scalar $K = K(z)$. ϕ is expressed as $\phi = z + \frac{p}{\rho g}$. In this way, Darcy's law can be written as:

$$v_0 = -\frac{K}{\rho g}(\frac{\partial p}{\partial z} + \rho g) \tag{3.94}$$

or:

$$v_0 = -\frac{k}{\eta}(\frac{\partial p}{\partial z} + \rho g) \tag{3.95}$$

where $K = k_p\rho g/\eta$. k_p $[m^2]$ is the coefficient of *permeability* of the porous medium, ∂p is the pressure drop over the distance ∂z, and η $[Pa \cdot s]$ is kinematic viscosity (Bear, 1972). In the case of horizontal flow, Eq. (3.95) is often written as:

$$\frac{\partial p}{\partial z} = -\frac{\eta}{k_p}v_0 \tag{3.96}$$

The factor $\frac{\eta}{k_p}$ is therefore an expression of the flow resistance (or viscous friction coefficient). By the substitution of the superficial velocity, $v_0 = \epsilon_l v$ (Eq. (3.70)), we have:

$$\frac{\partial p}{\partial z} = -\frac{\eta}{k_p}\epsilon_l v = -\frac{\Lambda}{\epsilon_l}v \tag{3.97}$$

where in this study Λ expresses the viscous friction coefficient ($\frac{\eta}{k_p}\epsilon_l^2$). It is given by the viscosity coefficient for the liquor, η_l, and the permeability (porosity) of the chip plug, k_{pc}. The idea is that when the chip plug moves faster than the free liquor, the friction force acts with a positive sign on the liquor, and with a negative sign on the chip plug, as if the liquor where flowing counter-current the chips. The work of flow on the two phases are the same, i.e the friction coefficients are the same. Note that even though this viscous term is included in the flow equation for the chip plug, such as for the free liquor, we have not regarded the chip plug as a viscous medium, such as the free liquor is.

The coefficient of permeability depends on the characteristics of the medium through which the flow goes.

In flow through porous media, there is not a sharp difference between laminar and turbulent flow regimes. This means that significant inertia forces occur at much lower Reynold numbers than in e.g. one-phase flow through pipes. Bear (1972) writes about this:

As the specific discharge increases, Darcy's law, which specifies a linear relationship between the specific discharge and the hydraulic gradient, has been shown by many investigators to be invalid. Fig. 3.8 shows a schematic picture of these results.

Figure 3.8: Schematic classification of flow through porous media (Bear, 1972)

In flow through conduits, the Reynolds number (Re), a dimensionless number expressing the ratio of inertial to viscous forces, is used as a criterion to distinguish between laminar flow occurring at low velocities and turbulent flow (see any text book on fluid mechanics). The critical Re between laminar and turbulent flow in pipes is around 2100. *By analogy, a Reynolds number is defined also for flow through porous media:*

$$Re = \frac{v_0 d \rho}{\eta} \tag{3.98}$$

where d is some length dimension of the porous matrix. Often the mean grain diameter is used as the length dimension. In practically all cases, Darcy's law is valid as long as the Reynolds number based on average grain diameter does not exceed some value between 1 *and* 10 *(Bear, 1972). The three regions that may be distinguished in flow through porous media are, see Fig. 3.8:*

1. *At low Reynolds numbers (i.e. at low velocity for a constant d and η), we have a region where the flow is laminar, viscous forces are predominant, and the linear Darcy's law is valid. The upper limit of this range is at a value of Re between* 1 *and* 10.

2. *As Re increases, we observe a transition zone. At the lower end of this zone, we have the passage from the laminar regime, where viscous forces are predominant, to another laminar regime where inertial forces govern the flow. At the upper end of the transition zone, we have a gradual passage to turbulent flow. Some authors suggest Re 100 for the upper limit of the laminar flow regime, which is often referred to as the nonlinear laminar flow regime.*

3. *At high Re, we have turbulent flow.*

Independent of these results, Forchheimer (1901) was the first to propose a modification of Darcy's law including both first and second power of the velocity, i.e. actually in the case of nonlinear laminar flow regime: [8]

$$\frac{\partial p}{\partial z} = a_1 v_0 + a_2 |v_0| v_0 \tag{3.99}$$

As argued by Forchheimer (1901), the deviation from Darcy's law for flow through porous media, which can be attributed to the addition of the second power of the velocity term in Eq. (3.99), is due to influence from inertial forces on the flow, rather than turbulence. The reason for this is that the second order term in this equation is not proportional to the viscosity.
Härkönen (1984) gives a review of proposed expressions for $k_{pc} = k_p$. Härkönen found a special form of Eq. (3.99), the socalled *Ergun equation* (Ergun, 1952), to fit best his data:

$$\frac{\partial p_l}{\partial z} = -\frac{150\eta_l}{d^2}\frac{\epsilon_c^2}{\epsilon_l^3} v_0 - \frac{1.75\rho_l}{d}\frac{\epsilon_c}{\epsilon_l^3}|v_0| v_0 \tag{3.100}$$

By the substitution $v_0 = \epsilon_l(v_c - v_l)$, Härkönen expresses the friction coefficient Λ as:

$$\Lambda = R_1\frac{\epsilon_c^2}{\epsilon_l} + R_2\epsilon_c \mid v_c - v_l \mid \tag{3.101}$$

where $R_1 = \frac{150\eta_l}{d^2}[\frac{kg}{m^3 s}]$ and $R_2 = \frac{1.75\rho_l}{d}[\frac{kg}{m^4}]$ are estimated parameters from a pilot laboratory digester. Due to the reasons that are mentioned in the in Sec. 3.3.3, different results are reported. $R_1 = 2.12 \cdot 10^4$ (Härkönen, 1984), respective $4.6 \cdot 10^3$ (Härkönen, 1987), and $R_2 = 9.62 \cdot 10^6$ (Härkönen, 1984), respective $3.9 \cdot 10^6$ (Härkönen, 1987).
This means that the experiments by Härkönen show that the force of inertia is significant although the term (i.e. $-v\frac{\partial v}{\partial z}$, see Eq. (3.165)) is "small" compared to the other terms which are included in the momentum balances. However, the Reynolds number, as defined in Eq. (3.98), is in the range $0.8 - 15$, at velocity $3mm/s$, void fraction 0.5, viscosity $3.51 \cdot 10^{-4}$, and grain diameter in the range $0.2 - 3.4mm$ according to these R_1, R_2 numbers. This means, according to Fig. 3.8 that we have a flow regime mainly in the laminar area. However, a grain diameter of $1cm$ is probably more realistic. This gives a Reynolds number of 43, and according to Fig. 3.8 we have a flow regime in the nonlinear laminar area.
The conclusion of this is that even though the force of inertia for the liquor is

[8] Often, this form is referred in context with one-phase flow. In that case $|v_0|v_0 = v_0^2$ as long as $v_0 \geq 0$. Further, $|v_0|$ is also written as $\sqrt{v_0 v_0}$.

"small" compared to other terms (like gravity and pressure forces), it is significant compared to the viscous normal force which causes turbulent flow. Hence, the latter is typically small as well ("very small"). Note also that the friction factor Eq. (3.101) is a function of the porosity (ϵ_l). Less porosity, i.e. higher compaction of chips, means higher friction. This explains the structure of the equation.

A good overview of different derivations of Darcy's law for saturated flow using different conceptual models of the porous medium, can be found in Bear (1972). These are based on the motion equations in porous media and use the basic principles underlying the theory of hydrodynamics.

Note that Darcy's law, and the generalization Eq. (3.99) are simple steady state momentum balances. In Sec. 3.6.1, we include this effect in the general form of the momentum balances. In the derivation, we show that the viscous friction force can be considered as a part of the generalized stress tensor, i.e. a "pressure-like" term, c.f. page 77.
Another way to consider this force is to regard it as a part of the *molecular momentum transport*, τ_{ij} (Bird et al., 1960). In the momentum balance (Navier Stokes equation) for the z component, the following terms represent this:

$$\frac{\partial \tau_{xz}}{\partial x} + \frac{\partial \tau_{yz}}{\partial y} + \frac{\partial \tau_{zz}}{\partial z} \tag{3.102}$$

where for a Newtonian fluid with constant viscosity, η, c.f. Appendix B:

$$\begin{aligned}
\tau_{xz} &= -\eta(\frac{\partial v_z}{\partial x} + \frac{\partial v_x}{\partial z}) \\
\tau_{yz} &= -\eta(\frac{\partial v_z}{\partial y} + \frac{\partial v_y}{\partial z}) \\
\tau_{zz} &= -2\eta\frac{\partial v_z}{\partial z} + \frac{2}{3}\eta(\nabla v)
\end{aligned}$$

These equations state that the shear force per unit area is proportional to the negative of the local velocity gradient, and is known as *Newton's law of viscosity*. Substitution gives:

$$\eta(\frac{\partial^2 v_z}{\partial x^2} + \frac{\partial^2 v_z}{\partial y^2} + \frac{\partial^2 v_z}{\partial z^2}) \tag{3.103}$$

Then, a way to derive Darcy's law is to average the Navier Stokes equations over a representative elementary volume. Irmay (1958) found:

$$\eta(\frac{\partial^2 \bar{v}_z}{\partial x^2} + \frac{\partial^2 \bar{v}_z}{\partial y^2}) = -[\beta(1-n)^2/n^3 d^2]v_0 \tag{3.104}$$

where β is a parameter, and n is the porosity. Thus, we see that the viscous eddy diffusion, $(\eta\frac{\partial^2 v}{\partial z^2})$, is molecular momentum transport as well. This is also called viscous normal force.

In this study, we use the friction force as proposed by Härkönen (1987) and denote it F_Λ where:

$$F_\Lambda = \Lambda(v_c - v_l) \tag{3.105}$$

This is regarded as a *volume force*, i.e. with dimension N/m^3.

Sliding friction

It can be experimentally verified that the sliding force of friction has a magnitude that, for most practical purposes is proportional to the normal force **N** pressing one body against one other (see e.g. Alonso and Finn (1983)). The constant of proportionality is called the coefficient of friction μ such that the force of sliding friction for the chip plug against the side walls (the digester shell) is:

$$dF = \mu N = \mu p_c dA = \mu p_c \Pi d dl \tag{3.106}$$

for a cylindrical slice of the reactor with diameter d and height dl. Härkönen regards this as a volume force:

$$\frac{dF}{dV} = \frac{\mu p_c \Pi d dl}{\frac{1}{4}\Pi d^2 dl} = \frac{4\mu p_c}{d} \tag{3.107}$$

In the sequel we denote this as F_μ.

The characteristics of the movement of the chip plug

Paper pulp in water has a *pseudo plastic* behaviour (Bird et al., 1960). According to Newton's law of viscosity, Eq. (B.5), a plot of τ_{xy} versus $-(dv_x/dy)$ for a given fluid gives a straight line through the origin, and the slope of this line is the viscosity of the fluid at a given temperature and pressure, i.e. constant viscosity η (see Fig. 3.9). Pseudo plastic behaviour is an example of so-called non-Newtonian behaviour where η decreases with increasing rate of shear $(-dv_x/dy)$.

It is probable that the chip plug has qualitatively the same properties as "paper pulp in water". As a consequence, the coefficient of viscosity for the chip plug is hard to determine. Further, it is probable that, as for the liquor, the viscous normal force is very small compared to gravity, pressure forces etc. Hence, we do no assumptions about if the movement is a viscous flow, and the viscous normal force (eddy diffusion) is therefore neglected. However, although the dispersive movement is physically connected to this phenomenon, the dispersive effect is included in our model, c.f. assumption 1 at page 52. Hence, the chip movement is not a pure *plug flow*, i.e. we assume non-flat radial velocity profiles, giving axial mixing.

3.4.2 Compressibility

Because the chip pressure only acts between the individual chips and not on the surrounding liquor (c.f. Sec. 3.3.3), the nature of the compressibility of the chip bed differs from that of, for instance, an air bulb surrounded by entrapped liquor inside the chips. Here, the air and liquor pressures are steady state equal $(= p_l)$,

Figure 3.9: A summary of steady-state non-Newtonian two-parameter models (the Newtonian model is shown for reference) (Bird et al., 1960)

c.f. Eq. (3.42). This means that the compressibility of the air bulb is totally reversible. Compression followed by free expansion gives unchanged bulb volume. In contrast, in the chip bed, variations in the liquor pressure does not influence the chip pressure. Hence, the compaction only has to do with inter-constellation of the chips. In this way, variations in the volume fraction of chips means that it is the number of chips per m^3 which varies. What happens is the same as in unconsolidated materials of inelastic grains. Bear (1972) writes about this:

Experience has shown that in soils, deformation occurs as an integrated result of the usually irreversible microscopic movements of many irregular particles under stress patterns set up by the applied load and the random geometry of the individual grain-to-grain contact. After removing the cause of motion, each particle will find itself under a new stress system that, while requiring small local adjustments that may take some time, will not return the particles to their original positions. Changes in position will continue until a new equilibrium is reached. Hence, we have inelastic deformation. This also means that the response of the stresses on the soil depends on the loading history. This is especially so in granular unconsolidated materials. In rocks, or in consolidated materials we have an approximately elastic deformation.
Another important observation is that since it takes some time for the porosity, n, or void ratio, $e = n/(1-n)$, to change, the effective stress remains at first unchanged and then varies gradually. This means that any increment in the total stress (i.e. the sum of the effective stress and the hydrostatic pressure) produces an immediate response in the form of a pressure rise in the water above the equilibrium that existed initially. Then, this pressure is reduced as the effective stress increases, and e decreases as drainage of water takes place. This is the process of

consolidation.

In our problem, the chip bed is regarded as a granular unconsolidated soil of inelastic chips. Hence, the elasticity (or compressibility) of the chip bed is irreversible. Changes in the chip pressure give inelastic deformation. This mechanism is described in the model by not letting the chip pressure act on the free liquor explicitly, i.e. the chip pressure is not a part of the normal stresses for the liquor phase. At present time, no tests that are known to the author are made in order to study this irreversibility in full-scale digesters. Laboratory tests, however, indicate that the compressibility is not reversible in small pilot digesters (Härkönen, 1994).

3.5 Mass and component balances

This section contains a derivation of the mass balances. These include both overall balances for the two phases and component balances. The overall balances give a dynamic equation for the compaction of chips and a continuity equation which the liquor velocity is solved from. The densities of lignin, carbohydrates, entrapped and free alkali and dissolved solids are solved from the component balances.
Four different phenomena are considered. These are vertical convection, chemical reaction, interphase diffusion and vertical dispersion.

3.5.1 The main section

A general definition of the conservation of mass is given in Appendix C. For the chip plug, Eq. (C.1) is expanded in the following form:

$$\frac{d}{dt}\iiint_{V_c} \rho_c dV_c = -\oiint_{A_c} \rho_c \mathbf{v_{c,j}}^T \mathbf{n} dA_c \tag{3.108}$$

Here, the reaction term is not present because the chemical reactions only act inside the chips.

We substitute $dV_c = \epsilon_c dV$ from Eq. (3.10) and $dA_c = \epsilon_c dA$ from Eq. (3.9):

$$\frac{d}{dt}\iiint_{V} \rho_c \epsilon_c dV = -\oiint_{A} \rho_c \epsilon_c \mathbf{v_{c,j}}^T \mathbf{n} dA \tag{3.109}$$

The use of Gauss' theorem (see e.g. Edwards and Penny (1986)) gives:

$$\frac{d}{dt}\iiint_{V} \rho_c \epsilon_c dV = -\iiint_{V} \nabla(\rho_c \epsilon_c \mathbf{v_{c,j}}^T \mathbf{n}) dV \tag{3.110}$$

We use $\mathbf{v_{c,j}}^T \mathbf{n} = v_{c,j}$ where $\mathbf{v_{c,j}}^T = [0 \quad 0 \quad v_{c,j}]$. By assuming smooth solutions, i.e. no discontinuities, and constant control volumes according to the Euler formulation of partial differential equations, we divide the equation by the elementary

control volume V and get the following partial differential equation [9]:

$$\frac{\partial}{\partial t}(\rho_c \epsilon_c) = -\nabla(\rho_c \epsilon_c v_{c,j}) \tag{3.111}$$

$v_{c,j}$ is defined by Eq. (3.73): [10]

$$\rho_c \epsilon_c v_{c,j} = \rho_c \epsilon_c v_c + j_c \tag{3.112}$$

where $j_c = j_{c,z} + j_{c,\gamma}$. This gives:

$$\frac{\partial}{\partial t}(\rho_c \epsilon_c) = -\frac{\partial}{\partial z}(\rho_c \epsilon_c v_c) - \frac{\partial j_{c,z}}{\partial z} - \frac{\partial j_{c,\gamma}}{\partial \gamma} \tag{3.113}$$

From Eq. (3.74) we have the dispersive term:

$$\frac{\partial j_{c,z}}{\partial z} = -D_c \frac{\partial^2(\rho_c \epsilon_c)}{\partial z^2} \tag{3.114}$$

and from Eq. (3.76) we have the net mass transfer from the chips to the free liquor:

$$\frac{\partial j_{c,\gamma}}{\partial \gamma} = D_{EA}(\rho_{EA,el} - \rho_{EA,fl}) + D_{ds}(\rho_{ds,el} - \rho_{ds,fl}) \tag{3.115}$$

By this, the overall mass balance equation for the chips related to an elementary volume of mass (REV) can be written as:

$$\frac{\partial}{\partial t}(\rho_c \epsilon_c) = -\frac{\partial}{\partial z}(\rho_c \epsilon_c v_c) - \Delta(D\rho) + D_c \frac{\partial^2}{\partial z^2}(\rho_c \epsilon_c) \tag{3.116}$$

where $\rho_c = (\alpha_{lig} + \alpha_{carb})\rho_{ODW} + \rho_{EA,el} + \rho_{ds,el} + \rho_{air} + \rho_{w,el}$ from Eq. (3.64). Substitution gives:

$$\begin{aligned}\frac{\partial}{\partial t}(\rho_c \epsilon_c) = \; & \frac{\partial}{\partial t}(\epsilon_c(\alpha_{lig} + \alpha_{carb})\rho_{ODW}) + \frac{\partial}{\partial t}(\epsilon_c(\rho_{EA,el} + \rho_{ds,el})) \\ & + \frac{\partial}{\partial t}(\epsilon_c \rho_{air}) + \frac{\partial}{\partial t}(\epsilon_c \rho_{w,el})\end{aligned}$$

Without losing information, we can separate Eq. (3.116) into the following four component balances where $\rho_{lig,mass}$, $\rho_{carb,mass}$, $\rho_{EA,el,mass}$, and $\rho_{ds,el,mass}$ are regarded as independent:

$$\begin{aligned}\frac{\partial}{\partial t}\rho_{lig,mass} = \; & \frac{\partial}{\partial t}(\epsilon_c \alpha_{lig} \rho_{ODW}) = -\frac{\partial}{\partial z}(\epsilon_c \alpha_{lig} \rho_{ODW} v_c) \\ & - r_{lig} \rho_{ODW} \epsilon_c + D_c \frac{\partial^2}{\partial z^2}(\epsilon_c \alpha_{lig} \rho_{ODW})\end{aligned} \tag{3.117}$$

$$\frac{\partial}{\partial t}\rho_{carb,mass} = \frac{\partial}{\partial t}(\epsilon_c \alpha_{carb} \rho_{ODW}) = -\frac{\partial}{\partial z}(\epsilon_c \alpha_{carb} \rho_{ODW} v_c) \tag{3.118}$$

[9] When the Euler formulation of PDE's is used, the control volume is fixed in space and hence, $\frac{\partial z}{\partial t} = 0$. Then, $\frac{d\rho}{dt} = \frac{\partial \rho}{\partial t}$.

[10] We neglect the Soret effect, c.f. Appendix B.

$$\begin{aligned}
& -r_{carb}\rho_{ODW}\epsilon_c + D_c\frac{\partial^2}{\partial z^2}(\epsilon_c\alpha_{carb}\rho_{ODW}) \\
\frac{\partial}{\partial t}\rho_{EA,el,mass} &= \frac{\partial}{\partial t}(\epsilon_c\rho_{EA,el}) = -\frac{\partial}{\partial z}(\epsilon_c\rho_{EA,el}v_c) \qquad (3.119)\\
& -(b_{lig}r_{lig}\rho_{ODW}\epsilon_c + b_{carb}r_{carb}\rho_{ODW}\epsilon_c) \\
& -D_{EA}(\rho_{EA,el} - \rho_{EA,fl}) + D_c\frac{\partial^2}{\partial z^2}(\epsilon_c\rho_{EA,el}) \\
\frac{\partial}{\partial t}\rho_{ds,el,mass} &= \frac{\partial}{\partial t}(\epsilon_c\rho_{ds,el}) = -\frac{\partial}{\partial z}(\epsilon_c\rho_{ds,el}v_c) \qquad (3.120)\\
& +(1+b_{lig})r_{lig}\rho_{ODW}\epsilon_c + (1+b_{carb})r_{carb}\rho_{ODW}\epsilon_c \\
& -D_{ds}(\rho_{ds,el} - \rho_{ds,fl}) + D_c\frac{\partial^2}{\partial z^2}(\epsilon_c\rho_{ds,el})
\end{aligned}$$

Because $\rho_{w,el}$ is expressed as a function of $\alpha_{lig}, \alpha_{carb}, \rho_{EA,el}, \rho_{ds,el}$ and T_c (c.f. Eqs. (3.46) and (3.31)), $\frac{\partial}{\partial t}(\epsilon_c\rho_{w,el})$ can be expressed by Eqs. (3.117)-(3.120) and (3.212).

Further, note that Eqs. (3.117)-(3.120) form a set of four equations with five unknown "densities"; $\alpha_{lig}, \alpha_{carb}, \rho_{EA,el}, \rho_{ds,el}$ and ϵ_c. These unknowns are, however, five degrees of freedom. The four equations can therefore be separated into five equations. This is discussed in the final remarks at the end of this section. The separation gives the following parabolic partial differential equation for the volume fraction of chips:

$$\frac{\partial\epsilon_c}{\partial t} = -\frac{\partial}{\partial z}(\epsilon_c v_c) + D_c\frac{\partial^2\epsilon_c}{\partial z^2} \qquad (3.121)$$

Note that we have included the convective part $\frac{\partial v_c}{\partial z}$ here because this influences the amount of chips in the control volume Adz. Eq. (3.121) is essential in the model. Note that it actually expresses the *volume balance* for the chips. In the following, it will be referred to as the *compaction equation* (c.f. the definition of compaction in Sec. 3.3.6).

As a consequence:

$$\frac{\partial(\rho_{air}\epsilon_c)}{\partial t} = \rho_{air}\frac{\partial\epsilon_c}{\partial t} = \rho_{air}(-\frac{\partial}{\partial z}(\epsilon_c v_c) + D_c\frac{\partial^2\epsilon_c}{\partial z^2}) \qquad (3.122)$$

where ρ_{air} is given from Eq. (3.43).

A similar derivation gives the following overall mass balance equation for the free liquor:

$$\frac{\partial}{\partial t}(\rho_l\epsilon_l) = -\frac{\partial}{\partial z}(\rho_l\epsilon_l v_l) + \Delta(D\rho) + D_l\frac{\partial^2}{\partial z^2}(\rho_l\epsilon_l) \qquad (3.123)$$

where $\rho_l = \rho_{EA,fl} + \rho_{ds,fl} + \rho_{w,fl}$ from Eq. (3.65). This gives:

$$\frac{\partial}{\partial t}(\rho_l\epsilon_l) = \frac{\partial}{\partial t}(\epsilon_l\rho_{EA,fl}) + \frac{\partial}{\partial t}(\epsilon_l\rho_{ds,fl}) + \frac{\partial}{\partial t}(\epsilon_l\rho_{w,fl})$$

and:

$$\frac{\partial}{\partial t}\rho_{EA,fl,mass} = \frac{\partial}{\partial t}(\epsilon_l \rho_{EA,fl}) = -\frac{\partial}{\partial z}(\epsilon_l \rho_{EA,fl} v_l) \tag{3.124}$$
$$+D_{EA}(\rho_{EA,el} - \rho_{EA,fl}) + D_l \frac{\partial^2}{\partial z^2}(\epsilon_l \rho_{EA,fl})$$
$$\frac{\partial}{\partial t}\rho_{ds,fl,mass} = \frac{\partial}{\partial t}(\epsilon_l \rho_{ds,fl}) = -\frac{\partial}{\partial z}(\epsilon_l \rho_{ds,fl} v_l) \tag{3.125}$$
$$+D_{ds}(\rho_{ds,el} - \rho_{ds,fl}) + D_l \frac{\partial^2}{\partial z^2}(\epsilon_l \rho_{ds,fl})$$

Because $\rho_{w,fl}$ is expressed as a function of $\rho_{EA,fl}$ and $\rho_{ds,el}$ (c.f. Eq. (3.54)), $\frac{\partial}{\partial t}(\epsilon_l \rho_{w,fl})$ can be expressed by Eqs. (3.124)-(3.125).

As for the chip phase, we can separate the dynamics of ϵ_l from the dynamics of $\rho_{EA,fl}$ and $\rho_{ds,el}$. This gives the following parabolic partial differential equations for the volume fraction of free liquor:

$$\frac{\partial \epsilon_l}{\partial t} = -\frac{\partial}{\partial z}(\epsilon_l v_l) + D_l \frac{\partial^2 \epsilon_l}{\partial z^2} \tag{3.126}$$

As a consequence:

$$\frac{\partial(\rho_w \epsilon_l)}{\partial t} = \rho_w \frac{\partial \epsilon_l}{\partial t} = \rho_w(-\frac{\partial}{\partial z}(\epsilon_l v_l) + D_l \frac{\partial^2 \epsilon_l}{\partial z^2}) \tag{3.127}$$

where ρ_w is the specific weight of water.

By Eqs. (3.12), (3.121) and (3.126), we get the two-phase form of the continuity equation:

$$\frac{\partial v_l}{\partial z} = \frac{1}{1-\epsilon_c}((v_l - v_c)\frac{\partial \epsilon_c}{\partial z} - \epsilon_c \frac{\partial v_c}{\partial z} + (D_c - D_l)\frac{\partial^2 \epsilon_c}{\partial z^2}) \tag{3.128}$$

This elliptic equation is used to compute the free liquor velocity.

In addition, the above separations give the final form of the component balances as:

$$\frac{\partial \alpha_{lig}}{\partial t} = -v_c \frac{\partial \alpha_{lig}}{\partial z} - r_{lig} + D_c \frac{\partial^2 \alpha_{lig}}{\partial z^2} \tag{3.129}$$
$$\frac{\partial \alpha_{carb}}{\partial t} = -v_c \frac{\partial \alpha_{carb}}{\partial z} - r_{carb} + D_c \frac{\partial^2 \alpha_{carb}}{\partial z^2} \tag{3.130}$$
$$\frac{\partial \rho_{EA,el}}{\partial t} = -v_c \frac{\partial \rho_{EA,el}}{\partial z} - \rho_{ODW}(b_{lig} r_{lig} + b_{carb} r_{carb}) \tag{3.131}$$
$$-\frac{D_{EA}}{\epsilon_c}(\rho_{EA,el} - \rho_{EA,fl}) + D_c \frac{\partial^2 \rho_{EA,el}}{\partial z^2}$$
$$\frac{\partial \rho_{ds,el}}{\partial t} = -v_c \frac{\partial \rho_{ds,el}}{\partial z} - \rho_{ODW}[(1+b_{lig}) r_{lig} + (1+b_{carb}) r_{carb}] \tag{3.132}$$
$$-\frac{D_{ds}}{\epsilon_c}(\rho_{ds,el} - \rho_{ds,fl}) + D_c \frac{\partial^2 \rho_{ds,el}}{\partial z^2}$$

$$\frac{\partial \rho_{EA,fl}}{\partial t} = -v_l \frac{\partial \rho_{EA,fl}}{\partial z} + \frac{D_{EA}}{\epsilon_l}(\rho_{EA,el} - \rho_{EA,fl}) + D_l \frac{\partial^2 \rho_{EA,fl}}{\partial z^2} \quad (3.133)$$

$$\frac{\partial \rho_{ds,fl}}{\partial t} = -v_l \frac{\partial \rho_{ds,fl}}{\partial z} + \frac{D_{ds}}{\epsilon_l}(\rho_{ds,el} - \rho_{ds,fl}) + D_l \frac{\partial^2 \rho_{ds,fl}}{\partial z^2} \quad (3.134)$$

The reaction kinetics then only influences the mass balances through mass transfer inside the chips.

Some remarks

Model states and degrees of freedom

Through the model derivation, we have assured that no mass either comes into being or disappears. Further, we have assured that some components are expressed by linear combinations of the others, and not as state variables. Such variables are called *reaction invariants*. This is also a result of the mass balances. Considering Eq. (3.110) and the corresponding equation for the free liquor phase:

$$\frac{d}{dt}\iiint_V \rho_c \epsilon_c dV = -\iiint_V \nabla(\rho_c \epsilon_c \mathbf{v_{c,j}}^T \mathbf{n}) dV$$

$$\frac{d}{dt}\iiint_V \rho_l \epsilon_l dV = -\iiint_V \nabla(\rho_l \epsilon_l \mathbf{v_{l,j}}^T \mathbf{n}) dV$$

the sum of the left-hand sides are:

$$\frac{d}{dt}\iiint_V (\rho_c \epsilon_c + \rho_l(1-\epsilon_c)) dV = \frac{d}{dt}\iiint_V (\rho_l + (\rho_c - \rho_l)\epsilon_c) dV = 0 \quad (3.135)$$

and the sum of the right-hand sides are:

$$-\iiint_V \nabla(\rho_c \epsilon_c \mathbf{v_{c,j}}^T \mathbf{n} + \rho_l \epsilon_l \mathbf{v_{l,j}}^T \mathbf{n}) dV = 0 \quad (3.136)$$

The potential Ψ is defined as $\nabla\Psi = (\rho_c \epsilon_c \mathbf{v_{c,j}}^T \mathbf{n} + \rho_l \epsilon_l \mathbf{v_{l,j}}^T \mathbf{n})$, which by use of Eq. (3.136) gives:

$$\iiint_V \nabla^2 \Psi dV = 0 \quad (3.137)$$

This is the continuity equation for the total mass flow in the digester (Härkönen, 1984). In this way, Eq. (3.135) or (3.136) yields the overall constraint for the two mass balances such that they are fulfilled. In our model, we have three constraints connected to this. These are:

1. The elementary control volumes are constant, i.e. the sum of the volume fraction of chips and free liquor is 1; Eq. (3.12).
2. The volume of a single chip is constant, i.e. the sum of the volume fraction of entrapped liquor and solid materials is 1; Eq. (3.16) and (3.44).

3. The sum of the volume fraction of the components in the free liquor is 1; Eq. (3.53).

These three constraints make the constraint Eq. (3.135) or (3.136) to be fulfilled. This means that it is the water components in the two phases that are reaction invariants in our model, c.f. Eqs. (3.46) and (3.54).

The separation of the equations

According to assumption 2 in Sec. 3.2.1, the chip volume is kept constant through the digestion process. The compaction of chips is, however, influenced by the process of delignification and degradation of the carbohydrates. This is explained in the section about the chip pressure in Sec. 3.3.3. When the chips become softer and change their shape, the chip pressure is reduced. Thus, the reaction kinetics influences the compaction of chips through the momentum transfer. Hence, because this is an additional information about the mechanism of the motion of the mass, ϵ_c and α_{lig} are two degrees of freedom in the system. The consequence of this is that the dynamics of ϵ_c can be separated from the dynamics of the four chip components. Note, however, that since the lignin is a part of the chips, the momentum transport of the lignin (which influences the dynamics connected to the vertical movement) is totally dependent on the momentum transport of chips (it is exactly the same "driving force"). Fig. 3.10 illustrates how these variables influence each other through the mass- and momentum transport. The same ar-

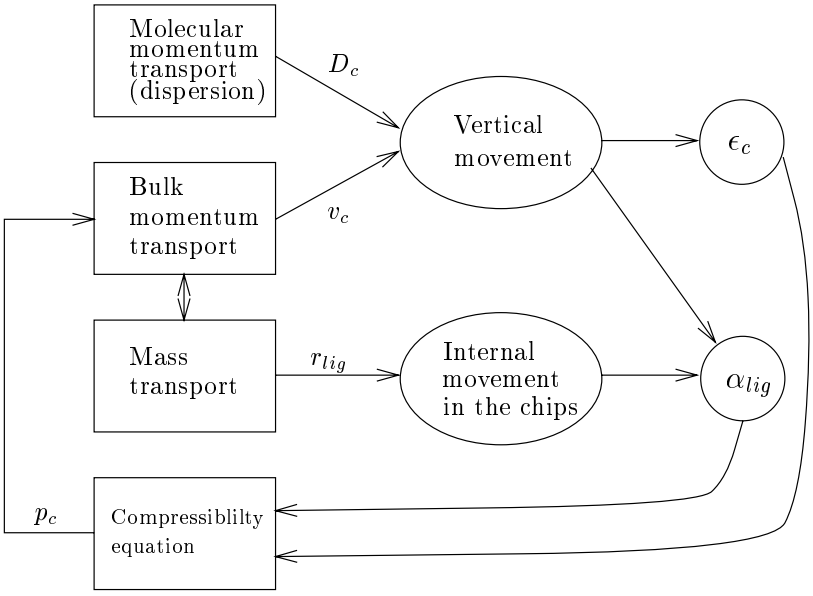

Figure 3.10: Cause-and-effect diagram for ϵ_c and α_{lig}

gument applies regarding the other components. Finally, note that this enforces

us to describe the compressibility equation as $p_c = p_c(\epsilon_c, \kappa)$ in Eq. (3.6), and not as $\epsilon_c = \epsilon_c(p_c, \kappa)$ in Eq. (3.67).

Convection

In the separation of the mass balances, we have included the convective part $\frac{\partial v_c}{\partial z}$ in the compaction equation Eq. (3.121), and hence not in the wood component balances. Equivalently for the free liquor. The reason for this is that e.g. the content of lignin in a representative elementary volume of mass is described by the content of lignin in a representative chip in this volume, and not by the total amount of lignin in the volume (the amount of lignin in one chip times the number of chips in the volume). This is in accordance with what was discussed about the separation of α_{lig} and ϵ_c above.

Diffusion

The density variables $\rho_{EA,el}$ and $\rho_{EA,fl}$ are defined such that diffusion occurs whenever $\rho_{EA,el} \neq \rho_{EA,fl}$. Further, when $\rho_{EA,el} = \rho_{EA,fl}$ (i.e. no diffusion) these have to be defined relative to different volumes, here V_{ODW} respective V_{fl} (c.f. Eqs. (3.32) and (3.47)) as the respective mass differ. Note also that the respective sums of the diffusion terms in Eqs. (3.116) and (3.123), (3.119) and (3.124), and (3.120) and (3.125) equal zero, as we consider mass transfer relative to an elementary volume, which has to balance in the two phases. However, the respective sums of the diffusion terms in Eqs. (3.131) and (3.133), and (3.132) and (3.134) do not equal zero, as we consider mass transfer relative to different volumes, that do not balance in the two phases.

Dispersion

Consider the differentiation of Eq. (3.117):

$$\begin{aligned}\alpha_{lig}\frac{\partial \epsilon_c}{\partial t} + \epsilon_c \frac{\partial \alpha_{lig}}{\partial t} &= -\alpha_{lig}\frac{\partial}{\partial z}(\epsilon_c v_c) - \epsilon_c v_c \frac{\partial \alpha_{lig}}{\partial z} - r_{lig}\epsilon_c \\ &\quad + D_c(\underbrace{\alpha_{lig}\frac{\partial^2 \epsilon_c}{\partial z^2}}_{(a)} + \underbrace{\epsilon_c \frac{\partial^2 \alpha_{lig}}{\partial z^2}}_{(b)} + \underbrace{2\frac{\partial \epsilon_c}{\partial z}\frac{\partial \alpha_{lig}}{\partial z}}_{(c)})\end{aligned}$$

By the dispersive motion of the chips, the terms marked (a) and (b) are included in the respective equations Eqs. (3.121) and (3.129) since ϵ_c and α_{lig} are influenced by the same vertical movement. The term marked (c) has to do with mutual influence with respect to the vertical movement, c.f. the conception of *covariance* between x and y; $Var(x+y) = Var(x) + Var(y) + 2Cov(x,y)$. By the same argument as given to Eqs. (3.117)-(3.120), this term equals zero because ϵ_c and α_{lig} are two degrees of freedom.

To a sum-up, Eqs. (3.121), and (3.129)-(3.134) which give the compaction of chips and the densities of the respective components, result in state equations in a state-space description of the model. In addition Eq. (3.128) is used to compute the free liquor velocity.

3.5.2 The extraction section

The equations valid in the main section are used here regarding the mass and component balances for the chips. With respect to the free liquor, however, numerical adaptation is necessary. This is due to the discontinuity in the free liquor velocity at this location, as cooking liquor from above and wash water from below enter the section and leave together through the extraction line, see Fig. 3.1.

3.5.3 The top section

Because it is impossible to determine both density and volume from the mass balance, the mass densities (and volume fractions) are fixed in the derivation of the balance equations, giving the chip and liquor levels as state variables. Component balances and an equation for the volume fraction of chips are formulated ad hoc. The dispersion terms are neglected at this location. In the following, subscript in and o denote respective the mass into the digester and out of this section.

The level equations

Here, the mass balance for the chip plug is expressed as:

$$\frac{d}{dt}\int\int\int_V \rho_c dV = m_{c,in} - m_{c,o} \tag{3.138}$$

where $m_{c,in}[kg/s]$ is the mass flow of chips into the digester, $m_{c,o}$ is the mass flow out of the section, and $dV = Ah_c^{'}$ is the total volume of the section. This volume includes chips and liquor when the chip level is below the liquor level, and chips and steam above the liquor level when the chip level is above the liquor level, see Fig. (3.2). $h_c^{'}$ is the chip level relative to h_t (the distance from the digester bottom to the lower boundary of the top section); $h_c = h_c^{'} + h_t$, and A is the cross-section area. By assuming the mass density as constant, Eq. (3.138) gives the following ordinary differential equation for the chip level:

$$\frac{d}{dt}h_c = \dot{h}_c = \frac{1}{A\rho_c\epsilon_c}(m_{c,in} - m_{c,o}) \tag{3.139}$$

The mass flow is expressed as $m_c = A\rho_c\epsilon_c v_c = \rho_c q_c$ where $q_c = A\epsilon_c v_c$ is the volume flow according to Dupuit's assumption Eq. (3.68). This gives:

$$\dot{h}_c = \frac{1}{A\rho_c\epsilon_c}(\rho_{c,in}q_{c,in} - \rho_{c,o}q_{c,o}) \tag{3.140}$$

In the transition from Eq. (3.138) to (3.139), ρ_c and ϵ_c are assumed to be constant. Hence, $\rho_c = \rho_{c,o} = \rho_{c,in}$ has to be satisfied in Eq. (3.140). However, it is the volume

flow variations which change the chip level. Hence, the volume fraction of chips this is maintained in the equation. This gives:

$$\dot{h}_c = \frac{1}{A\epsilon_c}(q_{c,in} - A\epsilon_{c,o}v_{c,o}) \tag{3.141}$$

$q_{c,in}$ is treated as a manipulated variable (process input), where $\epsilon_{c,in}$ is embedded. In Sec. 3.3.6, $q_{c,in}$ is recalculated in terms of the chip meter speed. Substitution of Eq. (3.83) gives the final form of the chip level equation:

$$\dot{h}_c = \frac{1}{A\epsilon_c}(\frac{RPM}{k_{rpm}} - A\epsilon_{c,o}v_{c,o}) \tag{3.142}$$

An equivalent equation to Eq. (3.141) can be derived for the free liquor:

$$\dot{h}_l = \frac{1}{A(1-\epsilon_c)}(q_{l,in} - A(1.0-\epsilon_{c,o})v_{l,o}) \tag{3.143}$$

Eq. (3.84) in Sec. 3.3.6 gives the volume flow of liquor in the feed $q_{l,in}$ as a function of the liquor-to-wood ratio, L/W. Substitution of Eqs. (3.84) and (3.83) in Eq. (3.143) gives:

$$\dot{h}_l = \frac{1}{A(1-\epsilon_c)}(\frac{(L/W)RPM\rho_{dc,in}}{k_{rpm}\cdot 10^3} - A(1.0-\epsilon_{c,o})v_{l,o}) \tag{3.144}$$

Thus, we have an inherent control loop for the feed liquor volume flow through the L/W-ratio in the model.

Volume fraction of chips

Assuming a linear relationship to the chip level, the volume fraction of chips is expressed as:

$$\epsilon_c = \begin{cases} 0.356 & \text{if } h_c < 1.0m \\ 0.356 + k_{ts}h_c & \text{otherwise} \end{cases} \tag{3.145}$$

where k_{ts} is an empiric coefficient. A discussion of this equation is given in Appendix F.

Component balances

Although ρ_c and ρ_l are assumed to be constant in Eqs. (3.142) and (3.144), it is necessary to model these as to include the influence of chip level variations on the delignification. The component balances are expressed as:

$$\dot{\alpha}_{lig} = -v_c\frac{(\alpha_{lig} - \alpha_{lig,in})}{h_c'} - r_{lig} \tag{3.146}$$

$$\dot{\alpha}_{carb} = -v_c\frac{(\alpha_{carb} - \alpha_{carb,in})}{h_c'} - r_{carb} \tag{3.147}$$

$$\dot{\rho}_{EA,el} = -v_c\frac{(\rho_{EA,el} - \rho_{EA,el,in})}{h_c'} - \rho_{ODW}(b_{lig}r_{lig} + b_{carb}r_{carb}) \tag{3.148}$$

$$-\frac{D_{EA}}{\epsilon_c}(\rho_{EA,el}-\rho_{EA,fl})$$

$$\dot{\rho}_{ds,el} = -v_c\frac{(\rho_{ds,el}-\rho_{ds,el,in})}{h_c^{'}} - \rho_{ODW}[(1+b_{lig})r_{lig} \tag{3.149}$$

$$+(1+b_{carb})r_{carb}] - \frac{D_{ds}}{\epsilon_c}(\rho_{ds,el}-\rho_{ds,fl})$$

$$\dot{\rho}_{EA,fl} = -v_c\frac{(\rho_{EA,fl}-\rho_{EA,fl,in})}{h_l^{'}} + \frac{D_{EA}}{\epsilon_l}(\rho_{EA,el}-\rho_{EA,fl}) \tag{3.150}$$

$$\dot{\rho}_{ds,fl} = -v_c\frac{(\rho_{ds,fl}-\rho_{ds,fl,in})}{h_l^{'}} + \frac{D_{ds}}{\epsilon_l}(\rho_{ds,el}-\rho_{ds,fl}) \tag{3.151}$$

The division by $h_c^{'}$ implicates that the chemical reactions proceed longer as the chip level, and thus the residence time of the chips, increases.

The liquor velocity, v_l, is computed from Eq. (3.128).

To a sum-up for this section Eqs. (3.142) and (3.144) which give the respective levels, and Eqs. (3.146)-(3.151) which give the densities of the respective components, form state equations in a state-space description of the model. In addition Eq. (3.128) is used to compute the free liquor velocity. What is somewhat special here compared to the main section is that the overall mass balances for the two phases give two state equations (the chip- and liquor levels) instead of one (volume fraction of chips). The reason for this is the special feature of this section, where we consider the volumes of the two phases as two degrees of freedom.

The error of accuracy resulting from the simplified description of this section, is assumed to be of minor importance in light of the small percentage of volume which covers this section, compared to the total volume of mass in a typical digester.

A remark about the component balances

An alternative formulation of the convection terms in these equations is $(\rho_{in}q_{i,in} - \rho q_{i,o})/(A\epsilon_i h_i^{'}), i = c,l$ where ρ is the respective component. However, this formulation is neither perfect. Note that the components comprise the mass in a representative chip, or elementary volume of free liquor. Thus, ρ is not influenced by the amount of chips or liquor in the section. Hence, the velocity gradient is not included in these equations in the main section, as commented in the remarks in Sec. 3.5.1. The resulting error in using this alternative formulation is largest when $\rho = \rho_{in}$ and simultaneously $q_{i,o} \neq q_{i,in}$.
This discussion illustrates the weakness of using the Euler-formulation of the PDE's in this problem. As already commented, it is impossible to compute both the density and the volume from a mass balance.

3.5.4 The outlet section

The volume fraction of chips in the outlet device (see Fig. 3.3) can be expressed by the macroscopic balance:

$$\dot{\epsilon}_{c,out} = \frac{1}{V_{outlet}}(q_c - q_{c,out}) \tag{3.152}$$

where V_{outlet} is the volume of the section, and $q_{c,out}$ is given by Eq. (3.175) or (3.176). $q_c = A\epsilon_c v_c$, where v_c is given from Eq. (3.173).
The liquor velocity into the section is computed from the continuity equation:

$$v_l = \frac{q_{l,out} + q_{c,out} - q_{bn} - q_c}{A\epsilon_l} \tag{3.153}$$

where $q_{l,out}$ is given by Eq. (3.174) or (3.177). q_{bn} is the liquor flow through the bottom nozzles.

The component balances may be formulated by the same type of equations as for the inlet section.

3.6 Momentum balances

In this section, momentum balances for the two phases are derived, including boundary conditions.

3.6.1 The main section

A general definition of the conservation of momentum is given in Appendix C. We distinguish between two types of forces which act on the control volume:

- Body forces, here gravity

$$\iiint_V \rho \mathbf{g} dV \tag{3.154}$$

- Surface forces, here pressure and friction forces

$$\oiint_A \sigma \mathbf{n} dA \tag{3.155}$$

  This is discussed in Sec. 3.4.1.

The chip plug

For the chip plug, Eq. (C.2) is expanded in the following form:

$$\frac{d}{dt}\iiint_{V_c}\rho_c\mathbf{v_c}dV_c = -\oiint_{A_c}\rho_c\mathbf{v_c}\mathbf{v_{c,j}}^T\mathbf{n}dA_c + \iiint_{V_c}\rho_c\mathbf{g}dV_c \\ -\oiint_{A_c}(p_c^{'}+p_l)\mathbf{n}dA_c - \iiint_{V}F_\Lambda dV - \iiint_{V}F_\mu dV \tag{3.156}$$

where $F_\Lambda = \Lambda(v_c - v_l)$, $F_\mu = \frac{4\mu p_c}{d}$, and $\mathbf{g}$ is the vector of gravity acceleration. $\mathbf{v_c}$ is the velocity of momentum, which equals the average velocity, i.e. here the vertical velocity ($\mathbf{v_c} = [0 \quad 0 \quad v_c]^T$).

Substitution of $dV_c = \epsilon_c dV$ and $dA_c = \epsilon_c dA$ gives:

$$\frac{d}{dt}\iiint_{V}\rho_c\epsilon_c\mathbf{v_c}dV = -\oiint_{A}\rho_c\epsilon_c\mathbf{v_c}\mathbf{v_{c,j}}^T\mathbf{n}dA + \iiint_{V}\rho_c\epsilon_c\mathbf{g}dV \\ -\oiint_{A}(p_c^{'}+p_l)\mathbf{n}\epsilon_c dA - \iiint_{V}F_\Lambda dV - \iiint_{V}F_\mu dV \tag{3.157}$$

We use $p_c^{'}\epsilon_c = p_c$ (c.f. Eq. (3.90)), and Gauss' theorem:

$$\frac{d}{dt}\iiint_{V}\rho_c\epsilon_c\mathbf{v_c}dV = -\iiint_{V}\nabla(\rho_c\epsilon_c\mathbf{v_c}\mathbf{v_{c,j}}^T\mathbf{n})dV + \iiint_{V}\rho_c\epsilon_c\mathbf{g}dV \\ -\iiint_{V}(\nabla p_c + \epsilon_c\nabla p_l)dV - \iiint_{V}F_\Lambda dV - \iiint_{V}F_\mu dV \tag{3.158}$$

Note that ∇ is not acting on ϵ_c in the liquor pressure term, while it implicitly does on the chip pressure term. The former is a result of the sum of two contributions; (1) from the "end surfaces" of the control volume, A_e, and (2) from the "intermediate surface", i.e. the surface of the side wall (the digester shell) and the interphase surface, A_i, see Fig. 3.11. This gives:

$$\oiint_{A}p_l\epsilon_c\mathbf{n}dA = \iint_{A_e}p_l\epsilon_c\mathbf{n}dA_e + \iint_{A_i}p_l\epsilon_c\mathbf{n}dA_i \tag{3.159}$$

p_l in the integral over the "intermediate surface", A_i, is constant with respect to ∇. We use of Gauss' theorem on Eq. (3.159):

$$\iiint_{V}[\nabla(p_l\epsilon_c) + p_l\nabla\epsilon_c]dV = \iiint_{V}\epsilon_c\nabla p_l dV \tag{3.160}$$

Actually, this is not the formal way to express this result because the Gauss' theorem requires closed surfaces. Note that we consider a problem in which there are movements in two spatial directions (radial and axial, this is why for instance ϵ_c can variate axially), and we only describe the axial variation explicitly. In contrast to the mass balances, where the mass of each phase can be considered as

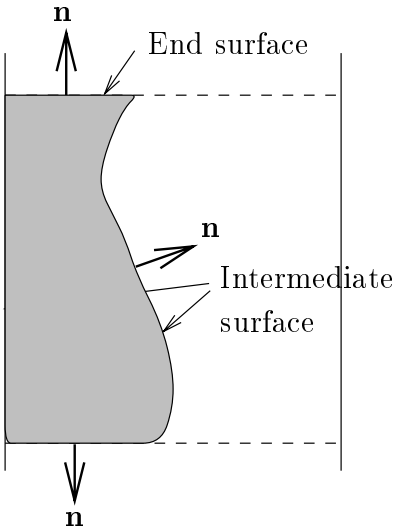

Figure 3.11: Control volume in stratified flow ((Ytrehus, 1987))

being uniformly distributed in the control volume (the distributed volume model), here we have to consider each phase as a compact medium where the interphase surface gives a contribution in the pressure terms (the collected volume model), c.f. Fig. 3.11. While p_c is defined with ϵ_c implicit, this contribution cannot be expressed explicitly here.

Equivalently as for the derivation of the mass balances, this gives the partial differential equation:

$$\frac{\partial}{\partial t}(\rho_c \epsilon_c v_c) = -\nabla(\rho_c \epsilon_c v_c v_{c,j}) + \rho_c \epsilon_c g - \frac{\partial p_c}{\partial z} - \epsilon_c \frac{\partial p_l}{\partial z} - F_\Lambda - F_\mu \tag{3.161}$$

When we only consider the left-hand side and the first term on the right-hand side, these can be expanded by:

$$v_c \frac{\partial(\rho_c \epsilon_c)}{\partial t} + \rho_c \epsilon_c \frac{\partial v_c}{\partial t} = -v_c \nabla(\rho_c \epsilon_c v_{c,j}) - \rho_c \epsilon_c v_{c,j} \nabla v_c \tag{3.162}$$

The sum of the first term on the left- and right-hand sides is the mass balance Eq. (3.111), and equals zero. Then, by the substitution $\rho_c \epsilon_c v_{c,j} = \rho_c \epsilon_c v_c + j_c$ where $j_c = j_{c,z} + j_{c,\gamma} = -D_c \frac{\partial(\rho_c \epsilon_c)}{\partial z} + \rho_c \epsilon_c v_{c,\gamma}$, and by using the divergence operator, this gives:

$$\rho_c \epsilon_c \frac{\partial v_c}{\partial t} = -\rho_c \epsilon_c v_c \frac{\partial v_c}{\partial z} + D_c \frac{\partial(\rho_c \epsilon_c)}{\partial z} \frac{\partial v_c}{\partial z} - \rho_c \epsilon_c v_{c,\gamma} \frac{\partial v_c}{\partial z} \tag{3.163}$$

By substituting Eq. (3.163) in (3.161) we get:

$$\begin{aligned}\frac{\partial v_c}{\partial t} &= -v_c\frac{\partial v_c}{\partial z} + \overbrace{\frac{D_c}{\rho_c\epsilon_c}\frac{\partial(\rho_c\epsilon_c)}{\partial z}\frac{\partial v_c}{\partial z}}^{a} - \overbrace{v_{c,\gamma}\frac{\partial v_c}{\partial z}}^{b} + g - \frac{1}{\rho_c\epsilon_c}\frac{\partial p_c}{\partial z} \\ &\quad -\frac{1}{\rho_c}\frac{\partial p_l}{\partial z} - \frac{1}{\rho_c\epsilon_c}\Lambda(v_c - v_l) - \frac{1}{\rho_c\epsilon_c}F_\mu\end{aligned} \tag{3.164}$$

where $F_\Lambda = \Lambda(v_c - v_l)$.

In light of the low velocities which occur in a real vessel (typically 1-6 mm/s), one may query the inclusion of the dynamics in v_c (i.e. the acceleration of the chip plug), the force of inertia (i.e. the convective momentum term $-v_c\frac{\partial v_c}{\partial z}$), and the terms which are marked a and b in these equations, since these terms normally are negligible compared to the others. We neglect the terms a and b, c.f. assumption 5 about momentum transfer in Sec. 3.2.2, but include the former two. It is well known that these have important stabilizing effects, c.f. assumption 6 in the same section. This is further discussed in Ch. 7.

As a result, we have the following hyperbolic partial differential equation, from where the chip velocity is computed:

$$\begin{aligned}\frac{\partial v_c}{\partial t} &= -v_c\frac{\partial v_c}{\partial z} + g - \frac{1}{\rho_c\epsilon_c}\frac{\partial p_c}{\partial z} - \frac{1}{\rho_c}\frac{\partial p_l}{\partial z} \\ &\quad -\frac{1}{\rho_c\epsilon_c}\Lambda(v_c - v_l) - \frac{1}{\rho_c\epsilon_c}F_\mu\end{aligned} \tag{3.165}$$

The free liquor

For the free liquor, Eq. (C.2) is expanded in the following form:

$$\begin{aligned}\frac{\partial}{\partial t}\iiint_{V_l}\rho_l\mathbf{v_l}dV_l &= -\oiint_{A_l}\rho_l\mathbf{v_l}\mathbf{v_{l,j}}^T\mathbf{n}dA_l + \iiint_{V_l}\rho_l\mathbf{g}dV_l \\ &\quad -\oiint_{A_l}p_l\mathbf{n}dA_l + \iiint_{V}F_\Lambda dV\end{aligned} \tag{3.166}$$

where the dry friction force against the side walls is neglected. The viscous friction term has opposite sign compared to the equation for the chip phase, c.f. Eq. (3.105). A similar derivation as for the chip plug gives:

$$\frac{\partial v_l}{\partial t} = -v_l\frac{\partial v_l}{\partial z} - \frac{1}{\rho_l}\frac{\partial p_l}{\partial z} + g - \frac{1}{\rho_l\epsilon_l}\Lambda(v_l - v_c) \tag{3.167}$$

The only unknown variable in this equation is the liquor pressure, p_l. For this phase, we do not have an equation of state that relates it to the density of the free liquor because of the incompressibility assumption. This is expressed in Eq. (3.12), which results in Eq. (3.128).

There has been suggested different iterative methods to estimate p_l (see e.g. (Patankar, 1980)). These are based upon the condition that the pressure has to satisfy the continuity equation. Instead of increasing the complexity of the model by including such an estimator, the approach of neglecting the dynamics in Eq. (3.167) is made. Note that the incompressibility assumption does not imply $\frac{\partial v_l}{\partial t} \equiv 0$. However, as argued for the chip plug, the term is normally small compared to the other terms. Further, as we have included the acceleration of the chip plug, this simplification does not complicate the numerical solution considerably. Moreover, even though this acceleration may be substantial under transient periods, these periods will be very short due to the incompressibility. Hence, resulting shock waves through the liquor phase cannot be traced. The resulting stationary elliptic equation is then solved for the pressure gradient:

$$\frac{\partial p_l}{\partial z} = -\rho_l v_l \frac{\partial v_l}{\partial z} + \rho_l g - \frac{1}{\epsilon_l}\Lambda(v_l - v_c) \tag{3.168}$$

If the boundary conditions for the liquor pressure (i.e. the steam pressure and respective the up- and down-stream pressures of the valves in the extraction line, in the wash- and dilution water lines, and in the blow line) are perfectly controlled, these are "driving forces" in the model. Alternatively, if the liquor flows (i.e. velocities) through these valves are perfectly controlled, these will be the driving forces. The application of this is mainly a question of whether the blow flow is a one- or two-phase flow. In the case of two-phase flow, it is necessary to calculate p_l to determine v_l and vice versa. Hence, the resulting set of equations form algebraic loops. When one-phase flow in the blow flow is assumed, this simplifies the numerical solution of the model. These two alternatives are referred to as respective *Alt.1* and *Alt.2* in the sequel. This is discussed further in Secs. 3.6.4 and 4.3.

Further, by substituting Eq. (3.168) in Eq. (3.165), we have:

$$\begin{aligned}\frac{\partial v_c}{\partial t} = &-v_c\frac{\partial v_c}{\partial z} - \frac{1}{\rho_c\epsilon_c}\frac{\partial p_c}{\partial z} + (1 - \frac{\rho_l}{\rho_c})g \\ &-\frac{1}{\rho_c\epsilon_c\epsilon_l}\Lambda(v_c - v_l) - \frac{1}{\rho_c\epsilon_c}F_\mu\end{aligned} \tag{3.169}$$

where the force of inertia for the liquor has been neglected. Hence, the effect of p_l (or its gradient), and its variation due to variations in ϵ_c etc., are implicitly included in Eq. (3.169). Note, however, that calculation of p_l also is necessary for the calculation of the air volume in the chips (c.f. Eq. (3.42)). Further, the liquor level in the digester is often estimated by a measurement of the liquor pressure in the bottom of the digster. Perhaps the greatest disadvantage of *Alt.1* is that it may limit the use of the model in practical applications due to the required measure accuracy of the liquor boundary pressures.

3.6.2 The top section

In the top of the digester (see Fig. 3.2), the mass flow from the top separator is actually decoupled from the bulk flow in the digester. The convective momentum

into the section is therefore a bump (impulse) against the top of the mass. This tiny effect on the velocity out of the section is neglected. As boundary condition for Eq. (3.168) we have:

$$p_l = p_s + \frac{3}{2}\rho_l g h_l - \frac{3}{2}\frac{h_l^{'}}{\epsilon_l}\Lambda(v_l - v_c) \tag{3.170}$$

An estimate for the chip velocity is made by using a numerical adaptation to Eq. (3.165).

3.6.3 The extraction section

Alt.1

In the extraction line (see Fig. 3.1), there is a control valve which is controlled by the valve opening $u_{extr}[m^3/(kg/m)^{-1/2}]$. The pressure down-flow the valve, $p_{l,extr}$ (a boundary condition for Eq. (3.168)) is assumed to be known. The flow through the valve is a sum of the two flows coming from the cooking zone above, and from the wash zone below. Thus, the pressure up-flow the extraction valve, p_l, is a function of the steam pressure, p_s. p_l is computed from Eq. (3.168).

The liquor velocity which gives the boundary condition for Eq. (3.128), may be written as:

$$v_{l,extr} = u_{extr}\sqrt{p_l - p_{l,extr}}/(A\epsilon_l) \tag{3.171}$$

The characteristic of the extraction valve is assumed to be known (u_{extr} includes the valve gain). ϵ_l is the volume fraction of liquor in the zone, and A is the cross section area of the digester.

Alt.2

The liquor flow through the valve, $q_{extr}[m^3/s]$ is a known boundary condition. Hence by Eq. (3.69), the liquor velocity is gives as:

$$v_{l,extr} = q_{extr}/(A\epsilon_l) \tag{3.172}$$

The vertical liquor velocities through the section are given by the continuity equation Eq. (3.128).

3.6.4 The outlet section

The pulp flows into the blow line which has a considerable smaller diameter than the digester, see Fig. 3.3. Appendix D shows that variable cross section area does not influence the momentum balance equations. From Eq. (3.165) we have:

$$\begin{aligned}\frac{\partial v_c}{\partial t} &= -v_c\frac{\partial v_c}{\partial z} + g - \frac{1}{\rho_c\epsilon_c}\frac{\partial p_c}{\partial z} - \frac{1}{\rho_c}\frac{\partial p_l}{\partial z} \\ &\quad -\frac{1}{\rho_c\epsilon_c}F_\Lambda - \frac{1}{\rho_c\epsilon_c}F_\mu + K_\omega(1 - e^{-\omega/\Omega})\end{aligned} \tag{3.173}$$

where $K_\omega(1-e^{-\omega/\Omega})[m/s]$ is the relationship between the bottom scraper speed, ω, and the chip velocity (i.e. the additional driving force for the chip plug). $\Omega[rpm]$ is a parameter. This function has to be established experimentally.

The flow of chips and liquor out of this section is dependent on the opening and characteristics of the blow valve. Further, the transport of chips is helped by the liquor flow. This means that if there is no flow of liquor, there is no outflow of chips either. No data has been found in the literature on the flow characteristics of the blow flow.

Alt.1

Similar as for the extraction section, the liquor flows through the blow valve, and through the side and bottom nozzle valves may be written as:

$$q_l = u_{valve}\sqrt{p_l - p_{bp}} \tag{3.174}$$

where u_{valve} are the control inputs, and p_{bp} are the boundary pressures.

The chip out-flow is a function of the valve opening and its characteristics, u_{out}, the dilution flow, q_{dil}, and the amount of chips in the section (i.e. the chip pressure p_c). We may write this as:

$$q_{c,out} = \begin{cases} K_{out} \cdot u_{out}\sqrt{p_c} & \text{if } q_{dil} > 0 \\ 0 & \text{otherwise} \end{cases} \tag{3.175}$$

where K_{out} $[m^3/(s\sqrt{Pa})]$ is a parameter, and the chip pressure is assumed to be zero downstream the blow valve ($\epsilon_c \leq 0.356$).

Alt.2

The respective flows are expressed as:

$$q_{c,out} = \epsilon_c q_{bf} \tag{3.176}$$

$$q_{l,out} = \epsilon_l q_{bf} \tag{3.177}$$

where q_{bf} is the controlled blow flow $[m^3/s]$.

3.7 Energy balances

This section presents a dynamic model of temperature profiles for the chip plug and the free liquor, based on the conservation law of energy which is stated in Appendix C.

The energy balances support the mass and momentum equations through the chemical reactions (the Arrhenius coefficients, Eq. (3.3)), the diffusion rate coefficients, Eqs. (3.4) and (3.5), and the air volume inside the chips, Eq. (3.42). In

addition, some other temperature dependent parameters connected to the energy balances in the steam zone will be presented in this section.

The boundary conditions are defined by separate ordinary differential equations for volumes bounded to the external control variables.

3.7.1 The main section

In the following, we concentrate on the movement of the chip plug. The derivation is similar for the free liquor.

For the chip plug, Eq. (C.3) is expanded in the following way:

$$\frac{d}{dt}\iiint_{V_c}\rho_c E_c dV_c = -\oiint_{A_c}\rho_c \mathbf{v_{c,j}}^T \mathbf{n} E_c dA_c \tag{3.178}$$

$$-\oiint_{A_c}\mathbf{n}^T\mathbf{v_c}p_c^{'}dA_c - \oiint_{A_c}\mathbf{n}^T\mathbf{v_c}p_l dA_c \tag{3.179}$$

$$-\iiint_{V}\mathbf{n}^T\mathbf{v_c}F_\Lambda dV - \iiint_{V}\mathbf{n}^T\mathbf{v_c}F_\mu dV$$

$$-\oiint_{A_c}\mathbf{Q}_{cz}^T\mathbf{n}dA_c - \oiint_{A_c}\mathbf{Q}_{clw}^T\mathbf{n}dA_c$$

The first term on the right-hand side represents the convection, The second term is the internal pressure work. The third term represents the external pressure work, and then follows the interphase friction (viscous) work and the dry friction work against the side walls of the vessel. Finally, we have vertical heat of conduction, and the sum of the interphase heat of conduction and that through the digester shell. We only consider the vertical component of $v_{c,j}$ in the work terms, v_c.

We substitute $dV_c = \epsilon_c dV$ and $dA_c = \epsilon_c dA$ in the equation:

$$\frac{d}{dt}\iiint_{V}\rho_c\epsilon_c E_c dV = -\oiint_{A}\rho_c\epsilon_c \mathbf{v_{c,j}}^T \mathbf{n} E_c dA \tag{3.180}$$

$$-\oiint_{A}\mathbf{n}^T\mathbf{v_c}p_c^{'}\epsilon_c dA - \oiint_{A}\mathbf{n}^T\mathbf{v_c}p_l\epsilon_c dA$$

$$-\iiint_{V}\mathbf{n}^T\mathbf{v_c}F_\Lambda dV - \iiint_{V}\mathbf{n}^T\mathbf{v_c}F_\mu dV$$

$$-\oiint_{A}\mathbf{Q}_{cz}^T\mathbf{n}\epsilon_c dA - \oiint_{A}\mathbf{Q}_{clw}^T\mathbf{n}\epsilon_c dA$$

The pressure work can be expressed as (c.f. Eq. (D.9) and Eq. (3.90)):

$$-\oiint_{A}\mathbf{n}^T\mathbf{v_c}p_c^{'}\epsilon_c dA - \oiint_{A}\mathbf{n}^T\mathbf{v_c}p_l\epsilon_c dA = -\oiint_{A}\mathbf{n}^T\mathbf{v_c}(p_c + p_l\epsilon_c)dA$$

$$\Downarrow \mathit{Gauss}$$

$$
\begin{aligned}
&= -\iiint_V \nabla(\mathbf{n}^T \mathbf{v_c}(p_c + p_l\epsilon_c))dV \\
&\quad +p_c \iiint_V \nabla(\mathbf{n}^T \mathbf{v_c})dV \\
&\quad +p_l \iiint_V \nabla(\mathbf{n}^T \mathbf{v_c}\epsilon_c)dV \\
&= -\mathbf{n}^T \mathbf{v_c}\epsilon_c \nabla(p_c + p_l)
\end{aligned}
$$

This gives:

$$
\begin{aligned}
\frac{d}{dt}\iiint_V \rho_c\epsilon_c E_c dV \;=\; & -\iiint_V \nabla(\rho_c\epsilon_c {\mathbf{v_{c,j}}}^T \mathbf{n} E_c)dV && (3.181)\\
& -\iiint_V \mathbf{n}^T\mathbf{v_c}\nabla p_c dV - \iiint_V \mathbf{n}^T\mathbf{v_c}\epsilon_c\nabla p_l dV \\
& -\iiint_V \mathbf{n}^T\mathbf{v_c}F_\Lambda dV - \iiint_V \mathbf{n}^T\mathbf{v_c}F_\mu dV \\
& -\iiint_V \nabla(\mathbf{Q}_{cz}^T\mathbf{n}\epsilon_c)dV - \iiint_V \nabla(\mathbf{Q}_{clw}^T\mathbf{n}\epsilon_c)dV && (3.182)
\end{aligned}
$$

In our model, ${\mathbf{v_{c,j}}}^T = [0 \quad 0 \quad v_{c,j}]$, ${\mathbf{v_c}}^T = [0 \quad 0 \quad v_c]$, and $\mathbf{Q}_i^T = [0 \quad 0 \quad Q_i]$. This gives $\mathbf{n}^T\mathbf{v_{c,j}} = v_{c,j}$, $\mathbf{n}^T\mathbf{v_c} = v_c$, , and $\mathbf{Q}_i^T\mathbf{n} = Q_i$. Similar as in the derivation of the mass balances, this gives the partial differential equation:

$$
\begin{aligned}
\frac{\partial}{\partial t}(\rho_c\epsilon_c E_c) \;=\; & -\nabla(\rho_c\epsilon_c v_{c,j}E_c) - v_c\frac{\partial p_c}{\partial z} - v_c\epsilon_c\frac{\partial p_l}{\partial z} && (3.183)\\
& -F_\Lambda v_c - F_\mu v_c - \frac{\partial}{\partial z}(Q_{cz}\epsilon_c) - \nabla(Q_{clw}\epsilon_c)
\end{aligned}
$$

where ∇ operates on z and γ. We expand this equation by writing:

$$
\begin{aligned}
\overbrace{E_c\frac{\partial}{\partial t}(\rho_c\epsilon_c)}^{a} + \rho_c\epsilon_c\frac{\partial E_c}{\partial t} \;=\; & \overbrace{-E_c\nabla(\rho_c\epsilon_c v_{c,j})}^{b} - \rho_c\epsilon_c v_{c,j}\nabla E_c \\
& -v_c\frac{\partial p_c}{\partial z} - \epsilon_c v_c\frac{\partial p_l}{\partial z} \\
& -F_\Lambda v_c - F_\mu v_c \\
& -\epsilon_c\frac{\partial Q_{cz}}{\partial z} - Q_{cz}\frac{\partial \epsilon_c}{\partial z} - \nabla(Q_{clw}\epsilon_c)
\end{aligned}
$$

The terms $a + b$ comprise the mass balance for the chip plug, Eq. (3.111), times E_c. Further, by Eqs. (3.73), (3.74) and (3.75):

$$
\begin{aligned}
\rho_c\epsilon_c v_{c,j}\nabla E_c \;&= (\rho_c\epsilon_c v_c + j_{c,z} + \rho_c\epsilon_c v_{c,\gamma})\nabla E_c \\
&= \rho_c\epsilon_c v_c\frac{\partial E_c}{\partial z}\underbrace{-D_c\frac{\partial(\epsilon_c\rho_c)}{\partial z}\frac{\partial E_c}{\partial z}}_{\star} + \rho_c\epsilon_c v_{c,\gamma}\frac{\partial E_c}{\partial \gamma}
\end{aligned}
$$

Here, the term, $\star$, describes the "dispersion-thermo" effect, a Dufour-like effect which is discussed in Appendix B. This is neglected [11] (assumption 1 in Sec. 3.2.2). This gives:

$$\begin{aligned}\epsilon_c\rho_c\frac{\partial E_c}{\partial t} = & -\epsilon_c\rho_c v_c\frac{\partial E_c}{\partial z} - \epsilon_c\rho_c v_{c,\gamma}\frac{\partial E_c}{\partial \gamma} \\ & -v_c\frac{\partial p_c}{\partial z} - \epsilon_c v_c\frac{\partial p_l}{\partial z} \\ & -v_c F_\Lambda - v_c F_\mu \\ & -\epsilon_c\frac{\partial Q_{cz}}{\partial z} - Q_{cz}\frac{\partial \epsilon_c}{\partial z} - \nabla(Q_{clw}\epsilon_c)\end{aligned} \tag{3.184}$$

The specific energy, E_c, consists of internal energy U_c, kinetic energy $\frac{1}{2}v_c^2$ and potential energy Φ, where $\nabla\Phi = \frac{\partial\Phi}{\partial z} = -g$:

$$E_c = U_c + \frac{1}{2}v_c^2 + \Phi \tag{3.185}$$

In this equation we introduce the specific *enthalpy*, by definition:

$$H \triangleq U + \frac{p}{\rho} \tag{3.186}$$

Here:

$$U_c = H_c - \frac{p_c^{'}}{\rho_c} - \frac{p_l}{\rho_c} = H_c - \frac{p_c}{\rho_c\epsilon_c} - \frac{p_l}{\rho_c} \tag{3.187}$$

H_c can generally be written: [12]

$$H_c = H_c(T_c, p_c^{'}, p_l, \mathbf{c}_c) \tag{3.188}$$

where $\mathbf{c}_c$ is a vector of the respective mass fractions in the chips [kg dry content /kg ODW]:

$$\mathbf{c}_c = [\alpha_{lig} \quad \alpha_{carb} \quad \rho_{EA,el}/\rho_{OWD} \quad \rho_{ds,el}/\rho_{OWD} \quad \rho_{w,el}/\rho_{OWD}] \tag{3.189}$$

Then:

$$\frac{\partial U_c}{\partial t} = \frac{\partial H_c}{\partial t} - \frac{1}{\rho_c\epsilon_c}\frac{\partial p_c}{\partial t} + \frac{p_c}{(\rho_c\epsilon_c)^2}\frac{\partial(\rho_c\epsilon_c)}{\partial t} - \frac{1}{\rho_c}\frac{\partial p_l}{\partial t} + \frac{p_l}{\rho_c^2}\frac{\partial\rho_c}{\partial t} \tag{3.190}$$

where:

$$\begin{aligned}\frac{\partial H_c}{\partial t} = & \left(\frac{\partial H_c}{\partial T_c}\right)_{p_c^{'},p_l,\mathbf{c}_c}\frac{\partial T_c}{\partial t} \\ & +\left(\frac{\partial H_c}{\partial p_c^{'}}\right)_{T_c,p_l,\mathbf{c}_c}\frac{\partial p_c^{'}}{\partial t} \\ & +\left(\frac{\partial H_c}{\partial p_l}\right)_{T_c,p_c^{'},\mathbf{c}_c}\frac{\partial p_l}{\partial t} \\ & +\left(\frac{\partial H_c}{\partial \mathbf{c}_c}\right)_{T_c,p_c^{'},p_l}\frac{\partial \mathbf{c}_c}{\partial t}\end{aligned} \tag{3.191}$$

[11] This may be included in the uncertainty of the vertical conduction term Q_{cz}.

[12] See e.g. (Singstad, 1992) for a comprehensive discussion of these thermodynamic results.

The following coefficients are by definition or from thermodynamic results: [13]

$$(\frac{\partial H_c}{\partial T_c})_{p_c',p_l,\mathbf{c}_c} = C_{pc} \tag{3.192}$$

$$(\frac{\partial H_c}{\partial p_c'})_{T_c,p_l,\mathbf{c}_c} = v_c - T_c(\frac{\partial v_c}{\partial T_c})_{p_c',p_l,\mathbf{c}_c} = \frac{1}{\rho_c} \tag{3.193}$$

$$(\frac{\partial H_c}{\partial p_l})_{T_c,p_c',\mathbf{c}_c} = v_c - T_c(\frac{\partial v_c}{\partial T_c})_{p_c',p_l,\mathbf{c}_c} = \frac{1}{\rho_c} \tag{3.194}$$

$$(\frac{\partial H_c}{\partial \mathbf{c}_c})_{T_c,p_c',p_l} = \Delta\mathbf{h}_r^T \tag{3.195}$$

where:

$$\Delta\mathbf{h}_r = \begin{bmatrix} \Delta h_{lig} \\ \Delta h_{carb} \end{bmatrix} \tag{3.196}$$

Further we have:

$$\frac{\partial p_c'}{\partial t} = \frac{1}{\epsilon_c^2}(\epsilon_c\frac{\partial p_c}{\partial t} - p_c\frac{\partial \epsilon_c}{\partial t}) \tag{3.197}$$

Note that ρ_c is constant when $\mathbf{c}_c$ is constant, i.e. there is no thermic expansion of the chip volume (c.f. assumption 3 in Sec. 3.2.2).

$$-(\frac{\partial v_c}{\partial T_c})_{p_c',p_l,\mathbf{c}_c} = (\frac{\partial \rho_c}{\partial T_c})_{p_c',p_l,\mathbf{c}_c} = 0 \tag{3.198}$$

This gives from Eq. (3.190):

$$\frac{\partial U_c}{\partial t} = C_{pc}\frac{\partial T_c}{\partial t} + \Delta\mathbf{h}_r^T\frac{\partial \mathbf{c}_c}{\partial t} + \frac{1}{\rho_c^2}\frac{\partial \rho_c}{\partial t}(\frac{p_c}{\epsilon_c} + p_l) \tag{3.199}$$

where

$$\frac{\partial \rho_c}{\partial t} = -v_c\frac{\partial \rho_c}{\partial z} - \frac{1}{\epsilon_c}\Delta(D\rho) \tag{3.200}$$

is Eq. (3.116) when Eq. (3.121) is subtracted. Again, we have neglected the mass dispersion.

$\Delta\mathbf{h}_r^T\frac{\partial \mathbf{c}_c}{\partial t}$ only contains the heat of reaction. We write this as:

$$\frac{\partial \mathbf{c}_c}{\partial t} = \begin{bmatrix} -r_{lig} \\ -r_{carb} \end{bmatrix} \tag{3.201}$$

By using assumption 4 in Sec. 3.2.2, we have:

$$\Delta\mathbf{h}_r^T\frac{\partial \mathbf{c}_c}{\partial t} = -\Delta h_{lig}r_{lig} - \Delta h_{carb}r_{carb} \approx -\Delta h_r(r_{lig} + r_{carb}) = -\Delta h_r r \tag{3.202}$$

This term expresses that the chemical reactions are exothermic. Eq. (3.185) then gives:

$$\begin{aligned}\frac{\partial E_c}{\partial t} &= \frac{\partial U_c}{\partial t} + \frac{\partial(\frac{1}{2}v_c^2)}{\partial t} + \frac{\partial \Phi}{\partial t} \\ &= C_{pc}\frac{\partial T_c}{\partial t} - \Delta h_r r - \frac{1}{\rho_c^2}(\frac{p_c}{\epsilon_c} + p_l)(v_c\frac{\partial \rho_c}{\partial z} + \frac{1}{\epsilon_c}\Delta(D\rho)) + v_c\frac{\partial v_c}{\partial t}\end{aligned} \tag{3.203}$$

[13] See e.g. Sonntag and Van Wylen (1991).

Further we have:

$$\begin{aligned}\frac{\partial U_c}{\partial z} &= \frac{\partial H_c}{\partial z} - \frac{\partial}{\partial z}(\frac{p_c}{\rho_c \epsilon_c}) - \frac{\partial}{\partial z}(\frac{p_l}{\rho_l}) \\ &= C_{pc}\frac{\partial T_c}{\partial z} + \frac{1}{\rho_c^2}\frac{\partial \rho_c}{\partial z}(\frac{p_c}{\epsilon_c} + p_l) \end{aligned} \tag{3.204}$$

where we have used that $\Delta \mathbf{h}_r^T \frac{\partial \mathbf{c}_c}{\partial z} = 0$ (there is no heat of reaction caused by the convective transport of mass). Eq. (3.185) then gives:

$$\begin{aligned}\frac{\partial E_c}{\partial z} &= \frac{\partial U_c}{\partial z} + \frac{\partial(\frac{1}{2}v_c^2)}{\partial z} + \frac{\partial \Phi}{\partial z} \\ &= C_{pc}\frac{\partial T_c}{\partial z} + \frac{1}{\rho_c^2}\frac{\partial \rho_c}{\partial z}(\frac{p_c}{\epsilon_c} + p_l) + v_c\frac{\partial v_c}{\partial z} - g \end{aligned} \tag{3.205}$$

Further:

$$\frac{\partial E_c}{\partial \gamma} = (\frac{\partial H_c}{\partial T_c})_{p_c', p_l, \mathbf{c}_c}\frac{\partial T_c}{\partial \gamma} = \bar{C}_p\frac{\partial T_c}{\partial \gamma} \tag{3.206}$$

where $\bar{C}_p = f(C_{p,w} + C_{p,liq})$ is a function of the respective two heat capacities. This may be expressed by:

$$\rho_c \epsilon_c v_{c,\gamma}\frac{\partial E_c}{\partial \gamma} \approx \epsilon_c \bar{C}_p(T_c - T_l)\Delta(D\rho) \tag{3.207}$$

Substituting these expressions into Eq. (3.184), we get:

$$\begin{aligned}\rho_c C_{pc}\frac{\partial T_c}{\partial t} &- \rho_c \Delta h_r r - \frac{1}{\rho_c}(\frac{p_c}{\epsilon_c} + p_l)(\overbrace{v_c\frac{\partial \rho_c}{\partial z}}^{c} + \frac{1}{\epsilon_c}\Delta(D\rho))\overbrace{+\rho_c v_c\frac{\partial v_c}{\partial t}}^{m} \\ &= -v_c\rho_c C_{pc}\frac{\partial T_c}{\partial z}\overbrace{-\frac{v_c}{\rho_c}\frac{\partial \rho_c}{\partial z}(\frac{p_c}{\epsilon_c} + p_l)}^{c}\overbrace{-v_c\rho_c v_c\frac{\partial v_c}{\partial z}}^{m}\overbrace{+v_c\rho_c g}^{m} \\ &\quad -\bar{C}_p(T_c - T_l)\Delta(D\rho)\overbrace{-\frac{v_c}{\epsilon_c}\frac{\partial p_c}{\partial z} - v_c\frac{\partial p_l}{\partial z}}^{m} \\ &\quad \overbrace{-\frac{v_c}{\epsilon_c}F_\Lambda - \frac{v_c}{\epsilon_c}F_\mu}^{m} - \frac{\partial Q_{cz}}{\partial z} - \frac{Q_{cz}}{\epsilon_c}\frac{\partial \epsilon_c}{\partial z} - \frac{1}{\epsilon_c}\nabla(Q_{clw}\epsilon_c) \end{aligned} \tag{3.208}$$

Here, we note that the terms marked c cancel out and the terms marked m comprises the momentum balance equation for the chip plug, Eq. (3.165). Further, the terms connected to the interphase mass transfer, $\Delta(D\rho)$, are neglected (assumption 1 in Sec. 3.2.2).

The terms for heat of conduction are expressed by Fourier's law, c.f. Appendix B:

$$Q_{cz} = -k_{cz}\frac{\partial T_c}{\partial z} \tag{3.209}$$

giving:

$$\frac{\partial Q_{cz}}{\partial z} = -k_{cz}\frac{\partial^2 T_c}{\partial z^2} \tag{3.210}$$

and finally, the last term for heat of conduction, which expresses interphase transfer and transfer through the digester shell, can be written as:

$$\nabla(Q_{clw}\epsilon_c) = (k_{cl}(T_c - T_l) + k_{cw}(T_c - T_a))\epsilon_c \tag{3.211}$$

The temperature for the chip plug is then given by the parabolic equation:

$$\begin{aligned}\frac{\partial T_c}{\partial t} &= -v_c\frac{\partial T_c}{\partial z} + [\rho_c \Delta h_r r + k_{cz}(\frac{\partial^2 T_c}{\partial z^2} + \frac{1}{\epsilon_c}\frac{\partial \epsilon_c}{\partial z}\frac{\partial T_c}{\partial z}) \\ &\quad -k_{cl}(T_c - T_l) - k_{cw}(T_c - T_a)]/(C_{pc}\rho_c)\end{aligned} \tag{3.212}$$

and equivalently for the free liquor phase:

$$\frac{\partial T_l}{\partial t} = -v_l\frac{\partial T_l}{\partial z} + [k_{lz}(\frac{\partial^2 T_l}{\partial z^2} + \frac{1}{\epsilon_l}\frac{\partial \epsilon_l}{\partial z}\frac{\partial T_l}{\partial z}) - k_{cl}(T_l - T_c) - k_{lw}(T_l - T_a)]/(C_{pl}\rho_l) \tag{3.213}$$

The factors which include the heat capacities are expressed as $C_{pc}\rho_c = C_{p,w}((\alpha_{lig} + \alpha_{carb})\rho_{ODW} + \rho_{ds,el}) + C_{p,liq}(\rho_{EA,el} + \rho_{w,el})$ and $C_{pl}\rho_l = C_{p,w}\rho_{ds,fl} + C_{p,liq}(\rho_{EA,fl} + \rho_{w,fl})$.

The first term on the right-hand side of Eq. (3.212) describes the heat of convection, i.e. heat connected to vertical convection of mass. The second term expresses the heat of chemical reaction, and the third term describes vertical heat of conduction. Note that the term $k_{lz}\frac{1}{\epsilon_l}\frac{\partial \epsilon_l}{\partial z}\frac{\partial T_l}{\partial z}$ accounts for compaction gradients. The fourth term represents heat of conduction between the two phases, and the last term accounts for heat of conduction through the side walls of the vessel.
Eq. (3.213) contains the same type of terms, except for the heat generation by the chemical reactions.

3.7.2 The steam zone

When the mass leaves the top separator, it comes immediately in contact with high pressure steam to be heated rapidly up near to the cooking temperature of about 170^oC. The colder mass makes the steam condense on the surfaces of the chip and the free liquor. This contributes to the water balance as well. The zone is illustrated in Fig. 3.12.

There are three phases in this zone; the chips, the excess of free liquor from the top separator, and the high pressure steam. The steam is assumed to be saturated, well mixed, and perfectly controlled; both with respect to pressure and temperature. An energy balance for this phase is therefore not considered. The steam temperature, T_s, and pressure, p_s, are then control inputs in the model. Because the steam is saturated, the free liquor does not evaporate.

Figure 3.12: The steam zone

The chips and the free liquor fall down through the steam with final velocities given by the mechanical energy balance:

$$\begin{aligned} \text{Kinetic energy} &= \text{Lost potential energy} \\ \frac{1}{2}v_i^2 &= g(h_s - h_i) \\ v_i &= \sqrt{2g(h_s - h_i)} \end{aligned}$$

By using $v_{c,s} = \frac{1}{2}v_c$ and $v_{l,s} = \frac{1}{2}v_l$, mass and momentum balance equations for the chips and the free liquor are not derived for this zone. Then, it is not possible to set up a macroscopic energy balance. Instead, we use a numerical adaption of the microscopic balance as derived for the main section. It may be argued that the above velocity equations are rather rough estimates. However, with respect to the liquor velocity, the lower part of the fall is not a free fall when the liquor level is below the chip level (typically a difference of $1.5 - 2.0$ meters). Condensation of steam occurs, however, here on the free liquor.

Since the mass falls fast in this zone, the vertical heat of conduction terms are negligible.
The heat transfer between the steam and the mass consists of *latent heat of conden-*

sation and *sensible heat transfer*. The former can be written as (see e.g. Coulson and Richardson (1977)):

$$Q_{cond,i} = D_{cond,i}\frac{\rho_{air}}{\epsilon_i}(\xi_s - \xi_i)\lambda_w \tag{3.214}$$

with dimension $J/(sm^3$ of phase $i)$. The volume fraction of the respective phase, ϵ_i, is a function of the feed flow of chips and liquor, i.e. the L/W-ratio. The specific latent heat of condensation, λ_w, is equal to the latent heat of vaporization of water. By means of the least squares method, and data from thermodynamic tables (see e.g. Coulson and Richardson (1977)), a second order function of temperature, T, for λ_w is derived, see Fig. 3.13:

$$\lambda_w = 2501.6 - 2.275T - 0.0018T^2 \tag{3.215}$$

This function tells how many kilo Joule which are transfered to the chips or the free liquor when 1 kg of water is condensed on their respective surfaces. Their surfaces are assumed to have the temperature T_i, $i = c, l$.

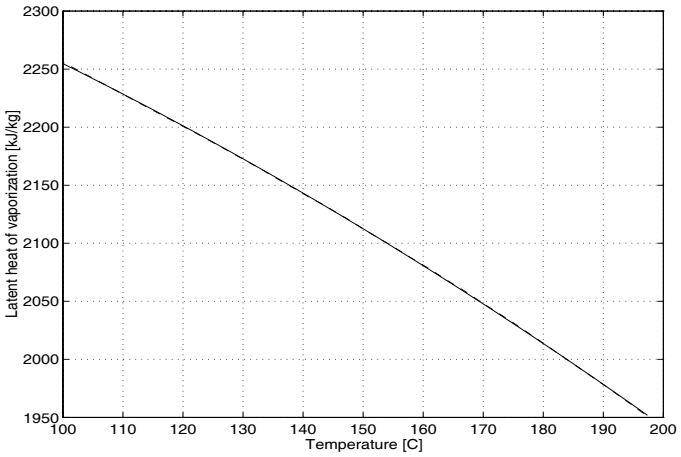

Figure 3.13: The temperature dependency for the latent heat of vaporization of water. The second order approximation (solid line) and data from thermodynamic tables (dashed line).

ξ_s is the *absolute humidity* for the saturated steam (i.e. 100% relative humidity), while ξ_i is the absolute humidity for the saturated steam at the surface of phase i, corresponding to the temperature of the steam at the surface. The humidity can be expressed as:

$$\xi = [p_{s,p}/(p_s - p_{s,p})]\frac{M_{water}}{M_{air}} \tag{3.216}$$

where $M_{water} = 18.0\frac{kg}{kmol}$, $M_{air} = 29.0\frac{kg}{kmol}$ and the steam pressure is given as $p_s = p_{s,p} + p_{air}$. The *partial saturated pressure* for the steam, $p_{s,p}$, is also uniquely dependent on temperature. From thermodynamic tables, the following 2nd order polynomial is derived, see Fig. 3.14:

$$p_{s,p} = 10^3(941.0770 - 18.8947T_s + 0.1055T_s^2) \tag{3.217}$$

Alternatively, we may use the *Clausius -Clapeyron* equation (see e.g. Sonntag and Van Wylen (1991)):

$$p_{s,p} = p_{s,p,0} e^{\frac{\lambda_{w,0} M_{water}}{R}(\frac{1}{T_{s,0}+273.2} - \frac{1}{T_s+273.2})} \tag{3.218}$$

where $(p_{s,p,0}, T_{s,0}, \lambda_{w,0})$ is a point on the saturated steam curve.

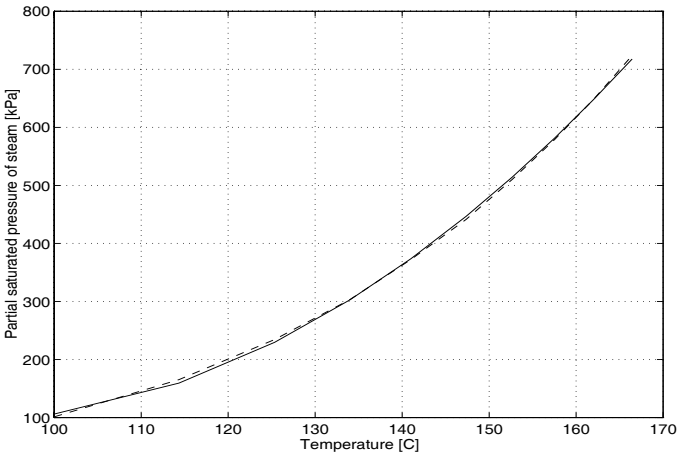

Figure 3.14: The temperature dependency for the partial saturated pressure of steam. The second order approximation (solid line) and data from thermodynamic tables (dashed line).

At $(101.3kPa, 100^oC, 2257.6kJ/kg)$ we have:

$$p_{s,p} = 101.3 \cdot 10^3 e^{4887.8(\frac{1}{373.2} - \frac{1}{273.2+T_s})} \tag{3.219}$$

[14] The density of dry air is approximated by using the equation of state for an ideal gas (Eq. (3.41)) $pV = nRT$, which gives:

$$\rho_{air} = \frac{n_{air}}{V} M_{air} 10^{-3} = \frac{p_{air}}{RT_{air}} M_{air} 10^{-3} \tag{3.220}$$

where T_{air} has dimension $[K]$. With $[^oC]$ as dimension for T_{air}, and by using $T_{air} = T_s$, we have:

$$\rho_{air} = 29.0 \cdot 10^{-3} \frac{p_{air}}{R(273.16 + T_s)} mol \tag{3.221}$$

where $p_{air} = p_s - p_{s,p}$.

This gives the latent heat transfer by condensation:

$$Q_{cond,i} = 18.0 \cdot 10^{-3} \lambda_w(T_i) \frac{D_{cond,i}}{R(T_s + 273.16)\epsilon_i} (p_{s,p}(T_s) - p_{s,p}(T_i)) \tag{3.222}$$

[14] It should be noted that Eq. (3.217) gives e.g. about $24kPa$ lower value at $T_s = 170^oC$ compared to Eq. (3.219). This corresponds to a temperature difference of about 3^oC in the chip temperature.

Note that the steam pressure, p_s, is cancelled out. The sensible heat transfer can be written equivalently Eq. (3.211) as:

$$k_{is}(T_i - T_s) \tag{3.223}$$

Finally, the heat transfer through the digester shell is:

$$k_{iw}(T_i - T_a) \tag{3.224}$$

Due to the short residence times in this zone, the heat of reaction is ignored. The chip and the free liquor temperatures are then given by:

$$\frac{dT_{c,s}}{dt} = -v_{c,s}\frac{T_{c,s} - T_s}{h_s - h_c} + [Q_{cond,c} - k_{cl}(T_{c,s} - T_s) - k_{cw}(T_{c,s} - T_a)] /(C_{pc}\rho_c) \tag{3.225}$$

$$\frac{dT_{l,s}}{dt} = -v_{l,s}\frac{T_{l,s} - T_s}{h_s - h_l} + [Q_{cond,l} - k_{lz}(T_{l,s} - T_s) - k_{lw}(T_{l,s} - T_a)] /(C_{pl}\rho_l) \tag{3.226}$$

The consumption of steam due to the condensation, makes it necessary to add steam continuously. Otherwise, the pressure and temperature in the steam will decrease, and the steam will not stay saturated. The kilo-flow of added steam, $[kg$ water $/s]$ accounts both for this condensation and also for varying liquor level in the digester. These variations act on the steam pressure/temperature and also on the humidification. A good energy control structure for the high pressure steam should therefore include both a humidification loop, and a temperature, or pressure, loop.

3.7.3 The top section

When the chips have settled on the top of the mass, see Fig. (3.2), we assume that the free liquor, which enters simultaneously, is still in the steam zone. This means that the free liquor covers the chips while it flows down and settles on the liquor level where it becomes a part of the top section. Hence, there is no steam-chip contact in this section, and thus either no condensation. Further, the free liquor which comes from the steam zone, and becomes a part of the top section, is continuously replaced by new liquor coming from above. Hence, there is either no steam-liquor contact in this section.
The chip and the free liquor temperatures, $T_{c,t}$ and $T_{l,t}$, are given by macroscopic balances similar to Eqs. (3.225) and (3.226), (c.f. Eqs. (3.212) and (3.213)):

$$\begin{aligned}\frac{dT_{c,t}}{dt} = &-v_c\frac{T_{c,t} - T_{c,s}}{h_c'} + [\rho_c \Delta h_r r \\ &+k_{cz}(\frac{\partial^2 T_{c,t}}{\partial z^2} + \frac{1}{\epsilon_c}\frac{\partial \epsilon_c}{\partial z}\frac{\partial T_{c,t}}{\partial z}) \\ &-k_{cl}(T_{c,t} - T_{l,s}) - k_{cw}(T_{c,t} - T_a)]/(C_{pc}\rho_c)\end{aligned} \tag{3.227}$$

$$\begin{aligned}\frac{dT_{l,t}}{dt} = &-v_l\frac{T_{l,t} - T_{l,s}}{h_l'} + [k_{lz}(\frac{\partial^2 T_{l,t}}{\partial z^2} + \frac{1}{\epsilon_l}\frac{\partial \epsilon_l}{\partial z}\frac{\partial T_{l,t}}{\partial z}) \\ &-k_{lz}(T_l - T_s) - k_{lw}(T_l - T_a)]/(C_{pl}\rho_l)\end{aligned} \tag{3.228}$$

where $T_{c,s}$ and $T_{l,s}$ are the respective phase temperatures in the steam zone.

3.7.4 The outlet section

Regarding the chip phase, the equation for the main section is used. The free liquor temperature is given by the inlet temperature of the diluting water, see Fig. 3.3.

3.7.5 The liquor circulations

The zones which cover the liquor circulation screens define boundary conditions for the energy balance of the liquor. Regarding the chip phase, the equation for the main section is used. In the energy balance for the liquor, a convection term is added, which describes the net input energy flow for the respective heat exchanger:

$$\frac{\partial T_{l,circ}}{\partial t} = \frac{\partial T_l}{\partial t} - q_{circ}\frac{(T_l - T_{he})}{A\epsilon_{l,i}z_i} \tag{3.229}$$

$\frac{\partial T_l}{\partial t}$ is given by Eq. (3.213), q_{circ} is the respective circulation volume flow, $\epsilon_{l,i}$ is the volume fraction of liquor in the zone, z_i is the length of the zone, and T_{he} is the controlled temperature on the secondary side of the respective heat-exchanger. Hence, the temperature controls of the heat-exchangers are implicitly included in the model by assuming perfect control.

3.8 Rescaling of the equations

There are mainly two reasons for rescaling a mathematical model which is based on physical quantities:

1. There may be large numerical differences between the values of some of the time differential variables. This causes the final state space model to become artificially stiff.
2. The model parameters are lumped into fewer parameters. In this way, e.g. parameter estimation is facilitated. In our context, this also means that the resulting parameters become *dimensionless groups* which have got their name in the literature. Thus, some characteristics of our model may easily be compared to other flow-models.

In our model, we are primarily interested in reducing the artificial stiffness. The model is made dimensionless by rescaling the variables by the characteristic quantities as given in Table 3.2. The dimensionless variables are (see e.g. Bird et al. (1960)) $z^* = z/d$, $t^* = t/t_0$, $v^* = v/v_0$, $p^* = (p - p_0)/(\rho_0 v_0^2)$, $T^* = T/T_0$, and $\rho^* = \rho/\rho_0$. Because the volume fractions and mass fractions are dimensionless and normalized, these are not rescaled. The result is that the state variables have values in the same numerical range. This is a great advantage in the numerical solution. Note that the rescaling does not change the gain between the inputs and

Symbol	Description	Dimension
d	cross section diameter used as reference length	m
p_0	reference pressure	Pa
ρ_0	reference density	kg/m^3
v_0	reference velocity	m/s
T_0	reference temperature	^oC
t_0	$= d/v_0$ characteristic time variable	s

Table 3.2: Characteristic quantities for the rescaling of the model variables

outputs in the model. The dimensionless partial differential equations are here shown for the main section.

$$\frac{\partial \epsilon_c}{\partial t^*} = -\frac{\partial}{\partial z^*}(\epsilon_c v_c^*) + \frac{1}{Pe_c}\frac{\partial^2 \epsilon_c}{\partial z^{*2}} \tag{3.230}$$

$$\frac{\partial v_l^*}{\partial z^*} = \frac{1}{1-\epsilon_c}((v_l^* - v_c^*)\frac{\partial \epsilon_c}{\partial z^*} - \epsilon_c \frac{\partial v_c^*}{\partial z^*} + (\frac{1}{Pe_c} - \frac{1}{Pe_l})\frac{\partial^2 \epsilon_c}{\partial z^{*2}}) \tag{3.231}$$

$$\frac{\partial \alpha_{lig}}{\partial t^*} = -v_c^* \frac{\partial \alpha_{lig}}{\partial z^*} - t_0 r_{lig} + \frac{1}{Pe_c}\frac{\partial^2 \alpha_{lig}}{\partial z^{*2}} \tag{3.232}$$

$$\frac{\partial \alpha_{carb}}{\partial t^*} = -v_c^* \frac{\partial \alpha_{carb}}{\partial z^*} - t_0 r_{carb} + \frac{1}{Pe_c}\frac{\partial^2 \alpha_{carb}}{\partial z^{*2}} \tag{3.233}$$

$$\frac{\partial \rho_{EA,el}^*}{\partial t^*} = -v_c^* \frac{\partial \rho_{EA,el}^*}{\partial z^*} - t_0 \rho_{ODW}(\frac{b_{lig} r_{lig}}{\rho_{EA,0}} \tag{3.234}$$

$$+\frac{b_{carb}\rho_{carb}}{\rho_{EA,0}}) - \frac{1}{Sc_{EA}\epsilon_c}(\rho_{EA,el}^* - \rho_{EA,fl}^*) + \frac{1}{Pe_c}\frac{\partial^2 \rho_{EA,el}^*}{\partial z^{*2}}$$

$$\frac{\partial \rho_{ds,el}^*}{\partial t^*} = -v_c^* \frac{\partial \rho_{ds,el}^*}{\partial z^*} + t_0 \rho_{ODW}(\frac{(1+b_{lig})r_{lig}}{\rho_{ds,0}} \tag{3.235}$$

$$+\frac{(1+b_{carb})r_{carb}}{\rho_{ds,0}}) - \frac{1}{Sc_{ds}\epsilon_c}(\rho_{ds,el}^* - \rho_{ds,fl}^*) + \frac{1}{Pe_c}\frac{\partial^2 \rho_{ds,el}^*}{\partial z^{*2}}$$

$$\frac{\partial \rho_{EA,fl}^*}{\partial t^*} = -v_l^* \frac{\partial \rho_{EA,fl}^*}{\partial z^*} + \frac{1}{Sc_{EA}\epsilon_l}(\rho_{EA,el}^* - \rho_{EA,fl}^*) + \frac{1}{Pe_l}\frac{\partial^2 \rho_{EA,fl}^*}{\partial z^{*2}} \tag{3.236}$$

$$\frac{\partial \rho_{ds,fl}^*}{\partial t^*} = -v_l^* \frac{\partial \rho_{ds,fl}^*}{\partial z^*} + \frac{1}{Sc_{ds}\epsilon_l}(\rho_{ds,el}^* - \rho_{ds,fl}^*) + \frac{1}{Pe_l}\frac{\partial^2 \rho_{ds,fl}^*}{\partial z^{*2}} \tag{3.237}$$

$$\frac{\partial v_c^*}{\partial t^*} = -v_c^* \frac{\partial v_c^*}{\partial z^*} - \frac{\rho_{c,0}}{\rho_c^{*'}\epsilon_c}\frac{\partial p_c^*}{\partial z^*} - \frac{\rho_{l,0}}{\rho_c^{*'}}\frac{\partial p_l^*}{\partial z^*} + \frac{1}{Fr} - \frac{d}{v_0^2}\frac{1}{\epsilon_c \rho_c^{*'}}F_\mu \tag{3.238}$$

$$-\frac{\rho_{c,0}}{\rho_c^{*'} Re_{\Lambda,c}\epsilon_c}(v_c^* - v_l^*) \tag{3.239}$$

$$\frac{\partial p_l^*}{\partial z^*} = -\frac{\rho_l^{*'}}{\rho_{l,0}} v_l^* \frac{\partial v_l^*}{\partial z^*} + \frac{\rho_l^{*'}}{\rho_{l,0}}\frac{1}{Fr} - \frac{1}{Re_{\Lambda,l}(1-\epsilon_c)}(v_l^* - v_c^*) \tag{3.240}$$

$$\frac{\partial T_c^*}{\partial t^*} = -v_c^* \frac{\partial T_c^*}{\partial z^*} + \frac{\rho_c^* \rho_{c,0} d\Delta h_r r}{v_0 T_0 (C_{pc}\rho_c)^{*'}} \tag{3.241}$$

$$+\frac{1}{Re_c Pr_c}(\frac{\partial^2 T_c^*}{\partial z^{2*}}+\frac{1}{\epsilon_c}\frac{\partial \epsilon_c}{\partial z^*}\frac{\partial T_c^*}{\partial z^*})$$
$$-St_{cl}(T_c^*-T_l^*)-St_{cw}(T_c^*-T_a^*)$$

$$\frac{\partial T_l^*}{\partial t^*} = -v_l^*\frac{\partial T_l^*}{\partial z^*}+\frac{1}{Re_l Pr_l}(\frac{\partial^2 T_l^*}{\partial z^{2*}}+\frac{1}{\epsilon_l}\frac{\partial \epsilon_l}{\partial z^*}\frac{\partial T_l^*}{\partial z^*}) \tag{3.242}$$
$$-St_{lc}(T_l^*-T_c^*)-St_{lw}(T_l^*-T_a^*)$$

The *Peclet numbers* $Pe_c = v_0 d/D_c$ and $Pe_l = v_0 d/D_l$ respectively express the relationship between the convective and the dispersive terms for the chip plug and the free liquor, the *Schmidt numbers* $Sc_{EA} = v_0/(D_{EA}d)$ and $Sc_{ds} = v_0/(D_{ds}d)$ express the relationship between the convective mass transport and the interphase mass transfer of alkali and dissolved solids between the two phases. The *Froude number* $Fr = v_0^2/(dg)$ expresses the relationship between the force of inertia and the force of gravity, while the *Reynolds numbers* $Re_{\Lambda,i} = \rho_{i,0}v_0/(\Lambda d)$ express the relationship between the force of inertia and the viscous friction force between the phases. [15] $(C_{pi}\rho_i)^{*'}$ and $\rho_i^{*'}$ are $C_{pi}\rho_i$ and ρ_i, with the respective reference values $\rho_{EA,0}$, $\rho_{ds,0}$ and $\rho_{w,0}$ inserted.

The *Stanton numbers*:

$$St_{ij} = \frac{Nu_{ij}}{Re_i Pr_i},\ Nu_{ij} = \frac{d^2 k_{ij}}{k_{iz}} \tag{3.243}$$

express the relationship between the interphase heat of conduction and the vertical heat of convection. Nu_{ij} are the *Nusselt numbers* $i = c, l$, $j = c, l, w$. The products between the *Reynolds numbers* and the *Prandtl numbers*:

$$Re_c Pr_c = \frac{(C_{pc}\rho_c)^{*'}dv_0}{k_{cz}}$$
$$Re_l Pr_l = \frac{(C_{pl}\rho_l)^{*'}dv_0}{k_{lz}}$$

express the relationship between the heat transport by the vertical convection and the vertical conduction.

Note that the products between the Reynolds numbers and Prandtl numbers are not just parameters, but include time differential variables. The reason for not extracting only parameters in these numbers is that it is not possible to separate $\rho_{EA,el}$, $\rho_{ds,el}$ etc. from $(C_{pc}\rho_c)^{*'}$.

[15] The Reynolds number is normally used as the name of the dimensionless group expressing the relationship between the force of inertia, $\rho_{i,0}v_0^2/d$, and the viscous eddy diffusion force, $\eta v_0/d^2$, (Bird et al., 1960). There has not been found any name for the dimensional group $\rho_{i,0}v_0/(\Lambda d)$ in the literature. Since the viscous eddy diffusion force is neglected in this study and Λv_0 is a viscous force as well, the term Reynolds number with subscript Λ is used for this expression.

Chapter 4

Numerical solution

4.1 Introduction

Numerical solution of the Navier-Stokes (NS) equations, i.e. dynamic mass- and momentum balances, [1] is widely known to be a nontrivial task. As one can imagine, a two-phase form of the NS equation, such as the one considered in this study, is not offering fewer problems. The key problem is connected to the momentum balances, where small perturbations in the pressure fields place large requirements on the numerical algorithms in the calculation of the velocity (Patankar, 1980). Moreover, as discussed earlier, we have omitted the term for turbulent diffusion. Often, this is included in the momentum balance, since this is an important term for numerical stability reasons as well. In this form, the equation is denoted *parabolic*. When this term is omitted, the balance equation is *hyperbolic*. In hyperbolic equations, the numerical stability is strongly dependent on the boundary conditions.
In this study, the finite difference method (FDM) is used to solve the PDEs. One advantage of this method (compared to the other main category of methods; the finite element methods (FEM)) is that it is quite straitforward to implement.

This chapter includes discussions on some selected topics which are related to the numerical solution of the model. These are the method which is used for the spatial discretization, a discussion of the model structure, and some other aspects connected to simulator tuning. The numerical solution of this problem is critical. Hence, we have given this broader attention.

[1] The term Navier-Stokes equation refers actually to the dynamic momentum balance equation for constant density and viscosity (Bird et al., 1960). However, it is common to refer to the set of mass- and momentum balance equations in the general form, as the Navier-Stokes equations as well.

4.2 Spatial discretization

The mass and momentum balances

The PDEs describing the mass and momentum balances are discretized in the vertical direction z by the MAC (Marker And Cell) method (Welch, Harlow, Shannon and Daly, 1966). This is a *staggered grid* method where the mass and momentum balances are solved in overlapping control volumes, see Fig. 4.1. The diagonal terms, i.e. $\partial\rho/\partial z(z = z_m)$ in the mass balances, are approximated by mid point differences $((\rho(z = z_{m+1}) - \rho(z = z_{m-1}))/\Delta z)$, while the cross terms, i.e. $\partial v/\partial z(z = z_m)$ in the mass balances, are approximated by central differences $((v(z = z_{m+1/2}) - v(z = z_{m-1/2}))/\Delta z)$. The same apply for the momentum balances.

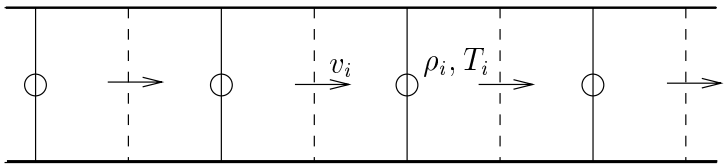

Figure 4.1: Staggered control volumes as used in the MAC method

This numerical discretization method is well suited for our model for two reasons. First, because of the parabolic structure of the mass balances. Second, and most important, because the model variables are dependent on both up- and downstream conditions. The advantages of the method are twofold. For a control volume for the mass balances, e.g. the discretized compaction equation Eq. (3.121) contains the difference between *adjacent* chip velocity components, i.e. the velocities at the boundaries of the control volume. Hence, only "reasonable" (i.e. uniform) velocity fields will have the possibility of being acceptable to the equation. Second, the pressure difference between two adjacent grid points for the mass balances becomes the natural driving force for the velocity component located between these grid points. Consequently, only "reasonable" pressure fields will be acceptable as solutions (Patankar, 1980).

The energy balances

The convection is dominant as the vertical heat transfer is concerned, see Sec. 5.1. Hence, the downstream temperatures have no significant influence on the temperature at a given location. Therefore, solving the vertical heat transfer terms by central differences is numerically unsuccessful. The PDEs are instead discretized by the Euler backward method, see e.g. Mitchell and Griffiths (1990).

4.3 Resulting model structure

The resulting set of equations from the spatial discretization is a complex nonlinear coupled and mixed set of both ordinary differential equations (ODEs) and algebraic equations. In a compact form, the model can be written as:

$$\dot{\mathbf{x}}_1(t) = \mathbf{f}_1(\mathbf{x}_1(t), \mathbf{x}_2(t)) \tag{4.1}$$

$$0 = \mathbf{f}_2(\mathbf{x}_1(t), \mathbf{x}_2(t)) \tag{4.2}$$

where $\mathbf{x}_1(t)$ and $\mathbf{x}_2(t)$ are vectors of the differential and algebraic variables respectively. *Alt.1* (c.f. Sec. 3.6.1), comprises a set of *semi-explicit* equations. This means that all variables are expressed explicitly on the left-hand side, but there are also algebraic loops between variables (hence the name semi-explicit).

The algebraic loops are comprised by the calculation of the liquor pressure, p_l, and the liquor velocity, v_l in *Alt.1* (c.f. the discussion at the end of Sec. 3.6.1). This form is classified as a *semi-explicit nonlinear DAE* (Differential Algebraic Equations). Here, $(\partial f_2/\partial y)^{-1}$ exists and is bounded in a neighbourhood of the exact solution. In *Alt.2* the algebraic loops are omitted because the liquor flows are controlled variables. Hence, this formulation is *explicit nonlinear DAE*.

Eq. (4.1) is a special case of the general fully-implicit nonlinear DAE:

$$\mathbf{F}(t, \mathbf{x}(t), \dot{\mathbf{x}}(t)) = 0 \tag{4.3}$$

The following discussion is based on Brenan, Campbell and Petzold (1989), where a comprehensive discussion of numerical solution of such systems can be found.

A property known as the *index* plays a key role in the classification and behaviour of DAEs.

Definition *The minimum number of times that all or part of the DAE Eq. (4.3) must be differentiated with respect to t in order to determine $\dot{\mathbf{x}}$ as a continuous function of $\mathbf{x}, t$, is the index of the DAE.*

Accordingly, ODEs (explicit and implicit) have index zero. Hence, ODEs are special cases of DAEs. This means that DAEs require more stringent criteria to guarantee a unique solution than is the case for ODEs. Hence, the numerical solutions of DAEs require more attention to the numerical algorithms and the *initial conditions* than is the case for ODEs. This leads us to another key property regarding DAEs, *consistent initial conditions*, which is defined in the following statements:

1. *The solution of the linear constant coefficient DAE*

$$A\dot{\mathbf{x}} + B\mathbf{x} = f \tag{4.4}$$

can involve derivatives of order $k-1$ (where k is the index) of the forcing function f if the DAE is higher index.

2. *Not all initial conditions of Eq. (4.4) admit a smooth solution if $k \geq 1$. Those that do admit solutions are called consistent initial conditions.*

3. *Higher index DAEs can have hidden algebraic constraints.*

Even though the statements above are valid for linear constant coefficient DAEs, a generalization to nonlinear DAEs locally may be made. The theory is still under development for nonlinear systems.

Our DAE (4.1) as *Alt.1* is a semi-explicit index one system. Such systems are an important subset of index one systems which arise frequently in problems in science and engineering. It is notable that initial conditions (as for ODEs) only have to be specified for the *differential variables*, and not for the *algebraic variables*. This is because the algebraic variables are all given semi-explicitly as functions of the differential variables. However, the semi-explicit form means that an iterative equation solver is needed to solve the algebraic loops. This is not the case when the model is formulated as *Alt.2*. Hence, in this case the DAE is an (explicit) index zero system.

As an important model reduction step, the momentum balance equation for the chip plug could be solved as a steady-state equation (i.e. as an algebraic equation). This will reduce the stiffness in the model considerably and speed up the simulations a lot (c.f. the discussion about the eigenvalues in Sec. 6.2.3). When we omit the force of inertia, this gives:

$$v_c^* = v_l^* + Re_{\Omega,c}\frac{\rho_c^{*'}\epsilon_c}{\rho_{c,0}}(-\frac{\rho_{c,0}}{\rho_c^{*'}\epsilon_c}\frac{\partial p_c^*}{\partial z^*} - \frac{\rho_{l,0}}{\rho_c^{*'}}\frac{\partial p_l^*}{\partial z^*} + \frac{1}{Fr} - \frac{d}{v_0^2}\frac{1}{\epsilon_c\rho_c^{*'}}F_\mu) \tag{4.5}$$

The total DAE (*Alt.1*) is now still of index one (since v_c^* still can be solved explicitly), but the attention to the specification of consistent initial conditions must now be intensified. In *Alt.2*, however, the index is increased to index one. This is further discussed in Sec.7.3.

Consider the resulting DAE, *Alt.1*, when Eq. (3.168) is replaced by Eq. (3.167), i.e. the dynamic momentum balance for the liquor. Since p_l only occurs implicit in Eq. (3.167), the resulting DAE is index two. However, as discussed in Sec. 3.6.1, there are no practical reasons for our model to keep the index two structure. Hence, index reduction is essential when considering DAEs. However, index reduction is not always possible or desirable. The special treatment of index two and higher index systems, as well as index reduction methods are discussed broadly by Brenan et al. (1989).

Finally, note that the use of Eq. (3.169), i.e. *Alt.2*, gives fewer equations in the DAE, compared to *Alt 1.* Hence, this has (limited) effect on the simulation speed as well. In the simulations which are shown in this thesis, *Alt.2* is used where the momentum balance for the chip plug is retained as a dynamic equation (index zero DAE).

4.4 Some further numerical aspects

In the previous section, the attention to the specification of consistent initial conditions was stressed. Apart from a proper specification of boundary conditions, smooth solutions of nonlinear DAEs require attention to some other important topics as well:

1. Choice of model parameters, e.g. mass-, friction-, and heat transfer coefficients.
2. Tuning of the input variables, e.g. feed flows and densities, liquor circulation temperatures etc.
3. The number of spatial discretization grids.
4. Algorithm for the time integration, time-step size and limits for the numerical tolerance.

The implicit Adams-Moulton and Gear predictor-corrector methods, see e.g. Shampine and Gordon (1990), are used in the simulations which are presented in this thesis. Note that the accuracy of the solution depends on the sum of the spatial and time discretization errors.

Chapter 5

Simulation results

In this chapter, the properties of the model are investigated. First, a steady-state dimensional analysis, i.e. quantitative analysis of the included effects, is treated in Sec. 5.1. Next, steady-state profiles are discussed in Sec. 5.2. Finally, the dynamic behaviour of the model is analysed in Sec. 5.3. The conditions in a typical industrial Kamyr digester, as referred to in Appendix I, have been simulated. The results have been evaluated by running audits with recognized persons within the pulp and paper industry (Christensen, Kleppe and Kirkebak, 1994).

The numerical solution is based on a spatial discretization of the PDEs into 21 grid points. The grid spacing is 1 metre in the cooking zone, 2 metres in the upper part and 4 metres in the lower part of the wash zone. This results in 226 state (or ordinary differential) equations and a corresponding number of algebraic equations. Referring to the profiles that are shown, the horizontal axis denotes the vertical distance from the bottom of the vessel, see Fig. 5.1. The extraction screens are located at $26m$, the cooking circulation screens at $33m$, while the top section starts at $38.5m$.

5.1 Dimensional analysis

In this section, the size of each term in the equations, and their relative importance at steady-state, are analysed for the two operating points; the high production rate (HPR) and the low production rate (LPR). The values are calculated for a point at the end of the cooking zone, i.e. at level $28m$ above the bottom of the vessel, see Fig. 5.1.

Lignin and carbohydrate balances

$$\frac{\partial \alpha_{lig}}{\partial t^*} = \overbrace{-v_c^* \frac{\partial \alpha_{lig}}{\partial z^*}}^{a} \overbrace{-t_0 r_{lig}}^{b} + \overbrace{\frac{1}{Pe_c} \frac{\partial^2 \alpha_{lig}}{\partial z^{*2}}}^{c}$$

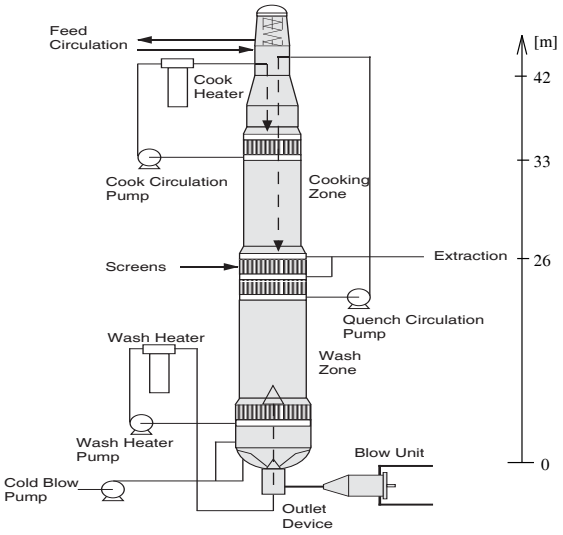

Figure 5.1: The horizontal axis in the profile plots

$$\frac{\partial \alpha_{carb}}{\partial t^*} = \overbrace{-v_c^* \frac{\partial \alpha_{carb}}{\partial z^*}}^{d} \overbrace{-t_0 r_{carb}}^{e} + \overbrace{\frac{1}{Pe_c} \frac{\partial^2 \alpha_{carb}}{\partial z^{*2}}}^{f}$$

The values for each term in the above equations are shown for the two operating points in Table 5.1. This shows that both the convective and the reactive terms

Term	HPR	LPR
a	0.0177	0.0115
b	-0.0186	-0.0126
c	0.0009	0.0011
d	0.0135	0.0088
e	-0.0143	-0.0098
f	0.0008	0.0010

Table 5.1: Steady-state values of the terms in the wood solid equations

are most important, as they have values in the same order, whereas the dispersive terms in this case comprise only $10 - 12\%$ of the former ones. This is due to the low value of the chosen dispersion coefficient.

Effective alkali balances

$$\frac{\partial \rho^*_{EA,el}}{\partial t^*} = \overbrace{-v_c^* \frac{\partial \rho^*_{EA,el}}{\partial z^*}}^{a} \overbrace{-t_0 \rho_{ODW} \left(\frac{b_{lig} r_{lig}}{\rho_{EA,0}} + \frac{b_{carb} \rho_{carb}}{\rho_{EA,0}} \right)}^{b}$$

$$\frac{\partial \rho^*_{EA,fl}}{\partial t^*} = \overbrace{-v_l^* \frac{\partial \rho^*_{EA,fl}}{\partial z^*}}^{e} \overbrace{+\frac{1}{Sc_{EA}}(\rho^*_{EA,el} - \rho^*_{EA,fl})}^{f} \overbrace{+\frac{1}{Pe_l}\frac{\partial^2 \rho^*_{EA,fl}}{\partial z^{*2}}}^{g}$$

$$\overbrace{-\frac{1}{Sc_{EA}}(\rho^*_{EA,el} - \rho^*_{EA,fl})}^{c} \overbrace{+\frac{1}{Pe_c}\frac{\partial^2 \rho^*_{EA,el}}{\partial z^{*2}}}^{d}$$

The values for each term are shown for the two operating points in Table 5.2. The

Term	HPR	LPR
a	0.0409	0.0303
b	−0.0842	−0.0574
c	0.0411	0.0278
d	0.0022	−0.0007
e	0.0378	0.0280
f	−0.0400	−0.0273
g	0.0022	−0.0007

Table 5.2: Steady-state values of the terms in the alkali equations

chemical consumption and the interphase diffusion are equally important as the convection terms. Dispersion has about the half influence as for the solids.

Dissolved solids balances

$$\frac{\partial \rho^*_{ds,el}}{\partial t^*} = \overbrace{-v_c^* \frac{\partial \rho^*_{ds,el}}{\partial z^*}}^{a} \overbrace{+t_0 \rho_{ODW}\left(\frac{(1+b_{lig})r_{lig}}{\rho_{ds,0}} + \frac{(1+b_{carb})r_{carb}}{\rho_{ds,0}}\right)}^{b}$$

$$\overbrace{-\frac{1}{Sc_{ds}}(\rho^*_{ds,el} - \rho^*_{ds,fl})}^{c} \overbrace{+\frac{1}{Pe_c}\frac{\partial^2 \rho^*_{ds,el}}{\partial z^{*2}}}^{d}$$

$$\frac{\partial \rho^*_{ds,fl}}{\partial t^*} = \overbrace{-v_l^* \frac{\partial \rho^*_{ds,fl}}{\partial z^*}}^{e} \overbrace{+\frac{1}{Sc_{ds}}(\rho^*_{ds,el} - \rho^*_{ds,fl})}^{f} \overbrace{+\frac{1}{Pe_l}\frac{\partial^2 \rho^*_{ds,fl}}{\partial z^{*2}}}^{g}$$

The values for each term are shown for the two operating points in Table 5.3. The same comments apply here as for the effective alkali balances. At the low production rate for the free liquor component, the dispersion comprises as much as $40-50\%$ of the convection. The reason for this is shown in Fig. 5.7; the profile curvature is here substantial. Hence, this is a numerically important term even at steady-state. [1] (Note that the same dispersion coefficient is applied for the two

[1] Note that by use of the MAC-method in the spatial discretization (where central differences are used), in cases where the convection is dominating, the generated negative numerical dis-

Term	HPR	LPR
a	-0.0298	-0.0164
b	0.0812	0.0553
c	-0.0499	-0.0329
d	-0.0015	-0.0060
e	-0.0440	-0.0214
f	0.0487	0.0323
g	-0.0047	-0.0109

Table 5.3: Steady-state values of the terms in the equations for the dissolved solids

phases.)

The compaction equation

$$\frac{\partial \epsilon_c}{\partial t^*} = \overbrace{-v_c^* \frac{\partial \epsilon_c}{\partial z^*}}^{a} \overbrace{-\epsilon_c \frac{\partial v_c^*}{\partial z^*}}^{b} \overbrace{+\frac{1}{Pe_c} \frac{\partial^2 \epsilon_c}{\partial z^{*2}}}^{c}$$

The values for each term are shown for the two operating points in Table 5.4. It

Term	HPR	LPR
a	-0.0373	-0.0264
b	0.0366	0.0262
c	0.0007	0.0002

Table 5.4: Steady-state values of the terms in the compaction equation

appears that the convective terms are equally important. The dispersive term is here neglible (0.4% of the convection in the LPR case).

The momentum balances

$$\frac{\partial v_c^*}{\partial t^*} = \overbrace{-v_c^* \frac{\partial v_c^*}{\partial z^*}}^{a} \overbrace{+\frac{1}{Fr}(1.0 - \frac{\rho_l^{*'}}{\rho_c^{*'}})}^{b} \overbrace{-\frac{\rho_{c,0}}{\rho_c^{*'} \epsilon_c} \frac{\partial p_c^*}{\partial z^*}}^{c}$$
$$\overbrace{-\frac{\rho_{c,0}}{\rho_c^{*'} Re_{\Lambda,c} \epsilon_c \epsilon_l}(v_c^* - v_l^*)}^{d} \overbrace{-\frac{d}{v_0^2} \frac{1}{\epsilon_c \rho_c^{*'}} F_\mu}^{e}$$

persion may result in numerical instability. This is, however, true only when the convection is driven mainly either by up- or downstream conditions. In our case, the convection is driven both by up- and downstream conditions. Hence, numerical instability does not occur.

$$\frac{\rho_{l,0}}{\rho_l^{*'}}\frac{\partial p_l^*}{\partial z^*} = \overbrace{-v_l^*\frac{\partial v_l^*}{\partial z^*}}^{f}\overbrace{+\frac{1}{Fr}}^{g}\overbrace{-\frac{\rho_{c,0}}{\rho_c^{*'}}\frac{1}{Re_{\Lambda,l}\epsilon_l}(v_l^*-v_c^*)}^{h}$$

The values for each term are shown at respective level $28m$ in the cooking zone (CZ) and level $22m$ in the wash (WZ) zone, for the two operating points in Table 5.5. It appears that all the included terms are important in the momentum bal-

Term	HPR CZ	HPR WZ	LPR CZ	LPR WZ
a	0.0511	-0.0020	0.0266	0.0043
b	$6.6339 \cdot 10^4$	$7.7597 \cdot 10^4$	$6.5281 \cdot 10^4$	$7.4625 \cdot 10^4$
c	$-5.6867 \cdot 10^4$	$-1.1157 \cdot 10^4$	$-5.6198 \cdot 10^4$	$-1.7882 \cdot 10^4$
d	$-5.2345 \cdot 10^2$	$-7.9920 \cdot 10^4$	$-3.3346 \cdot 10^2$	$-4.6741 \cdot 10^4$
e	$-8.9484 \cdot 10^3$	$-8.8335 \cdot 10^3$	$-8.7497 \cdot 10^3$	$-1.0002 \cdot 10^4$
f	-0.0422	0.0035	-0.0224	-0.0073
g	$1.22625 \cdot 10^6$	$1.22625 \cdot 10^6$	$1.22625 \cdot 10^6$	$1.22625 \cdot 10^6$
h	$2.7649 \cdot 10^2$	$4.4106 \cdot 10^4$	$1.7659 \cdot 10^2$	$2.6525 \cdot 10^4$

Table 5.5: Steady-state values of the terms in the momentum equations

ance for the chip plug, except for the force of inertia which is neglible. Concerning the liquor balance, the force of gravity is dominating. The viscous force of friction comprises only about 3% in the wash zone at high production rate, and less in the other cases.

The values for the two terms in the viscous friction coefficient Eq. (3.101):

$$\Lambda = \overbrace{R_1\frac{\epsilon_c^2}{\epsilon_l}}^{a} + \overbrace{R_2\epsilon_c \mid v_c - v_l \mid}^{b} \tag{5.1}$$

are shown for respective locations in the cooking and wash zones, for the two operating points in Table 5.6.

Term	HPR CZ	HPR WZ	LPR CZ	LPR WZ
a	$2.2951 \cdot 10^3$	$2.5450 \cdot 10^3$	$2.3181 \cdot 10^3$	$2.7970 \cdot 10^3$
b	$7.4370 \cdot 10^2$	$1.7553 \cdot 10^4$	$5.1030 \cdot 10^2$	$1.3225 \cdot 10^4$

Table 5.6: Steady-state values of the terms in the viscous friction coefficient

The viscous friction terms are relatively small in the cooking zone, but more considerable in the wash zone. This is due to the co-current wash flow, and is described by the b-term. Thus, this friction term comprises a strong nonlinearity in the model.

The energy balances

$$\frac{\partial T_c^*}{\partial t^*} = \overbrace{-v_c^* \frac{\partial T_c^*}{\partial z^*}}^{a} \overbrace{+\frac{\rho_c^* \rho_{c,0} d\Delta h_r r}{v_0 T_0 (C_{pc}\rho_c)^{*'}}}^{b} \overbrace{+\frac{1}{Re_c Pr_c}\left(\frac{\partial^2 T_c^*}{\partial z^{2*}} + \frac{1}{\epsilon_c}\frac{\partial \epsilon_c}{\partial z^*}\frac{\partial T_c^*}{\partial z^*}\right)}^{c} \overbrace{-St_{cl}(T_c^* - T_l^*)}^{d} \overbrace{-St_{cw}(T_c^* - T_a^*)}^{e}$$

$$\frac{\partial T_l^*}{\partial t^*} = \overbrace{-v_l^* \frac{\partial T_l^*}{\partial z^*}}^{f} \overbrace{+\frac{1}{Re_l Pr_l}\left(\frac{\partial^2 T_l^*}{\partial z^{2*}} + \frac{1}{\epsilon_l}\frac{\partial \epsilon_l}{\partial z^*}\frac{\partial T_l^*}{\partial z^*}\right)}^{g} \overbrace{-St_{lc}(T_l^* - T_c^*)}^{h} \overbrace{-St_{lw}(T_l^* - T_a^*)}^{i}$$

The values for each term are shown for the two operating points in Table 5.7. For

Term	HPR	LPR
a	$-4.9989 \cdot 10^{-5}$	$-3.3510 \cdot 10^{-4}$
b	$2.8393 \cdot 10^{-2}$	$1.9303 \cdot 10^{-2}$
c	$-8.9111 \cdot 10^{-9}$	$-2.4724 \cdot 10^{-9}$
d	$-2.8039 \cdot 10^{-2}$	$-1.8681 \cdot 10^{-2}$
e	$-3.0401 \cdot 10^{-4}$	$-2.8687 \cdot 10^{-4}$
f	$-4.6053 \cdot 10^{-3}$	$-3.0571 \cdot 10^{-3}$
g	$-1.1368 \cdot 10^{-8}$	$-1.1102 \cdot 10^{-8}$
h	$4.6549 \cdot 10^{-3}$	$3.1042 \cdot 10^{-3}$
i	$-4.9540 \cdot 10^{-5}$	$-4.7047 \cdot 10^{-5}$

Table 5.7: Steady-state values of the terms in the energy equations

the chip phase, the heat of reaction and the heat of conduction from the liquor are the most significant contributions. As to the liquor phase, the convection and the heat of conduction from the chips are the most significant. The vertical heat of conduction and the heat of conduction through the walls are neglible for both phases.

Conclusions

The results show that most of the included effects are important in the mass balances in this model from a steady-state dimensional analysis point of view.

The exception is the mass dispersion in most of the equations. Regarding the dispersion effect in the mass balance for the dissolved solids, this is of importance. We have chosen the dispersion coefficient small enough so that it has limited influence at steady-state. This is based on a guess, and should be proven by plant experiments. As commented upon in assumption 1 under mass transfer in Sec. 3.2.2, this effect is included for generality, as to give the opportunity to study the effect and to facilitate the numerical solution in the tuning of the model.
With respect to the momentum balances, the forces of inertia are neglible in both phases. The balance equation for the free liquor is mainly affected by the force of gravity.
In the energy balances, the vertical heat of diffusion and the heat of conduction through the walls are neglible for both phases.
What does not come out of this analysis is the importance of the individual terms under dynamic transients. Generally, terms that are of little importance at steady-state may dynamically be of greater importance. Examples are the force of inertia and the mass dispersion. In Sec. 5.3, it is illustrated that the latter may be considerable in this process, while the force of inertia is not. The dynamic and relative importance of the individual state variables in the model does neither come out of this analysis. Examples are the two pairs of the diffusive components. This is further discussed in Ch. 7. Finally, we have either not compared the steady-state results at different locations in the vessel. The chosen locations in this analysis are, however, likely to give representative results.

5.2 Steady-state profiles

Figs. 5.2-5.13 show the computed steady-state profiles for the two operating conditions as referred in Table I.3. In these results, there is no air in the chips, i.e $\epsilon_{air,atm} = 0$. This is discussed in Sec. 5.3.2.

1. **Components**

   (a) **Lignin and carbohydrate concentrations.** According to (Christensen et al., 1982), about 20% of the lignin, 40% of the hemicelluloses, 10% of the celluloses, and all the volatile extractives are removed during the initial delignification stage. We assume that this only occurs in the pre-impregnation tower, i.e. before the chips enter the digester. Assuming 42.2% celluloses, 27.2% hemicelluloses, 28.3% lignin, and 2.3% extractives in the chips entering the pre-impregnation tower (see e.g. Smook (1989)), this gives mass fractions $\alpha_{lig} = 0.227$ and $\alpha_{carb} = 0.543$ in the feed chips to the digester. This corresponds to a Kappa number of about 195 ($c_\kappa = 0.153$). Fig. 5.2 shows how the concentrations decrease smoothly down towards the end of the cooking zone where the reactions are stopped (or quenched) by displacement of the hot liquor with dilute wash liquor from below. Hence, no significant decrease occurs in the wash zone. The final Kappa number of about 60, see Fig. 5.3, corresponds to a pulp that is used for production of liner grades. The final yield of about 42% may seem somewhat low at this Kappa

number. Conventional kraft pulping of Norway spruce typically gives about 10% higher yield (Kleppe, 1978).
The H-factor profiles are shown in Fig. 5.4. The H-factor is higher at the high production rate than at the low production rate. This is because the reaction rates are higher at high production rate (due to higher cooking temperature), despite the lower residence time. Note that we have reduced the feed alkali concentration, and increased the cooking temperature such that the final Kappa number is about the same at the two production rates. Hence, the H-factors differ. When the H-factor is used in digester control, however, it is common to charge the same amount of alkali, and change the cooking temperature such that the H-factor is the same. The H-factor profile is commonly plotted as the area under the curve for the relative reaction rate. This is shown in Fig. 5.5.

(b) **Concentrations of effective alkali.** According to the nominal operating points, the concentration of effective alkali in the feed flow to the digester, i.e. in the transport circulation between the pre-impregnation tower and the digester, is about $25 g/l$ at high, and $23 g/l$ at low production rate. As the chemical reactions proceed, the alkali is consumed; giving a declining profile down towards the extraction. A typical operational objective is to achieve about 70% of the feed concentration in the in the cooking circulation ($33m$). Fig. 5.6 shows the steady-state profiles according to this. In the wash zone, the pure wash liquor [2] extracts the residual alkali in the chips by counter-current *diffusion washing*. Further, the concentration of entrapped alkali is below the concentration of free alkali in the cooking zone, while the opposite situation is the case in the wash zone. This is due to the dynamics caused by the diffusion process. With the applied diffusion rate coefficient, the results show that the steady-state difference between the concentration in the chips and in the free liquor is relatively small, about $0.08 g/l$ at the extraction at high production rate, and about $0.04 g/l$ at low production rate. This means that the diffusion rate of alkali is nearly as fast as the net vertical convective transport (i.e. the difference between the chip and liquor velocities). Further, this means that the liquor-to-wood-ratio (L/W) is low enough so as to prevent external mass transfer limitation, as far as the alkali is concerned. In other words, the diffusion of alkali is not a steady-state limiting factor. Fig. 5.10 shows the steady-state profile of pH according to Eq. (I.3).

(c) **Concentrations of dissolved solids.** According to the nominal lignin and carbohydrate concentrations in the feed as described above, α_{lig} and α_{carb} have been reduced respectively by $0.283 - 0.227 = 0.056 kg/kg$ ODW and $0.694 - 0.543 = 0.151 kg/kg$ ODW. This gives a total amount of dissolved solids in the liquor of $\rho_{ds,feed} = (0.056 + 0.151) kg/kg$ ODW $\cdot \rho_{ODW} \approx 82.2 kg/m^3$ ODW. We assume that the diffusion process has

[2] For simplicity we assume that the injected wash liquor is pure water. Usually, it is first brown stock wash filtrate (Smook, 1989).

levelled out the concentration difference in the entrapped and free liquor during the transport through the upstream processes.
Fig. 5.7 shows a smooth increase in the cooking zone down towards the extraction screens due to the chemical reactions. In the wash zone, the pure wash water extracts the residual solids in the chips up towards the extraction likewise as for the alkali. The concentration of free dissolved solids is below the concentration of entrapped dissolved solids in the whole vessel due to the dynamics caused by the diffusion process.
With the applied diffusion rate coefficient, the results show that the steady-state difference between the concentration in the chips and in the free liquor is considerable; about $14.2 g/l$ at the extraction at high production rate, and about $9.8 g/l$ at low production rate. Even higher differences appear outside the extraction zone. Note that about $1/3$ of the concentration of entrapped materials at the extraction screens, is retained in the chips in the discharged pulp, at both production rates. This result means that the diffusion of dissolved solids is a steady-state limiting factor, and there may be room for a better wash efficiency. These results depend on the operational conditions such as the dilution factor, and how pure the wash water is at the entrance.

(d) **Concentrations of water.** Fig. 5.8 clearly shows the ingenuity of washing counter-current instead of co-current. There is a smooth increase in the chip water concentration in the cooking zone down towards the extraction. This is due to the interphase diffusion of the residuals, which replaces these with water (c.f. the discussion about the conceptual model in Sec. 3.3.2). The effect is, however, limited by the fact that the chips move faster than the free liquor in this zone. In the wash zone, the inclination is greater, despite reduced diffusion coefficient, as described below. This is because the free liquor is diluted by cleaner, or more dilute, liquor coming from below.

(e) **Chip and liquor densities.** Fig. 5.9 shows how the chip density decreases downwards in the whole vessel as the chemical reaction and diffusion processes remove solid materials with higher specific weight than water. The free liquor density is greatest at the extraction, as the free dissolved solids concentration here is greatest. Note that it is the density difference between the two phases that is the "driving force" for the autonomous vertical motion of the chip plug. Hence, these profiles influence the profile for the compaction of chips as described below.

(f) **Diffusion coefficients.** As shown in Fig. 5.10, there are three different regions that characterize the diffusion coefficient profile. This is due to the fact that there are three different variables that affect the coefficient; the temperature, the yield and pH, c.f. Eq. (3.4). In the upper part of the cooking zone, the temperature is high, pH is high, and the yield is high. Looking at the profile downwards in the cooking zone, the temperature slightly increases, pH is reduced, and the yield is reduced as well. The result is that the coefficient increases. This shows that possibly all the three variables influence the coefficient. However,

as shown in the upper part of the wash zone ($15 - 26m$), pH and especially the temperature are dramatically reduced, but the yield is nearly constant. This shows how strongly the temperature influences the diffusion coefficient.

2. **Chip mass movement.** Fig. 5.11 shows the profiles of the compaction of chips (computed by Eq. (3.80)), and the chip pressure (Eq. (3.6)), and Fig. 5.12 shows the chip velocity profile. The compaction of chips increases down towards the extraction screens. This is mostly due to gravity and the delignification (c.f. the discussion about the chip pressure in Sec. 3.3.3). Thereby, the chip velocity is reduced. In the wash zone, the gradients are considerably smaller than in the cooking zone. This is due to the reduced (stopped) delignification and due to the lift from the wash water. The figures show that the profiles depend on the operational conditions. This is in agreement with the results as reported by Johnsson (1971) and Härkönen (1984). The results from the industrial runs as reported by Neretnieks (1974b) indicate as well that most of the compaction of the chips occurs in the cooking zone. Further, the profile for the chip velocity is in agreement with residence time measurements, accomplished by the use of radioactive tracers, as reported in KAMYR (1993). These indicate that it is nearly independent of location in the wash zone.
   Fig. 5.11 also shows the chip pressure profile. It is similar to the compaction profile. We observe that, with respect to these steady-state profiles, the increased compaction of chips in the cooking zone has stronger influence on the chip pressure than the reduced Kappa number has (c.f. Fig. 3.6). Further, it is the increased compaction due to the gravity that increases the chip pressure. This means that the increased compaction due to the delignification is not great enough to increase the chip pressure (as a net effect). This is discussed further in Sec. 5.3.1.
   It may be argued that the compaction of chips at the extraction screens is a critical factor in the operation of digesters (Härkönen, 1994). This value may be a key indicator of how the digester is running.
   The total residence time in the digester is about 2.6 hours at the high-, and 3.8 hours at the low production rate. The mass consistency in the discharged pulp is about 8.1% at the high-, and 9.0% at the low production rate. The dilution factor according to Eq. (3.86) is about 0.91 at the high, and 0.90 at the low production rate ($k_n = 62.0$ and $k_d = 83.3$).

3. **Liquor mass flow.** Due to the incompressibility assumption, the liquor pressure and velocity are directly mutually dependent. The liquor velocity increases downwards in the cooking zone, as shown in Fig. 5.12. This is due to the positive gradient of the compaction (increased flowing resistance), and the negative gradient of the chip velocity (c.f. Eq. (3.128)). The velocity is driven by the controlled extraction flow (or the suction pressure from the extraction pump through the screens). Note that the liquor velocity is lower than the chip velocity in this zone. This prevents external mass transfer limitation, as discussed in the comments to assumption 3 about interphase diffusion in Sec. 3.2.2. Equivalent conditions arise in the wash zone where the velocity is negative, denoting that the flow is directed upwards. This

causes the discontinuity at the extraction screens. Near the digester bottom, i.e. between the inlets from the side- and bottom nozzles ($4m$), some of the liquor from the side nozzles flows down through the blow unit to fulfill the liquor mass balance given by the operating flow rates.
The liquor pressure increases in a straight line from about $11bar$ in the top to about $7bar$ in the bottom. This is mainly due to gravity, c.f. Table 5.5.

4. **Energy flows.** Fig. 5.13 shows the temperature profiles for the two phases at the two operating points. The temperatures at $42m$ denote the steam temperatures. It appears that the heat transfer from the high pressure steam to the liquor is greater than to the chips, resulting in a considerable temperature difference (about 20^oC at high production rate, and about 14^oC at low production rate) in this zone. The reason for this is the longer residence time for the liquor in the steam zone. The temperature rise in the liquor is, however, limited by larger heat capacity and more mass compared to the chip phase. Further, the large increase in the chip temperature from the steam zone to the top section is due to the heat conduction from the liquor and the exothermic chemical reactions. The temperature rise from the top and down towards the cooking circulation screens is also due to the exothermic reactions. The increase in this area is about $1.7^oC/m$ at the high production rate (about 6.3% increase), and about $1.1^oC/m$ at the low production rate (about 4.4% increase). Further, the exothermic heat generation is considerable lower in the lower part of the cooking zone (about $0.13^oC/m$, i.e. 0.4% increase), at the high production rate, and about $0.06^oC/m$, i.e. 0.2% increase, at the low production rate). The influence from the exothermic reactions are here considerably smaller due to lower reaction level in this area. Christensen et al. (1982) reports about a temperature gradient of about $1.0^oC/m$ for kraft cooks in the cooking zone. At the cooking circulation screens, the liquor temperature is affected by the controlled cooking circulation temperature of 170^oC vs. 160^oC at the high- and low production rates. This also affects the chip temperature to a certain degree. Hence, the interphase heat transfer is considerable but not dominating in the cooking zone. The temperature difference between the two phases is about 3.4^oC at both production rates at this point.
Below the extraction screens, i.e. in the wash zone, the chips are rapidly cooled down by the wash water which has a temperature of 90^oC at the inlet in the bottom. At the location where the quench circulation screens normally are, i.e. just below the extraction screens (about $25m$), the liquor temperature is about 132^oC at high- and about 128^oC at low production rate. This corresponds typically to the controlled temperature in this circulation when this is in operation. Hence, this indicates that the quench circulation may be closed, as often is the case in running digesters. The temperature difference between the two phases, at this point, is about 19^oC at high- and about 24^oC at low production rate.

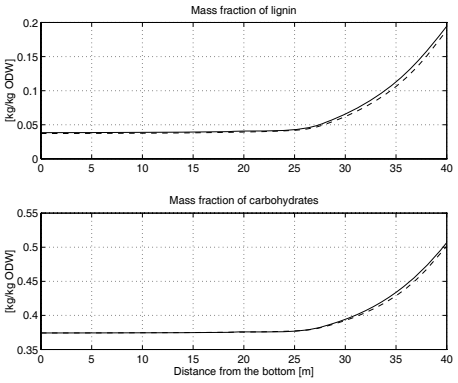

Figure 5.2: Steady-state profiles of the mass fractions of lignin and the carbohydrates at high (solid line) and low (dashed line) production rate.

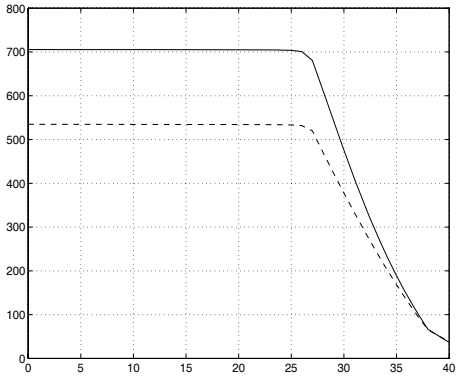

Figure 5.4: Steady-state profiles of the H-factor at high (solid line) and low (dashed line) production rate.

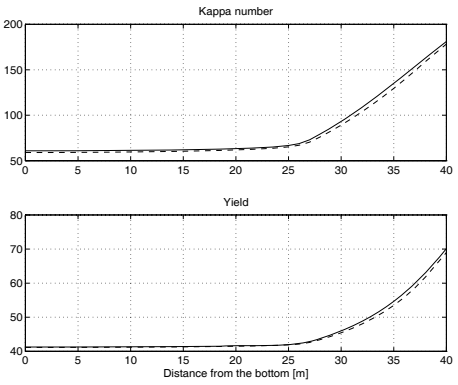

Figure 5.3: Steady-state profiles of the Kappa number and yield (in %) at high (solid line) and low (dashed line) production rate.

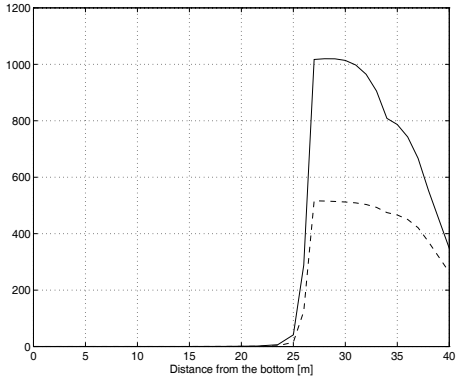

Figure 5.5: Steady-state profile of the relative reaction rate (dimensionless) as defines the H-factor as the area under the curve accodring to Eq. (2.3). The solid line shows the result at high production rate, whereas the dashed line shows the result at low production rate.

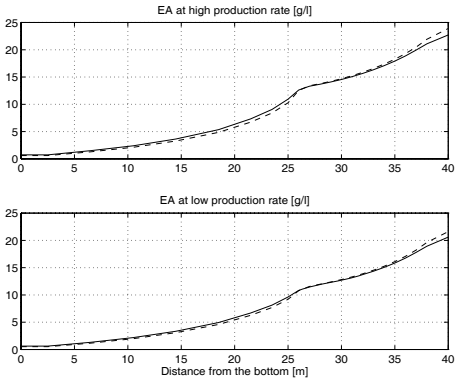

Figure 5.6: Steady-state profiles of the concentrations of entrapped (solid line) and the free (dashed line) effective alkali at the two production rates.

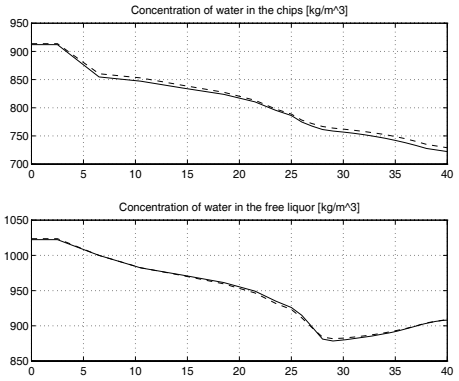

Figure 5.8: Steady-state profiles of the concentration of water in the chips and in the free liquor at high (solid line) and low (dashed line) production rate.

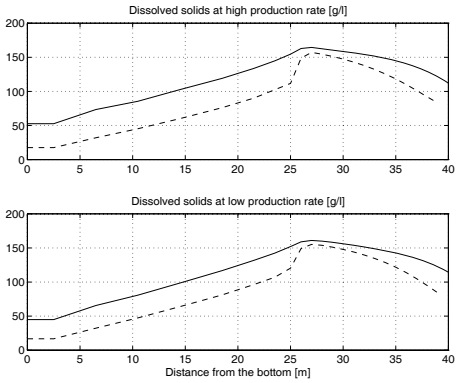

Figure 5.7: Steady-state profiles of the concentrations of entrapped (solid line) and the free (dashed line) dissolved solids at the two production rates.

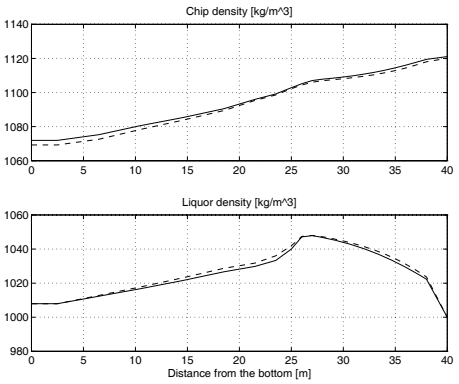

Figure 5.9: Steady-state profiles of the chip and free liquor density at high (solid line) and low (dashed line) production rate.

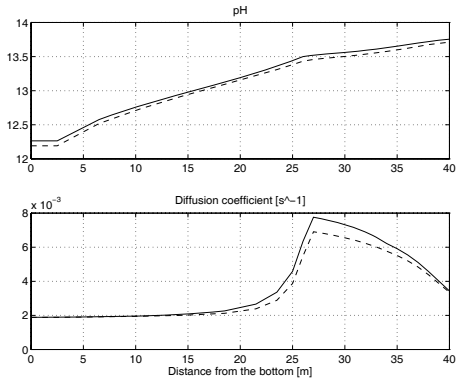

Figure 5.10: Steady-state profiles of pH and the diffusion rate coefficient for the alkali at high (solid line) and low (dashed line) production rate.

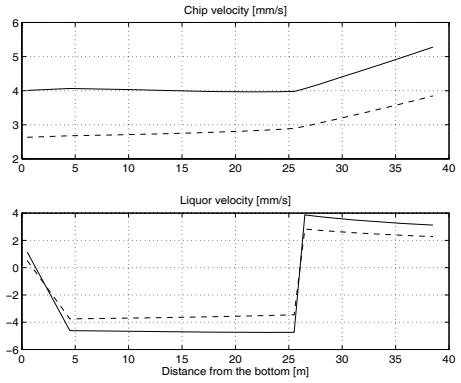

Figure 5.12: Steady state profiles of the chip plug- and free liquor velocity at high (solid line) and low (dashed line) production rate.

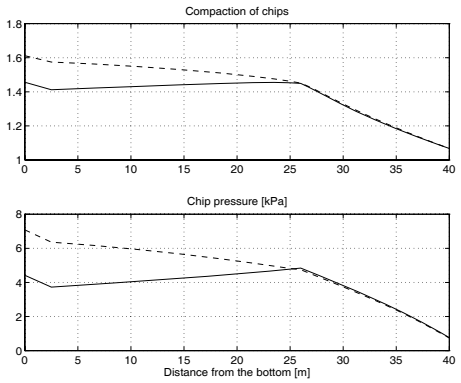

Figure 5.11: Steady-state profiles of the compaction of chips and the chip pressure at high (solid line) and low (dashed line) production rate.

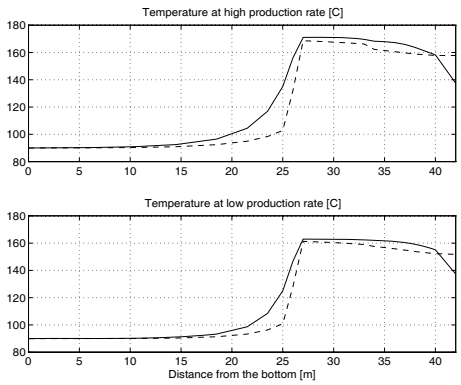

Figure 5.13: Steady state profiles of the chip plug (solid line) and the free liquor (dashed line) temperatures at the two production rates.

5.3 Dynamic behaviour

In this section, the dynamic qualities of the model are investigated. A number of selected scenarios are shown and discussed. First, the sensitivity of the model is studied. This is done both with respect to some of the important manipulated variables in Sec. 5.3.1, and to some important process disturbances in Sec. 5.3.2. Finally, a short-stop is simulated, which illustrates a planned operational change. The steady-state point of operation at the high production rate (see Appendix I) is used as the starting point for the simulations. A control loop for the liquor level

is included, where the extraction flow is the manipulated variable. In the courses where the chip level is controlled, the blow flow is the manipulated variable. We use PI-controllers such that the steady-state control errors are zero.

5.3.1 Sensitivity to manipulated variables; temperature-, alkali-, and residence time changes

In this section, we study the results from a 5% change in the manipulated variables that are primarily used to control the temperature, the concentration of alkali, and the residence time. The study is divided into two parts; (1) no chip level control, and (2) chip level control included. The chosen manipulated variables in case (1) are; the steam-, cooking circulation-, and lower wash circulation temperature, the alkali concentration in the feed (i.e. from the transport circulation), and the wash water flow through the side nozzles. In addition, the chip meter speed and the chip level set-point is included in case (2).

At simulation time, $t = 1$ hour, the 5% change (i.e. reduction) is made as a first order step in the respective manipulated variable (i.e. one at each scenario). The filter time constant is 12.5 minutes. The steam temperature is reduced from 175^oC to 166.25^oC, the cooking circulation temperature from 170^oC to 161.5^oC,, the lower wash circulation temperature from 90^oC to 85.5^oC, the alkali feed from $25.0g/l$ to $23.75g/l$, the wash water flow through the side nozzles from $2800.0l/min$ to $2660.0l/min$, the chip meter speed from $21.3rpm$ to $20.2rpm$, and the chip level from $41.50m$ to $39.43m$.
From the results, we may deduce something on how the relative importance of these variables is, with respect to the influence on the pulp quality, and the other key variables that are modelled for the process. [3]

The liquor circulation flows are held at the operating point in all the courses.

No chip level control

Figs. 5.14-5.19 show the effect on the chip level, the residence time for chips, the compaction of chips at the extraction screens, the Kappa number and the concentration of entrapped dissolved solids in the blow flow, and the concentration of effective alkali in the extraction flow.

[3] It should be noted that such a comparison is dependent on the measure range of the variables, i.e. how much the 5% change yields. In this study, we assume that the measure ranges start at respective $0^oC, 0g/l, 0l/min, 0rpm$, and $0m$. In the case of e.g. the chip level, however, a common measure range has dimension %, the nominal level corresponds to say 50%, and 0% corresponds to some metres below this. Thus, a 5% reduction is typically considerable less than the 2 metres which we operate with. Equivalently for the other variables.

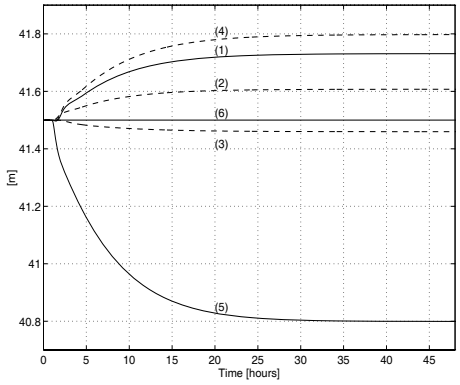

Figure 5.14: Chip level after a 5% reduction in the steam temperature (1), cooking circulation temperature (2), lower wash circulation temperature (3), alkali feed (4), and wash water flow (5), when the chip level is not controlled. (6) is the set-point.

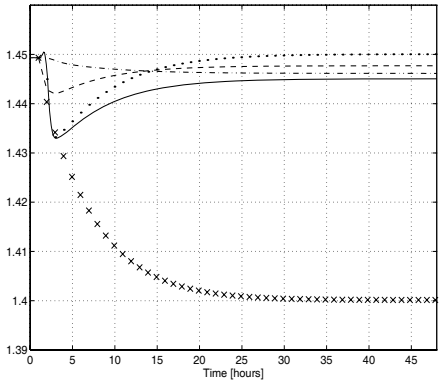

Figure 5.16: Chip packing at the extraction screens after a 5% reduction in the steam temperature (solid line), cooking circulation temperature (dashed line), lower wash circulation temperature (dashed-dotted line), alkali feed (dotted line), and wash water flow (+ line), when the chip level is not controlled.

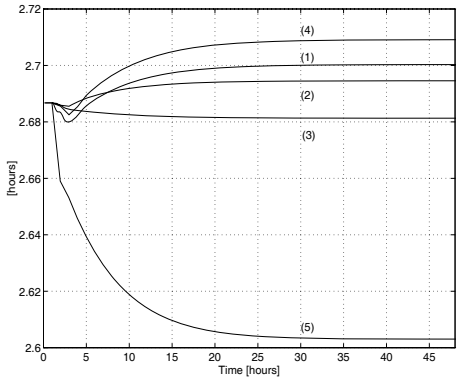

Figure 5.15: Residence time after a 5% reduction in the steam temperature (1), cooking circulation temperature (2), lower wash circulation temperature (3), alkali feed (4), and wash water flow (5), when the chip level is not controlled.

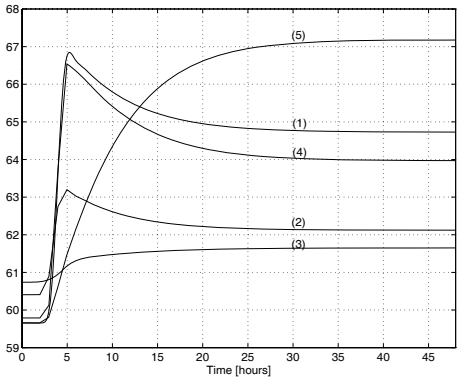

Figure 5.17: Kappa number in the blow flow after a 5% reduction in the steam temperature (1), cooking circulation temperature (2), lower wash circulation temperature (3), alkali feed (4), and wash water flow (5), when the chip level is not controlled.

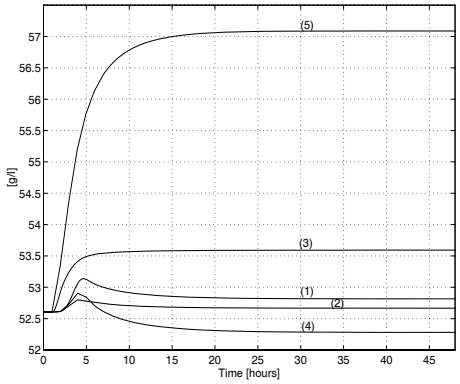

Figure 5.18: Concentration of entrapped dissolved solids in the blow flow after a 5% reduction in the steam temperature (1), cooking circulation temperature (2), lower wash circulation temperature (3), alkali feed (4), and wash water flow (5), when the chip level is not controlled.

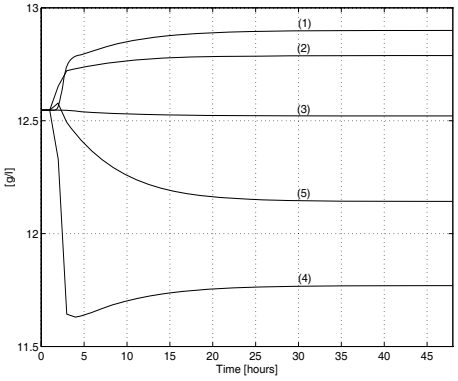

Figure 5.19: Concentration of free effective alkali in the extraction flow after a 5% reduction in the steam temperature (1), cooking circulation temperature (2), lower wash circulation temperature (3), alkali feed (4), and wash water flow (5), when the chip level is not controlled.

We observe from the figures that the influence from the wash water flow (i.e. the manipulated variable that control the wash effect) has the strongest gain to all the variables under consideration, except for the effective alkali concentration. The latter is naturally influenced strongest by the alkali feed. Hence, because the wash water flow lifts the chip plug, and thus has a strong impact on the chip level, we may conclude that the manipulated variables that have the strongest influence on the residence time for the chips also have the strongest impact on the pulp quality. This shows the importance of modelling the residence time for the chips in the digester.
Further, as may be expected, the influence from the lower wash circulation temperature is weak compared to the others, and the influence from the steam temperature and the alkali charge are comparable except from the influence on the alkali concentration. Finally, the effect of the reduction in the cooking circulation temperature is weaker than from the steam temperature.
The settling times are influenced mostly by the long-term chip level dynamics. Hence, they are about the same, c.f. Fig. 5.14.

Figs. 5.20-5.33 show some more of the dynamic properties of the model in the case where the steam- and cooking circulation temperatures are reduced. The figures highlight an important property of the model; the coupling between the residence time for the chips and the chemical reactions. In Fig. 5.20 it is shown how the chip and liquor temperatures decrease at the cooking screens, and in the six grid points downflow the screens, after the cooking circulation temperature drop. Due to this, the chemical reaction rates are reduced, and thus the Kappa number increases as shown in Fig. 5.22. Because of this increase, the chip pressure is increased as well, see Fig. 5.30. As a result, the chip plug is retarded in the cooking zone upstream

the cooking circulation screens, see Fig. 5.24 at $1-2$ hours; an effect that limits the Kappa number increase through increased residence time for the chips. The result of this is that the compaction of chips increases in this part of the digester, see Fig. 5.26. The mechanism that stabilizes this process is discussed in Appendix G.

In the scenario with the steam temperature drop, Fig. 5.24 also shows that the chip velocity is varying in four characteristic time periods (the same occurs in the scenario with the cooking circulation temperature drop, but this is not visible in these figures). The four time periods are characterized by the dominating effects from the interplay between the gravity, the chip pressure gradient, the viscous friction force between the phases, and the dry friction force between the chips and the vessel walls.

1. The initial increase in the chip velocity is mainly caused by the increased individual chip weight, as a result of the raised Kappa number.

2. The subsequent decrease is due to the decined gravity increase, and the reduced chip pressure gradient. The latter is caused by the fact that the chip pressure increases more upstream than downstream due to the Kappa number increase. At this point, an acceleration in the chip plug is initiated. Also due to the chip pressure increase, the friction force between the chips and the vessel walls increase.

3. Next, the chip velocity is increased again. In this period, the above-mentioned chip plug acceleration is dominating. Moreover, this acceleration is amplified downwards in the cooking zone (see Figs. 5.25, 5.29 and 5.30). This means that the resulting mass and momentum transports through the chip plug acts as a pulse which is amplified downwards in this zone. [4] In this way, the Kappa number and the chip pressure increase more downstream than upstream in the cooking zone. Thus, more chips move out than into a grid-section, and as a result, the compaction of chips decrease more downstream than upstream. This is shown in Figs. 5.26 and 5.27. The figures show, however, an initial increase in the compaction before the reduction. When the acceleration pulse reaches a grid boundary, more chips first move into the grid section compared to what leaves. Next, more chips move out of the grid section compared to what enters due to the mentioned amplification. This phenomenon appears first in the wash zone in the scenario when the cooking circulation temperature drops, see Fig. 5.28.
   In the wash zone, the increase in the chip velocity, and the decrease in the compaction are less downstream than upstream, see Fig. 5.28. Hence, the increase in the chip pressure is still greater downstream than upstream, despite the increase in the Kappa number being lower as well, see Figs. 5.31 and 5.23.
   Note, however, that the downstream changes are results of the transport delay as well.
   As a result of this chip velocity increase, the residence time is reduced, see Fig. 5.15.

[4] The amplification is caused by the model structure and the vertical profiles of the Kappa number, the compaction of chips, and the chip pressure.

4. Finally, the reduction in the chip velocity is caused by the increased friction force between the chips and the vessel walls. This retardation causes the chip level to increase, see Fig. 5.14. Because of these two effects, the residence time for the chips increases, see Fig. 5.15.

After some time, approximately $2-3$ hours for the discharged pulp, the Kappa number drops. This is caused by the mentioned chip level increase. Note that the feed flow of chips is constant. Since the residence time in the cooking zone is further increased by this, the Kappa number is reduced, see Fig. 5.21. Due to the chip level increase, the compaction in the top section (Eq. (3.145)) increases as well, see the lower curve in Fig. 5.26. This is further discussed in Appendix F. The following three effects contribute to the increase in the compaction in the whole vessel, see Fig. 5.26, 5.27 and 5.28.

i) Higher chip level means longer residence time, reduction in the Kappa number, and thus an increase in the compaction.

ii) Higher Kappa number means higher individual chip weight.

iii) More chips in the top section means higher total weight of chips in this section.

As a result, the chip pressure is further increased, see Fig. 5.29. Hence, when the Kappa number has reached its maximum value and only decreases slightly further on, the chip pressure is influenced most by the compaction of chips.

Fig. 5.32 shows the concentration of entrapped dissolved solids at three different locations in the digester. The concentration decreases in the cooking zone below the cooking circulation screens, in the same manner as shown at the extraction screens. This is due to the reduced delignification as a result of the temperature reduction. Above the cooking circulation screens, there is an increase in the concentration due to the increased residence time because of the increased chip level. The response in the wash zone is initially influenced by the above mentioned "acceleration pulse" that in a transient period of time moves mass with higher concentration from upstream into the grid-section that we consider. The long-term reduction is the transport delay response from the upstream reduction. Fig. 5.33 shows how the concentration of free effective alkali increase due to the reduced chemical reactions, as less alkali is consumed.

Similar responses to the above appear after decreasing the alkali concentration. When the lower wash circulation temperature and the wash water flow drop, the curves behave more first order like, as the effect from these changes, and from the resulting chip level act in the same direction.

We observe from the above that there is a large spread in time between important dynamic effects in the digester. Viewing the Kappa number of the discharged pulp (Fig. 5.23), the initial increase has a duration of $2-3$ hours while steady-state is reached after approximately 24 hours.

Finally, note how the chip pressure is influenced by the Kappa number and the compaction of chips in Figs. 5.29, 5.30 and 5.31, c.f. Eq. (3.6). The increased Kappa number influences the chip pressure stronger than the decreased compaction does, especially in the cooking zone (c.f. the discussion above). This happens irrespective if the chip level is controlled or not (see the next section). The reason for this is

that the variation in the compaction is relatively small. This is different from the location dependency as discussed in the section about the chip mass movement in Sec. 5.2. In that case, due to the gravity, the change in the compaction is great enough to dominate the influence on the chip pressure.

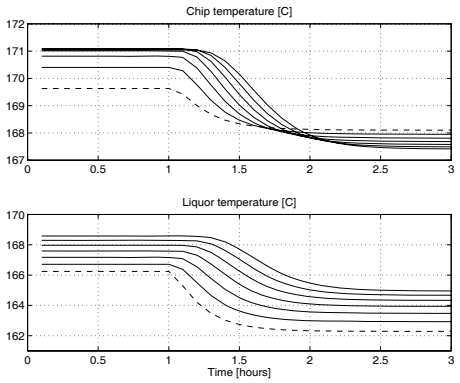

Figure 5.20: Cooking zone temperature downstream the cooking circulation screens when the cooking circulation temperature is reduced, and the chip level is not controlled. The temperature at the screens is plotted as dashed line. C.f. Fig. 5.13.

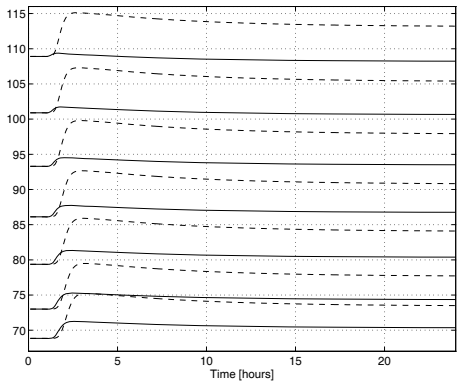

Figure 5.22: The Kappa number in the cooking zone below the cooking circulation screens when the cooking circulation temperature (solid line) and steam temperature (dashed line) are reduced, and the chip level is not controlled. C.f. Fig. 5.3.

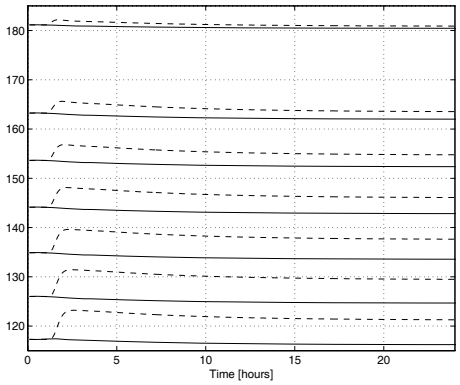

Figure 5.21: The Kappa number above the cooking circulation screens when the cooking circulation temperature (solid line) and steam temperature (dashed line) are reduced, and the chip level is not controlled. C.f. Fig. 5.3.

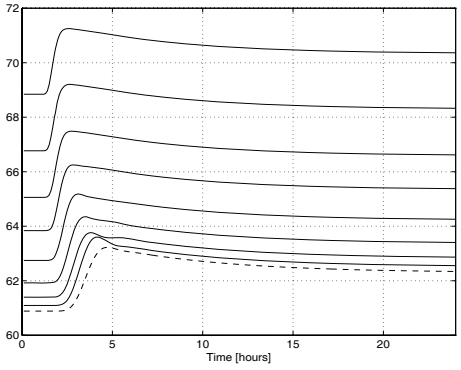

Figure 5.23: The Kappa number in the wash zone when the cooking circulation temperature is reduced, and the chip level is not controlled. The dashed line shows the discharged pulp. C.f. Fig. 5.3.

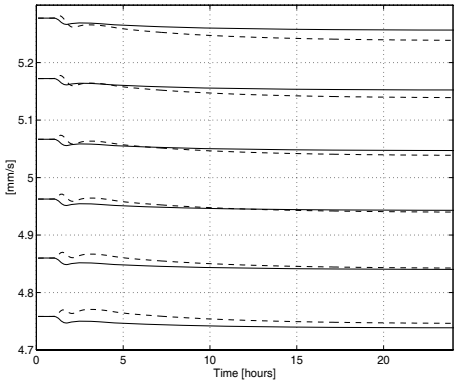

Figure 5.24: The chip velocity above the cooking circulation screens when the cooking circulation temperature (solid line) and steam temperature (dashed line) are reduced, and the chip level is not controlled. C.f. Fig. 5.12.

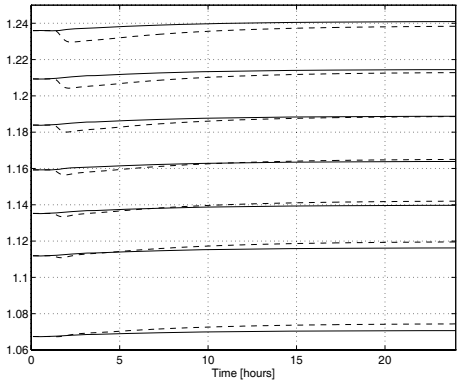

Figure 5.26: Compaction of chips above the cooking circulation screens when the cooking circulation temperature (solid line) and steam temperature (dashed line) are reduced, and the chip level is not controlled. C.f. Fig. 5.11.

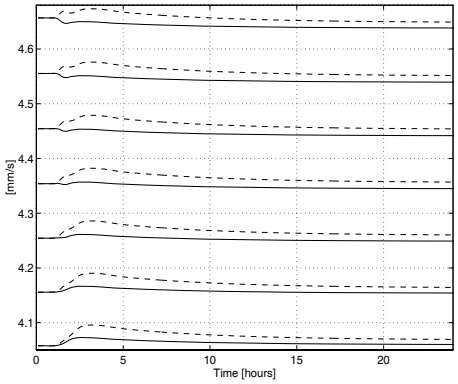

Figure 5.25: The chip velocity in the cooking zone below the cooking circulation screens when the cooking circulation temperature (solid line) and steam temperature (dashed line) are reduced, and the chip level is not controlled. C.f. Fig. 5.12.

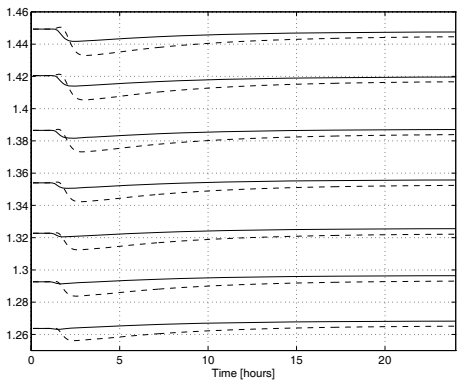

Figure 5.27: Compaction of chips in the cooking zone below the cooking circulation screens when the cooking circulation temperature (solid line) and steam temperature (dashed line) are reduced, and the chip level is not controlled. C.f. Fig. 5.11.

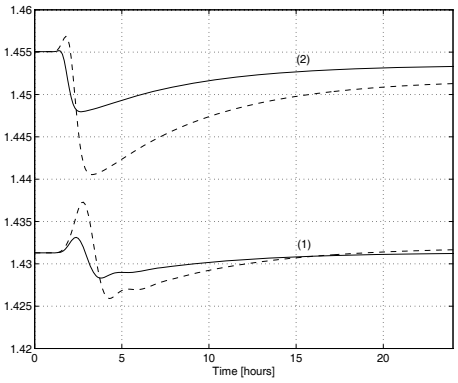

Figure 5.28: Compaction of chips in the wash zone at $11m$ (1), and $23m$ (2), when the cooking circulation temperature (solid line) and steam temperature (dashed line) are reduced, and the chip level is not controlled.

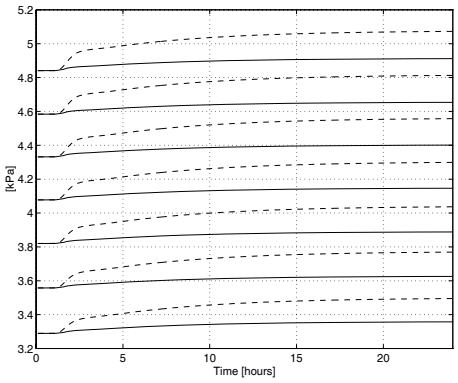

Figure 5.30: Chip pressure in the cooking zone below the cooking circulation screens when the cooking circulation temperature (solid line) and steam temperature (dashed line) are reduced, and the chip level is not controlled. C.f. Fig. 5.11.

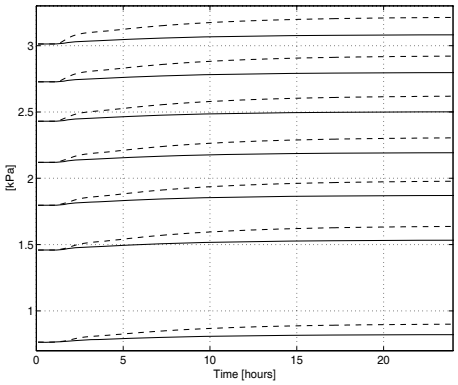

Figure 5.29: Chip pressure above the cooking circulation screens when the cooking circulation temperature (solid line) and steam temperature (dashed line) are reduced, and the chip level is not controlled. C.f. Fig. 5.11.

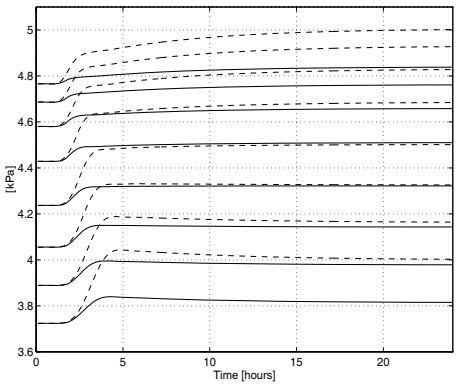

Figure 5.31: Chip pressure in the wash zone when the cooking circulation temperature (solid line) and steam temperature (dashed line) are reduced, and the chip level is not controlled. C.f. Fig. 5.11.

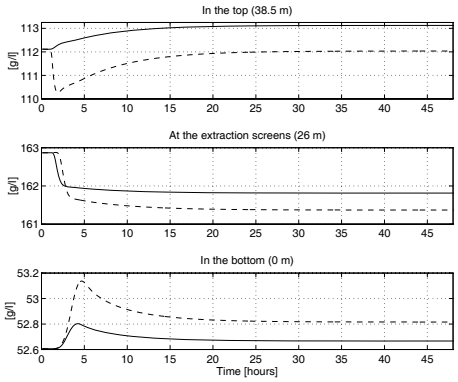

Figure 5.32: Concentration of entrapped dissolved solids when the cooking circulation temperature (solid line) and steam temperature (dashed line) are reduced, and the chip level is not controlled.

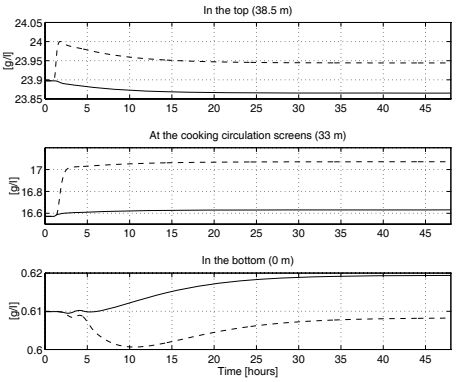

Figure 5.33: Concentration of free effective alkali when the cooking circulation temperature (solid line) and steam temperature (dashed line) are reduced, and the chip level is not controlled.

Chip level control included

The same study is performed as in the previous section, in the case when the chip level is controlled by the blow flow. We add the chip meter speed and the chip level set-point as manipulated variables. Figs. 5.34-5.42 show the effect on the blow flow, the chip level, the residence time for chips, the compaction of chips at the extraction screens, the Kappa number and the concentration of entrapped dissolved solids in the blow flow, and the concentration of free effective alkali in the extraction flow.

The steady-state gain from the effective alkali feed to the Kappa number in the discharged pulp ($5.3 units/(g/l)$) corresponds well to reported results from the Peterson digester (Lunde and Mikaelsen, 1994). The results from the other manipulations were not successful in that work, due to operational problems during the collection of data.

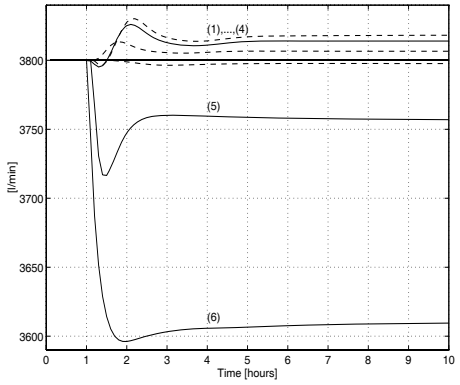

Figure 5.34: Blow flow after the drop in the steam temperature (1), cooking circulation temperature (2), lower wash circulation temperature (3), alkali charge (4), wash water flow (5), and chip meter speed (6) when the chip level is controlled. The set-point is at $3800 l/min$.

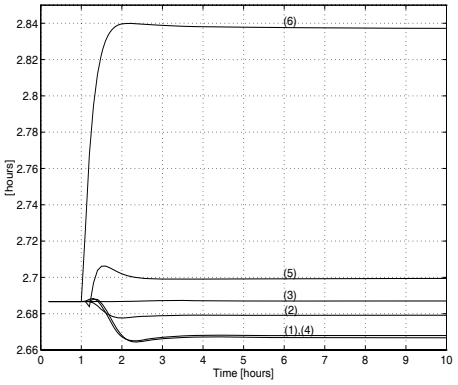

Figure 5.36: Residence time after a 5% reduction in the steam temperature (1), cooking circulation temperature (2), lower wash circulation temperature (3), alkali feed (4), wash water flow (5), and the chip meter speed (6), when the chip level is controlled.

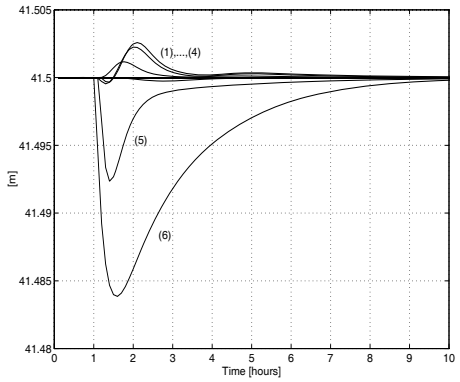

Figure 5.35: Chip level after the drop in the steam temperature (1), cooking circulation temperature (2), lower wash circulation temperature (3), alkali charge (4), wash water flow (5), and chip meter speed (6) when the chip level is controlled. The set-point is at $41.5m$.

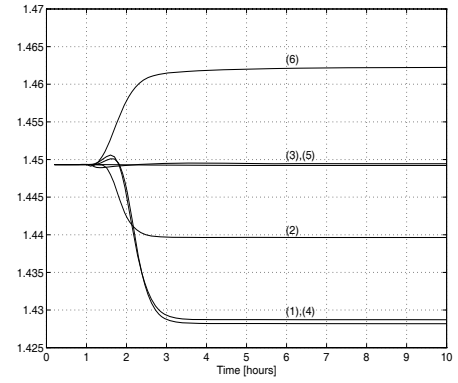

Figure 5.37: Chip packing at the extraction screens after a 5% reduction in the steam temperature (1), cooking circulation temperature (2), lower wash circulation temperature (3), alkali feed (4), wash water flow (5), and the chip meter speed (6), when the chip level is controlled.

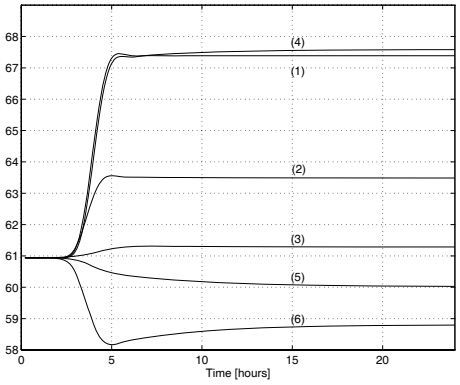

Figure 5.38: Kappa number in the blow flow after a 5% reduction in the steam temperature (1), cooking circulation temperature (2), lower wash circulation temperature (3), alkali feed (4)), wash water flow (5), and the chip meter speed (6), when the chip level is controlled.

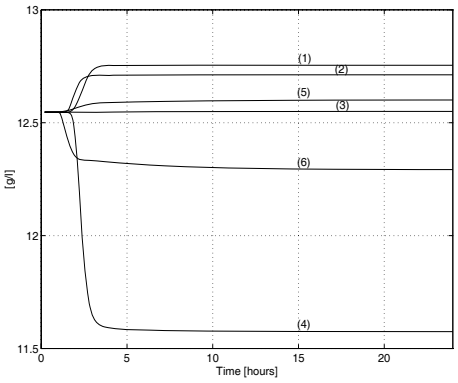

Figure 5.40: Concentration of free effective alkali in the extraction flow after a 5% reduction in the steam temperature (1), cooking circulation temperature (2), lower wash circulation temperature (3), alkali feed (4), wash water flow (5), and the chip meter speed (6), when the chip level is controlled.

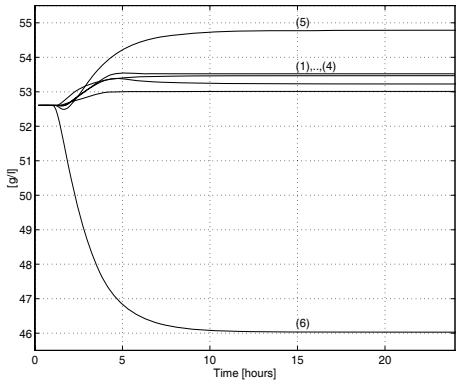

Figure 5.39: Concentration of entrapped dissolved solids in the blow flow after a 5% reduction in the steam temperature (1), cooking circulation temperature (2), lower wash circulation temperature (3), alkali feed (4), wash water flow (5), and the chip meter speed (6), when the chip level is controlled.

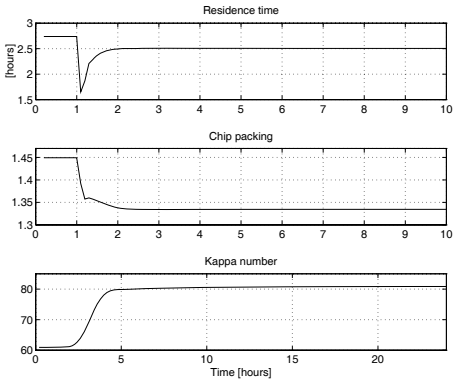

Figure 5.41: Residence time, chip packing at the extraction screens, and Kappa number in the blow flow after a 5% reduction in the chip level set-point.

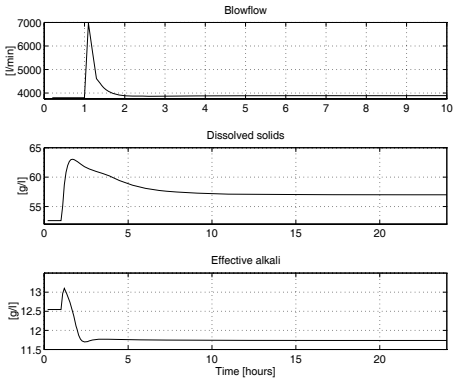

Figure 5.42: Blow flow, concentration of entrapped dissolved solids in the blow flow, and concentration of free effective alkali in the extraction flow after a 5% reduction in the chip level set-point.

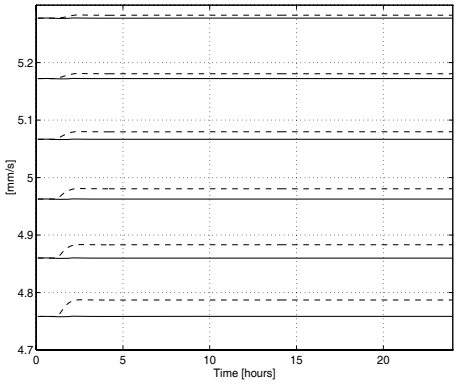

Figure 5.43: The chip velocity above the cooking circulation screens when the cooking circulation temperature (solid line) and steam temperature (dashed line) are reduced, and the chip level is controlled. C.f. Fig. 5.12.

We observe from the figures that the chip level change has a dominating impact on the residence time, chip packing, and the Kappa number, compared to the other manipulations (c.f. the results from the previous case). Next, the steam temperature and the alkali feed have the second strongest impact on Kappa number. Further, the cooking circulation temperature and the chip meter speed have about the same influence on Kappa number with opposite signs. We observe as well that the influences from the wash water flow and the chip meter speed have positive gains to the Kappa number. The reason for this is shown in Fig. 5.34; the chip level control reduces the blow flow, and thus the residence time for the chips is increased, c.f. Fig. 5.36. Note especially that the influence from the wash water flow in this case is dramatically reduced compared to the case where the chip level is not controlled, c.f. Figs. 5.14-5.19. Thus, the blow flow and the wash water flow counteract on the chip velocity (and thus the residence time). The lift force from the wash water flow and the pull force from the blow flow almost cancel the effect of each other. Since the chip meter speed has the strongest effect on the chip level, this gives a greater response on the blow flow as well. Thus, when we disregard the chip level set-point change, the impact on the residence time is greatest as well, c.f. Fig. 5.36. Because the chip level control increases the blow flow in the scenarios where the cooking temperature- and alkali feed are reduced, the gains to the Kappa number are larger in this case compared to the previous case. Further, the figures show a good correspondence between the responses from the Kappa number and the chip packing. This relationship is clearer in this case compared to the previous case. The settling times are fairly equal in the first four scenarios. Regarding the latter three scenarios, the settling times are greatly influenced by the chip level control, c.f. Fig. 5.35. Note also the considerable shorter settling times in this case compared to the previous case.

Figs. 5.43-5.56 show some more of the dynamic properties of the model in the scenarios where the steam- and cooking circulation temperatures are reduced. Compared to the previous case, Figs. 5.43 and 5.44 show that the chip plug is accelerated immediately downstream the cooking circulation screens after the reduction in the cooking circulation temperature, while the plug velocity is practically unchanged upstream the screens. The explanation to this is that the blow flow increase (see Fig. 5.34) also accelerates the chip plug, and thus compensates for the retardation upstream of the screens due to the Kappa number increase. As explained in the previous case, it is this retardation that causes the chip level to increase.

Figs. 5.48-5.50 show that the chip pressure increases less in this case. This is due to increased weight of the chip plug when the chip level increases, as discussed in the previous section.

Fig. 5.51 shows how the concentration of entrapped dissolved solids decreases at the extraction screens, in the same manner as in the previous case. However, in the scenario with the reduction in the cooking circulation temperature, the concentration is practically unchanged above the cooking circulation screens, due to the controlled chip level.

In Fig. 5.53, it is shown how the Kappa number increases along the digester as a propagating wave downwards through the vessel. We observe from Figs. 5.23 and 5.56 that the positive flanks of the curves are about the same in the two cases. This shows that the influence from the chip level is neglible in this initial transient period of time.

Some conclusions

- The responses are more "first order like" when the chip level is controlled. Moreover, in this case the manipulated variables that primarily influence the residence time (i.e. the chip meter speed and the wash water flow) have less influence on the Kappa number than have those which control the cooking temperature and the alkali concentration. From this, we see that the chip level control has a potential to improve the digester control under these types of disturbances, and especially those which directly affect the motion of the chip plug.
- The above result means as well that the chip velocity has less influence on the Kappa number than the chip level does, compare Figs. 5.15 with 5.36, and 5.17 with 5.38. Hence, the residence time itself is not that important as the combined effect of the chip level and the chip velocity. Changing the residence time by the chip level has greater influence than changing it by the chip velocity.
- Fig. 5.57 shows a comparison of the final Kappa number when the chip velocity is computed from the momentum balance, and when it is held constant at the initial profile. From this, we may conclude that when the chip level is tightly controlled, computing the chip velocity is not critical for Kappa number prediction under these type of disturbances, at 5% variations. Note,

however, that this assumes that the velocity profile is given. For this, we need the momentum balance equation for the chip plug. However, the situation is different regarding the concentrations of dissolved solids and effective alkali.

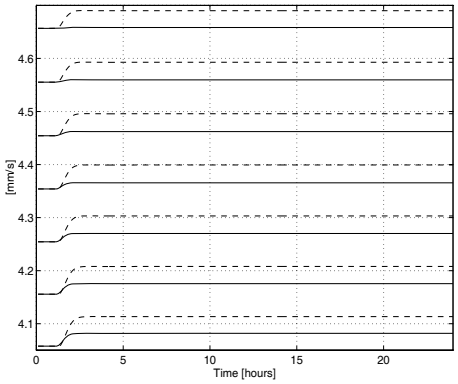

Figure 5.44: The chip velocity in the cooking zone below the cooking circulation screens when the cooking circulation temperature (solid line) and steam temperature (dashed line) are reduced, and the chip level is controlled. C.f. Fig. 5.12.

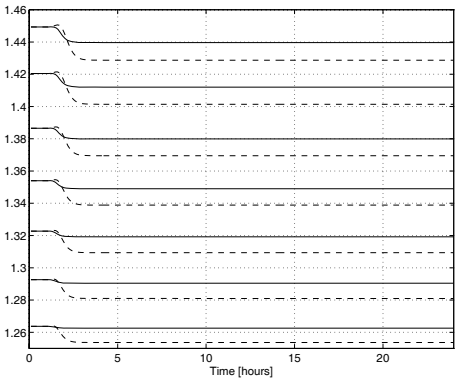

Figure 5.46: Compaction of chips in the cooking zone below the cooking circulation screens when the cooking circulation temperature (solid line) and steam temperature (dashed line) are reduced, and the chip level is controlled. C.f. Fig. 5.11.

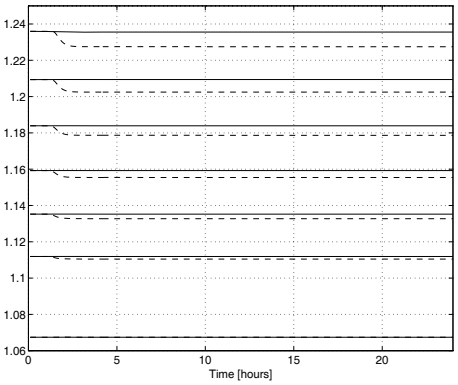

Figure 5.45: Compaction of chips above the cooking circulation screens when the cooking circulation temperature (solid line) and steam temperature (dashed line) are reduced, and the chip level is controlled. C.f. Fig. 5.11.

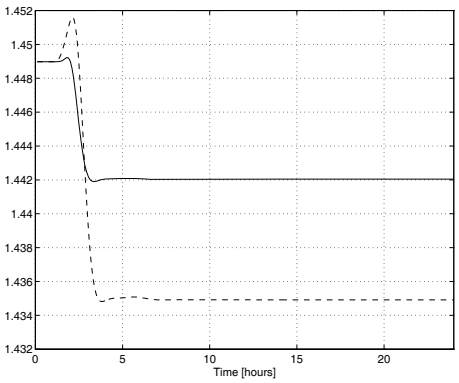

Figure 5.47: Compaction of chips in the wash zone at $19m$ when the cooking circulation temperature (solid line) and steam temperature (dashed line) are reduced, and the chip level is controlled.

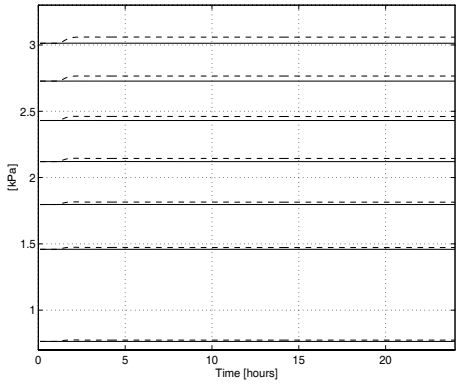

Figure 5.48: Chip pressure above the cooking circulation screens when the cooking circulation temperature (solid line) and steam temperature (dashed line) are reduced, and the chip level is controlled. C.f. Fig. 5.11.

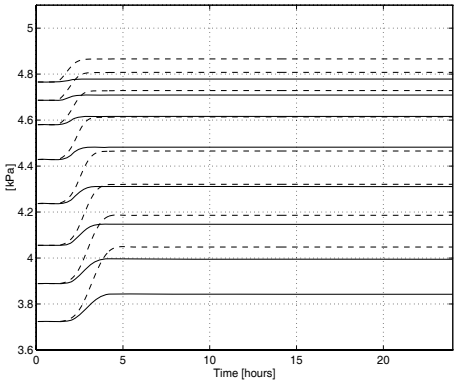

Figure 5.50: Chip pressure in the wash zone when the cooking circulation temperature (solid line) and steam temperature (dashed line) are reduced, and the chip level is controlled. C.f. Fig. 5.11.

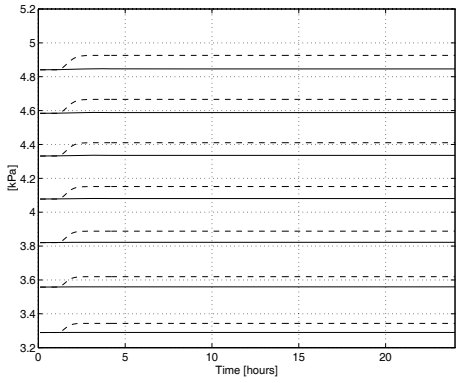

Figure 5.49: Chip pressure in the cooking zone below the cooking circulation screens when the cooking circulation temperature (solid line) and steam temperature (dashed line) are reduced, and the chip level is controlled. C.f. Fig. 5.11.

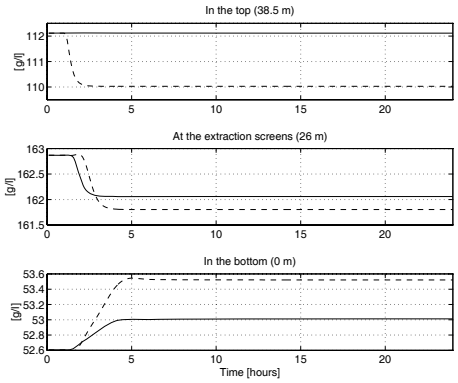

Figure 5.51: Concentration of entrapped dissolved solids when the cooking circulation temperature (solid line) and steam temperature (dashed line) are reduced, and the chip level is controlled.

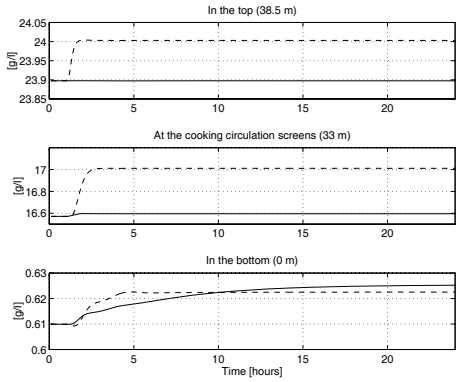

Figure 5.52: Concentration of free effective alkali when the cooking circulation temperature (solid line) and steam temperature (dashed line) are reduced, and the chip level is controlled.

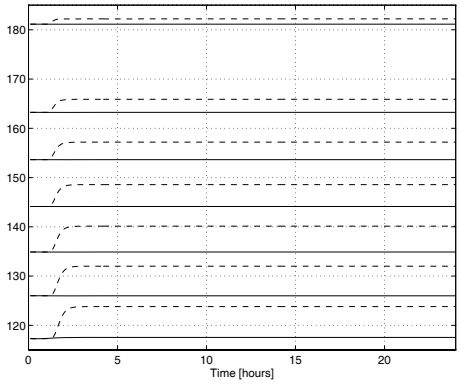

Figure 5.54: The Kappa number above the cooking circulation screens when the cooking circulation temperature (solid line) and steam temperature (dashed line) are reduced, and the chip level is controlled. C.f. Fig. 5.3.

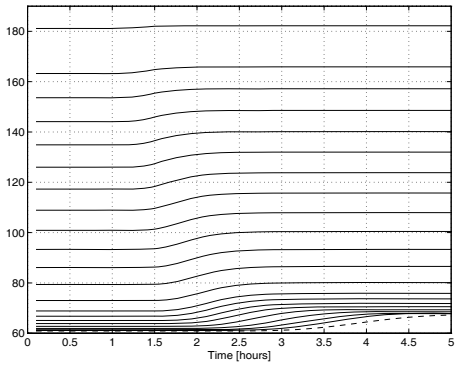

Figure 5.53: Kappa number along the vessel when the steam temperature is reduced, and the chip level is controlled. The dashed line shows the discharged pulp.

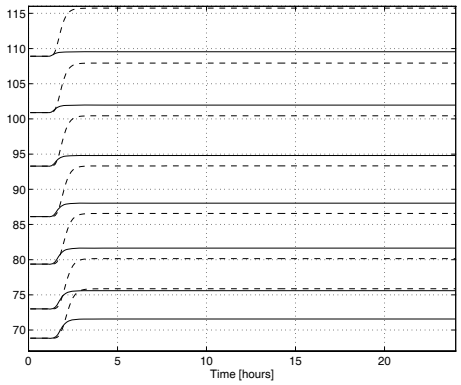

Figure 5.55: The Kappa number in the cooking zone below the cooking circulation screens when the cooking circulation temperature (solid line) and steam temperature (dashed line) are reduced, and the chip level is controlled. C.f. Fig. 5.3.

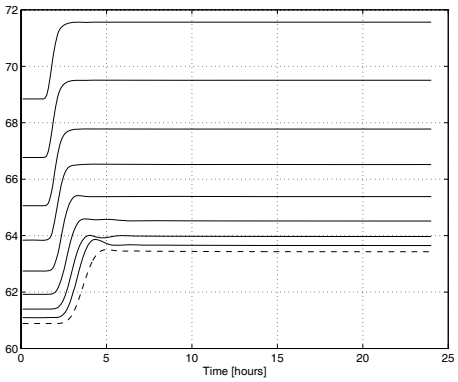

Figure 5.56: Kappa number in the wash zone when the cooking circulation temperature is reduced, and the chip level is controlled. The dashed line denotes the discharged pulp.

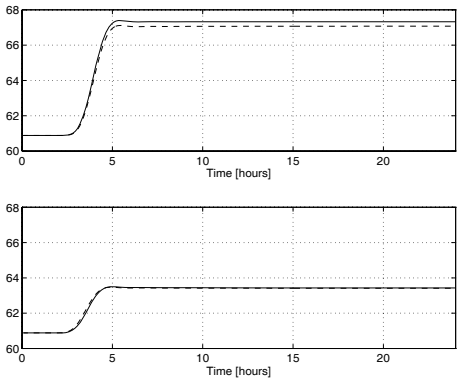

Figure 5.57: Kappa number in the blow flow when the steam temperature is reduced (upper figure), and when the cooking circulation temperature is reduced (lower figure), the chip level is controlled, and the chip velocity is computed by the momentum balance equation (solid line), and when it is held constant at the initial values (dashed line).

5.3.2 Sensitivity to some common operational disturbances; changes in feed chip reactivity, -lignin and -air content

As commented in Sec. 1.2.3, quality changes in the uncooked chips is a common disturbance source in the operation of digesters.

Variable reactivity occurs mainly when mixtures of hard- and softwood are used. This type of disturbance was also considered by Christensen et al. (1982). In the simulations, this effect is illustrated by changing the frequency factor, A_1, for the lignin reactions by a 5% step, from 1.0 to 0.95 in the feed flow. Then, as the mass moves downwards in the column, the factor A_1 is changed accordingly for the equations corresponding to the grid point (or slice) at which the step front (or actually the average due to the dispersion effect) is at current time. The step front is calculated based on the convective chip velocity, v_c.

Variability in the feed chip lignin content occurs when there are changes in the wood age, species of softwood (or hardwood), summer/winter wood, place of growth, sap content etc. The mass fraction of lignin is increased by 5%, from 0.230 to 0.242 in the simulations.

Air in the chips is a result of incomplete pre-steaming. The air reduces the chip density, and thus the "driving force" for the autonomous vertical motion of the chip plug. In the simulations, the air content is increased from zero to 5% in the

feed flow (i.e. $\epsilon_{air,atm}$ Eq. (3.40)). Then, likewise as for the reactivity change, $\epsilon_{air,atm}$ is changed accordingly for the equations corresponding to the grid point at which the step front is at current time. The final vertical profile of the air content is shown in Fig. 5.65.

The chip and liquor levels are both controlled during the scenarios.

Figs. 5.58-5.64 show the effect on the blow flow, the chip level, the residence time, the compaction of chips at the extraction screens, the Kappa number and the concentration of entrapped dissolved solids in the blow flow, and the concentration of free effective alkali in the extraction flow. We observe from the figures that the results are similar to what was found in the chip level control case in the previous section. The air content has greatest impact on the residence time for chips and the concentration of dissolved solids, whereas the influence on the Kappa number is neglible. Further, the impact on the chip packing is greatest from the air content as well. Except for the responces from the concentrations of dissolved solids and alkali, the influence from the lignin reactivity is greater than from the concentration of lignin in the feed chips.
Note the large settling times for the responses from the air content. This may be related to the long transport delay. Regarding the other responses, the settling times are much influenced by the chip level control in this case as well, c.f. Figs. 5.58 and 5.59.

Fig. 5.65 shows the steady-state vertical profiles of the air content at respective 5% and 10% in the uncooked chips at atmospheric pressure and 20^oC. It appears that the concentration of air in the vessel is fairly linear with respect to the concentration in the uncooked chips. Fig. 5.66 shows how the chip packing and the Kappa number are dependent on the air content at the two levels. It appears that the chip packing is largely influenced by the reduced chip weight due to this, meaning that the vertical motion of the chip plug is dramatically affected. Hence, the blow flow has to be increased considerably, to keep the chip level at the set point, c.f. Fig. 5.67. In this way, the concentration of wood in the discharged flow is reduced.

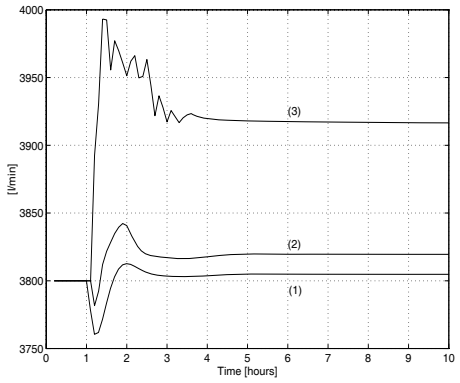

Figure 5.58: Blow flow after the 5% change in the feed lignin mass fraction (solid line), lignin reactivity (dashed line), and air content (dashed-dotted line). The set-point is at $3800 l/min$.

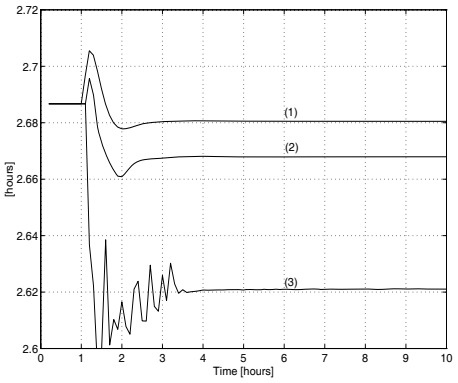

Figure 5.60: Residence time after the 5% change in the feed mass fraction of lignin (1), lignin reactivity (2), and increase in the chip air content (3).

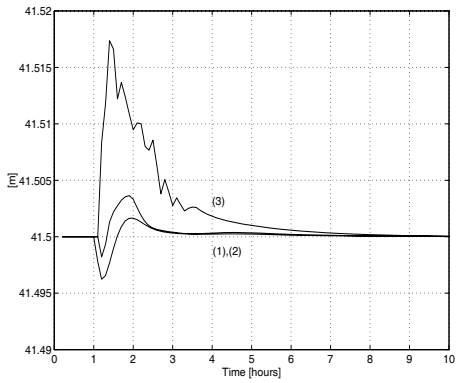

Figure 5.59: Chip level after the 5% change in the feed lignin mass fraction (solid line), lignin reactivity (dashed line), and air content (dashed-dotted line). The set-point is at $41.5m$.

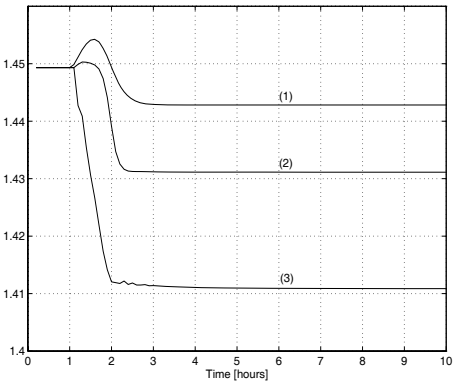

Figure 5.61: Chip packing at the extraction screens after the 5% change in the feed mass fraction of lignin (1), lignin reactivity (2), and increase in the chip air content (3).

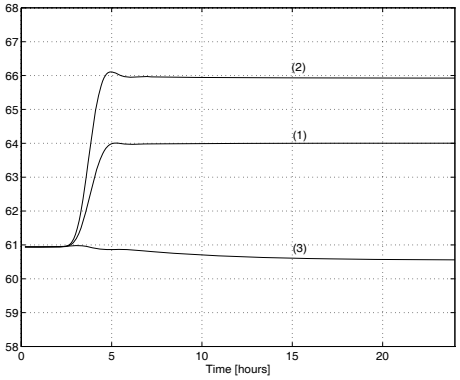

Figure 5.62: Kappa number in the blow flow after the 5% change in the feed mass fraction of lignin (1), lignin reactivity (2), and increase in the chip air content (3).

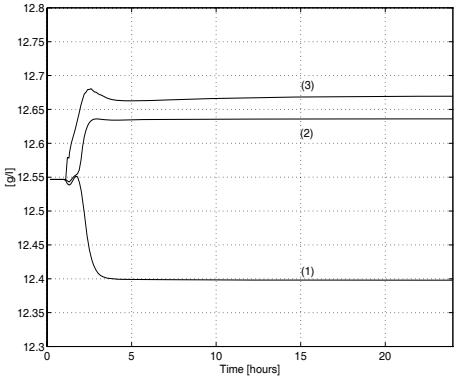

Figure 5.64: Concentration of free effective alkali in the extraction flow after the 5% change in the feed mass fraction of lignin (1), lignin reactivity (2), and increase in the chip air content (3).

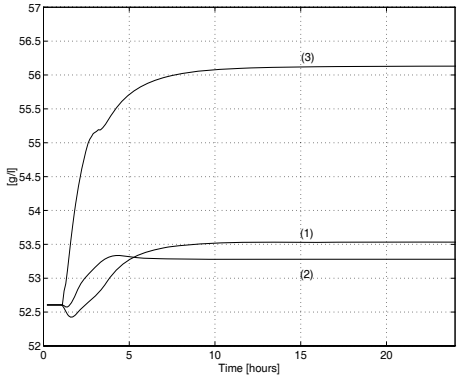

Figure 5.63: Concentration of entrapped dissolved solids in the blow flow after the 5% change in the feed mass fraction of lignin (1), lignin reactivity (2), and increase in the chip air content (3).

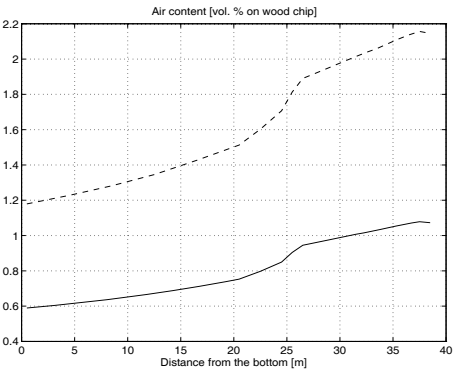

Figure 5.65: Steady-state profiles of the volume % of air in the chips when the air content in the uncooked chips at atmospheric pressure and 20^oC is 5% (solid line) and 10% (dashed line).

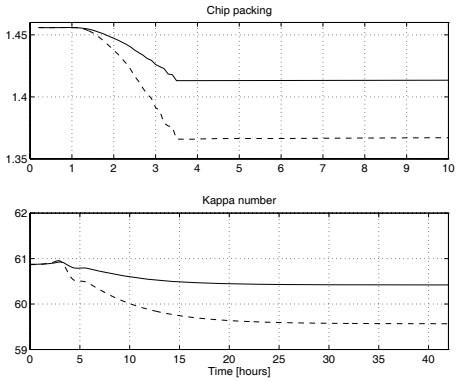

Figure 5.66: Chip packing at the extraction screens and the Kappa number in the blow flow after charging chips with air content 5% (solid line) and 10% (dashed line) at atmospheric pressure and 20^oC.

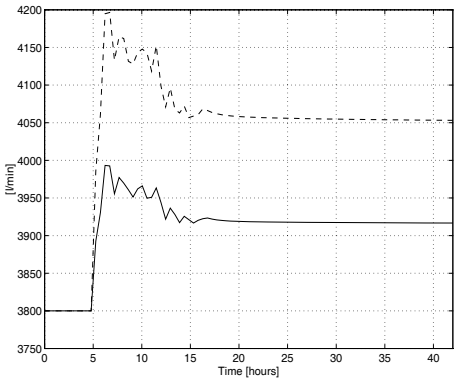

Figure 5.67: The blow flow after charging chips with air content 5% (solid line) and 10% (dashed line) at atmospheric pressure and 20^oC.

5.3.3 Short-stop

When operational problems occur in downflow processes in the pulping mill, the digester has to be stopped for a while until the problems are solved and the downflow processes again are able to receive the pulp. This situation typically occurs frequently in real plant operations. Because the pulp quality is not measured and the chip- and liquor levels go beyond their respective measurement ranges in such stopping-periods, useful information may be achieved by simulation.

In such operational changes, the operators have certain procedures to follow. For illustrative reasons in this case study, we have somewhat simplified such a procedure for a short-stop up to five hours, and subsequent startup of the process. Since the model is not valid at extremely low Kappa number levels, the stopping period is shortened to 100 minutes, and lasts from time 2.3 hours to 4 hours.

Initially, there are steady-state conditions and no automatic chip-, and liquor level control. At time, $t = 1$ hour, the steam- and cooking circulation temperatures are reduced by 1.7^oC (i.e. 1^oC/hour of stop according to the procedure). One hour later, the procedure starts of stopping the respective flows. First, the cooking- and lower wash circulation flows, then 12.5 minutes later the chip feed flow and the blow flow, and finally 5 minutes later the wash water flows through the side- and bottom nozzles and the extraction flow are stopped. To achieve a soft stop, the temperatures and some of the flows are stopped through first order step changes with filter time constants in the range $3 - 13$ minutes.

In the procedure of start-up, the extraction flow is first opened. This is because the liquor level has been increased considerably during the stop period, see Fig.

(5.70). At the same time, the chip feed is started. Further, with intervals 3, 4, 3, and 56 minutes respectively, the wash water flows, the blow flow, the lower wash circulation flow, and the cooking circulation flow are started. Finally, the steam- and cooking circulation temperatures are raised to their normal levels.
In this way, the liquor level is reduced, and the chip level is increased against their respective set-point values, c.f. Figs. (5.69) and (5.70). At the point where the chip level reaches the set-point, both the level controllers are turned to automatic control. [5]

Fig. (5.68) shows how the chip temperature in the digester top and at the cooking circulation screens decreases before the stopping time 2.3 hours. The subsequent increase is due to the heat of reaction. Further, at start-up when colder chips (137^oC) enter the vessel, a drastic temperature decrease below the nominal values is followed by a smooth increase against these.

Fig. (5.69) shows how the chip level first increases about $70cm$ before it is reduced. The increase is due to the rapid closure of the blow flow when, at the same time, the chip feed is rather slowly decreased. Then, the chip level decrease is due to the contraction of the chip mass when the Kappa number is reduced. It reaches its minimum value at about 4 hours. The net reduction in the chip level is about 1.7 metres.

The liquor level increases almost through the whole stopping period, see Fig. (5.70). This is both due to the same reason as for the initial chip level first increase, but mostly due to the displacement of the liquor in the vessel during the contraction of the chip mass as explained above.

Fig. (5.71) shows a 3D-plot of the Kappa number profile as a function of time. The total Kappa number reduction in the discharged pulp is about 40 units, see Fig. (5.72). The figures illustrate that the dispersive effect in the chip plug is considerable in a transient period like this. The 40-unit decrease in the discharged pulp is smaller than the maximum decrease in the digester, see Fig. (5.72). Hence, there is a considerable amount of mixing in the wash zone after the start-up. This is shown in Fig. 5.73. This figure reveals a weakness in the model as well. The Kappa number increase in the top section ($40m$), at about 2.7 hours, is due to the chip velocity increase as explained below, c.f. Eqs. (3.146)-(3.151). This weakness is the description of the component balances in the top section, see the remarks in Sec. 3.5.3.

When the blow flow is stopped, the chip velocity in the whole column is immediately retarded as shown in Fig. (5.74). As a result, the compaction of chips is increased, see Figs. (5.75) and (5.76). There is only a slight increase in the cooking zone. This is due to the subsequent acceleration of the chip plug, which is caused by the wash water stop. Thus, the viscous friction force in the wash zone is dramatically reduced, and the chips settle on the digester bottom; the compaction of chips increases considerably in the wash zone. Further, because the vertical movement is stopped in the bottom, the chip plug eventually settles down; the

[5] The controllers have only P-function and operate around the steady-state points. Hence, the steady-state control errors are zero.

chip velocity goes to zero. As a result of the Kappa number decrease, the compaction of chips is increased in the cooking zone ($2.5-4$ hours). In the wash zone, however, the compaction is reduced. The reduction is larger more downstream. This is caused by the fact that the compaction increase is larger downstream as a result of the blow flow stop. Hence, the chip pressure increases more downstream as well, see Fig. (5.78). The result is that the chip plug reverses, see Fig. (5.74) ($2.5-4$ hours). Note that this chip plug movement is not due to elasticity, c.f. the section about compressibility in Sec. 3.3.3. The movement is described as inelastic deformation. Hence, the over-shots in the chip velocity and the compaction, denoting a higher order system, have to do with chips that push each other in both vertical directions (i.e. chip pressure changes). In this context, it should be noted that the force of inertia is neglible during the whole period (as is the case at steady-state as well, c.f. Sec. 5.1). Hence, even though the weight of the chip plug is large, the force of inertia is small because the velocity is low.

After the start-up, the result of starting the extraction flow and the wash water flow before the blow flow, is that the compaction of chips increases dramatically from both sides against the extraction area, see Figs. (5.75) and (5.76). This increase appears about 4 hours later in the bottom. The peak around the extraction area is "damped" in the chip pressure as shown in Figs. (5.77) and (5.78).

Because the wash water flows are continued 5 minutes after the blow flow is stopped, the liquor velocity in the wash zone is increased considerably as shown in Fig. (5.79). As a result, the concentrations of free alkali and dissolved solids are reduced dramatically in the wash zone. Figs. (5.80) and (5.81) show how the free and entrapped concentrations of the two components approach during the stopping period. Because no alkali is supplied during this period, the concentrations in the cooking zone decrease as the alkali is consumed during the chemical reactions. This decrease is reflected at the extraction screens as well. Hence, the concentration of alkali may be a limiting factor for the Kappa number reduction during longer stop periods and lower feed concentrations. Note that the concentrations at the extraction screens are influenced by the changes in both zones. The increase in the concentrations of dissolved solids at the extraction screens after the start-up is due to the accumulated concentration in the cooking zone during the stopping period.

A conclusion to the results of this scenario, where the digester is run in rather extreme conditions, is that valuable information may be retrieved, despite certain model deficiencies. In addition to gaining a better understanding about the physical behaviour of the mass during the stop, such information may also be used in designing improved stop- and start procedures. It appears that better knowledge about the dispersion coefficient may improve the prediction of the Kappa number in the blow flow after these type of transients.

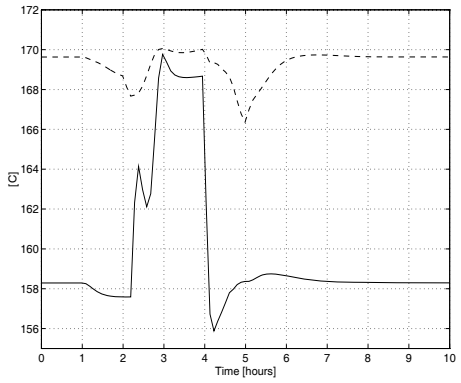

Figure 5.68: Chip temperature in the top section (solid line) and at the cooking circulation screens (dashed line) during the short-stop

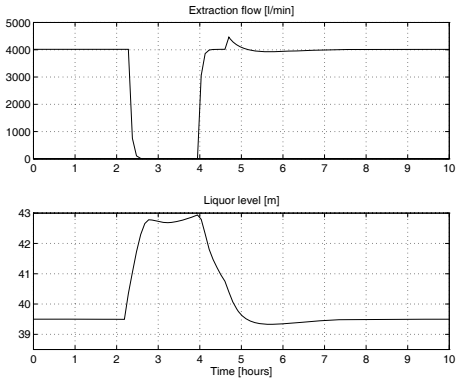

Figure 5.70: Extraction flow and liquor level during the short-stop

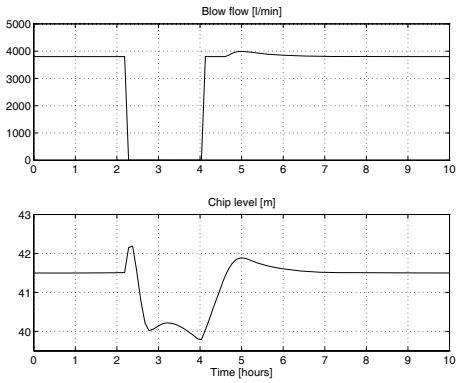

Figure 5.69: Blow flow and chip level during the short-stop

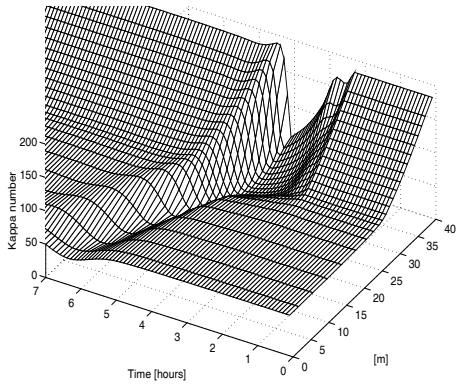

Figure 5.71: 3D-plot of the Kappa number lapse during the short-stop

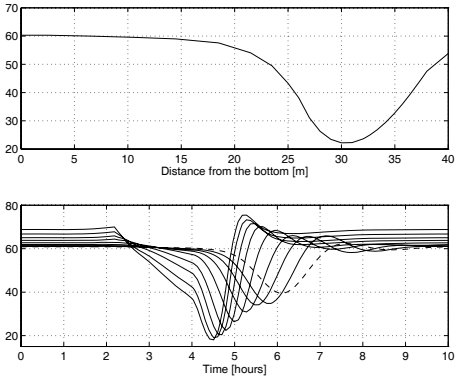

Figure 5.72: Kappa number profile at time 4.1 hours (upper figure), and the Kappa number lapse in the wash zone (lower figure)during the short-stop. The dotted line shows the discharged pulp.

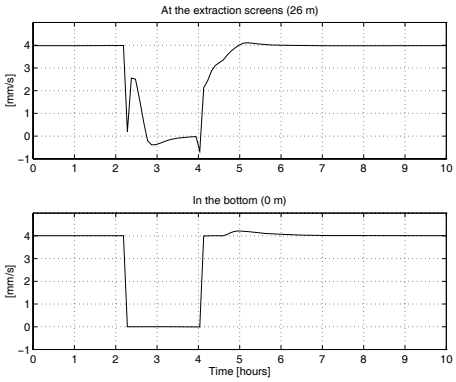

Figure 5.74: Chip velocity during the short-stop

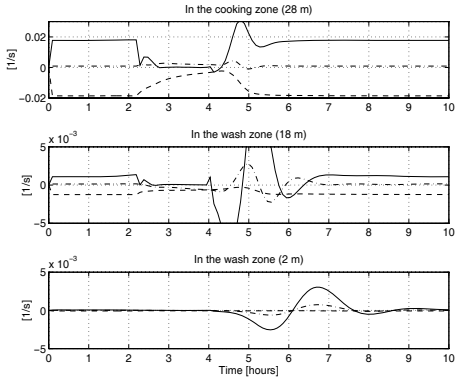

Figure 5.73: The convection (solid line), reaction (dashed line), and the dispersion (dashed-dotted line) terms in the equation for the mass balance of lignin Eq. (3.232) during the short-stop

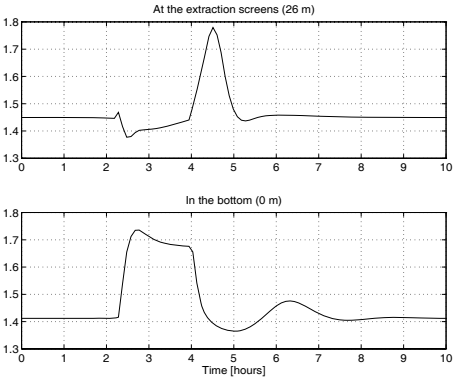

Figure 5.75: Compaction of chips during the short-stop

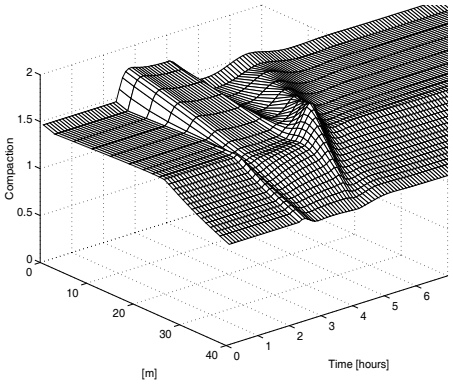

Figure 5.76: 3D-plot of the compaction of chips during the short-stop

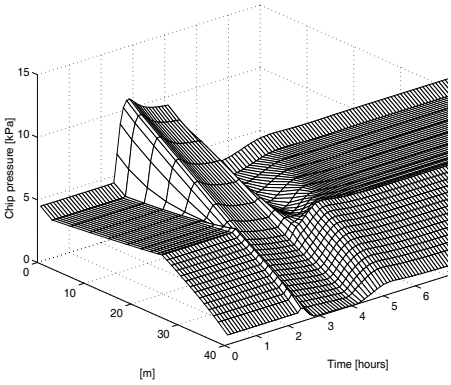

Figure 5.78: 3D-plot of the chip pressure during the short-stop

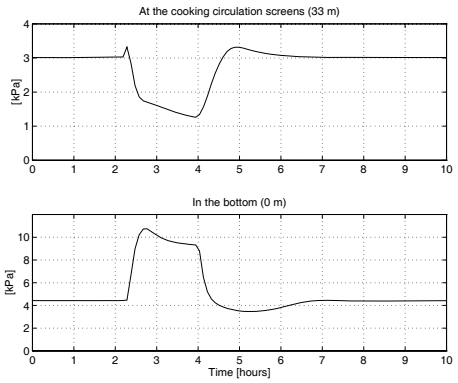

Figure 5.77: The chip pressure during the short-stop

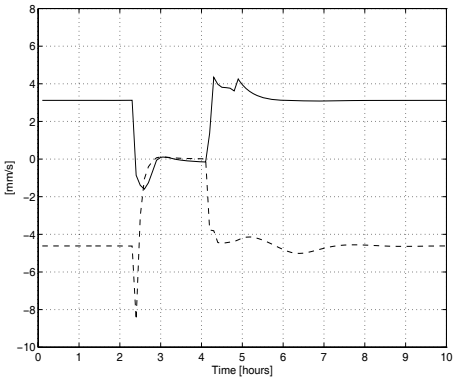

Figure 5.79: The liquor velocity in the cooking zone (solid line) and in the wash zone (dashed line), during the short-stop

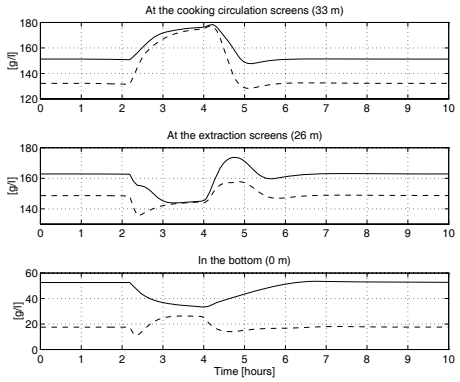

Figure 5.80: Concentration of entrapped (solid line) and free (dashed line) dissolved solids during the short-stop

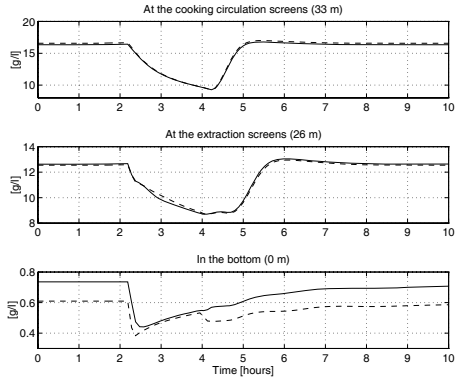

Figure 5.81: Concentration of entrapped (solid line) and free (dashed line) effective alkali during the short-stop

Chapter 6

Linear analysis

This chapter includes discussions on selected topics on linear analysis of the proposed model. It is assumed that the reader is partly familiar with the terms that are used. To investigate the properties of the model, both operating points for the digester are used. These are denoted HPR (the high production rate) and LPR (low production rate).

Linearizing process models give additional opportunities to analyse the process, as the main part of the available analysis methodology is based on linear models. One may query the validity of the results from a linear analysis of our process model which is fundamentally nonlinear. Linear models, in this context, are only valid in a limited region around the operating point at which the linearization is made. When we know that the digester mainly operates at fixed operating points, like at a low and a high production rate, and the perturbations around these points mainly are limited, such linear results may be valid. Hence, the results from the analysis may give valuable information about the process, that otherwise is not possible to achieve. Such information may be used both in the design (or redesign) of the process, and perhaps most important, in control system design.
In the proceeding sections, focus is placed on the dynamics in the model. The Jacobian matrix is investigated in Sec. 6.2. In particular, which state variables are affected by the slow versus fast dynamics in the process are revealed. The stability of the model is discussed as well. In Sec. 6.3, we make a controllability analysis. Such information is valuable in the design of control structures for the digester. Dynamic simulation of the linearized models, so as to compare with the non-linear model, is not considered.

6.1 Model linearization and tools for analysis

6.1.1 Linearization

The linearization of the resulting state space model Eq. (4.1) around a steady-state operating point, gives a linear constant coefficient state space model of the form:

$$\dot{\mathbf{x}} = A\mathbf{x} + B\mathbf{u} \tag{6.1}$$

$$\mathbf{y} = C\mathbf{x} + D\mathbf{u} \tag{6.2}$$

where $\mathbf{x} \in \Re^n$ is the state vector, $\mathbf{u} \in \Re^r$ is a vector of manipulated (or input) variables, and $\mathbf{y} \in \Re^m$ is a vector of measurements (or outputs). A, B, C and D are constant matrices of appropriate dimensions. Here, the values of $\mathbf{x}$, $\mathbf{u}$, and $\mathbf{y}$ denote variations about the steady-state operating point $(\mathbf{x^s}, \mathbf{u^s}, \mathbf{y^s})$. The A matrix is denoted the *Jacobian matrix*, or the system matrix. Note that the algebraic equation Eq. (4.2) is included in Eq. (6.1) through the coefficient matrices.

The perturbation levels for the states, x_i, and for the manipulated variables, u_i, are $0.01 + 10^{-5} \cdot \mid w_i^s \mid$, $w_i^s = x_i^s, u_i^s$, $i = 1, .., n$ and r respectively. Thus, the respective elements in $\mathbf{x}$ and $\mathbf{u}$ are weighted to account for differences in the numerical values.

6.1.2 Transfer functions and singular value decomposition

In what follows, it is convenient to discuss the model properties in the frequency domain. Hence, the concept of *transfer functions* is introduced. In multivariable systems, i.e. when several in- and outputs are considered simultaneously, we consider *transfer function matrices* (or *transfer matrices*). The transfer matrix, $H_p(s) \in \Re^{m \times r}$, for the process is defined as:

$$\mathbf{y}(s) = H_p(s)\mathbf{u}(s) \tag{6.3}$$

where $\mathbf{u}(s)$ and $\mathbf{y}(s)$ are the input and outputs. In multivariable systems the *directions* of the in- and output vectors, i.e. the combinations of the individual vector elements, are of interest. These are analysed using *singular value decomposition (SVD)* (see e.g. Strang (1988) for details). The transfer matrix, $H_p(s)$, is decomposed into three matrices:

$$H_p(s) = W(s)\Sigma(s)V^H(s) \tag{6.4}$$

where $W(s) \in \Re^{m \times m}$ is the decomposition of the output space, $V(s) \in \Re^{r \times r}$ is the decomposition of the input space. These are unitary. $\Sigma(s) \in \Re^{m \times r}$ contains a zero sub-matrix when $m \neq r$, and a diagonal positive semi-definite matrix $\Sigma_1(s) \in \Re^{k \times k}$, $k = min\{r, m\}$ of *singular values* arranged in descending order. The largest singular value, denoted $\overline{\sigma}$, expresses the largest multivariable gain in the system, and the smallest singular value, denoted $\underline{\sigma}$, expresses the smallest non-zero multivariable gain.
The Euclidean (or 2-norm) condition number of $H_p(s)$ is defined as $\gamma = \overline{\sigma}/\underline{\sigma}$.

Referring to the frequency plots that are shown, the frequency axis has dimension radians per dimensionless time (t/t_0 seconds where $t_0 = 750sec$). The interval $1.0 \cdot 10^{-3} - 1.0 \cdot 10^3$ covers time constants between 4.7 seconds and 1309 hours (i.e. approximately steady-state). Hence, $frequency = 1.0$ corresponds to a time constant of $T = 2\Pi \cdot 12.5 = 78.5$ minutes.

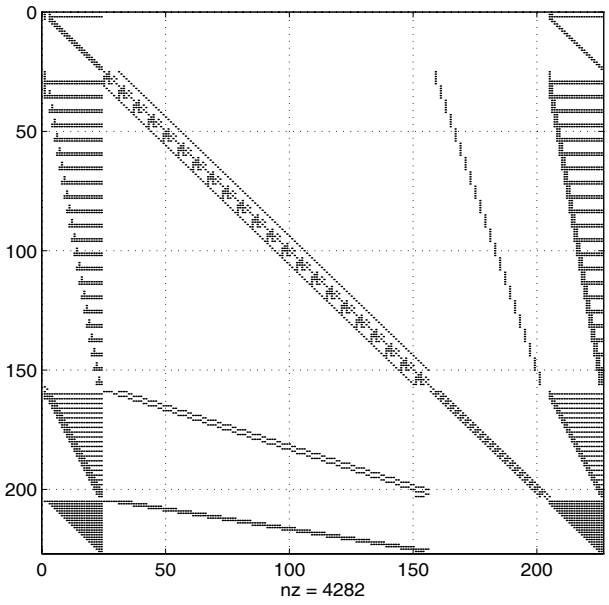

Figure 6.1: Visualization of the sparsity pattern in the Jacobian matrix

6.2 The Jacobian matrix

Fig. 6.1 shows the sparsity pattern of the Jacobian matrix.

According to Eq. (4.1), $A = (\partial \mathbf{f}_1 / \partial \mathbf{x})$. This matrix has the same sparsity pattern in the two operating points, whereas the values of the elements differ. The latter means that the process gains (and hence also the dynamics) are different in the two cases. The reason is the nonlinearity in the original model. The Jacobian is a real matrix, i.e. its elements are real-valued.
Referring to the figure, the states are ordered sequentially as follows: the chip- and liquor levels (state no. 1 and 2), volume fraction of chips (state no. 3 to 24), chip and liquor components (state no. 25 to 156), chip and liquor temperatures (state no. 157 to 204), and chip velocity (state no. 205 to 226). The variables that are distributed, i.e. all but the levels, are ordered in the subsequent slices from the top to the bottom in the digester.

6.2.1 The matrix elements

The figure shows that out of totally $226 \cdot 226 = 51076$ elements in the matrix, only 4282 of them are non-zero. These are plotted as dots in the figure. As a large majority of variables do not affect each other, the matrix is sparse. In fact, the result is typical to solutions of problems that are approximated by replacing a distributed system by a series of stirred tanks. Parameters are placed in a band along the main diagonal. In our case, the band width is essentially three along

the horizontal and vertical axis in the matrix, which means that the states in the neighbouring-slices up- and downstream both influence, and are dependent on, the respective state in a given slice. This results from the use of the MAC-scheme in the spatial discretization, c.f. Ch. 4. Note that due to the specific ordering of the state variables, the inter-relationships between for instance the wood and liquor components in the same slice accidentally appear along the diagonal band as well. Hence, the band width is wider than three elements in the middle part of the matrix that corresponds to these variables. The inter-relationships between the model variables can be studied by comparing the matrix elements with the model equations in Ch. 3. An example of this is that the volume fraction of chips, ϵ_c, in all downstream slices influence the liquor component variables, the liquor temperature, and the chip velocity in a given slice. This results from the incompressibility assumption for the free liquor, i.e. the continuity equation Eq. (3.128). Thus, changes in ϵ_c in a given location result in changes in the liquor velocity in the whole vessel. Hence, all the model variables that are directly affected by the liquor velocity are affected, denoted by a dot in Fig. 6.1. This gives the upper triangular shape of the shown sub-matrices.

The Jacobian matrix is strongly ill-conditioned with respect to matrix inversion and linear equation solution. This means that the sensitivity is high to the solutions of the algebraic equations to errors in the problem formulation. The ill-conditioness is expressed by the condition number, γ, for the matrix. The Euclidean condition number is about $3 \cdot 10^{10}$ and $2 \cdot 10^{11}$ for HPR and LPR respectively. Note that these numbers are greater than $1/sqrt(eps) = 6.7 \cdot 10^8$, where *eps* is the machine precision.

6.2.2 The eigenvalues

An analysis of the autonomous dynamics may give valuable insight into the model, e.g. information about the choice of state variables. Based on this, we may decide what improvements can be made so as to achieve a well-conditioned problem. This has influence on both dynamic simulation of the open loop model, and control.

Even though the Jacobian matrix is ill-conditioned, it may have a well-conditioned eigenproblem. The eigenproblem results from diagonalization of the state space model Eq. (6.1). All eigenvalues at the two operating points are distinct, which means that a full set of independent eigenvectors exists. This means that diagonalization is possible (see e.g. (Strang, 1988)). The diagonalized (or canonical) form is expressed as:

$$\dot{\mathbf{q}} = \Lambda \mathbf{q} + H \mathbf{u} \tag{6.5}$$

$$\mathbf{y} = F \mathbf{q} + D \mathbf{u} \tag{6.6}$$

where $\mathbf{q} \in \Re^{\mathbf{n}}$ is the state vector for the system, $\Lambda \in \Re^{n \times n}$ is the eigenvalue matrix, $H = M^{-1}B \in \Re^{n \times r}$, $F = CM \in \Re^{m \times n}$, and $M \in \Re^{n \times n}$ is the eigenvector

matrix [1] (see any textbook on linear algebra).

Fig. 6.2 shows the real part of the eigenvalues of A.

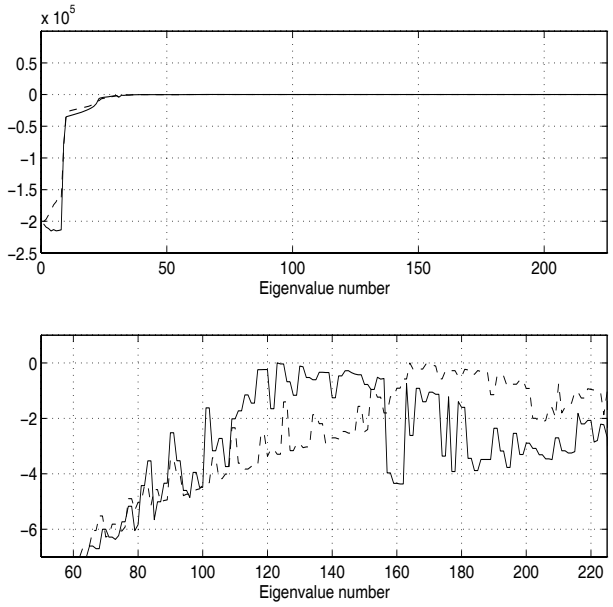

Figure 6.2: The real part of the eigenvalues of the Jacobian at high production rate (solid line), and low production rate (dashed line)

Some eigenvalues are real, whereas the others appear as complex conjugate pairs. To the latter, the entries in the corresponding eigenvectors are complex conjugate pairs as well. [2] Because of the canonical transformation $\mathbf{x} = M\mathbf{q}$ in the diagonalization of the system, the absolute value (or length) of the corresponding eigenvector entries tells about the weight, or degree of influence, from the eigenvalue under consideration to the corresponding physical state variable in the state vector, $\mathbf{x}$.

It appears from Fig. 6.2 that eigenvalue no. 123 at the high production rate, respective no. 164 at the low production rate, are close to zero, i.e. the origin [3] ($3.8 \cdot 10^{-3}$ at HPR, respective $5.4 \cdot 10^{-3}$ at LPR). Fig. 6.3 shows the elements in eigenvector no. 123 (real) at HPR. The corresponding vector at LPR contains essentially the same result. It appears that the largest values are those that correspond to the chip and liquor levels (largest for the liquor level (element number

[1] Note that even though the eigenvector matrix, M, is strongly ill-conditioned as well (the condition number is respectively $8.3 \cdot 10^8$ and $1.6 \cdot 10^8$ at the two operating points), the back-multiplication $A' = M\Lambda M^{-1}$ gives A' close to the original A matrix.

[2] This is always the case (see any textbook on linear algebra).

[3] From linear algebra, we know that the corresponding eigenvectors, to the eigenvalues in the origin, are in the nullspace of A. Further, a zero eigenvalue signals that A has linearly dependent columns and rows; A is singular and its determinant is zero. Diagonalization is, however, as mentioned possible.

2)). Hence, these are mostly affected by this dynamics, corresponding to time constants respectively about 55 and 40 hours. The liquor components are also affected by this dynamics, though much less than the levels.

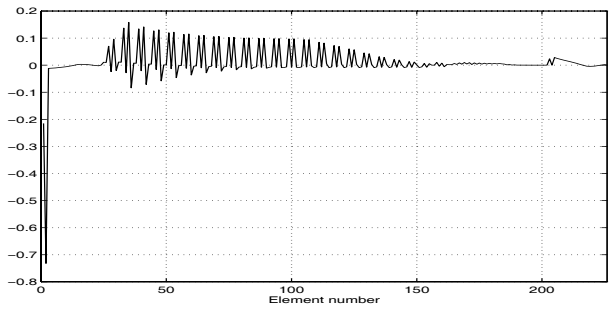

Figure 6.3: The absolute values of the elements in the eigenvector which correspond to the smallest eigenvalue in the Jacobian matrix at the high production rate

The eigenvalues nos. 1 to 21 are the largest (all real). $2.0 \cdot 10^5$ corresponds to a time constant of about $3.8ms$. This is the fastest autonomous dynamics in the model. It appears from the corresponding eigenvectors that only the chip velocity at the respective locations in the vessel is influenced by these. The physical interpretation of this is that the acceleration of the chip plug is extremely high.

The span between the fastest and the slowest dynamics in the model is about $6 \cdot 10^7$, c.f. the condition number as commented on page 166.

In the same way, information about the middle-range dynamics can be analysed. As an example, the chip level, the compaction of chips in the bottom of the digester, and the wood and liquor components in the wash zone are most affected by the dynamics corresponding to time constants in the range $1 - 6$ hours. The latter may be attributed to the low reaction rates and consumption of alkali in this zone, where both the temperature, the concentration of alkali, and the amount of residual lignin are low.

6.2.3 Discussion

- The Jacobian matrix is strongly ill-conditioned. This has two reasons:
  - First, the largest entries in the matrix are of order 10^7. These correspond to the gains from the concentration of lignin and the volume fraction of chips, to the chip velocity (c.f. the compressibility equation Eq. (3.6)). This means as well that the largest singular value (multivariable gain) of the matrix is related to the chip velocity. [4] Note that this ill-conditioness results even though the model states are rescaled (normalized), see Sec. 3.8.

[4] From linear analysis we have $\overline{\sigma}(A) \geq \max_{i,j} \mid a_{i,j} \mid$ where $a_{i,j}$ are the entries in the matrix A.

  - Second, the equations for the chip- and liquor levels, Eqs. (3.142) and (3.144), are almost pure integrators (singularities).
    The chip level, Eq. (3.142), is slightly damped, due to the compaction equation in the top section, Eq. (3.145), and the weight change of the chip plug that changes the amount of discharged wood.
    Liquor level changes, Eq. (3.144), are weakly damped by the process downflow due to the buoyant force on the chip plug that influences the amount of discharged wood.
    The "zero" eigenvalue is, however, positive at both operating points. This means that the linear model is open loop unstable. However, from the simulation of the nonlinear model, we know that this is stable. Hence, the nonlinear model includes some stabilizing mechanisms that do not appear in the linear model due to numerical approximations. [5]
    This depends on how strong the nonlinearities are.

- The above discussion means that the ill-conditioness of the Jacobian is reduced by:
  - Solving the momentum balance equation for the chip plug as a steady-state equation. This removes the chip velocity from the state vector, and hence reduces the maximum singular value.
  - Including stable control loops for the chip- and liquor levels. By this, the integrators are moved into the left half plane, and the minimum singular value is increased.

6.3 Controllability analysis

In this section, SISO (Single Input Single Output) control loops for the chip- and liquor levels are included.

Controllability is commonly treated in the meaning *state controllability* by Kalman's definitions (Kalman, 1960), (Kalman, Ho and Narendra, 1963). State controllability of distributed systems are extended by Herget (1967). This is only briefly discussed here.
In the following, focus is made on the other main type of controllability, denoted *input-output controllability* (sometimes also denoted as functional controllability). As the name tells, this is based on an input-output model. This section starts by selecting a vector of outputs as property variables, and a vector of input variables which we in advance know affects these properties. The controllability analysis is twofold. (1) For SISO controllability, we study transfer functions (gains and phase angles). (2) For MIMO (multi input multi output) controllability, we consider singular value decomposition (SVD) (gains, and in- and output directions), where the condition number plays a key role. Some conclusions are given in the last section.

[5] *..in an applied setting where noise and imprecision exists, the answer to the question of existence will almost always be technically "yes" even though perfectly accurate data might lead to a "no" answer (Moore, 1978).*

6.3.1 Selection of inputs and outputs

The selection of output variables is a question of what properties are of interest to control. In Sec. 3.2.3, the quality variables are defined as the Kappa number κ_{bf} and the concentration of entrapped dissolved solids in the blow pulp $\rho_{ds,el,bf}$, and the concentration of effective alkali in the extraction flow $\rho_{EA,fl,ex}$. As we in this study focus the residence time for the chips in the digester, τ, we included this as well as a property that is of interest to investigate the controllability of. Thus, the property vector is defined as: [6]

$$\mathbf{y} = \begin{bmatrix} \tau \\ \kappa_{bf} \\ \rho_{ds,el,bf} \\ \rho_{EA,fl,ex} \end{bmatrix} \tag{6.7}$$

The chosen quality measures are dependent on the three factors; temperature, concentration of alkali and residence time. Regarding the influence from the temperature, the results in Sec. 5.3.1 indicate that the steam temperature, T_s, is of most importance. Further, the alkali concentration is controlled by the concentration in the feed to the top of the digester, $\rho_{EA,in}$. The residence time is determined by the chip level (which is controlled by the blow flow) and the chip velocity. We include the chip level set point, $h_{c,sp}$, as manipulated variable. The chip velocity is externally affected directly by the liquor flows and the production rate, c.f. Eq. (3.169). The production rate is controlled by the feed flow of chips, $q_{c,in}$. The liquor flow in the cooking zone is controlled by the L/W-ratio, Eq. (3.84), while in the wash zone, it is controlled by the wash water flow. We omit the influence from the L/W-ratio since the influence on the residence time is limited compared to the influence from the wash water flow, c.f. Table 5.6 in Sec. 5.1. The influence from the wash water flow, q_{wash}, is, however, considerable (see Sec. 5.3.1).
From this, we define the vector of manipulated variables as:

$$\mathbf{u} = \begin{bmatrix} T_s \\ \rho_{EA,in} \\ q_{wash} \\ q_{c,in} \\ h_{c,sp} \end{bmatrix} \tag{6.8}$$

The chip- and liquor levels are controlled in the same way as explained in Sec. 5.3. Note that the regulatory control of all the inputs are implicitly included in the model.

The chosen input-output pair Eqs. (6.7)-(6.8) defines a 4×5 system for our process model. Note that since each of the four outputs represents different state variables, these are linearly independent. Hence, only four linearly independent inputs are

[6] One may query why typical measurement variables in real plant operations are not included in this vector. The question of availability of gauges, their resolution, and the possibility to apply them in a plant, is a question of instrumentation rather than model properties. Moreover, if the chosen property vector is identifiable from the available measurements, this is a question of observability; a property which is not focused on in this study.

required to control these, if non of the inputs are in saturation. Whether these specific inputs are able to control the outputs, is also a question about the choice and location of the inputs. The advantage of having more inputs than outputs is that the system may still be controllable if one of the inputs goes into saturation. On the other hand, we may have included one more output to control our system.

Before we study the gains in the model, the in- and outputs are rescaled such that the rescaled u_i and y_i, denoted $u_i^{'}$ and $y_i^{'}$, have values between -1.0 and 1.0. The rescaling matrices are:

$$S_u = diag\{\frac{1}{185^oC}, \frac{1}{30g/l}, \frac{1}{3500l/min}, \frac{1}{25rpm}, \frac{1}{45m}\} \tag{6.9}$$

$$S_y = diag\{\frac{1}{3h}, \frac{1}{70}, \frac{1}{100g/l}, \frac{1}{20g/l}\} \tag{6.10}$$

The diagonal elements express the upper expected bounds for the respective in- and output variables.
The rescaled system is described by:

$$\mathbf{y}^{'}(\mathbf{s}) = S_y H_p(s) S_u^{-1} \mathbf{u}^{'}(\mathbf{s}) \tag{6.11}$$

Thus, the rescaled transfer matrix, $H_p^{'}(s) = S_y H_p(s) S_u^{-1}$, does not include artificial high or small gains due to the differences in the numerical values of the original in- and output variables in the chosen operating points (c.f. Sec. 3.8). Note, however, that some of the results in the following sections (transfer function gains, singular values, as well as the corresponding in- and output directions) are scaling dependent. Hence, the same comments apply here, as in the footnote on page 135 The phase curves, however, are not dependent on these factors.

6.3.2 About controllability

As a background for the controllability analysis in the proceeding sections, the term controllability is discussed in this subsection. Even though focus is placed on input-output controllability in this chapter, it may be necessary to pin-point what is special about state controllability for a distributed process like the continuous digester.

State controllability

The models that we build should be as simple as possible, and hence, the dimension of the state vector should not be unnecessarily large. Hence, the minimality of the state vector depends on the state controllability and -observability of the system (Aoki, 1990). Unlike stability, each of these two properties depend on a pair of matrices. Viewing Eqs. (6.1) and (6.2), the matrices A and B jointly determine the controllability property, and that of A and C the observability property. When the model possesses both of these properties, then the minimality of the state vector dimension is assured (Kalman, 1960).

Kalman's state controllability, as used in linear state space control theory, is defined as:

If any value of the state vector of a linear dynamic system can be achieved in finite time by the appropriate use of the manipulated variables, then all the states of the system are controllable.

This was originally made for mechanical systems. Based on this, the system (A, B) is controllable if the controllability matrix:

$$Q_c = [B, AB, A^2B, ..., A^{n-1}B] \tag{6.12}$$

has rank n which is the number of states in the system. The degree of controllability may be determined by the condition number of this matrix.
From this definition, we see that when $n \to \infty$, the condition number of Q_c also approaches infinity if the norm of A is greater than 1. Hence, for distributed systems this definition is useless, as the degree of controllability is dependent on the number of discretization grids (the finer the grid spacing, the less controllable is the system).
The physical interpretation of this is that the states that belong together, e.g. those which comprise the chip velocity profile, are tightly coupled like pearls on a string. This means that, for instance, manipulation of the chip velocity in a given grid point to say $1mm/s$, and manipulation of the chip velocity in one of the neighbour grid points to say $1m/s$, is obviously not possible or neither of interest. What may be of interest, however, is controllability of the chip velocity profile (and the other profiles), or the property measures for the process. The former means that the states which comprise the chip velocity profile are considered together as an *aggregated state*. The latter has to do with input-output controllability, as discussed in the next section.

Therefore, this theory has been extended for distributed systems (Herget, 1967). As it is generally complicated to analyse controllability for a specific system by this theory, this is not considered further here. In this context, it should be noted that the linear aggregation $\mathbf{x}' = P\mathbf{x}$, where $\mathbf{x}'$ is the vector of the twelve basic states $(h_c, h_l, \epsilon_c, \alpha_{lig}, ..., v_c)$ in the nonlinear PDE model, and P is a 12×226 projection matrix, neither leads to any answer about state controllability of $\mathbf{x}'$. The reason for this is that it is impossible to retrieve the information about our specific choice of the state vector $\mathbf{x}$ (i.e. number of discretization grids) back from the distributed state vector $\mathbf{x}'$. [7] Hence, aggregation in distributed systems has to be based on the PDE formulation of the model.

When transferring the model from the time domain to the frequency domain, only the modes that are both controllable and observable are preserved in the transfer matrix, $H_p(s)$. The consequence of this is that only the states that are both controllable and observable can be stabilized by feedback control (see e.g. Lunze (1992)). This means that if the state vector, $\mathbf{x}'$, in the PDE formulation of the model, is minimal (i.e. the corresponding linear system is balanced, i.e. of minimum realization), it is both state controllable and -observable. Further, finer

[7] It can be shown that the pseudo inverse P^+ of P, which is required in the computation of the transformed Jacobian matrix $A' = PAP^+$, don't exist. E.g. the matrix P^TP, in the left inverse $P^+ = (P^TP)^{-1}P^T$, has rank 12. This means that the columns or rows, which correspond to the individual grid states for the respective distributed variables, in P^TP are linearly dependent.

spatial discretization gives more modes (poles) and correspondingly more zeros in the the transfer matrix, $H_p(s)$. These zeros and poles almost cancel each other. In this way, the frequency responses of the respective transfer functions are almost the same when the number of grid points is above a certain limit.

Input-output controllability

It has been argued that Kalman's definition of controllability is rather limited compared to the use of the term in engineering practice. A number of alternative definitions appear in the literature (Rosenbrock, 1970), (Ziegler and Nichols, 1943), (Perkins, 1989). A key point is that controllability describes the inherent control characteristics of the system, and thus gives answer to how easy the system is to control. Moreover, the question of controllability is dependent on the objectives of the control.

Briefly, the question of input-output controllability is; "are the selected outputs controllable by the selected inputs?" In the following analysis, the system is controllable if the smallest singular value, $\underline{\sigma}$, of the transfer matrix is not zero (Rosenbrock, 1970). In this way, input-output controllability is a structural property and thus describes *structural controllability*, which means that the rank of the transfer matrix is equal to the number of outputs. Further, the degree of controllability is described by the condition number. High condition numbers, typically above 100, commonly indicate ill-conditioness and thus low degree of controllability. Here we assume that the scaling of the in- and outputs is proper (i.e. unit magnitude).

There are other factors which limit the controllability as well (Morari, 1983). In the linear plant representation:

$$\mathbf{y}(\mathbf{s}) = H_p(s)\mathbf{u}(\mathbf{s})$$

we want the outputs to equal their reference values (or set-points), $\mathbf{r}(\mathbf{s})$, i.e. $\mathbf{y}(\mathbf{s}) = \mathbf{r}(\mathbf{s})$. Hence, perfect control requires that the manipulated variables equal:

$$\mathbf{u}(\mathbf{s}) = -H_p^{-1}(s)\mathbf{r}(\mathbf{s}) \tag{6.13}$$

i.e. the controller inverts the process.

Controllability is limited when process inversion is not possible.

This occurs when:

- H_p^{-1} is unstable giving inverse responses (H_p has RHP-zeros)
- H_p has time delays (H_p^{-1} is non-causal)
- H_p^{-1} is large ($\underline{\sigma}$ is small) due to interactions, giving problems with input constraints.
- constraints in manipulators, gauges and other equipments

- H_p^{-1} is singular due to operating point changes

In addition, model uncertainty, giving sensitivity to disturbances, may also give problems with input constraints, or H_p^{-1} may be difficult to generate by other reasons (Skogestad, 1993).

In Sec. 6.2, the ill-conditioness in the system matrix A is discussed. As stated, this has to do with matrix inversion and linear equation solution ($b = Ax$). In the analysis of input-output systems, this has to do with both influence from input noise (or uncertainty), and controllability of the plant model.

- In the case of input noise, we consider the system

$$y(s) = H_v(s)v(s), \quad H_v(s) = (sI - A)^{-1}E$$

  where E is the input matrix, i.e. from the input noise to the states that define the noise. Here, the ill-conditioness of H_v has to do with full-block input uncertainty in the noise v, the sensibility of the measurements, and the internal plant couplings described by the matrix A.

- In the case of plant controllability, we consider the system

$$y(s) = H_p(s)u(s), \quad H_p(s) = C(sI - A)^{-1}B + D$$

  In this case the ill-conditioness of H_p has to do with the location and sensibility of the manipulators and measurements, in addition to the internal plant couplings described by the matrix A.

Note that the ill-conditioness of the system matrix A is reflected in H_v and H_p only if the respective (troublesome) states are excited and observed by the chosen in- and outputs. Hence, there is a close relationship between state controllability and input-output controllability.

6.3.3 Transfer functions

The following discussion treats the transfer functions between the input variables and the four outputs at high production rate. The results are qualitatively the same at the low production rate. Most important for SISO controllability are the phase angles. These can only be corrected for by a controller derivative function to a limited degree. With respect to the gains (magnitudes), these correspond well to the simulation results in Sec. 5.3.1 (Figs. 5.36,5.38,5.39,5.40).

The phase curves for the transfers from the wash water flow and the feed chip flow have been corrected for by -180^o, due to negative gain. Hence, e.g. an increase in the feed chip flow causes a decrease in the residence time, and vice versa. This is caused by the chip level control.

The influence on the residence time

The transfer functions between the respective inputs and τ are shown as functions of frequency in Fig. 6.4.

It appears from the phase curves that the influences from the wash water flow, the feed chip flow, and the chip level are good with respect to control for all frequencies in the range which is shown. The curves for the transfer functions from the wash water flow and the chip level do not decay at frequencies lower than about 10^4 ($0.5sec$). This is due to the fast acelleration of the chip plug. Note that for instance the transfer function from the chip level to the residence time may simply be described by a zero at about 0.1, a pole at about 2.0, and a gain. The gain from the chip level is dominating at higher frequencies. Further, it appears that the influences from the cooking temperature and the alkali feed are bad at frequencies above ω_{180} [8] about 1.0, corresponding to time constant 80 minutes.

These results mean that the residence time is best controlled by the manipulated variables which directly affect the vertical chip movement. The weak influences from the cooking temperature and the alkali feed at high frequencies may be explained by their long-term coupling through the reaction kinetics.

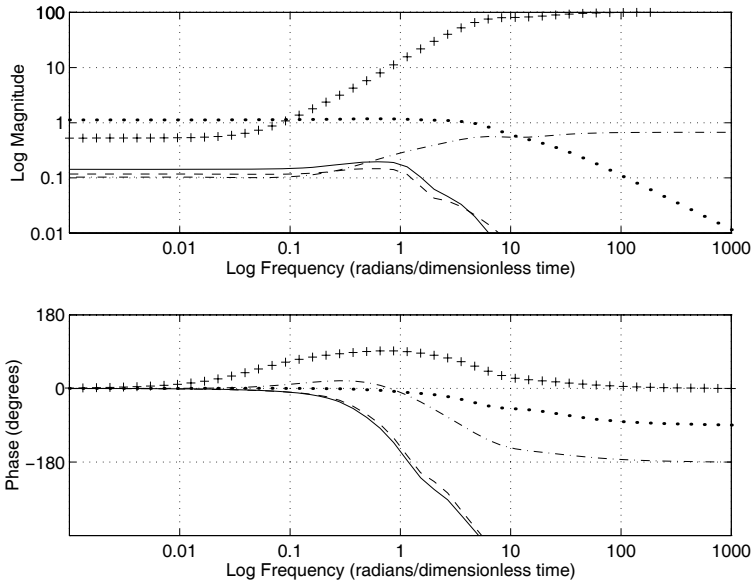

Figure 6.4: Bode plots of the transfer functions between the steam temperature (solid line), alkali feed (dashed line), wash water flow (dashed-dotted line), the feed chip flow (dotted line), the chip level (+ line), and the residence time for the chips at the high production rate.

[8] The frequency ω_{180} is defined as the lowest frequency where the phase curve cross -180 degrees.

The influence on the Kappa number

The transfer functions between the respective inputs and κ_{bf} are shown in Fig. 6.5.

We see from the phase curve that ω_{180} are about the same for all the channels (about 0.3, i.e. 4 hours). Further, all the curves decay dramatically at higher frequencies. This is typical for responses from transport delays. The results mean that the Kappa number cannot be controlled by the selected inputs on short time basis (say within a couple of hours). This is due to the slow dynamics connected to the reaction kinetics, and the transport delay from the top to the bottom in the digester. If the constraints in the actuators are similar, the SISO controllability of the Kappa number is about equal from the chosen manipulated variables (slightly better from the feed chip flow and the chip level than from the others).

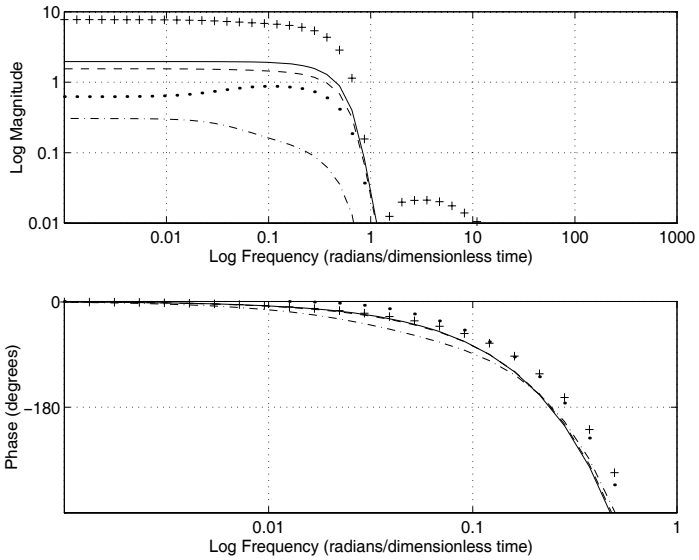

Figure 6.5: Bode plots of the transfer functions between the steam temperature (solid line), alkali feed (dashed line), wash water flow (dashed-dotted line), the feed chip flow (dotted line), the chip level (+ line), and the Kappa number in the blow flow at the high production rate.

The influence on the entrapped dissolved solids

The transfer functions between the respective inputs and $\rho_{ds,el,bf}$ are shown in Fig. 6.6.

It appears that there is no practical phase limitation in the transfer from the production rate (feed chip flow), although the gain at higher frequencies is low.

This may be explained by the fast chip level control loop and the considerable concentration gradient in the wash zone.
The transfer function from the wash water flow (which primarily is used to control the concentration of dissolved solids) has the lowest ω_{180}.
As for the Kappa number, the gains decay at higher frequencies from all the inputs.

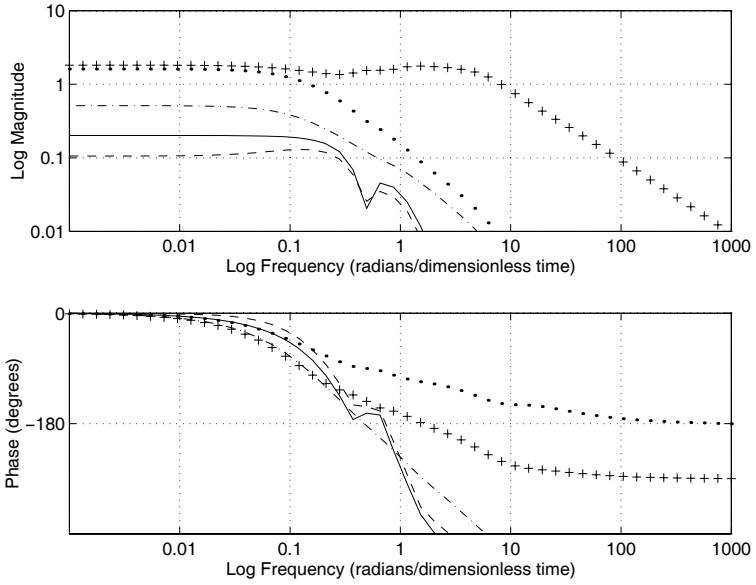

Figure 6.6: Bode plots of the transfer functions between the steam temperature (solid line), alkali feed (dashed line), wash water flow (dashed-dotted line), the feed chip flow (dotted line), the chip level (+ line), and the concentration of entrapped dissolved solids in the blow flow at the high production rate.

The influence on the free alkali

The transfer functions between the respective inputs and $\rho_{EA,fl,ex}$ are shown in Fig. 6.7.
The phase curves are about the same as for the previous case, except that the transfer from the feed chip flow has ω_{180} at about 20 (4 minutes). ω_{180} for the transfer from the alkali feed is about 0.6, corresponding to a time constant of about 2 hours.

6.3.4 Singular value decomposition

The four singular values and the Euclidean condition number for the resulting system transfer matrix are shown in Fig. 6.8. The latter is further discussed in Sec. 6.3.5.

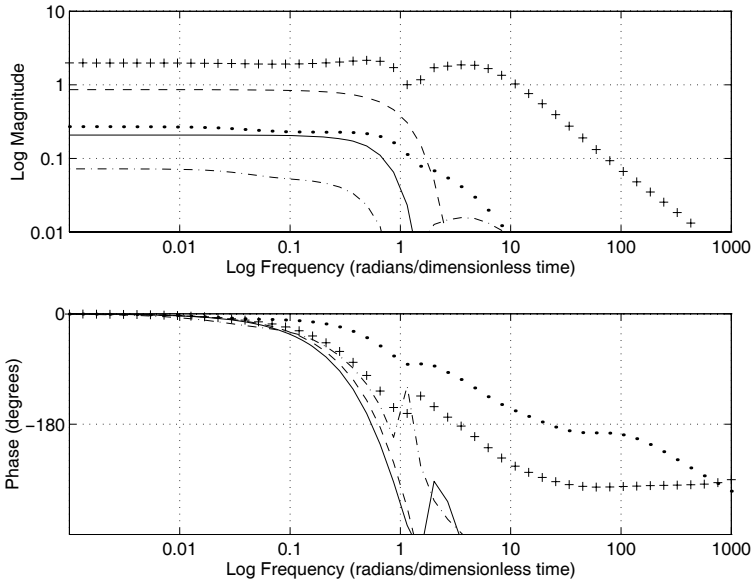

Figure 6.7: Bode plots of the transfer functions between the steam temperature (solid line), alkali feed (dashed line), wash water flow (dashed-dotted line), the feed chip flow (dotted line), the chip level (+ line), and the concentration of free alkali in the extraction flow at the high production rate.

The output matrix, W, has dimension 4×4 matrix, Σ is a 4×5 matrix, and V is a 5×5 input matrix. V has one row for each input. The first four column vectors describe the input directions (or singular directions) that have the singular values as gains as shown in Fig. 6.8. The resulting singular output directions are described by the respective column vectors in W. The latter column vector of V tells in which input direction these have no effect on the outputs (the corresponding "singular value" is zero). It appears that the matrix vectors are complex.

In Figs. 6.9 and 6.10, the respective first column vectors, as function of frequency, are shown at the high production rate. Fig. 6.9 shows the strongest input direction in the process model. This is the input direction which is required to achieve the largest multivariable gain (described by the largest singular value) on the output vector. The resulting output direction is shown in Fig. 6.10. It appears at the high production rate, at both low and high frequencies, the largest gain is achieved by manipulating the chip level strongest. When the inputs are excited in the shown direction, the Kappa number in the blow flow is most strongly influenced at low frequencies, while the residence time for the chips is most strongly influenced at high frequencies. The high frequency domain is, however, as already discussed of little interest for the pulp quality control. Note how the information about the phase in the transfer matrix is reflected in the relative phases between the inputs, and between the inputs and the outputs (i.e. the phase shifts from the input to the output directions). ± 180 degrees indicates a reduction in the respective

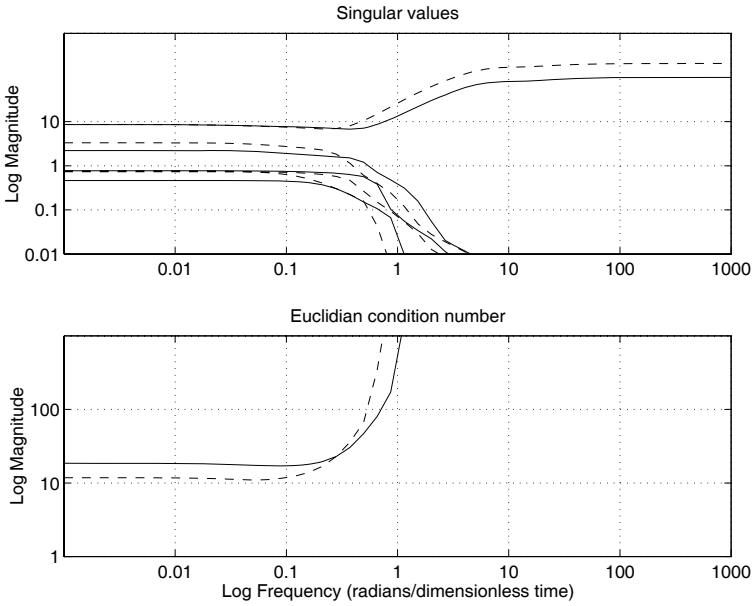

Figure 6.8: The four singular values and the Euclidean condition number for the transfer matrix at the high production rate (solid line) and the low production rate (dashed line).

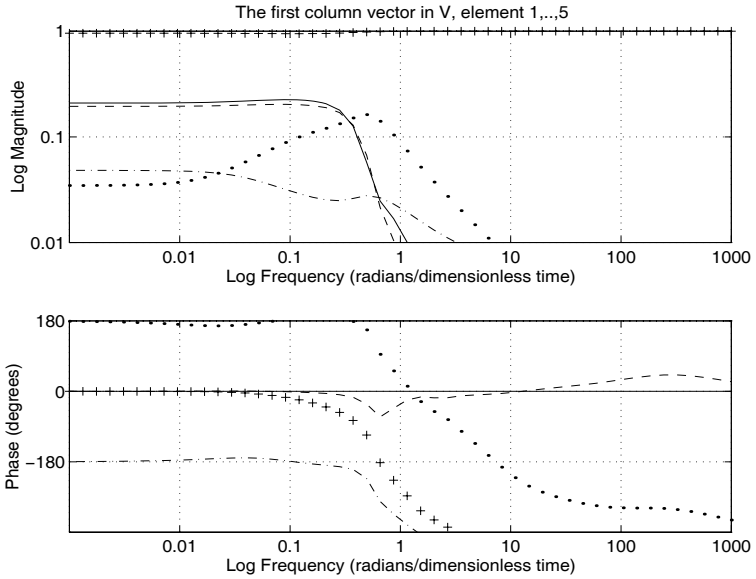

Figure 6.9: The strongest input direction for the transfer matrix at the high production rate. The subsequent elements are plotted as solid, dashed, dashed-dotted, dotted, and + marked lines.

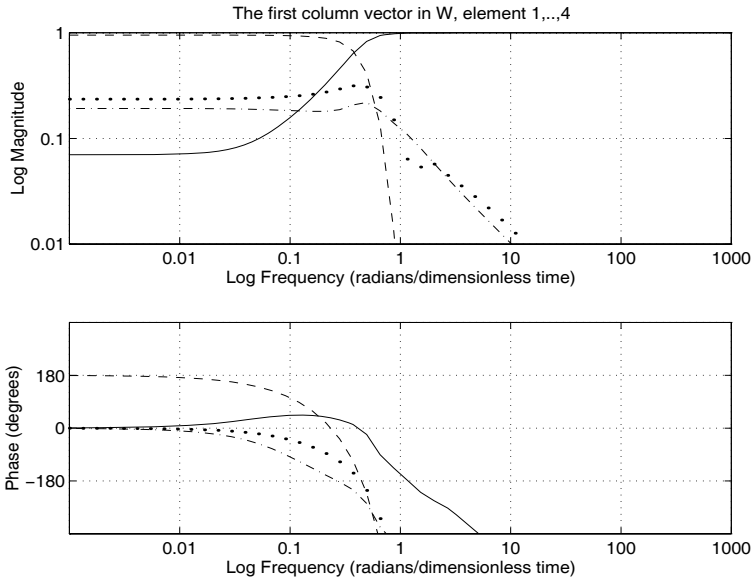

Figure 6.10: The strongest output direction for the transfer matrix at the high production rate. The subsequent elements are plotted as solid, dashed, dashed-dotted, and dotted lines.

variable compared to the variables which have phase 0 degrees. Further, the phases corresponding to the last four inputs and the outputs, are plotted relative to the first input (0 degrees).
The interpretation of these directions corresponds well to the results which are shown in Figs. 6.4 - 6.7.

At the low production rate, the results are mainly the same. Typically, the frequency where the curves for the residence time and the Kappa number cross, is lower, indicating that changes occur with larger time constants in this case (where the residence time is longer).

Figs. 6.11 and 6.12 show the respective fourth column vectors, i.e. the weakest in- and output directions that correspond to the smallest multivariable gain in the process model. The smallest singular value contains information of how close all 4×4 sub-transfer matrices are to be singular. Hence, this is the lower bound of the multivariable gain in the model. $\underline{\sigma}$ close to zero means that there is a path from the input that gives little influence on the output (giving large condition numbers).
It appears at the high production rate, at low frequencies, the smallest gain is achieved by controlling the residence time for the chips strongest by manipulating the steam temperature, the alkali charge, and the wash water flow strongest, and in the same direction. This corresponds well to the results in Fig. 6.4.
At high frequencies, the smallest gain is described by trying to control the Kappa number by manipulating the alkali feed strongest. As the Kappa number is badly

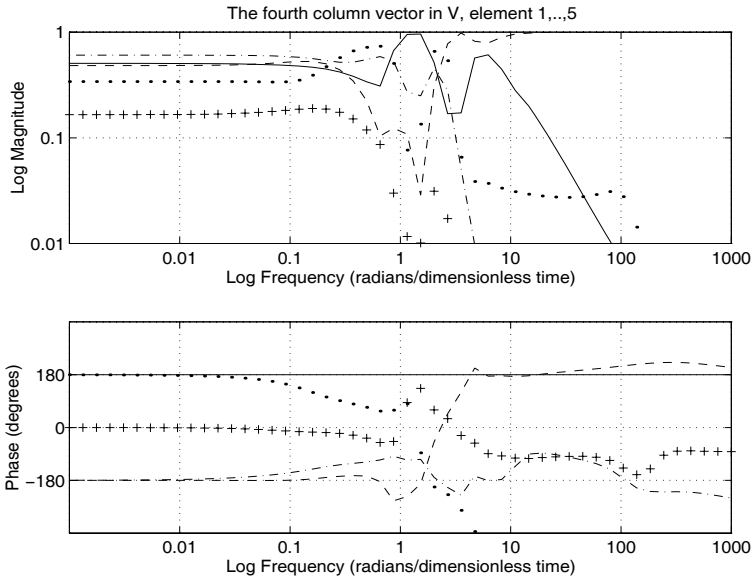

Figure 6.11: The weakest input direction for the transfer matrix at the high production rate. The subsequent elements are plotted as solid, dashed, dashed-dotted, dotted, and + marked lines.

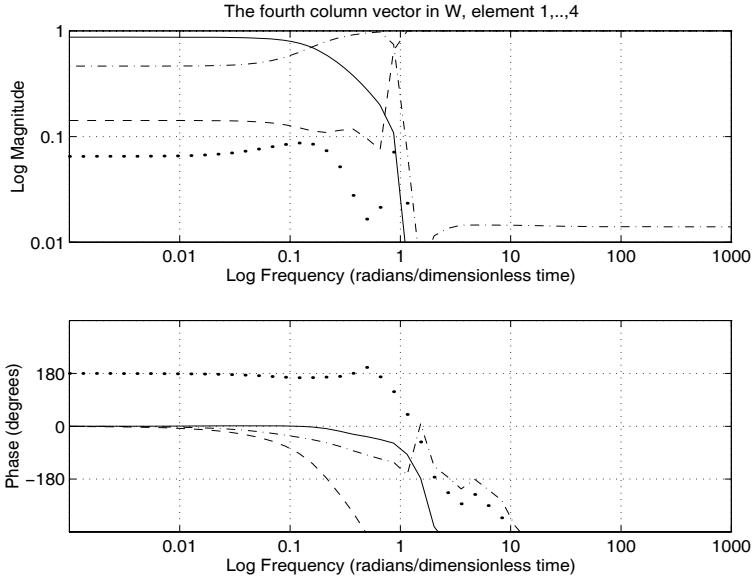

Figure 6.12: The weakest output direction for the transfer matrix at the high production rate. The subsequent elements are plotted as solid, dashed, dashed-dotted, and dotted lines.

controlled by any of the inputs in this frequency domain, this is only of theoretical interest.

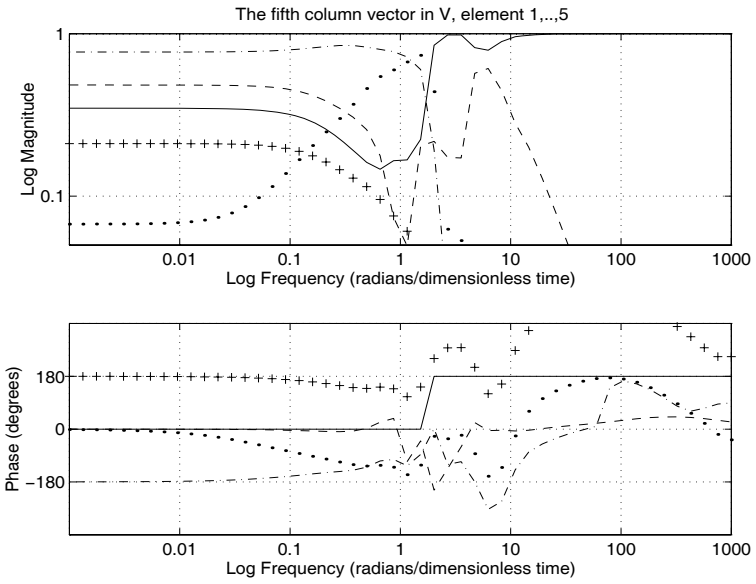

Figure 6.13: The input direction that gives no effect on the output at the high production rate. The subsequent elements are plotted as solid, dashed, dashed-dotted, dotted, and + marked lines.

Fig. 6.13 shows the absolute value of the last column vector in V, i.e. the input direction that gives no effect on the output. This means that the corresponding multivariable gain is zero. Note that the reason why this "no-effect"-input direction occurs, is that there are one more linearly independent inputs than outputs. Since only four linearly independent inputs are required to control these, if none of them are in saturation, the fifth input gives an opportunity to construct a (frequency dependent) direction in such way that the five inputs cancel the effect of each other on the outputs. This also explains why there are no actual transmission zeros in this system. However, we may also view this as there are transmission zeros at all frequencies in this particular direction. Non-square plants have commonly no transmission zeros (but some may have).

6.3.5 Discussion

. The input-output controllability analysis can be summarized as follows:

- By the chosen inputs, we may conclude the following with respect to SISO (decentralised) control structure selection:

- The residence time for the chips and the quality measures are all SISO controllable below certain frequencies (note that the former is a pre-condition for the latter). Especially, the residence time is SISO controllable by the wash water flow, the feed chip flow, and the chip level at almost all frequencies. At higher frequencies, the chip level is the best control input.
- As expected, the Kappa number can only be controlled on long time basis. If the constraints in the actuators are similar, the SISO controllability of the Kappa number is about equal by the chosen manipulated variables (slightly better from the feed chip flow and the chip level than from the others).
- The feed chip flow and the chip level set-point affect the concentration of dissolved solids in the blow flow strongest at low frequencies. The tranfer function from the feed chip flow (which often is a disturbance source) has no practical bandwidth limitation. In this case, the chip level set-point is the strongest manipulator to control this variable. The same comments apply for the control of the alkali concentration.

However, one should be careful to draw too conservative conclusions from this SISO based analysis. Moreover, with respect to input-output pairing, the controller and the disturbances should be considered as well. Hence, a full-block controller may be the best choice.

- For MIMO (full-block) control, the following should be considered:
  - The rank of the transfer matrix is 4, i.e. equal to the number of outputs (see Sec. 6.3.1). Hence, we have structural controllability. Otherwise, there is hope to control the outputs independently, as there will be zero gain for some directions of the outputs (Skogestad, 1994).
  - There are no transmission zeros in this system. Hence, the controllability is not limited due to RHP-zeros. It should be noted that transmission zeros (including RHP-zeros) occur when the model is made square. This generally indicates inverse responses and/or transport delays. In our plant, we have both. This means that the elements in our transfer matrix have RHP-zeros, even though the MIMO system has none.
  - According to Fig. 6.8, $\underline{\sigma}$ is small, i.e. less than 1.0 (about 0.5 at steady-state, at the high production rate). Hence, there are problems with input constraints for certain set-point changes (Skogestad, 1994). Considering the weakest in- and output directions (Figs. 6.11 and 6.12), this means that control of the residence time at low frequencies is badly accomplished by use of the steam temperature, the alkali charge, and the wash water flow as manipulated variables.

    However, the condition number is relatively small at low frequencies. The steady state values are respective about 19 and 12 at the high and low production rates. From this, we may conclude that the plant is fairly conditioned at low frequencies, i.e. up to about 0.7 (at HPR), that corresponds to time constants of about 2 hours. Condition numbers

above 100 commonly indicate ill-conditioness. This means that the outputs are not expected to be controllable by input variations less than 1%, when this is the sensitivity for the actuators, or equivalently, the measurements have to have 1% accuracy.
Further, it appears that the plant is strongly ill-conditioned at higher frequencies (denoted by high γ values). This corresponds well to the results, which are shown in Figs. 6.5, 6.6, and 6.7, and means that the quality measures are badly controlled on short time basis (especially, the control of the Kappa number is badly accomplished by use of the alkali charge, see Figs. 6.11 and 6.12). The reason for this is the slow dynamics connected to the reaction kinetics and the transport delay from the top to the bottom in the digester.
Moreover, the gain from the chip level set-point to the residence time is relatively large in this range, c.f. Figs. 6.4, 6.9, and 6.10. This is explained by the high gain from the chip velocity (which determines the residence time of the chips when the chip level is controlled) in the bottom to the top of the digester. This high gain is further explained by the the large negative eigenvalues of the A matrix, corresponding to the vertical chip acceleration, c.f. 6.2. Hence, we may state that these modes (or actually the chip velocity as one modus in the PDE model) are present in the transfer matrix, as these are input-output controllable and -observable.

Note that the condition number at the low production rate is lower than at the high production rate for low frequencies. This indicates, as expected, that it is easier to affect the process on long time basis, i.e. when the chip plug moves slower.

- From the frequency responses, it appears that the transfer functions include no integration. Hence, this is required in the controller if zero control error is to be achieved.

Chapter 7

Model reduction

"Models should be as simple as possible, but not simpler". The validity of this term is obvious when we consider the computational effort and the outline of the model.

In this chapter we discuss some ways to reduce the model. By this we mean that only the most important variables and effects are retained, and the numerical solution is simplified, such that the resulting model retains its ability to predict the pulp quality. Hence, we emphazise the approach of using physical knowledge in the model reduction (as far as the previous study has given us a correct physical knowledge about the effects that we emphazise in this study). The results from the previous chapters make a basis for this. It should be noted that the reasoning in what follows is mainly based on the steady-state analysis. Hence, we emphazise a model with satisfactory steady-state quality description. As the results in dynamic transients both are dependent on time and the operational point, the derivation of a "good" model is dependent on the prediction horizon. This is beyond the scope of this study. Note that terms that are "small" at steady-state or in some time periods, may be "large" (or considerable) in other time periods. Hence, these terms may run the process into quite another operating point than would be the case if they where not included.
Some of the simplifications which are discussed, are tested against some of the simulation results from Ch. 5.

7.1 The balance equations

The following sub-sections treat some selected mechanisms that reduce the model by retaining the first principles structure.

7.1.1 Mass balances

Wood components

When, as in this study, there is only one component of chemical agents in the model, the yield is in practice a unique function of the Kappa number in a limited

range around the operating point with respect to alkali and temperature variations. The reason is that the carbohydrate concentration is closely related to the lignin concentration. This is shown in Fig. 7.1 and is supported by plant data as reported in Christensen et al. (1982), see Fig. 7.2. These data cover a relatively wide range of operating conditions for kraft cooks. The figures show that our results fall within the 95% confidence interval for the referred data, and a 5% reduction in the steam temperature and the alkali feed concentration give no considerable deviations. As a result, α_{lig} and α_{carb} need not necessarily be regarded as being two states.

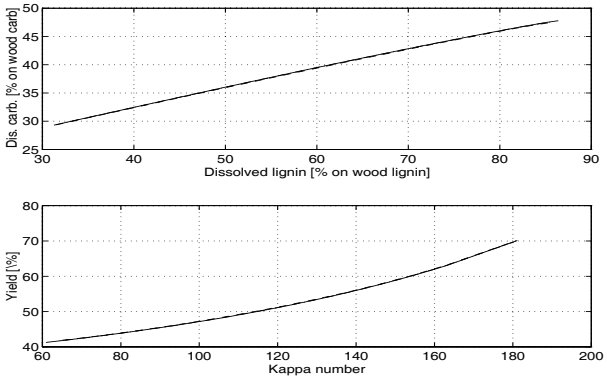

Figure 7.1: Amount of dissolved carbohydrates versus amount of dissolved lignin, and yield versus Kappa number, according to the model at plain high production rate (solid line), when the steam temperature is reduced 5% (dashed line), and when the effective alkali feed is reduced 5% (dashed-dotted line). In the latter two cases, the chip level is controlled. Steady-state conditions.

From the figures we have $\alpha_{carb} = f(\alpha_{lig})$. In what follows, we use a linear approximation of the function which is shown in Fig. 7.1: [1]

$$\alpha_{carb} = 0.36 + 0.84\alpha_{lig} \tag{7.1}$$

According to the orignial model, there is a nonlinear relation between the reaction rates for the carbohydrates and the lignin, as a function of location in the digester. This ranges from about 0.93 in the top, to about 0.59 in the bottom. The result is somewhat large compared to literature data. This may be caused by the choice of a high A_2-factor (see Eq. (3.2)), that gives a lower yield than is normal (c.f. Sec. 5.2). According to Gustafson et al. (1983), the carbohydrate reaction rate in the bulk delignification period is proportional to the lignin reaction rate as:

$$r_{carb} = 0.47 r_{lig} \tag{7.2}$$

The constant of proportionality is derived from data by Rekunen et al. (1980).

[1] Note that the axes in the upper figure in Fig. 7.1 have dimensions respectively $100(0.283 - \alpha_{lig})/0.283$ and $100(0.717 - \alpha_{carb})/0.717$ where 0.283 and 0.717 are the respective mass fractions in uncooked wood, c.f. Sec. 5.2.

Figure 7.2: Amount of dissolved non-lignin versus amount of lignin dissolved in kraft and soda pulping (from Christensen et al. (1982))

Mathematically, we can show that the yield is a function of the Kappa number in this case by the following. Eq. (3.77) gives:

$$\alpha_{lig} = \frac{\kappa \cdot f(\alpha_{lig})}{\frac{100}{c_\kappa} - \kappa} \tag{7.3}$$

i.e. $\alpha_{lig} = \alpha_{lig}(\kappa)$. Eqs. (3.77) and (3.78) then give:

$$Y = \frac{\alpha_{lig}(\kappa)}{\kappa} \frac{10^4}{c_\kappa} \tag{7.4}$$

Note also that this result is valid for all functions f except for 1.order linear functions without the constant term, i.e. $\alpha_{lig} = k \cdot \alpha_{carb}$, where k is any constant unequal zero. When k equal zero, we have:

$$\kappa = \frac{\frac{100}{c_\kappa}}{1+k} \tag{7.5}$$

i.e. κ is constant for every α_{lig} and α_{carb}.

The consequence of the above discussion in terms of model state reduction is that the carbohydrate component is omitted as a state variable.

Liquor components

Effective alkali

As shown in Fig. 5.6, the diffusion of alkali between the chips and free liquor

is so fast that there is no significant difference between the concentrations in the two liquor phases at steady-state. Hence, we define:

$$D_{EA} = \infty \tag{7.6}$$

as diffusion of the alkali is concerned. In this way, this concentration gradient is eliminated, and one state is omitted. We weight the effects that are included in the chip phase by w_1, and the effects that are included in the liquor phase by $(1 - w_1)$. Summation of Eqs. (3.234) and (3.236) with the respective weights, and defining:

$$\rho_{EA} = \rho_{EA,el} = \rho_{EA,fl} \tag{7.7}$$

as the only alkali component in the reduced model, gives:

$$\begin{aligned}\frac{\partial \rho^*_{EA}}{\partial t^*} &= -w_1 v^*_c \frac{\partial \rho^*_{EA}}{\partial z^*} - (1-w_1) v^*_l \frac{\partial \rho^*_{EA}}{\partial z^*} - w_1 t_0 \rho_{ODW} \left(\frac{b_{lig} r_{lig}}{\rho_{EA,0}}\right. \\ &\left. + \frac{b_{carb}\rho_{carb}}{\rho_{EA,0}}\right) + w_1 \frac{1}{Pe_c}\frac{\partial^2 \rho^*_{EA}}{\partial z^{*2}} + (1-w_1)\frac{1}{Pe_l}\frac{\partial^2 \rho^*_{EA}}{\partial z^{*2}}\end{aligned} \tag{7.8}$$

Note that the consequence of defining $D_{EA} = \infty$ is that $\frac{\partial \rho^*_{EA,el}}{\partial t^*} = \frac{\partial \rho^*_{EA,fl}}{\partial t^*}$, i.e. $\rho_{EA,el} = \rho_{EA,fl}$. Thus, $\frac{1}{Sc_{EA}\epsilon_c}(\rho^*_{EA,el} - \rho^*_{EA,fl}) = \frac{1}{Sc_{EA}\epsilon_l}(\rho^*_{EA,el} - \rho^*_{EA,fl}) = 0$.

Further, the definition of ρ_{EA} is (c.f. Sec. 3.3.2):

$$\rho_{EA,el} + \rho_{EA,fl} = \frac{m_{EA,el}V_{fl} + m_{EA,fl}V_{el}}{V_{el}V_{fl}} = 2\rho_{EA} \tag{7.9}$$

i.e.:

$$\rho_{EA} = \frac{m_{EA,el}V_{fl} + m_{EA,fl}V_{el}}{2V_{el}V_{fl}} \tag{7.10}$$

Dissolved solids, water and entrapped air

Since the difference between the concentrations of dissolved solids in the two liquor phases are significant (see Fig. 5.7), these have to be retained in the model if the wash efficiency is to be predicted. However, if the objective is only to predict the Kappa number, these components may not necessarily have to be calculated as these only are included in the calculation of the chip and liquor densities ρ_c and ρ_l (Eqs. (3.64) and (3.65)). These densities influence the vertical mass, momentum, and energy flows of the two phases through the force of gravity. Fig. 5.9 shows that these vary in the ranges $1070 - 1120 kg/m^3$ and $1010 - 1050 kg/m^3$ respectively. As these variations are relatively small $(4 - 5\%)$, we may simply use the mean values:

$$\rho_c = 1095 kg/m^3 \tag{7.11}$$

$$\rho_l = 1030 kg/m^3 \tag{7.12}$$

Alternatively, linear approximations between the referred end-points may be used. By this, if we assume that there is no entrapped air in the chips, we need not calculate the concentration of water.

The consequence of the above discussion in terms of reduction of the number of model states is that the two alkali components $\rho_{EA,el}, \rho_{EA,fl}$ are replaced by one, and the two components of dissolved solids $\rho_{ds,el}, \rho_{ds,fl}$ are omitted.

Mass dispersion

In Sec. 5.1 it is shown that the dispersive effect only constitutes some percent of the convection for most of the mass components at steady-state. The contribution in the equations for the dissolved solids is, however, more significant. Further, the short-stop scenario in Sec. 5.3.3 shows that the dispersion may be considerable in dynamic transients for the lignin as well.

In the previous section, we have discarded the computation of the dissolved solids. Moreover, we emphazise a model with satisfactory steady-state qualities. Hence, we omit the dispersion in the equations for the lignin and the volume fraction of chips. The alkali component, however, expresses the mean concentration in the chips and in the free liquor. As there is counter-current flow in the wash zone, discarding the dispersion gives numerical instability even if the equation is spatially discretized with the backward Euler method. Hence, we retain the dispersion for the alkali and the MAC-scheme in the spatial discretization for this equation.

Remark

The simplified model, which is discussed above, cannot be derived directly from the conservation law similarly to the procedure that is used in Ch. 3. Hence, the overall (i.e. total) mass balance for the two phases is not fulfilled. A consequence of this may be that it is more difficult to tune the model against real plant data, c.f. the discussion in Sec. 1.1.

7.1.2 Momentum balances

The simulation results from Sec. 5.1 (Table 5.5) and 5.3.3 show that the force of inertia is neglible at steady-state as well as in extreme dynamic transients. Hence, by discarding this effect, we do not reduce the accuracy in the solution considerably. The other included effects are, as shown in Table 5.5, of importance.

7.1.3 Energy balances

As shown in Table 5.7 in Sec. 5.1, the terms which describe vertical heat conduction and heat conduction through the digester walls are neglible compared to the other terms. Further, Fig. 5.13 shows that the temperatures in the two phases differ by about $2-7^oC$ in the cooking zone. If the required accuracy in the solution dictate that some mean value of these can be used as the chip temperature (meaning an

error compared to the original model of about 2.5 units in the Kappa number, c.f. Sec. 5.3), we define

$$k_{cl} = \infty \tag{7.13}$$

Equivalently as for the alkali, by summing the two temperature equations (3.241) and (3.242) with respective weights, w_2 and $1 - w_2$, defining:

$$T = T_c = T_l \tag{7.14}$$

as the only temperature variable in the reduced model, and dividing the resulting equation by 2, we get:

$$\frac{\partial T^*}{\partial t^*} = -w_2 v_c^* \frac{\partial T^*}{\partial z^*} - (1 - w_2) v_l^* \frac{\partial T^*}{\partial z^*} + w_2 \frac{\rho_c^* \rho_{c,0} d \Delta h_r r}{v_0 T_0 (C_{pc} \rho_c)^{*'}} \tag{7.15}$$

The consequence of the above discussion in terms of reduction of the number of model states is that the two temperature states are reduced to one.

7.1.4 Simulation results

Without changing the vertical discretization, the dimension of the resulting state space vector is reduced from 226 to 113. The weights in the combined alkali- and energy balances are chosen as $w_1 = w_2 = 0.37$ in the whole vessel. This is related to the mean volume (and mass) fraction of chips in the vessel, and the relative importance of the effects that are included in the chip phase compared to the free liquor phase in the original model.

Figs. 7.3 - 7.5 show some steady-state profiles of the reduced model compared to the original at the high production rate. There is a deviation of about 2 units in the final Kappa number, and about 2% in the yield. Fig. 7.4 shows a fairly good fit for the temperature and the alkali concentration in the cooking zone, while the correspondance in the upper part of the wash zone is rather bad. The reason for this may be that the influence from the effects that are included in the free liquor phase in the original model is less important in this part of the digester than the chosen weight of $1 - 0.37 = 0.63$ dictates. This illustrates how difficult a model reduction procedure of this kind may be.
The residence times are about the same (about 2.6 and 2.7 hours respectively in the original and the reduced model). The reduced model shows, however, a considerable higher compaction of chips at the extraction (26 m), see Fig. 7.5.

Fig. 7.6 shows how close the dynamic behaviour of the yield is in the reduced model compared to the original. It appears that the simplified computation of the mass densities gives rise to a slightly more disturbed responce. The main dynamics is, however, maintained in the reduced model.

7.2 Other structural changes

Some approaches which deviate from the first principles formulation are discussed in this section.

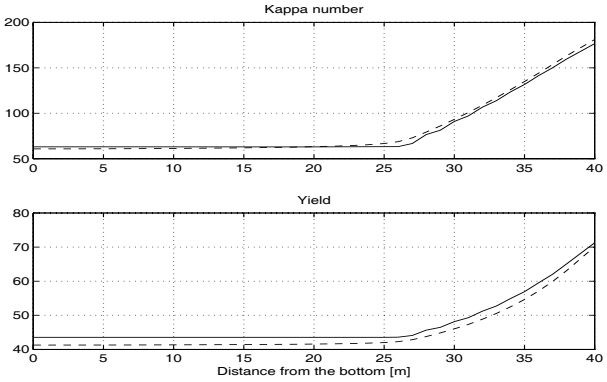

Figure 7.3: Steady-state profiles of the Kappa number and yield (in %). The solid line denotes the reduced model.

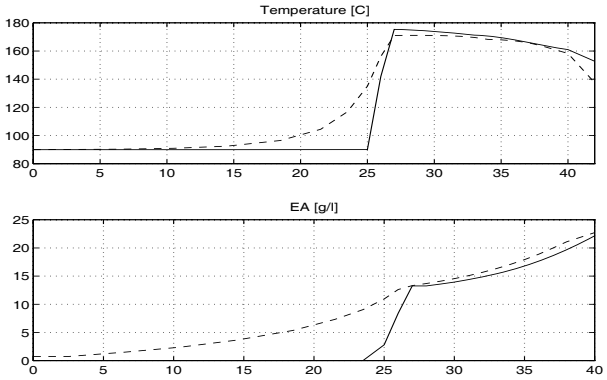

Figure 7.4: Steady-state profiles of the chip temperature and the concentration of effective alkali. The solid line denotes the reduced model.

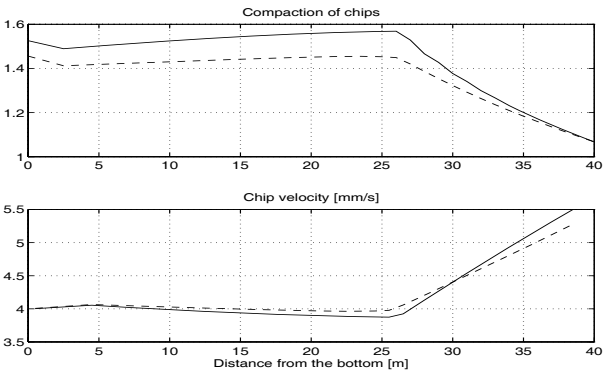

Figure 7.5: Steady-state profiles of the compaction of chips and the chip velocity. The solid line denotes the reduced model.

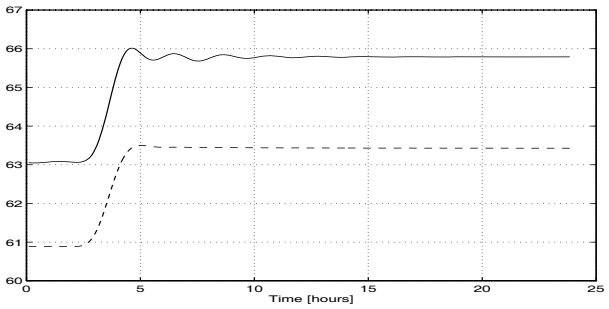

Figure 7.6: The Kappa number in the discharged pulp when the cooking circulation temperature is reduced 5%, and the chip level is controlled. The solid line denotes the reduced model.

7.2.1 Chip mass movement

If the flow dynamics in the model is simplified, the computing time will be dramatically reduced.

The mass- and the momentum transfer are two different mechanisms which are required to describe a moving substance. This means that the compaction of chips and the chip velocity are two degrees of freedom. Hence, they are state variables in the mass and momentum balance equations. This means that the compaction profile may generally be the same for different production rates (at different Kappa number levels etc.). Hence, when only the chip velocity profile is known, we cannot predict the value of the compaction (and vice versa). The compaction profile is only given by its value at some initial time and its time history. This is what characterizes states in state-space models.
It is important to stress this fact because one may be misled by the fact that these variables also affect each other. This is illustrated by the steady-state profiles in Sec. 5.2. Increasing compaction gives decreasing chip velocity. The reason is that the volume flow of chip, i.e. the product between ϵ_c and v_c (times the cross-sectional area), has to be equal down through the vessel at steady-state. In other words, there cannot be steady-state accumulation of chips anywhere in the vessel. Hence, in this case we can say something about the *shape* of the compaction profile when the velocity (or residence time) profile is known (and vise versa).
Further, the dynamics of the chip velocity (the vertical chip acceleration) is extremely fast compared to the other dynamics (c.f. Sec. 6.2).

This means that as an approximation, we may predict the velocity profile (c.f. Eq. (3.169)) when the *chip level* (affecting the force of gravity), *the Kappa number profile* (determining the chip pressure force gradient and the density difference between the chips and the free liquor), *the production rate* (determining the boundary conditions), and *the L/W-ratio and the dilution factor* (determining the viscous flow resistance) are given. These key process variables are the sources for the chip velocity profile (in the momentum equation) and, hence, also the compaction profile. The information that is required to achieve such a simplified description

of the bulk chip movement may be gained from parameter estimation techniques. Figs. 5.11 and 5.12 show that these profiles may be approximated by piecewise straight lines in the cooking and wash zones respectively. When we use the fact that the respective sub profiles for the cooking and wash zones coincidence near the extraction screens, we need three coefficients, $c_1,..,c_3$, for each profile. The respective profiles are then described as:

$$\epsilon_c = c_1 + c_2 z, \quad z \in [z_{top}, z_{extr} > \tag{7.16}$$

$$\epsilon_c = c_1 + (c_2 - c_3) z_{extr} + c_3 z, \quad z \in [z_{extr}, z_{bottom}] \tag{7.17}$$

$$v_c = c_4 + c_5 z, \quad z \in [z_{top}, z_{extr} > \tag{7.18}$$

$$v_c = c_4 + (c_5 - c_6) z_{extr} + c_6 z, \quad z \in [z_{extr}, z_{bottom}] \tag{7.19}$$

where the parameters $c_1,..,c_6$ may be estimated.

The information about the shape of the profiles is not included in the above approach. This may be included by the following two approaches. (1) the compaction profile may be computed as in the original model, as this represents much slower dynamics than for the chip velocity. (2) the application of Dupuit's assumption, Eq. (3.69), in the calculation of the chip velocity:

$$v_c = q_c/(\epsilon_c A)$$

This approach is pursued by Funkquist (1993).

We do not proceed with this reduction step further in this study, but rather stress that such an approach is possible when a detailed model of the flow dynamics in the vessel, as the original model in this thesis, is available for the use in parameter estimation. The concept of *neural nets* (see e.g. Wasserman (1989)) is particularly suited for this application.

7.2.2 Step response sub-models

In this section, we illustrate one important application of a SISO-model which is concerned with the chip level control. The model is derived from simulated data from the original model, and a comparison is made with a plant application.

When focus is made on specific parts of the process (i.e. some manipulated and measurement variables), simple step response models may be valuable in, for instance, controller design. In such cases, the plant is treated as a set of decoupled sub-systems, typically by using physical knowledge of the process. One such approach is treated by Allison et al. (1990) and Fuchs and Smith (1971), in chip level control, c.f. Sec. 2.6. Allison et al. (1990) uses the blow flow as manipulated variable in a Box-Jenkins model structure (Box and Jenkins, 1976). The model contains a gain of about $1.0\frac{\%/h}{m^3/h}$, a delay of typically $10-20$ minutes, and a time constant (pole) of about 1 hour. The time delay is assumed to be a high estimate. In addition, a noise model is included. Fuchs and Smith (1971) found time delays in the range $1-6$ minutes.

Fig. 7.7 shows the time response, in the original model at high production rate, of the chip level from a pulse pattern in the blow flow. The pulse height is 5% ($190l/min$) of the nominal value for the blow flow. From the results, no significant transport delay appears, and the level arrives at steady-state at about 20 hours.

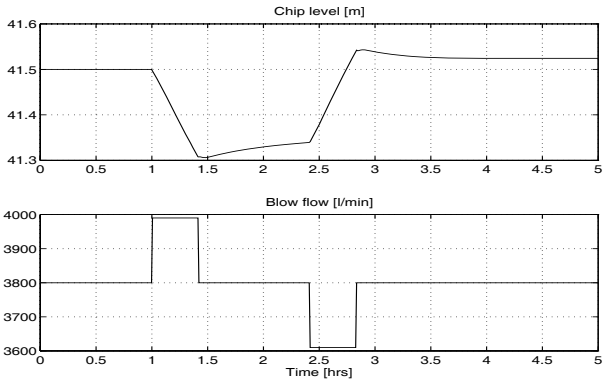

Figure 7.7: Time response of the chip level from a puls pattern in the blow flow at the high production rate

The time response has been identified by use of the Box-Jenkins-structure including one delay (i.e. 1 minute). The reason why the delay is included is that the sampling time is 1 minute. The following model was identified:

$$h_c(t) = \frac{-4.0 \cdot 10^{-5}}{1 - 0.9969 z^{-1}} q_{bf}(t-1) + w(t) \tag{7.20}$$

where $w(t)$ is white noise, and the standard deviation for the gain is $1.0 \cdot 10^{-7}$. This means that the gain is $-4.0 \cdot 10^{-5} \frac{m/min}{l/min}$, while the time constant is about 33 hours (i.e. practically an integrator).

Fig. 7.8 shows how good the generated model fits the original. The result is fairly encouraging. Note, however, that the original response includes additional dynamics to the pure integrator behaviour. This is caused by the complex interactions between the mass-, momentum-, and energy balances which are included in the model.

Note that the finding of no significant transport delay is a result of the extreme fast chip plug acceleration, c.f. Sec. 6.2, and no included manipulator-, and measure gauge dynamics. Hence, the results of $10-20$ minutes delay by Allison et al. (1990) may be explained by the latter.

The implication of the above results for the chip level control, see Fig. 7.9, is that with respect to rejection of input noise, which typically includes bias connected to:

- production rate changes
- top separation motor load changes (when this is used as an indication of high chip level conditions)

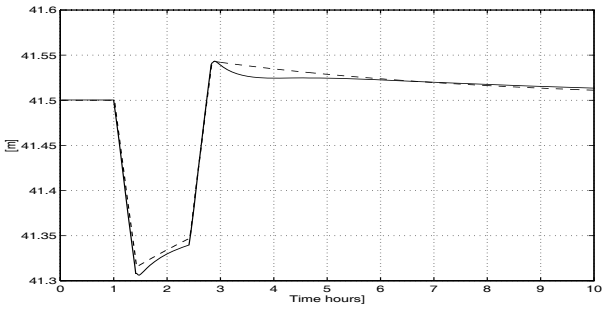

Figure 7.8: Comparison between the chip level responses of original (solid line) and the generated model

the controller has to include integration to achieve zero steady-state control error, e. Further, with respect to output noise, which typically includes:

- the feed flow of chips (a bias) including variations due to uneven filling in the chip meter etc.
- chip level measurement errors (see Sec. 8.3)
- chip volume flow variations in the digester, caused by Kappa number variations as discussed in Sec. 5.3 and Appendix F. Typically examples are:
  - wood density variations in the feed flow of chips, causing variations in the Kappa number of the uncooked chips
  - cooking temperature variations (due to steam feed problems, varying cooking circulation flow etc.)
  - variations in the alkali charge

either separate control loops are required for manipulation of these changes, or a PI-controller in the blow flow loop is necessary to achieve zero steady-state control error here as well. This is due to the bias in the feed flow of chips. Note, however, if the manipulators allow the controller gain to be raised sufficiently high, the steady-state control error may be fairly low without the inclusion of the I-function in the controller.
Regarding the latter to noise sources, the P-function in the controller is satisfactory as to achieve zero steady-state control error. Note that the transfer functions from the wood density in the feed chips, cooking temperature, alkali charge etc. to the chip level, include no integration (c.f. Sec. 5.3). Further, it appears from Fig. 5.14 that these may be described simply by first order transfer functions; $K_5 \frac{1}{s-b_1}$.
Note also that derivative function is not nesessary in these cases. Finally, we assume that the control of the blow flow is perfect, i.e. $q_{bf} = q_{bf}^{sp}$ (the set-point).

The success of application of such type of models as this may be illustrated by the results from Petrus and Allison (1990). By use of an adaptive controller, in one case the Kappa number variations were reduced by about 40% compared to earlier results.

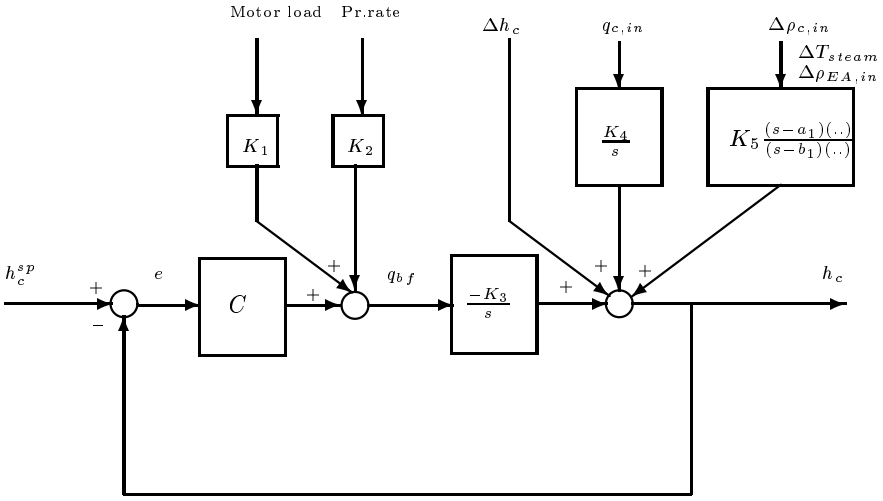

Figure 7.9: A conventional chip level control structure

7.3 Numerical solution

Chip plug acceleration

The momentum balance for the chip plug does not appear to be as easily solved as a steady-state equation. The main reason for this is that the system index of the resulting DAE is increased (from zero to one), c.f. Sec. 4.3. This means that the calculation of the chip velocity requires that the liquor velocity is known, and vice versa. Another complicating factor is that the resulting steady-state equation includes the multiplication of the chip velocity, v_c, by its absolute value. We do not proceed with this reduction step further in this study.

Spatial discretization of the PDEs

The selection of the number of spatial grid points along the vertical axis of the digester is a question of numerical accuracy in the solution. As commented in Sec. 4.4, this refinement has to be considered together with the time integration step size, because the total accuracy in the solution is given by the sum of the discretization error in the two directions.
The response of the model is more equal to the real process response as the number of grids is increased. This is discussed by e.g. Meisingset and Balchen (1994). Due to the uncertainty in the model description, the disturbances which influence the process and the ability of the process for disturbance rejection, the location and sensitivity of the actuators and gauges, there is always a limit to how much is known about the actual process mechanims. Hence, the validity of the model is limited irrespective of the finess in the spatial resolution. As a result, the model outputs are sensitive to the number of grid points, especially when this is lower

than a certain limit. This limit is therefore of special interest in the numerical solution of the model. This is also treated by Meisingset and Balchen (1994). Especially, it is notable that with respect to closed loop control, it is indicated that this grid limit is considerably lower than what is needed for open loop simulation. Hence, the above-mentioned reasons for the limit to how much is known about the actual process mechanisms, are analogous with respect to closed loop control; the feedback damps the effect of model uncertainty, and disturbances within the bandwidth of the closed loop system. This is one of the good properties of feedback control. These topics are not followed further in this study.

Chapter 8

Digester control

This chapter is concerned with the control of continuous digesters. Especially, we focus the control of the vertical movement of the chip plug, i.e. *residence time control*. This is treated in Sec. 8.3 and 8.4. As an introduction, the common control objectives are discussed in Sec. 8.1. A short review is given of conventional digester control in Sec. 8.2.
In a broader treatment of digester control, what we could call advanced control (model-based control) belongs as well. A number of such strategies have been developed for digester control, and are reported in the literature, c.f. Ch. 2. Time series models and adaptive structures are among the most frequent, see e.g. Dumont (1986) for a survey. This topic is not treated further in this thesis.

8.1 The control objectives

The pulp-, and pulping quality variables, as defined in Sec. 3.2.3, are influenced essentially by the temperature, T, the concentration of alkali, ρ_{EA}, and the residence time, τ. These variables have a high degree of interaction, see Fig. 8.1.

Further, apart from this interaction-problem, the control objectives are contradictory. Typically, keeping constant Kappa number and production rate, high wash efficiency, and low consumption of alkali, is a trade-off problem. Hence, decentralized control is not expected to yield the best control structure. Fig. 8.2 illustrates a general Kappa number control structure.

The control system for the digester has to handle the both fundamental main objectives for control systems:

- Set-point tracking
- Damping (or rejection) of noise/disturbances

Set-point changes are typically step-changes, or ramp-changes within a limited time interval. These include changes in:

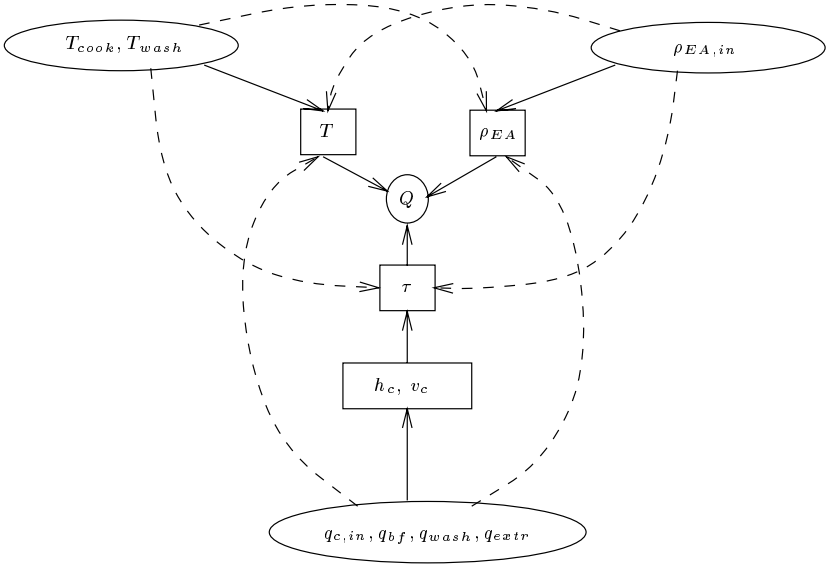

Figure 8.1: The interactions between the three basic factors with respect to quality (Q) control

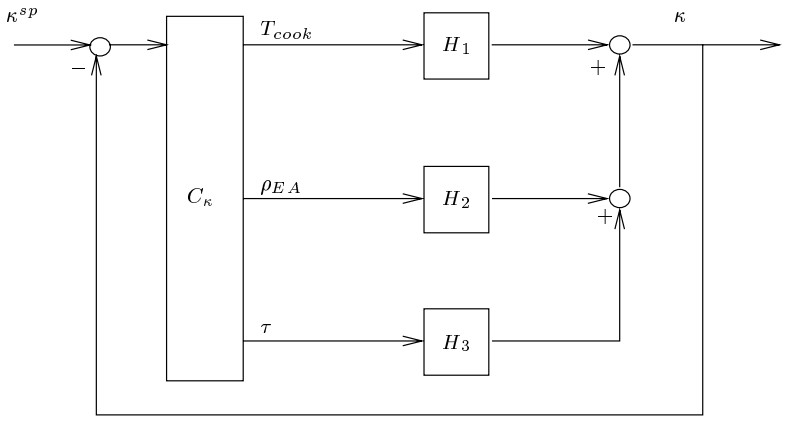

Figure 8.2: A general Kappa number control structure

- Production rate
- Grade (i.e. Kappa number level)
- Species of wood (typically softwood to hardwood, and vice versa)

Note that a change in species of wood in this context, assumes that the change is known, empirically or by measurements. These control problems are designed for feed-forward control. Thus, in the case of a change in species of wood, this control typically includes set-point changes for the cooking temperature, and/or

the alkali charge. Note that use of a model, in e.g. Kappa number prediction, may be beneficial in these type of applications.

Damping of noise is touched briefly in Sec. 7.2.2. The definition of the noise sources is problem dependent. For instance, production rate changes is included as a noise source for the chip level control system in Fig. 7.9. Further, changes in species of wood may be regarded as noise to the cooking temperature-, and/or the alkali charge-, and/or the chip level control loops. In Sec. 8.4, we define a vector of noise sources for the specific problem which is discussed there.

Digester control can be defined at different control levels. Thus, the different type of set-point changes and noise sources influence the different levels.

The upper control level can be defined as including the control of the pulp-, and pulping quality. In this way, set-point changes are defined as grade changes. A better Kappa number control will be used in most mills to shift the Kappa number target to achieve higher pulp yield, increased production or lower bleaching costs. Hence, improved digester control brings more effective use of chips, chemicals and energy.

At the second level of control we have:

- Residence time for the chips in the cooking zone
- Concentration of alkali in the cooking zone
- Cooking temperature
- Quench temperature
- Residence time for the chips in the wash zone
- Wash temperature
- Dilution factor

where the Kappa number is most influenced by the former four variables. Included at this level is the control of the blow consistency as well, c.f. Sec. 1.2.3.

To control these variables, we have at the third level:

- Chip- and liquor levels, feed flow of chips, blow flow, bottom scraper speed, wash water flow, controlling the residence times for the chips in the cooking and wash zones, and the blow consistency
- L/W-ratio and alkali charge, controlling the concentration of alkali in the cooking zone. Together with the control of the liquor level and the cooking temperature, these control the concentration of alkali in the chips such as to prevent external mass transfer limitation
- Steam- and cooking circulation temperature, controlling the cooking temperature
- Wash water- and wash circulation (upper and/or lower) temperature, controlling the quench- and wash temperatures
- Wash- and dilution flows controlling the dilution factor

Finally, at the bottom level, we have basic regulatory controls of valves, heat exchangers, engines etc.

8.2 Conventional control in general

By the term conventional control, we mean SISO or MISO control loops where the structure and tunings are not based on any mathematical model of the process. Typically, the controllers have the conventional PID-structure, or manual control is applied.

Conventional control structures are discussed widely in the literature, see e.g. (Lundqvist, 1982), (Granberg and Gustavsson, 1982), (Kleppe and Storebråten , 1982). In this section, we use the Peterson digester as an example to describe such a control structure. Some comments are given to how things are commonly done in other plants.

The Kappa number control of the Peterson digester, as reported in Kleppe and Storebråten (1982), was from the start-up based on an estimated (table based) H-factor, and the effective alkali concentration in the transfer- and cooking circulations. The H-factor is manually set, based on the chip meter speed and the temperature in the cooking circulation. The greatest problem for the Kappa number control is supposed to be a precise estimate of the H-factor. The white liquor charge is manually controlled, based on an estimated alkali-to-wood ratio, and measurements of the effective alkali concentration in the transfer- and cooking circulations. Thus, the white liquor flow to the top is matched to the feed of dry wood in order to provide the desired alkali concentration in the cooking circulation. In some digesters, the concentration can be corrected by additional charge after the impregnation stage. The control is often quite sluggish because of the manual settings, long time delays, and inaccurate measurements.
At the next level, the chip level is controlled by the blow flow and the bottom scraper speed, the liquor level by the extraction flow, and the cooking circulation temperature is adjusted according to the steam temperature. Production rate changes are made by keeping the estimated H-factor and the alkali-to-wood ratio constant. As discussed in the next section, especially the chip level control strategy varies from plant to plant.

It should be noted that Kappa number control, as in the example above, commonly is solved as a feed-forward control problem. However, in some newer installations on-line Kappa number gauges exists in the blow line. Since it is not possible, with today's technology, to measure directly in the cooking zone, closed loop control with such analysers is difficult due to the long transport delays. In some plants, however, successful results are reported, by the use of low gain feedback from the Kappa number gauge to the cooking temperature (Lundqvist, 1990).

8.3 Conventional residence time control

The model results reported in this thesis indicate that controlling the residence time for the chips in the digester is of great importance for controlling the pulp quality. This fact is discussed in the literature as well (Lundqvist, 1982), (Lundqvist,

1990), (Granberg and Gustavsson, 1982). Observations at the Peterson digester indicate a strong correlation between the Kappa number variations and the chip level variations.

The difficulties in the control of the residence time include, c.f. Eq. (3.169):

- Variations in the feed chip quality (content of lignin, air etc.), and amount (due to uneven filling in the chip meter)
- Small density differences between the chips and the free liquor, especially at low Kappa numbers
- Greater viscous friction between the two phases at higher production rates and higher dilution factors
- Variations in the L/W-ratio give varying viscous friction between the two phases in the cooking zone
- Interactions between different control loops in the system (chip level control in the pre-impregnation vessel and in the digester, dilution factor controls in the two vessels, blow consistency control, production rate control etc.)
- Variations in the friction between the chips and the digester shell at different wood species, and at extreme flow conditions (especially through the extraction screens). These disturbances may give hang-up of the chip plug, which is a serious operational failure situation

The residence time is determined by the chip level and the chip velocity. Hence, residence time control is conventionally accomplished by manipulation of the chip meter speed, the blow flow, and the bottom scraper speed. Since these control inputs are used for the chip level control, conventional residence time control is synonymous to control the chip level to be constant at the given production rate. Irrespective of how the residence time control is performed, good control of the chip level is essential for the control of the pulp quality. A good chip level control simplifies the other control loops. Especially, a prerequisite for good control of the alkali concentration, is a good chip- and liquor level control (Granberg and Gustavsson, 1982). As indicated in the fifth item above, the chip level control problem is especially difficult in two-vessel systems. Moreover, the simulation results in Sec. 5.3.1 indicate that the friction between the chips and the digester shell dominates the impact on the residence time after the transients caused by temperature, alkali, or chip density changes.

The chip level is conventionally controlled by manipulating the feed flow, or the discharged flow of chips, see Fig. 8.3.

Keeping the chip level constant, however, is not always equivalent to maintaining a constant residence time. The following discussion indicates that this depends on what the disturbances are, and hence how the chip level is controlled.

The simulation results in Sec. 5.3.1 indicate that a significant decrease in the cooking temperature, or the alkali charge, during otherwise stationary conditions, results in raised chip level if no compensation is made by the blow flow or the

Figure 8.3: The principles for chip level controls in two-vessel systems (Granberg and Gustavsson, 1982)

feed flow of chips. A similar increase will result from a significant increase in the feed chip lignin content (i.e. the chip density). In such situations, it is necessary to increase the blow flow instead of decreasing the chip meter speed in order to obtain a constant residence time (Granberg and Gustavsson, 1982). The reason to this is that the chip level increase is a result of Kappa number increase in the cooking zone. Hence, what should be controlled is the residence time for the chips which already are in the digester. The only way to adjust this, by the available manipulated variables, is by changing the outflow of chips. Such chip level variations are typically of low frequency.

A different situation occurs when there is a significant decrease in the filling of the chip meter. This means a decrease of the volumetric feed flow of chips, which, if no operational changes are made, results in a lower chip level. Such chip level variations are typically of high frequency, but may of course be of low frequency as well (including a bias). This disturbance is naturally best compensated for by increasing the chip meter speed in order to maintain the same residence time for the new chips that enter the digester. The assumption behind this strategy is either that the noise is measurable, or can be identified through, for instance, high frequency variations of the chip level.

In mill practice, the chip level is often controlled by a combination of these two strategies (Granberg and Gustavsson, 1982). The Kappa number variations (or the chip level variations) are used as a guideline to set the limits and tunings of these control loops. However, the control concept differ from mill to mill.

This control strategy has a disadvantage when the first type of noise occur. The two objectives of keeping constant production rate and constant residence time are contradictory. Lundqvist (1982) suggests two strategies for this. (1) At small chip density variations, the production rate can be controlled by keeping the blow flow constant, and manipulating the bottom scraper speed to get a constant blow consistency. Since it is difficult to measure the blow consistency directly, low frequency chip level variations are often interpreted as symptoms of this (c.f. the first strategy by Granberg and Gustavsson (1982) above). To keep the chip level constant, he suggests to control this by manipulating the chip meter speed. Note that this strategy implies (limited) residence time variations for the chips.
In strategy (2), this deficiency is considered. It is carried out at considerable chip density variations, and includes the same strategy, with the same limitations (relaxation of constant production rate), as that by Granberg and Gustavsson (1982), i.e. by manipulating the discharged pulp flow.
Again, when tuning the mix of these strategies, the Kappa number variations may be used as control performance criterion.

An alternative to these strategies is that implemented at the Peterson digester. Here, only the discharged pulp is manipulated in a cascade loop. The manipulation of the blow flow comprises the outer (or main) loop and accounts for small chip level variations, and the manipulation of the bottom scraper speed comprises the inner loop and accounts for larger chip level variations. Thus, the latter loop compensate for blow consistency variations, see Fig. 8.4.

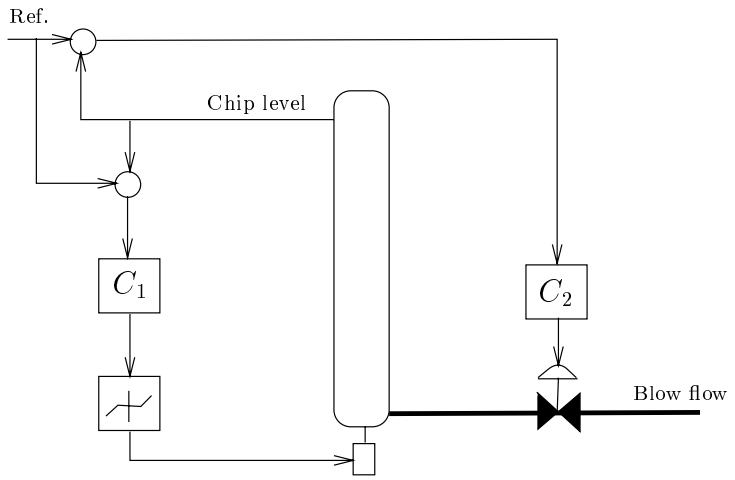

Figure 8.4: The chip level control strategy for the Peterson digester

With P-controllers, this is satisfactory for damping of noise of the first type which is discussed above. Further, the inclusion of integration function in the controllers accounts for the second type of noise (c.f. Sec. 7.2.2). The assumption behind this strategy is that the control loop has sufficient bandwidth to damp the noise caused by the varying chip meter filling. As mentioned above, these variations are typically of high frequency. Hence, this strategy may be less efficient than those discussed above. However, in two-vessel systems the feed flow of chips to the digester is determined by the chip level control of the pre-impregnation vessel. Thus, this variable is to be regarded as a noise source for the chip level control in the digester. Note further that this strategy not only implies the chip level to be controlled to a constant value; it implies the residence time to be controlled to a new value (active control, i.e. constant chip level- and changed chip velocity), c.f. the results in Sec. 5.3.1.

To control the blow consistency, an alternative is to manipulate the distribution of wash- and dilution water in the bottom of the digester. This strategy is common in the control of pre-impregnation vessels.

An assumption behind these conventional chip level control strategies is that the noise is not measurable. Otherwise, feed-forward control is an efficient strategy to control the set-points for the cooking temperature, alkali charge, or the chip level.

In the above discussion, maybe the most serious disturbance source for the chip level control loop is not mentioned. The chip level measurement is without exception a very noisy signal from available gauges. Strain gauges are used predominantly, but are characterized by poor resolution and extremely high measurement noise. In most modern control systems, signals from several gauges are combined to calculate a single composite level measurement. These measure problems complicate the design and tuning of the control loop, and has prompted the development of many heuristic control schemes (Cohen and Ryan, 1974). From this, we see that a model of the chip level may improve the operation of digesters in the effort of determining the correct level.

8.4 Improved residence time- and Kappa number control

The conventional residence time control strategies, as described above, are based on a fundamental misunderstanding. The philosophy behind these is that the chip level has to be kept constant, irrespective of the noise sources, to control the Kappa number. Figs. 5.38 and 5.62 illustrate that this is not the case. Moreover, **this control strategy may be worse than no control**; compare Fig. 5.17 with Fig. 5.38. Hence, to control the Kappa number by the residence time, one has to understand how the noise affects the residence time, and how the residence time influences the Kappa number. The model in this thesis may be a valuable tool for this, c.f. the discussion in Sec. 5.3.1. Figs. 5.36 and 5.60 illustrate that the

residence time has to be *controlled actively* to control the Kappa number by this strategy. This means that the objective for the residence time control should not imply that all chips get the same residence time, start the cook at the same location, or have the same velocity; they should have the same residence time relative to the noise that occurs. In other words; chips with different initial conditions should have different residence times.

Note that active residence time control is actually what the chip level control strategy by Lundqvist (1982), the second strategy by Granberg and Gustavsson (1982), and that in the control of the Peterson digester include; it is accomplished by changing the chip velocity and keeping the chip level constant. Chip velocity variations are measured indirectly by the changes in the chip level. However, as mentioned, the strategies fail to keep the Kappa number constant.

The chip level has to be controlled some way. Hence, an improved Kappa number control structure including active residence time control may be accomplished by:

1. Active control of the chip level *(S1)*
2. Active control of the chip velocity *(S2)*
3. Active control of both the chip level and the chip velocity *(S3)*
4. Indirect residence time control *(S4)*

Note that the residence time is input-output controllable, as discussed in Sec. 6.3.5, and that changing the residence time by the chip level has greater influence than changing it by the chip velocity (c.f. page 147).

In the following analysis, we focus on the two type of noise sources which are treated above:

1. Variations in the chip meter filling $(\Delta q_{c,in})$
2. Variations in the feed chip Kappa number, cooking temperature, or alkali feed $(\Delta \kappa_{in})$

These are assumed not to be directly measurable, only indirectly by either chip level variations (high respective low frequency variations) or Kappa number variations in the blow flow.

As argued by Lundqvist (1982), and Granberg and Gustavsson (1982), $\Delta q_{c,in}$ is best rejected by using the chip meter speed to control the chip level to be constant. In this way, all new chips get the same residence time as those which already are in the digester, and if all other conditions are held, the Kappa number will be constant. Hence, this strategy is not only the best, it is the only one that keeps the Kappa number to be constant.
This means that the Peterson strategy fails to keep the Kappa number constant by this noise, because the chip level control changes the residence time for the chips which already are in the digester. Hence, the Kappa number of these chips is changed, see curve (6) in Fig. 5.38.

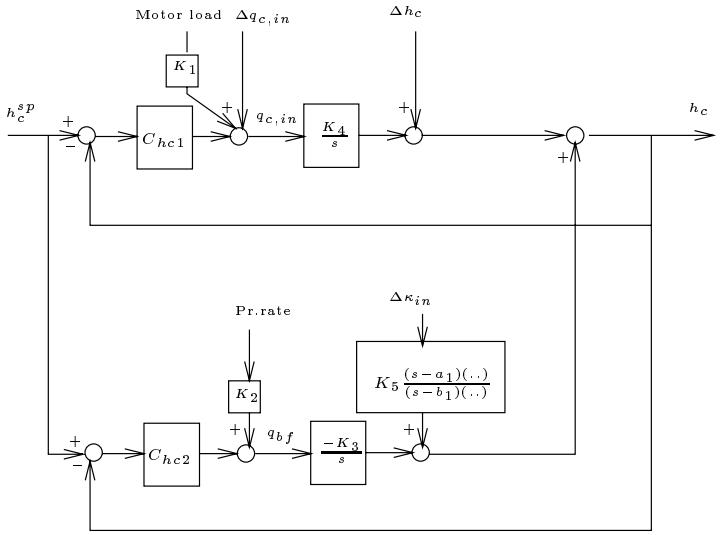

Figure 8.5: A chip level control structure

Further, $\Delta\kappa_{in}$ has to be corrected for by manipulating the chip velocity downstream and/or the chip level. A chip level control structure, where the blow flow is the manipulated variable for this noise, is shown in Fig. 8.5.

From the above discussion, we use the active residence time control strategies to treat the second type of noise, $\Delta\kappa_{in}$.

As already stated, to keep the chip level constant by this strategy is worse than no control. Hence, an increase in the Kappa number of the feed chips, for instance, should be corrected for by a reduction in the blow flow instead of an increase. This is accomplished by e.g. raising the set-point for the chip level. Thus, the residence time is further increased, c.f. Figs. 5.15 and 5.36 (note that without chip level control, the chip level is raised but the Kappa number is not held, c.f. Figs. 5.14 and 5.17).

8.4.1 Active chip level control

In strategy *S1*, the set-point for the chip level controller, h_c^{sp}, may be used to control the Kappa number in the blow flow directly in a feedback loop. Figs. 8.6-8.7 show the effect of this strategy compared to the results which are discussed in Sec. 5.3.2 and in the case of no chip level control. A PI-controller is needed to achieve zero control error (c.f. the discussion in Sec. 6.3.5). Note that the chip velocity is slightly reduced (c.f. the discussion about the conventional control strategies on page 207).

The parameters in the Kappa number controller are tuned fairly tight such that the gain margin is reduced to a minimum, see Fig. 8.8.

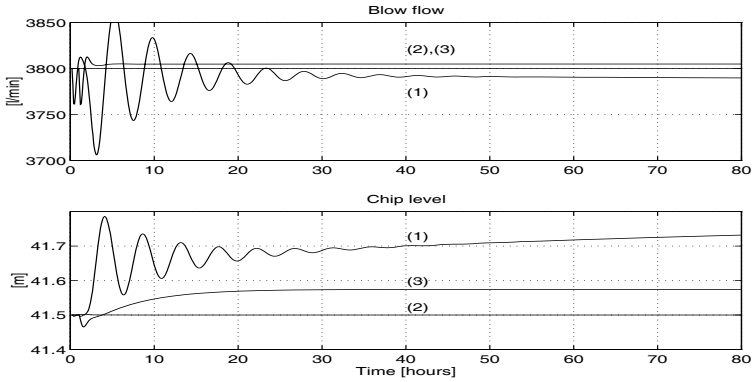

Figure 8.6: Blow flow and chip level during a 5% increase in the feed chip lignin content when the Kappa number is controlled by the chip level set-point (1), without Kappa number control but including chip level control (2), and without Kappa number- and chip level control (3). The set-points are respectively $3800 l/min$ and $41.5 m$.

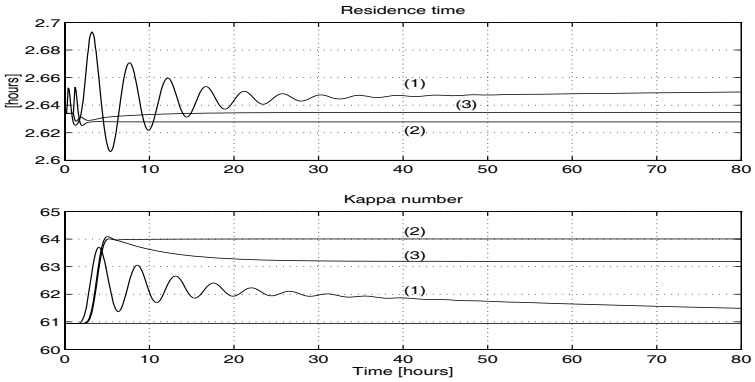

Figure 8.7: Residence time and the blow flow Kappa number during a 5% increase in the feed chip lignin content when the Kappa number is controlled by the chip level set-point (1), without Kappa number control but including chip level control (2), and without Kappa number- and chip level control (3). The set-point for the Kappa number is 60.9.

The Kappa number measure is, as already mentioned, suffering from large time delays. Hence, in the feedback loop, a low controller gain must be used. As a result, the settling time for the Kappa number in the blow flow becomes extremely long, c.f. Fig. 8.7. Therefore, to achieve a faster control, we may need an inner high gain loop which uses the low frequency chip level variations as an indication for the chip velocity variations. This is shown in Fig. 8.9. The chip velocity variations are estimated from a low pass filter (LPF), and the Kappa number controller updates its set-point, Δv_c^{sp}. The chip level control structure in Fig. 8.5 is denoted H_{hc}, and the transfer function from the chip level to the Kappa number is denoted $H_{h_{c,\kappa}}$.

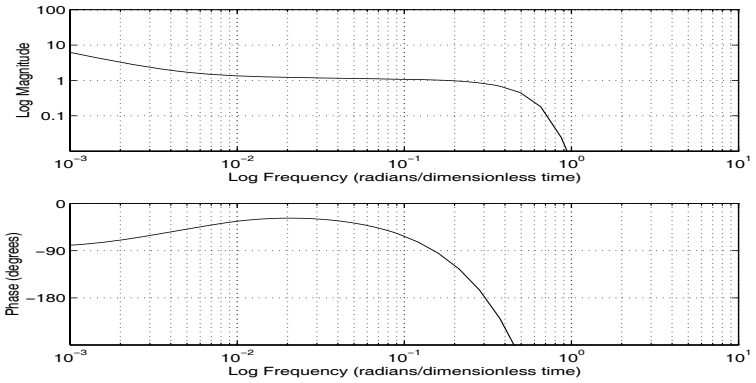

Figure 8.8: The closed loop transfer function in the active chip level control structure

We do not proceed this solution further here.

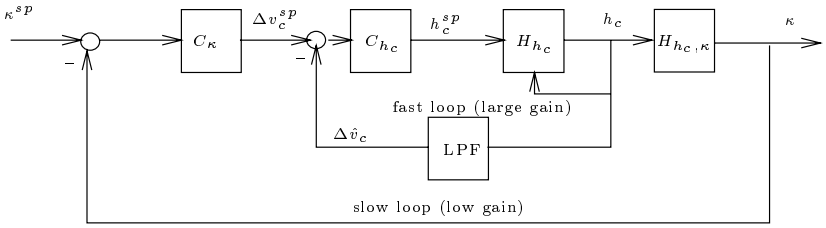

Figure 8.9: Kappa number control by active chip level control including internal feedback from the chip velocity variations

8.4.2 Active chip velocity control

In strategy *S2*, we have the problem to estimate the chip velocity. This may either be accomplished by the use of our mechanistic model, or by an estimation similar to that discussed in Sec. 7.2.1. Possible strategies for this include the blow flow or the wash water flow as control inputs, see Fig. 8.10. We assume that the chip level is not controlled.

8.4.3 Active chip level- and chip velocity control

A combination of *S1* and *S2* may give an improved solution. An advantage of using two control inputs (e.g. the blow flow and the wash water flow) to control the residence time, is that some degree of controllability is retained when one of the control inputs goes into saturation. By using a diagonal controller, however, we gain very little when the actuators are not in saturation. The reason for this

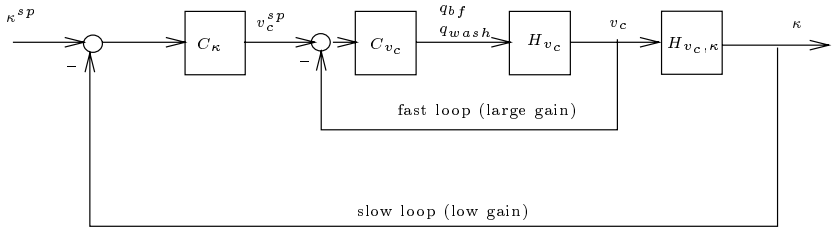

Figure 8.10: Kappa number control by active chip velocity control

is that when e.g. the chip level is tightly controlled by the blow flow, the influence from the wash water on the chip velocity in the cooking zone is weak. This is also discussed in Sec. 5.3.1; the lift force from the wash water flow and the pull force from the blow flow almost cancel the effect of each other. Hence, the best control structure may be a full 2×2 controller.

8.4.4 Indirect residence time control

Active residence time control may also indirectly be accomplished by omitting the continuous chip level control loop, and control the Kappa number directly by manipulating the blow flow or the wash water flow. In this case, we have to have a chip level control loop which is active only when the level falls outside certain limits. Figs. 8.11-8.14 show some responses from these approaches. The figures show that even though the settling times are still fairly long, one unit deviation of the Kappa number is achieved within a few hours. Again, the parameters in the Kappa number controllers are tuned tight such that the gain margins are fairly small, see Figs. 8.15-8.16.

Note finally that the production rate can be increased by higher chip level combined with higher chip velocity.

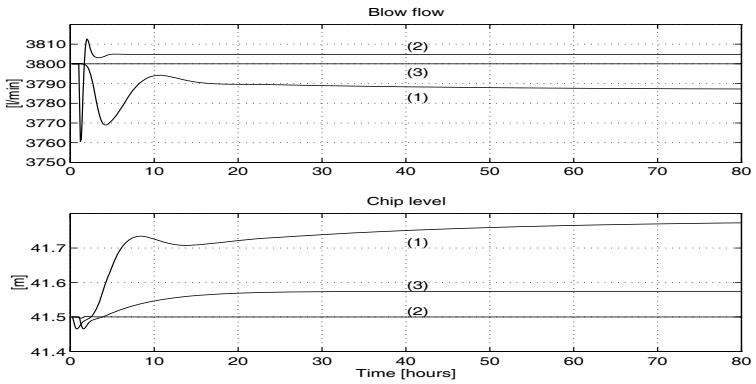

Figure 8.11: Blow flow and chip level during a 5% increase in the feed chip lignin content when the Kappa number is controlled by the blow flow (1), without Kappa number control but including chip level control (2), and without Kappa number- and chip level control (3). The set-points are respectively $3800 l/min$ and $41.5 m$.

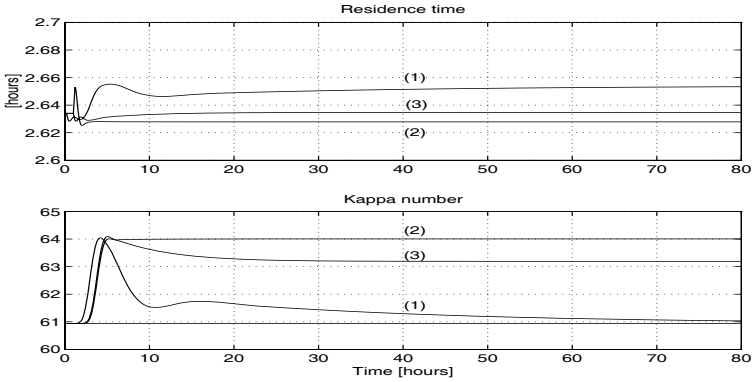

Figure 8.12: Residence time and the blow flow Kappa number during a 5% increase in the feed chip lignin content when the Kappa number is controlled by the blow flow (1), without Kappa number control but including chip level control (2), and without Kappa number- and chip level control (3). The set-point for the Kappa number is 60.9.

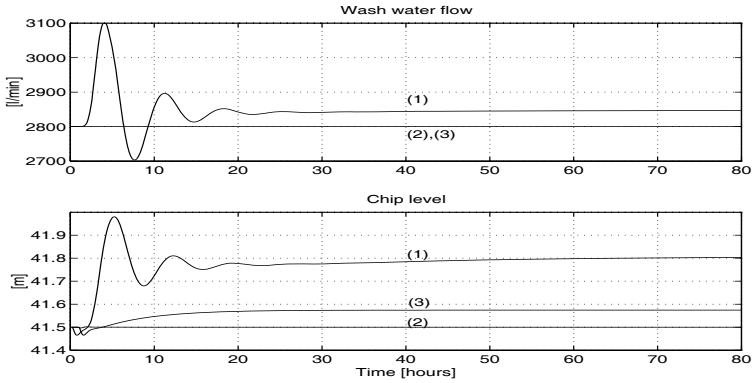

Figure 8.13: Wash water flow and chip level during a 5% increase in the feed chip lignin content when the Kappa number is controlled by the wash water flow (1), without Kappa number control but including chip level control (2), and without Kappa number- and chip level control (3). The set-points are respectively $3800 l/min$ and $41.5 m$.

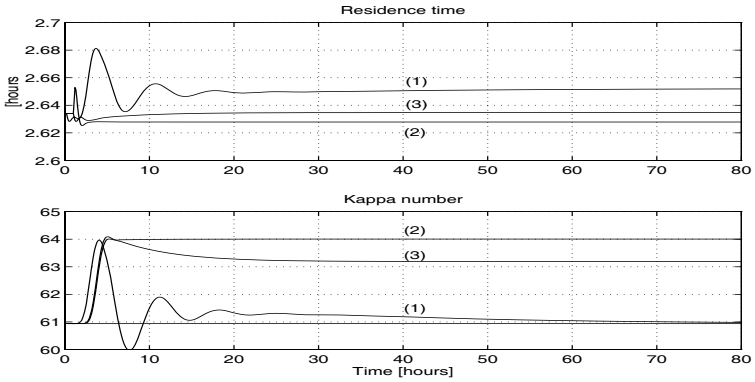

Figure 8.14: Residence time and the blow flow Kappa number during a 5% increase in the feed chip lignin content when the Kappa number is controlled by the wash water flow (1), without Kappa number control but including chip level control (2), and without Kappa number- and chip level control (3). The set-point for the Kappa number is 60.9.

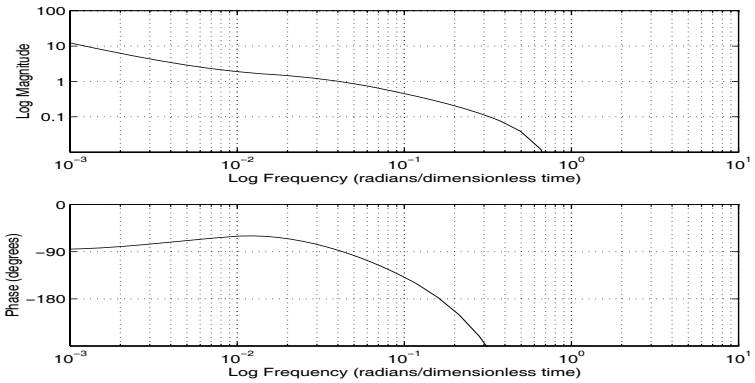

Figure 8.15: The closed loop transfer function in the indirect residence time control structure where the Kappa number is controlled by the blow flow

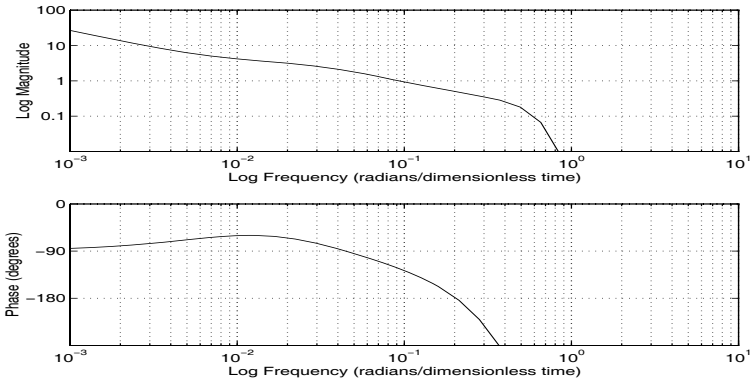

Figure 8.16: The closed loop transfer function in the indirect residence time control structure where the Kappa number is controlled by the wash water flow

Chapter 9

Discussion and conclusions

9.1 The model derivation and the analyses

A novel dynamic model of the continuous Kamyr digester has been developed. The availability of a number of earlier proposed models (Ch. 2) has facilitated our modelling. To understand the background of the proposed model, a detaild conceptual model has been discussed, including a number of model assumptions (Ch. 3). A special feature of this model is connected to the compressibility assumption for the chip plug. By considering the individual wood chips as being incompressible, the collection of chips, forming a continuous porous medium, is regarded as a granular unconsolidated soil by which the compressibility is irreversible (Sec. 3.4.2).

The model consists of a set of mass-, momentum-, and energy balances in two-phase form.
In the derivation of the mass balances, the separation of the component balances from the overall mass balances is essential. By this, a state equation for the compaction of chips is derived. Due to the Euler formulation of the PDEs, certain simplifications have been made for the upper part of the mass. In this part, the chip- and liquor levels are computed, as well as the first stage of delignification in the vessel.
The momentum (or force) balance equation for the chip plug may be regarded as the core of the model. This is needed in the dynamic prediction of the residence time for the chips. However, this equation is a bottleneck for the simulation speed because the acceleration of chip plug is extremely fast compared to the other dynamics which appear in the process (Sec. 6.2).
A special feature in the energy balances, is the condensation mechanism in the steam zone. Moreover, the temperature prediction in this zone is essential for the pulp quality prediction.
The proposed model describes the flow dynamics rather detailedly, and the kinetics more coarsely. We believe, however, that we have included the most important effects in the process so as to give a mathematical description that explains the physical behaviour of the mass inside the digester. The set of assumptions, the

model derivation, and the discussion around this, have brought a broader understanding of the model and the process.

The simulation results (Ch. 5) indicate that some effects are important, and some are not (Sec. 5.1). Further, the interactions between the delignification, the chip level, the compaction of chips, their residence time, and the pulp quality have been revealed. The compaction of chips occurs mostly in the cooking zone. In the wash zone, the lift of the chip plug by the wash water is considerable. The results indicate that the residence time for the wood chips has a dominating impact on the Kappa number when the chip level is not controlled, or controlled actively. Tight chip level control has a potential to improve the digester control. Further, it appears that the chip velocity has less influence on the Kappa number than the chip level does. This means that changing the residence time by the chip level has greater influence than changing it by the chip velocity. Hence, when the chip level is tightly controlled, computation of the chip velocity is not critical for Kappa number prediction. This supports the simplifications which are made in earlier proposed models. However, conventional residence time control seems to be based on the misunderstanding that constant chip level gives constant residence time and Kappa number under chip feed density variations. Our results (Ch. 8) indicate that active residence time control may give improved Kappa number control.
By this, we claim that it is important to include the interaction between the chip level and the chemical reactions in a continuous digester model for predicting pulp quality.

The simulation results also indicate that the model may be a valuable tool in the support for operational changes. By this, improved operating procedures during grade shifts, short-stops, etc. may be developed. The short-stop scenario in Sec. 5.3.3 indicates that axial mixing may be considerable during such changes.

Linear analysis tools are convenient for analysis of dynamics, process couplings, control structures, and process design. The analyses in this thesis indicate that the residence time for the chips, and the quality measures are input-output controllable in a limited frequency range. A MIMO control structure may be preferential for Kappa number, alkali concentration, and wash efficiency control.

Dependent on the application, reduced models may give satisfactory results. The reduction of the component balances indicates that they may be formulated by only three components; lignin, non-lignin and alkali, where only the first and the latter are described by time differential equations. Further, it may be argued that one temperature variable is satisfactory.

9.2 Model validation

The model has been validated by two means. First, acceptance for the results has been received from recognised persons within the pulp and paper community (Christensen, Kleppe and Kirkebak, 1994). This has been performed by running audits. These have included two types of discussions; (i) the model and the assumptions that it rests on, and (ii) the results from the simulation scenarios.
Second, we have compared the results with available process data (KAMYR, 1993), (Lunde and Mikaelsen, 1994).

9.3 Model weaknesses

The model analyses have revealed some weaknesses in the model. Among the model assumptions, the assumption of continuity in the chip plug is essential. Hence, the model cannot be used in prediction during extreme conditions like a hang-up. When a part of the chip plug hangs (typically at the extraction screens), the grid sections downflow are eventually depleted. In this way, continuity is not longer valid.
The description of the steam zone may be improved by including an energy balance for the steam, and in this way include the influence on the mass balance for water in the vessel. Especially in scenarios like a short-stop, this may be valuable.
For several reasons, the description of the top section (see Fig. 3.2) may be improved. The compaction of chips is described ad hoc, c.f. Eq. (3.145) and Appendix F. Further, the component balance equations in this section, Eqs. (3.146)-(3.151), are based on a numerical adaption. The weakness in the model related to this is revealed in the short-stop scenario in Sec. 5.3.3. Although we have assumed that the model error caused by these equations does not aggravate the accuracy of the solution too much, this weakness may as well be an explanation for the result that the chip level has a dominating impact on the Kappa number compared to the influence from the chip velocity. Formulation of the PDEs in the Lagrange form might give a better solution to these problems related to the steam zone and the top section.
We have made certain simplifications especially regarding the reaction kinetics, see page 46. This weakness is revealed typically at extremely low Kappa number levels. Hence, e.g. the stopping period in short-stop scenario is shortened as to give a proper solution.

9.4 Utilization of the model

From an operational perspective, the model is promising. The model results indicate that the many interacting effects in a digester may paint a confusing picture to operating personnel. Using the model as a predictive simulation tool may, hence, support operating personnel to make the correct decisions. Taking this further, the model may be used to develop model-based control schemes. The concept of *model predictive control (MPC)* (see Rawlings, Meadows and Muske (1994) for a survey), is one of the most successful approaches for processes with long time delays. Related to this is the ability of the model to support the instrumentation of digesters. The availability of gauges, the abilities for proper location, and the accuracy of existing gauges dictate this.
In addition to the new ability for developing improved operating procedures in plant operation, use of the model for redesign of the digester, and as a basis for training simulators should be considered as well.

Bibliography

Allison, J., Dumont, G. and Novak, L. (1991). Multi-Input Adaptive-Predictive Control of Kamyr Digester Chip Level, *The Canadian Journal of Chemical Engineering, vol.69, February* pp. 111–119.

Allison, J., Dumont, G., Novak, L. and Cheetham, W. (1990). Adaptive-Predictive Control of Kamyr Digester Chip Level, *AIChE Journal, July, vol.36, no.7* pp. 1075–1086.

Alonso, M. and Finn, E. (1983). *Physics*, Addison-Wesley Publishing Company.

Aoki, M. (1990). *State Space Modeling of Time Series*, Springer-Verlag.

Bäckström, C. (1960). Examensarbete, *Royal Institute of Technology, Stockholm* .

Bear, J. (1972). *Dynamics of fluids in porous media*, American Elsevier Publishing Company Inc.

Benko, J. (1964). The measurement of molecular weight of lignosulfonic acids and related materials by diffusion, *Tappi Journal (47)8* pp. 508–514.

Bird, R., Steward, W. and Lightfoot, E. (1960). *Transport Phenomena*, Wiley International Editions.

Box, G. and Jenkins, G. (1976). Time Series Analysis; Forecasting and Control, *Holden-Day, San Francisco* .

Brenan, K., Campbell, S. and Petzold, L. (1989). *Numerical Solution of Initial-Value Problems in Differential-Algebraic Equations*, North-Holland.

Burazin, M. (1986). *A Dynamic Model of Kraft-Anthraquinone Pulping*, PhD thesis, Lawrence University, The Institute of Paper Chemistry, Appleton, Wisconsin.

Burazin, M. (1988). Building a Mechanistic Model of Kraft-Anthraquinone Pulping Kinetics, *Tappi Journal, March,* pp. 165–169.

Christensen, T., Albright, L. and Williams, T. (1982). *A Mathematical Model of the Kraft Pulping Process, Report no 129*, PhD thesis, Purdue Laboratory for Applied Industrial Control, Purdue University, West Lafayette, Indiana.

Christensen, T., Ivan, M., Michaelsen, R., Lunde, G. and Zetterlund, U. (1994). Model Predictive Control of a Continuous Kamyr Digester at SCA-Nordliner, Munksund, Sweden, *Pulp and Paper Canada* **95**(12): 146+.

Christensen, T., Kleppe, P. and Kirkebak, P. (1994). Internal project meetings, *Peterson A/S, Moss, Norway* .

Christensen, T., Smith, C., Albright, L. and Williams, T. (1983). Dynamic modelling of the Kamyr digester: normal operation including hardwood-softwood swings, *Tappi Journal, vol.66, no.11* pp. 65–68.

Clarke, F. (1987). A kraft delignification model and its use in production optimization, *Pulp & Paper Canada, 88:6* pp. T197–T201.

Cohen, E. and Ryan, T. (1974). Continuous Digester Level Control Using Discrete Level Indication, *TAPPI Alkaline Pulping Conf., Seattle, 91* .

Coulson, J. and Richardson, J. (1977). *Chemical Engineering, Volume 1, 3rd ed.*

Darcy, H. (1856). Les Fontaines Publiques de la Ville de Dijon, *Dalmont, Paris* .

Dayal, B. (1992). *Feedforward neural networks for process modelling and control*, Master's thesis, Degree of Master Engineering, McMaster University, Toronto, Canada.

Dimmel, D., Shepard, D. and Brown, T. (1981). *Journal of Wood Chem.Technol., Vol.1* .

Dumont, G. (1986). Application of Advanced Control Methods in the Pulp and Paper Industry- A Survey, *Automatica, Vol.22, No.2* pp. 143–153.

Dupuit, J. (1863). Études Théoretiques et Pratiques sur le Mouvement des Eaux dans les Canaux Découverts et á Travers les Terrains Permeables, 2nd ed., *Dunod, Paris* .

Edwards, C. and Penny, D. (1986). *Calculus and Analytic Geometry, 2nd ed.*, Prentice-Hall International, Inc.

Ergun, S. (1952). Fluid flow through packed columns, *Chem.Eng.Prog., Vol.48* pp. 89–94.

Fogler, H. (1992). *Elements of chemical reaction engineering, 2nd ed.*, Prentice-Hall International Editions.

Forchheimer, P. (1901). Wasserbewegung durch Boden, *Z.Ver.Deutsch.Ing., 45* .

Fuchs, R. and Smith, C. (1971). Blow Flow Control of Continuous Digesters, *Tappi Journal, Vol. 54, No. 3* .

Funkquist, J. (1993). *On modelling and control of a continuous pulp digester*, Master's thesis, Department of Signals, Sensors & Systems, Automatic Control, Royal Institute of Technology, Stockholm.

Granberg, B. and Gustavsson, I. (1982). Kappa number control of Kamyr Digesters, *Proc. EUCEPA Symposium on Control Systems in Pulp and Paper Industry, Stockholm* pp. 116–125.

Gustafson, R., Sleicher, C., McKean, W. and Finlayson, B. (1983). Theoretical Model of the Kraft Pulping Process, *Ind.Eng.Chem.Process Des. Dev., vol. 22* pp. 87–96.

Hägglund, O. (1959). Examensarbete, *Royal Institute of Technology, Stockholm* .

Härkönen, E. (1984). *A mathematical model for two-phase flow*, Acta Polytechnica Scandinavia, Mechanical Engineering Series No. 88.

Härkönen, E. (1987). A mathematical model for two-phase flow in a continuous digester, *Tappi Journal, December* pp. 112–126.

Härkönen, E. (1994). Private correspondence.

Hartler, N. (1962). Penetrerings- och diffusionsforhålandena vid sulfatkoket, *Papper och Trä, no.7* pp. 365–374.

Hatton, J. (1973). Development of yield prediction equations in kraft pulping, *Tappi, vol.56, no.7* .

Herget, C. (1967). *Controllability of Distributed Parameter Systems*, PhD thesis, University of California, Los Angeles.

Horng, A., Mackie, D. and Ticky, J. (1987). Factors affecting pulp quality from continuous digesters, *Tappi Journal, December* pp. 75–79.

Ineropera, F. and De Witt, D. (1990). *Introduction to heat transfer*, Wiley International Editions.

Irmay, S. (1958). On the theoretical derivation of Darcy and Forchheimer formulas, *Trans. Amer. Geophys. Union no 4, 39* .

Jiménez, G., Gustafson, R. and McKean, W. (1989). Modelling Incomplete Penetration of Kraft Liquor, *Journal of pulp and paper science, vol. 15, no. 3* pp. 110–115.

Johansson, B., Mjöberg, J., Sandström, P. and Teder, A. (1984). Modified continuous kraft pulping-now a reality, *Svensk Papperstidning, no.10, vol.87* pp. 30–35.

Johnsson, L. (1971). Mathematical models of the kraft cooking process, *Technical report*, Chalmers University of Technology, Control Engineering Laboratory, Gothenburg, Sweden.

Jutila, E. (1979). *Applicability of Kraft Cooking Control Models*, PhD thesis, University of Oulu, Department of Process Engineering, Division of Control Engineering, Oulu, Finland.

Kalman, R. (1960). A Contribution to the Theory of Optimal Control, *Bol. Socied. Mat. Mexicana, 5, 102-119* .

Kalman, R., Ho, Y. and Narendra, K. (1963). Controllability of Linear Dynamical Systems, *Contributions to differential equations, 189-213* .

KAMYR (1970). Instruktion, Kamyr kontinuerliga kokeri med trykkimpregneringskärl och invändig toppseparator, *Instruction manual* .

KAMYR (1971). KALAB 3:71, *Internal document for Peterson A/S, Moss, Norway* .

KAMYR (1993). Residence time measurement in a continuous Kamyr digester, *Internal document for Peterson A/S, Moss, Norway* .

Kerr, A. (1970). The kinetics of kraft pulping, *APPITA, 24, 3* pp. 180–188.

Kerr, A. and Uprichard, J. (1976). The kinetics of Kraft Pulping - Refinement of a Mathematical Model, *APPITA, 30* pp. 48–54.

Kleinert, T. (1966). Mechanisms of Alkaline Delignification, *Tappi vol.49, no.2* pp. 53+.

Kleppe, P. (1970). Kraft Pulping, *Tappi vol.53, no.1* pp. 35+.

Kleppe, P. (1978). Progress in high yield kraft pulping, *Norsk Skogindustri no.6* .

Kleppe, P. and Storebråten, S. (1982). Strategies for and limitations in the control of a continuous digester, *Proceedings from EUCEPA Symposium on Control Systems in the Pulp and Paper Industry, Stockholm* pp. 87–95.

Koch Christensen, P. (1991). *Treforedlingskjemi*, Department of Chemical Engineering, Norwegian Institute of Technology, Trondheim.

Lee, J. and Datta, A. (1994). Nonlinear Inferential Control of Pulp Digesters, *AIChE Journal vol.40, no.1* .

Liao, Y. and Wu, S. (1976). A kamyr digester pulping process control by a time series approach, *IFAC* pp. 141–149.

Lunde, G. and Mikaelsen, R. (1994). Forstudie av koker-reguleringen ved Peterson A/S, *Internal document for Peterson A/S, Moss, Norway* .

Lundqvist, S. (1975). Matematisk model av kontinuerlig sulfatkokare, *SCAN FORSK 72*, Stockholm.

Lundqvist, S. (1982). State of the art in continuous digester control, *Proceedings from EUCEPA Symposium on Control Systems in Pulp and Paper Industry, Stockholm* pp. 99–108.

Lundqvist, S. (1990). Recent developments in continuous digester control, *Proceedings from EUCEPA Conference on New Available Techniques and Current Trends, Stockholm* pp. 222–333.

Lunze, J. (1992). *Feedback control of large-scale systems*, Prentice-Hall, New York.

Masùra, V. (1993). A mathematical model for kraft pulping expressed by a logarithmic straight-line equation, *Tappi Journal, vol.76, no.11* .

McKibbins, S. (1960). Application of Diffusion Theory to the Washing of Kraft Cooked Wood Chips, *Tappi Journal, vol. 43, no. 10* pp. 801–805.

Meisingset, H. and Balchen, J. (1994). Determining Necessary Model Resolution in Model Based Control of Distributed Parameter Processes, *Proceedings from the IFAC ADCHEM'94 International Symposium, Kyoto* pp. 483–488.

Michelsen, F. and Foss, B. (1993). Modelling and simulation of the mass flow and reaction kinetics in a continuous Kamyr steam/liquor phase digester, *Proceedings from the 35th SIMS Simulation Conference* pp. 277–291.

Michelsen, F. and Foss, B. (1994a). Modelling and simulation of the mass flow and reaction kinetics in a continuous Kamyr steam/liquor phase digester, *Modelling, Identification and Control, Vol.15, No.1* pp. 33–53.

Michelsen, F. and Foss, B. (1994b). Modelling of a Continuous Digester for Process Surveillance and Prediction, *Proceedings from the IFAC ADCHEM'94 International Symposium, Kyoto* pp. 552–557.

Michelsen, F. and Foss, B. (1995a). A Comprehensive Mechanistic Model of the Continuous Kamyr Digester, *Submitted to Applied Mathematical Modelling* .

Michelsen, F. and Foss, B. (1995b). A Dynamic Model of the Interaction between the Chemical Reactions and the Residence Time in the Continuous Kamyr Digester, *Submitted to Tappi Journal* .

Mitchell, A. and Griffiths, D. (1990). *The Finite Difference method in Partial Differential Equations*, John Wiley & Sons.

Moore, B. (1978). Singular value analysis in linear systems, *Proc. IEEE Conference on Decision and Control, pp 66-73* .

Morari, M. (1983). Design of resilient processing plants III, A general framework for the assessment of dynamic resilience.

Nelson, P. and Irvine, G. (1992). Tearing resistance in soda-AQ and kraft pulps, *Tappi Journal, January* pp. 163–166.

Neretnieks, I. (1974a). A mathematical model for continuous counter current adsorption, *Svensk Paperstidning, vol.77, no.11* pp. 407–411.

Neretnieks, I. (1974b). Note on some washing results with a Kamyr Hi-Heat washer, *Svensk Paperstidning, vol.77, no.13* pp. 486–490.

Norden, S. and Teder, A. (1979). Modified kraft processes for softwood bleached-grade pulp, *Tappi vol.62, no.7* pp. 49+.

Pankonin, B. (1979). *A dynamical model of the kraft pulping process*, Master's thesis, The Institute of Paper Chemistry, Appleton, Wisconsin.

Patankar, S. (1980). *Numerical Heat Transfer and Fluid Flow*, McGraw-Hill Book Company.

Pedersen, V. (1983). Kokeristyring, M.Peterson & Søn A/S, *Internal document for Peterson A/S, Moss, Norway* .

Perkins, J. (1989). Interactions Between Process Design and Process Control, *Preprints IFAC Symposium DYCORD 89, Maastricht, Netherlands* .

Peterson (1994). *Internal document for Peterson A/S, Moss, Norway* .

Petrus, C. and Allison, J. (1990). On the application of Generalized Predictive Control to Kamyr Digester Chip Level, *Pacific Paper Expo, Technical Conference, Program2:Process Control* .

Poppius, K. (1985). *Enhanced β-aryl ether cleavage in lignin model compounds caused by reduced species of anthraquinone under alkaline pulping conditions*, PhD thesis, The Finnish pulp and paper research institute, Helsinki, Report no.571.

Øgård, O. (1980). *Estimering og regulering av cellulosekoker*, Master's thesis, Department of Engineering Cybernetics, Norwegian Institute of Technology, Trondheim.

Rawlings, J., Meadows, E. and Muske, K. (1994). Nonlinear Model Predictive Control: A Tutorial and Survey, *Proceedings from the IFAC ADCHEM'94 International Symposium, Kyoto* .

Rekunen, S., Jutila, E., Lahteenmaki, E., Lönneberg, B. and Virkola, N. (1980). *Paperi ja Puu, 62, 80* .

Rosenbrock, H. (1970). *State-Space and Multivariable Theory*, Nelson, London, England.

Rydholm, S. (1967). *Pulping Processes*, Interscience Publishers, New York.

Saltin, J. (1992). A predictive dynamic model for continuous digesters, *Proceedings from Tappi Pulping Conference* pp. 261–267.

Sandström, P., Lindberg, H. and Teder, A. (1986). Development of modified kraft processes with a mathematical model for continuous digesters, *AIChE Forest Products Division, vol.1* pp. 31–43.

Sarkanen, K. and Ludwig, C. (1971). *Lignins occurrence, formation, structure and reactions*, John Wiley and Sons, Inc.

SCAN (1964). SCAN FORSK C17:64, *Technical report.*

Shampine, L. and Gordon, M. (1990). *Computer Solution of Ordinary Differential Equations*, W.H.Freeman & Company.

Singstad, P. (1992). *Modelling and multivariable control of high pressure autoclave reactors for polymerization of ethene*, PhD thesis, University of Trondheim, Norwegian Institute of Technology, Trondheim.

Sjöström, E. (1981). *Wood Chemistry*, Academic Press, New York.

Skogestad, S. (1993). Controllability analysis, *Talk notes from Norwegian Institute of Technology, Trondheim* .

Skogestad, S. (1994). *Multivariable feedback control - Analysis and design using frequency-domain methods, Course notes from Department of Chemical engineering, Norwegian Institute of Technology, Trondheim*, John Wiley & Sons.

Smith, C. and Williams, T. (1974). *Studies of the Mathematical Modelling, Simulation and Control of the Operation of a Kamyr Continuous Digester for the Kraft Process*, PhD thesis, Purdue University, West Lafayette, Indiana.

Smook, G. (1989). *Handbook for pulp & paper technologists*, Joint textbook committee of the paper industry.

Sonntag, R. and Van Wylen, G. (1991). *Introduction to Thermodynamics. Classical and Statistical, 3rd ed.*, John Wiley & Sons.

Stankovic, S., Majdanac, L. and Draskovic, S. (1976). Mathematical Modeling of the Sulfate Cooking Process, *Hem.Ind., 30, no.7* pp. 357–359.

Stone, J. (1957). The Effective Capillary Cross-Sectional Area of Wood as a Function of pH, *Tappi Journal, vol.40, no.7* pp. 539+.

Strang, G. (1988). *Linear algebra and its applications*, Harcourt Brace Jovanovich International Edition, San Diego.

Takeuchi, K., Komiyama, H. and Suzuki, M. (1979). The stop-and go method applied to simulation of a continuous kraft digester, *Tappi, 62, no.10* pp. 111–114.

Talton, J. and Cornell, R. (1987). Diffusion of sodium hydroxide in wood at high ph as a function of temperature and the extent of pulping, *Tappi Journal, March* pp. 115–118.

Teder, A. and Olm, L. (1981). Extended delignification by combination of modified kraft pulping and oxygen bleaching, *Paperi ja Puu, 63* pp. 315–326.

Terzaghi, K. (1943). *Theoretical Soil Mechanics*, John Wiley and Sons, Inc.

Terzaghi, K. (1960). *From Theory to Practice in Soil Mechanics*, John Wiley and Sons, Inc.

The MathWorks Inc., . (1994). *MATLAB, High-Performance Numeric Computation and Visualization Software, version 4.2.*, The MathWorks Inc., Cochituate Place, 24 Prime Park Way, Natick, Massachusetts 01760.

Tyler, D. (1981). *Predicting rejects from kraft cooking of overthick chips; a model incorporating caustic diffusion with delignification*, Master's thesis, University of Idaho, Moscow, ID.

Van Heiningen, A. (1993). Lecture notes, *Department of Chemical Engineering, University of New Brunswick, Fredricton, N.B.* .

Vanchinathan, S. and Krishnagopalan, G. (1993). Development of a dynamic model of kraft pulping based on liquor analysis, *Presentation at AIChE meeting, USA, Nov* .

Vroom, K. (1957). The H-factor: A means of expressing cooking times and temperatures as a single variable, *Pulp and Paper Magazine of Canada, vol.58, no.3* pp. 228–231.

Wasserman, P. (1989). Neural Computing, Theory and Practice, *Van Nostrand Reinhold, New York* .

Webster (1989). *Webster's Encyclopedic Unabridged Dictionary of the English Language*, Gramercy Books.

Welch, J., Harlow, F., Shannon, J. and Daly, B. (1966). The MAC method, *Report LA 3425, Los Alamos Scientific Laboratory, Los Alamos, N.M.* .

Wells, C., Johns, E. and Chapman, F. (1975). Computer control of batch digesters using a Kappa number model, *Tappi, vol. 58, No. 8* .

Wisnewski, P. (1994). *Mathematical models of the kraft cooking process*, Master's thesis, Purdue University, West Lafayette, USA.

Ytrehus, T. (1987). To - fase strømning, *EEU-kurs, Department of Applied Mechanics, Thermodynamics and Fluid Dynamics, Norwegian Institute of Technology, Trondheim* .

Zhong, Y., Bélanger, P. and Gendron, S. (1990). Parameter identification of the heating zone dynamics in the Kamyr digester, *Automatica, vol.26, no.3* pp. 629–631.

Ziegler, J. and Nichols, N. (1943). Process Lags in Automatic Control Circuits, pp. 433–444.

Appendix A

Porosity

Volumetric porosity

This material is taken from Bear (1972).

Let P be a mathematical point inside the domain occupied by the porous medium. Consider a volume ΔU_i (say having a shape of a sphere) much larger than a single pore or grain, for which P is the centroid. For this volume we may determine the ratio:

$$n_i \equiv n_i(\Delta U_i) = \frac{(\Delta U_v)_i}{\Delta U_i} \tag{A.1}$$

where $(\Delta U_v)_i$ is the volume of void space within ΔU_i. Obviously, if ΔU_i is too large, say in the order of magnitude of the entire field of flow, it is meaningless to assign the value n_i to the point P, i.e. to represent the ratio $\frac{(\Delta U_v)_i}{\Delta U_i}$ for the void space in the vicinity of P. This is especially true when the domain is inhomogeneous (e.g. layers of soil). To determine how small ΔU_i should be in order for n_i to represent the porous medium in the neighbourhood of P, we gradually reduce ΔU_i around P, determining the ratio $\frac{(\Delta U_v)_i}{\Delta U_i}$ for a sequence of volumes ΔU_i: $\Delta U_1 > \Delta U_2 > \Delta U_3 \cdots$. As the volumes in question pass through both the solid matrix and the void space, each volume ΔU_i will contain a "volume of solids", $(\Delta U_s)_i$, and a "volume of voids", $(\Delta U_v)_i$.
For large values of ΔU_i, the ratio may undergo gradual changes as ΔU_i is reduced (again when the domain is inhomogeneous). Below a certain value of ΔU_i, depending on the distance of P from boundaries of inhomogeneity, these changes or fluctuations tend to decay, leaving only small-amplitude fluctuations that are due to the random distribution of pore sizes in the neighborhood of P. However, below a certain value ΔU_0, we suddenly observe large fluctuations in the ratio n_i. This happens as the dimensions of ΔU_i approach those of a single pore. Finally, as $\Delta U_i \to 0$, converging on the mathematical point P, n_i will become either one or zero, depending on whether P is inside a pore or inside the solid matrix of the medium. Fig. A.1 shows the relationship between n_i and ΔU_i.

Figure A.1: Definition of porosity and representative elementary volume (from Bear (1972))

The *volumetric porosity* of the medium, $n(P)$, at a mathematical point P is defined as the limit of the ratio n_i as $\Delta U_i \rightarrow \Delta U_0$:

$$n(P) = lim_{\Delta U_i \rightarrow \Delta U_0} n_i\{\Delta U_i(P)\} = lim_{\Delta U_i \rightarrow \Delta U_0} \frac{(\Delta U_v)_i(P)}{\Delta U_i} \qquad (A.2)$$

For values of $\Delta U_i < \Delta U_0$, we must consider the actual presence of pores and solid particles; in this range there is no single value that can represent the porosity at P. The volume ΔU_0 is therefore the *representative elementary volume (REV)* or the *physical* (or *material*) point of the porous medium at the mathematical point P.
The limiting process in Eq. (A.2) is sometimes called the *extrapolated limit*. Obviously, the limit $\Delta U_i \rightarrow 0$ is meaningless. From the definition of the REV, it follows that its dimensions are such that the effect of adding or subtracting one or several pores has no significant influence on the value of n. We assume that both ΔU_0 and ΔU_v vary smoothly in the vicinity of P. Then:

$$n(P) = lim_{P' \rightarrow P} n(P') \qquad (A.3)$$

which means that n is a continuous function of the position of P within the porous medium.

Area and linear porosity

In a manner similar to that described for volume porosity, it is possible to define for a point P in the porous medium a *representative elementary area (REA)* and a corresponding *area porosity*. Equivalently, we can define a *representative elementary length (REL)* and a corresponding *linear porosity*.

It can be shown that the average values of the linear porosity, the area porosity, and the volume porosity are equal:

$$n_V(P) = n_A(P) = n_L(P) = n(P) \qquad (A.4)$$

We simply say that the porous medium has porosity $n(P)$.

A consequence of this is that the area porosity, defined as the average value of the *directional area porosity*, is **independent of direction**. Directional area porosity is the area porosity related to a REA plane whose normal is in a specific direction, say of the unit vector.

Appendix B

The multicomponent fluxes

The fundamental fluxes that arises in transport processes are discussed here. The material is adopted from Bird et al. (1960). The term *diffusion* is used in the general sense. The discussion is restricted to a multicomponent one-phase medium where the components have the same average velocity as the bulk medium. A diffusive movement is superimposed on this average flow.

In a flowing multicomponent medium there are three "mechanical driving forces" that tend to produce the movement of a species with respect to the mean fluid motion: 1) the concentration gradient, 2) the pressure gradient, and 3) external forces acting unequally on the various species. In addition, there is a "thermal driving force", expressed by the temperature gradient.

The expression for the *mass diffusion*, j_i, therefore consists of three contributions associated with the mechanical driving forces and one contribution associated with the thermal driving force:

$$j_i = j_i^{(x)} + j_i^{(p)} + j_i^{(g)} + j_i^{(T)} \tag{B.1}$$

i.e. the sum of terms describing *ordinary (concentration) diffusion*, $j_i^{(x)}$, *pressure diffusion*, $j_i^{(p)}$, *forced diffusion*, $j_i^{(g)}$, and *thermal diffusion*, $j_i^{(T)}$. In this study, the formulas for these mass fluxes are (c.f. Eqs. (3.74) and (3.75)):

$$\begin{aligned} j_i^{(x)} &= j_{i,z}^{(x)} + j_{i,\gamma}^{(x)} \qquad\qquad (B.2)\\ &\approx -D_i \nabla(\rho_i \epsilon_i) + \rho_i \epsilon_i v_{i,\gamma} \\ j_i^{(p)} &= j_i^{(g)} = j_i^{(T)} = 0 \qquad\qquad (B.3) \end{aligned}$$

The ordinary diffusion is, however, generally dependent, in a complicated way, on the concentration gradients of all the substances present. In this study, we have made certain approximations in this context (e.g. that the coefficients are not dependent on the spatial direction). The pressure diffusion term describes the net mass movement caused by the pressure gradient imposed on the system. The

tendency for a mixture to separate under a pressure gradient is very small, but use is made of this effect in centrifuge separations in which tremendous pressure gradients may be established. The forced diffusion term is of primary importance in ionic systems, in which the external force on an ion is equal to the product of the ionic charge and the local electric field. The thermal diffusion term describes the tendency for species to diffuse under the influence of a temperature gradient. It is described by

$$j_i^{(T)} = -D_i^T \nabla \ln T \tag{B.4}$$

This effect is generally quite small, except for special separation devices. In this study, we assume $D_i^T = 0$.

Figure B.1: Schematic diagram showing the approximate relations between fluxes and driving forces in a binary system. The associated transport coefficients are shown within brackets. From Bird et al. (1960)

Generally for a multicomponent system we have fluxes of momentum, energy, and mass, each resulting from an associated driving force as indicated by the main diagonal in Fig. B.1. Newton's law for constant ρ is:

$$\tau_{zx} = -\eta \frac{d}{dz}(\rho v_x) \tag{B.5}$$

Fourier's law for constant ρC_p is:

$$q_z = -k \frac{d}{dz}(\rho C_p T) \tag{B.6}$$

Fick's law for constant ρ is:

$$j_{A,z} = -D \frac{d}{dz}(\rho_A) \tag{B.7}$$

According to the thermodynamics of irreversible processes, there is a contribution to each flux owing to each driving force in the system. This "coupling" can occur

only between flux-force pairs that are tensors of equal order, or which differ in order by two. Consequently, in a multicomponent system,

- The momentum flux depends only upon the velocity gradients.
- The energy flux depends both on the temperature gradient (heat conduction) and on the mechanical driving forces (the "diffusion-thermo effect" or "Dufour effect").
- The mass flux depends both on the mechanical driving forces (ordinary, pressure and forced diffusion) and on the temperature gradient (the "thermal-diffusion effect" or "Soret effect").

Furthermore, the Onsager reciprocal relations for the thermodynamics of irreversible processes give information as to the interrelation of the two coupled effects; the Dufour and the Soret effects. In order to describe the Soret effect, an additional transport property (i.e. in addition to viscosity, thermal conductivity, and diffusivity) had to be introduced, namely the "thermal diffusion ratio" or the "Soret coefficient", depending upon the exact definition. Because of the interconnection of the Soret and Dufour effects, as described by the Onsager relations, this additional transport property will take care of the quantitative description of both phenomena (see the non-diagonal entries in Fig. B.1).

In this study, Eq. (B.4) comprises the Soret effect in the mass balances. In accordance with assumption 5 on page 54, it is neglected. The Dufour effect in the energy balances (i.e. the Dufour energy flux), is quite complex in nature, and is usually of minor importance. One differs between contributions resulting from inter-diffusion of the various species present and the Dufour effect.

Appendix C

Formulation of the conservation laws

Conservation of mass

The principle of conservation of mass states that the rate of change of mass in a control volume equals the rate at which mass enters the control volume minus the rate at which mass leaves the control volume minus the rate at which mass is converted inside the control volume.

In mathematical form this can be written:

$$\frac{d}{dt}\iiint_V \rho dV + \oiint_A \rho \mathbf{v}^T \mathbf{n} dA = \iiint_V r dV \tag{C.1}$$

where ρ is the local bulk density, $\mathbf{v}$ is the bulk velocity at the boundary A of the volume, and $\mathbf{n}$ is the unitary normal vector to the boundary surface, pointing outward. The first term on the left-hand side in Eq. (C.1) is the rate at which mass is accumulated in V. The second term is the net flux of mass *out* of V. The term on the right-hand side is the rate of conversion, i.e. the net rate at which the material is produced per unit volume in V due to reactions.

Conservation of momentum

The principle of conservation of momentum states that the rate of change of momentum in a control volume equals the rate at which momentum enters the control volume minus the rate at which momentum leaves the control volume plus the sum of all forces acting on the control volume.

In mathematical form this can be written:

$$\frac{d}{dt}\iiint_V \rho \mathbf{v} dV + \oiint_A \rho \mathbf{v}\mathbf{v}^T \mathbf{n} dA = \sum_k F_k \tag{C.2}$$

where ρ is the local bulk density, $\mathbf{v}$ is the bulk velocity at the boundary A of the volume, $\mathbf{n}$ is the unitary normal vector to the boundary surface pointing outward, and $\sum_k F_k$ is the sum of all forces acting on the control volume (body and surface forces). The first term on the left-hand side in Eq. (C.2) is the rate at which momentum is accumulated in V. The second term is the net flux of momentum *out* of V.

Conservation of energy

The principle of conservation of energy states that the rate of change of energy in a control volume equals the rate at which the energy enters the control volume minus the rate at which the energy leaves.

In mathematical form this can be written:

$$\frac{d}{dt}\iiint_V \rho E dV + \oiint_A \mathbf{n}^T \varphi_E dA = 0 \tag{C.3}$$

where E is accumulated energy per unit of mass in the volume V, φ_E is the directed flux of energy at the boundary A of the volume, and $\mathbf{n}$ is the unitary normal vector to the boundary surface, pointing outward. The first term in Eq. (C.3) is the rate at which energy is accumulated in V, while the second term is the net flux of energy *out* of V, i.e. *energy flux*.

Appendix D

Balance equations for a conic vessel

The mass and momentum balance equations for the main section are derived here with the inclusion of varying cross section area, $A = A(z)$ in the digester. Actually, this is a generalisation of the results in Sec. 3.6.1 about the dependency of varying volume fractions of chips and liquor on the momentum balance equation.

Mass balances

For illustration, we only consider the overall mass balance for the chip plug, and start from Eq. (3.109):

$$\frac{\partial}{\partial t}\iiint_V \rho_c \epsilon_c dV = -\oiint_A \rho_c \epsilon_c \mathbf{v_{c,j}}^T \mathbf{n} dA \tag{D.1}$$

Instead of using Gauss' theorem in its original form, we consider an infinitely small reactor element of length dz and cross section $A = A(z)$ as shown in Fig. D.1. By

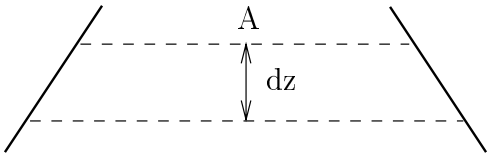

Figure D.1: A reactor element of length dz and cross section A

using Eq. (D.1) on this element gives:

$$\frac{\partial}{\partial t}(\rho_c \epsilon_c A dz) = (\rho_c \epsilon_c \mathbf{v_{c,j}}^T \mathbf{n} A)_z - (\rho_c \epsilon_c \mathbf{v_{c,j}}^T \mathbf{n} A)_{z+dz} \tag{D.2}$$

as we only consider the z-part of j_j, c.f. Sec. 3.5.1 (i.e. $\Delta(D\rho)$ is not included). We divide by dz and let $dz \to 0$:

$$A\frac{\partial}{\partial t}(\rho_c\epsilon_c) = -\frac{\partial}{\partial z}(\rho_c\epsilon_c v_{c,j}A) \tag{D.3}$$

as we have substituted for $\mathbf{v_{c,j}}$. Here, $\rho_c\epsilon_c v_{c,j} = \rho_c\epsilon_c v_c + j_j$ (c.f. Eq. (3.112)), where $j_j = j_z$.

$$A\frac{\partial}{\partial t}(\rho_c\epsilon_c) = -\frac{\partial}{\partial z}(\rho_c\epsilon_c v_c A) - \frac{\partial(j_z A)}{\partial z} \tag{D.4}$$

where, $\frac{\partial j_z}{\partial z} = -D_c\frac{\partial^2(\rho_c\epsilon_c)}{\partial z^2}$ (Eq. (3.114).

However, as $\mathbf{v_{c,j}}$ includes the interphase component, we have to integrate in this direction as well. By a similar derivation as above, and by summation, we have:

$$\begin{aligned}\frac{\partial}{\partial t}(\rho_c\epsilon_c) = &-\frac{\partial}{\partial z}(\rho_c\epsilon_c v_c) - \frac{\rho_c\epsilon_c v_c}{A}\frac{\partial A}{\partial z} - \Delta(D\rho) \\ &+D_c\frac{\partial^2}{\partial z^2}(\rho_c\epsilon_c) + \frac{D_c}{A}\frac{\partial(\rho_c\epsilon_c)}{\partial z}\frac{\partial A}{\partial z}\end{aligned} \tag{D.5}$$

The component balances are the same as in Sec. 3.5.1, while the $\frac{\partial A}{\partial z}$ terms include in the compaction equation Eq. (3.121). Note that the cross-term $\frac{D_c\epsilon_c}{A}\frac{\partial\rho_c}{\partial z}\frac{\partial A}{\partial z} = 0$ by the same argument as given in the remarks in Sec. 3.5.1.

Momentum balances

For illustration, we only consider the overall momentum balance for the chip plug, and start from Eq. (3.158):

$$\begin{aligned}\frac{\partial}{\partial t}\iiint_V \rho_c\epsilon_c\mathbf{v_c}dV = &-\oiint_A \rho_c\epsilon_c\mathbf{v_c}\mathbf{v_{c,j}}^T\mathbf{n}dA + \iiint_V \rho_c\epsilon_c\mathbf{g}dV \\ &-\oiint_A (p_c^{'} + p_l)\mathbf{n}\epsilon_c dA - \iiint_V F_\Lambda dV - \iiint_V F_\mu dV\end{aligned} \tag{D.6}$$

Again, we consider the infinitely small reactor element of length dz and cross section $A = A(z)$ as shown in Fig. D.1, and focus on the z direction. By using Eq. (D.6) on this element gives:

$$\begin{aligned}\frac{\partial}{\partial t}(\rho_c\epsilon_c\mathbf{v_c}Adz) = &(\rho_c\epsilon_c\mathbf{v_c}\mathbf{v_{c,j}}^T\mathbf{n}A)_z - ((\rho_c\epsilon_c\mathbf{v_c}\mathbf{v_{c,j}}^T\mathbf{n}A)_{z+dz} + \rho_c\epsilon_c\mathbf{g}Adz \\ &+((p_c^{'} + p_l)\mathbf{n}\epsilon_c A)_z - ((p_c^{'} + p_l)\mathbf{n}\epsilon_c A)_{z+dz} - F_\Lambda Adz - F_\mu Adz\end{aligned} \tag{D.7}$$

We substitute for $\mathbf{v_{c,j}}$ and $p_c = p_c^{'}\epsilon_c$, divide by dz, and let $dz \to 0$:

$$\begin{aligned}A\frac{\partial}{\partial t}(\rho_c\epsilon_c v_c) = &-\frac{\partial}{\partial z}(\rho_c\epsilon_c v_c v_{c,j}A) + A\rho_c\epsilon_c g - \frac{\partial(p_c A)}{\partial z} + p_c\frac{\partial A}{\partial z} \\ &-\frac{\partial(p_l\epsilon_c A)}{\partial z} + p_l\frac{\partial(\epsilon_c A)}{\partial z} - AF_\Lambda - AF_\mu\end{aligned} \tag{D.8}$$

When we only consider the left-hand side and the first term on the right-hand side, these can be expanded by:

$$Av_c\frac{\partial \rho_c\epsilon_c}{\partial t} + A\rho_c\epsilon_c\frac{\partial v_c}{\partial t} = -v_c\frac{\partial}{\partial z}(\rho_c\epsilon_c v_{c,j}A) - A\rho_c\epsilon_c v_{c,j}\frac{\partial v_c}{\partial z} \tag{D.9}$$

The first term on the left- and right-hand sides comprise the mass balance Eq. (D.3). As we omit j_j, $\rho_c\epsilon_c v_{c,j} = \rho_c\epsilon_c v_c$. This gives:

$$\begin{aligned} A\rho_c\epsilon_c\frac{\partial v_c}{\partial t} \;=\; & -A\rho_c\epsilon_c v_c\frac{\partial v_c}{\partial z} + A\rho_c\epsilon_c g \\ & -A\frac{\partial p_c}{\partial z} - A\epsilon_c\frac{\partial p_l}{\partial z} - AF_\Lambda - AF_\mu \end{aligned} \tag{D.10}$$

i.e. :

$$\frac{\partial v_c}{\partial t} = -v_c\frac{\partial v_c}{\partial z} + g - \frac{1}{\rho_c\epsilon_c}\frac{\partial p_c}{\partial z} - \frac{1}{\rho_c}\frac{\partial p_l}{\partial z} - \frac{1}{\rho_c\epsilon_c}F_\Lambda - \frac{1}{\rho_c\epsilon_c}F_\mu \tag{D.11}$$

Note that since both F_Λ and F_μ are functions of ϵ_c, we can equally well write:

$$\begin{aligned} -\frac{1}{\rho_c\epsilon_c}F_\Lambda \;&=\; -\frac{1}{\rho_c}F_\Lambda^{'} \\ -\frac{1}{\rho_c\epsilon_c}F_\mu \;&=\; -\frac{1}{\rho_c}F_\mu^{'} \end{aligned}$$

By this, Eq. (D.11) is independent of the cross section area A, i.e. equal to Eq. (3.165).

Appendix E

The yield and pH dependencies for the diffusion coefficient

With respect to the interphase diffusion coefficient, D_{EA}, Hägglund (1959) and Bäckström (1960) respectively found relationships between pH and the so-called *effective capillary cross-sectional area (ECCSA)*, and between the yield and ECCSA (see Fig. E.1 and E.2). ECCSA is a measure of the diffusion area in the wood chips.

Figure E.1: ECCSA as a function of pH for spruce wood blocks according to (Hägglund, 1959)

The experiments by Hägglund (1959) were, however, made on uncooked chips, while the experiments by Bäckström (1960) were made at $pH = 13.2$. At yield 100% and $pH = 13.2$, their results approximately coincide. As Fig. E.1 shows, ECCSA is constant with respect to pH at pH lower than $11 - 12$. During normal kraft cooking conditions, pH is in the range $12 - 13$ ($12 - 14$ when the impregnation stage is included). The pH dependency may be related to the swelling effect. $pH = 12.9$ is reported as a upper limit for the swelling effect by Talton and Cornell

Figure E.2: ECCSA as a function of yield for partially digested wood blocks at pH 13.2 according to (Bäckström, 1960)

(1987) (c.f. Sec. 2.3). However, the results by Hägglund (1959) indicate that the increase in ECCSA proceeds even above $pH = 12.9$.

The following derivation is adapted from Van Heiningen (1993). ECCSA is related to the diffusion coefficient by:

$$D = D_{Na^+-water}(T) \cdot ECCSA \tag{E.1}$$

where $D_{Na^+-water}(T)$ is the diffusion coefficient for Na^+ in a solution of highly diluted NaOH. ECCSA compensates for pH and yield (chip porosity) in the diffusion of Na^+ in the chips. By using the Stokes-Einstein relationship $\frac{D\eta}{T} = constant$, where η is coefficient of viscosity, we have the diffusion coefficient for white liquor as:

$$D_{wl}(T) = 1.6 \cdot 10^{-9} \frac{1.083}{2.0 \cdot \eta_w(T)} \frac{T}{290.0} \tag{E.2}$$

In the derivation, the value of D_{wl} at 17^oC is used as reference, and the kinematic viscosity of white liquor is two times the the viscosity of water η_w (which can be found from thermodynamic tables).

Appendix F

The compaction of chips in the top section

This appendix discusses why the estimate Eq. (3.145) is necessary. The discussion treats the deficiency of the model to predict strong chip- and liquor level variations as well.

In the derivation of Eqs. (3.142) and (3.144), the volume fraction of chips, ϵ_c, is assumed to be constant. This is because the formulation of the main section is based on the Euler-method which implies a fixed set of grid points in the space of the solution. Note at this point that the assumption behind the formulation of this section is that the model error does not aggravate the accuracy of the solution too much (assumption 1 in Sec. 3.2.4). To avoid confusion, we denote the volume fraction of chips $\epsilon_{c,top}$ in the sequel.
The variations in the weight of the chip plug, due to for instance feed chip volume flow variations, influence the compaction of chips in the mass. The only way this can be handled in our formulation of the model is to model the compaction in the top section ad hoc. Note, however, that for instance an increase in $\epsilon_{c,top}$, due to increased feed chip volume flow, is inconsistent with what is stated above, since such an increase should be handled by dividing the section volume into a new top section, and where the lower part is added to the original main section (which is formulated by PDEs). A possible problem solution would hence be a model with dynamically variating number of grid points, and thus dynamically variating number of equations. Such a solution would, however, be rather complex because new initial- and boundary conditions have to be defined at every time step. This discussion illustrates why a Lagrange-formulation of the PDEs (see e.g. Bird et al. (1960)) may be a more suitable solution of the problem, especially in the prediction of strong chip- and liquor level variations. The following discussion illustrates, however, that our approach may be a satisfactory solution of the problem.

Consider the two volumes of chips in Fig. F.1 where $\kappa_1 > \kappa_2$, i.e. $\epsilon_{c,1} < \epsilon_{c,2}$ and $m_{c,1} > m_{c,2}$. The chip levels are determined by the two factors:

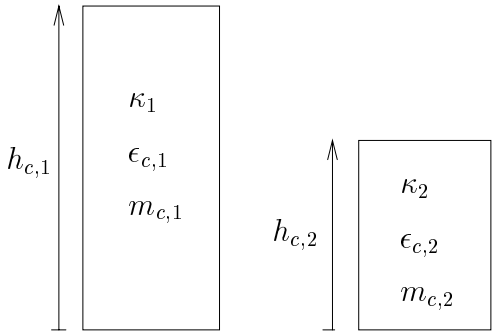

Figure F.1: To volumes of chips with different Kappa numbers.

1. Low Kappa numbers (κ_2) give low chip level ($h_{c,2}$) due to **softer chips** that are more conform. This is included in the model though the compressibility equation Eq. (3.6).
2. High Kappa numbers (κ_1) mean more solids in the chips, and hence more mass ($m_{c,1}$). This means **more weight**, and thus higher compaction. This is included in the model through the computation of the chip density, ρ_c, in Eq. (3.64) that influences the momentum balances.

When we consider the scenario in Sec. 5.3 where the cooking circulation temperature is reduced, a result of changed Kappa number is a retardation of the chip plug in the upper part of the cooking zone. This means that in a transient period of time, more chips enter than what leaves the top section. Note that the feed flow of chips is constant. Thus, the chip level increases (c.f. Fig. 5.14). This results irrespective of how small (narrow) the top section is modelled. As a result, there are three effects that limit this chip level increase:

1. Higher chip level means longer residence time for the chips. This results in lower Kappa number, and thus higher compaction of the chips (the first effect above).
2. Higher Kappa numbers mean increased individual chip weight, and thus higher compaction (the second effect above).
3. Even though the total number of chips in the digester is the same (assuming a constant discharge of chips as well), the number of chips in the top section is increased, as this was the reason for the chip level increase. (For the same reason, there are fewer chips in the other sections, described by lower compaction). Hence, the total weight of chips in the top section is increased. This results in higher compaction of chips in this section. In our model, we have to describe this effect ad hoc by the estimate Eq. (3.145), $\epsilon_{c,top} = \epsilon_{c,top}(h_c)$. Further, this increased compaction in the top section propagates downwards in the vessel. The result is lower chip level.

Thus, the compaction estimate Eq. (3.145) contributes to a more realistic model description during these process disturbances:

- Feed chip volume flow changes. By this, the number of chips, and hence the total weight of chips in the top section is changed.
- Feed chip density (i.e. Kappa number) changes, and feed chip reactivity. This influences the chip density and the chip pressure in the top section. The former means that the individual chip weight is changed, while the latter means that the chip plug either is retarded or accelerated in a transient period of time. The result is that the number of chips (and hence the chip weight) in the top section is changed.
- Downflow changes that retard or accelerate the chip plug in a transient period of time. This may be caused by changes in the Kappa number, liquor flows, and the pulp discharge in the bottom.

To sum-up, the estimate Eq. (3.145), $\epsilon_{c,top} = \epsilon_{c,top}(h_c)$ compensates for the discretization error that is introduced by solving the problem by the Euler-formulation. This contributes to chip volume flow changes as well as Kappa number changes, that both changes the compaction of chips and the chip level in the digester.
There is no conflict in the description of the compaction estimate due to changes in the Kappa number and the feed chip volume flow. Both influences the number of chips in the top section. In addition, when there is a change in the feed chip Kappa number or the feed chip reactivity, the individual chip density, as well as the chip pressure, in the top section are changed. These influence the momentum balances. It is important that the resulting model error does not aggravate the accuracy of the solution too much.

Appendix G

The mechanism that stabilizes the collapse of the chip plug

Consider the lignin balance Eq. (3.129) without the dispersive term (which is not important in this context):

$$\frac{\partial \alpha_{lig}}{\partial t} = -v_c \frac{\partial \alpha_{lig}}{\partial z} - r_{lig} \tag{G.1}$$

One may misleadingly think that there is inherent positive feedback in the model connected to the collapse of the chip plug due to the softening of the chips during the cook. For instance, higher temperature gives increased delignification r_{lig}. Thus, the Kappa number decreases and the compaction increases, as discussed in Ch. 5. The result is reduced chip velocity, and thus increased residence time for the chips. This again reduces the Kappa number further, and the process of positive feedback is supposed to be established.

The mechanism that stabilizes this process is the concentration gradient $\frac{\partial \alpha_{lig}}{\partial z}$ that decreases proportionally. Steady state, $-v_c \frac{\partial \alpha_{lig}}{\partial z}$ balances r_{lig} at new v_c and $\frac{\partial \alpha_{lig}}{\partial z}$ levels. Note also that the increase in r_{lig} is limited by the fact that it is a function of α_{lig} and $\rho_{EA,el}$; $r_{lig} = \alpha_{lig}\rho_{EA,el}A_1 e^{-E_1/(RT)}$. Each contribution is shown by the arrows in the steady state balance:

$$\overbrace{v_c}^{\downarrow}\ \overbrace{\frac{\partial \alpha_{lig}}{\partial z}}^{\downarrow} = -\overbrace{\alpha_{lig}}^{\downarrow}\ \overbrace{\rho_{EA,el}}^{\downarrow} A_1\ \overbrace{e^{-E_1/(RT)}}^{\uparrow} \tag{G.2}$$

This equation shows that Kappa number control is a matter of both chip velocity- (or residence time), alkali-, and temperature control. The simulation results in Ch. 5, and the analysis in Ch. 6, indicate that the process is stable.

Appendix H

Local velocity of sound for the chip plug

A derived variable from the compressibility equation Eq. (3.6) is the *local velocity of sound*. For the chip plug, this is defined as (see e.g. Bird et al. (1960)):

$$\nu_s = \sqrt{\partial p_c / \partial \epsilon_c} \tag{H.1}$$

where

$$\frac{\partial p_c}{\partial \epsilon_c} = -1.695 \cdot 10^4 \frac{1}{-0.831 + 0.139 ln(\kappa)} (\frac{\epsilon_c - 0.356}{0.831 - 0.139 ln(\kappa)})^{0.695} \tag{H.2}$$

A three-dimensional plot is shown in Fig. H.1. At Kappa number 60 and $\epsilon_c = 0.6$ ($p_c = 8.9kPa$), this velocity is $\nu_s = 248.2m/s$. This is comparable to the velocity of sound in air at atmospheric pressure and 0^oC, which is $331.5m/s$. The following derivation shows that typical values for the vertical chip velocity is far from the critical limit given by the local velocity of sound.

The compaction equation without the dispersive term can be written as:

$$\frac{\partial p_c}{\partial t} = -\nu_s^2 \epsilon_c \frac{\partial v_c}{\partial z} - v_c \frac{\partial p_c}{\partial z} \tag{H.3}$$

where $\nu_s^2 = (\partial \epsilon_c / \partial p_c)^{-1}$. Further, Eq. (3.165) can be written as:

$$\frac{\partial v_c}{\partial t} = -v_c \frac{\partial v_c}{\partial z} - \frac{1}{\rho_c \epsilon_c} \frac{\partial p_c}{\partial z} + y(z) \tag{H.4}$$

When we consider steady-state conditions and substitute Eq. (H.4) into Eq. (H.3), this gives:

$$(1 - \rho_c Ma^2) \frac{\partial v_c}{\partial z} = -\rho_c \frac{v_c}{\nu_s^2} y(z) \tag{H.5}$$

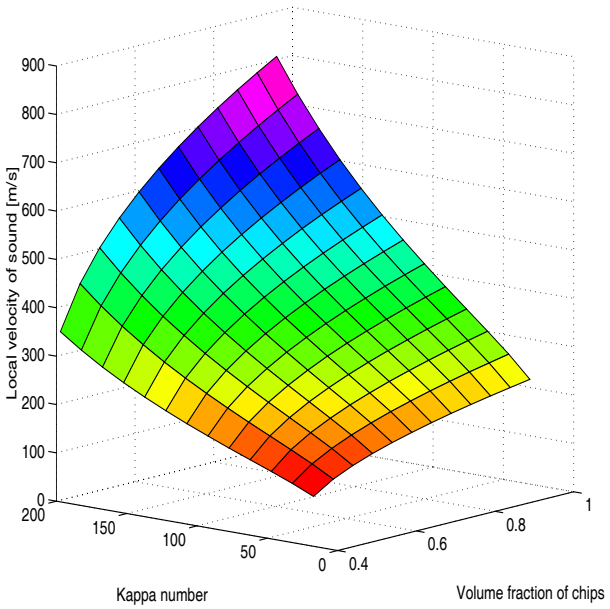

Figure H.1: 3D-plot of the equation for the local velocity of sound

where $Ma = \frac{v_c}{\nu_s}$ is the dimensionless group *Mach number*. The critical limit for the chip velocity is then given by the left-hand side of Eq. (H.5):

$$v_{c,crit} = \frac{\nu_s}{\sqrt{\rho_c}} \tag{H.6}$$

At Kappa number 60, $\epsilon_c = 0.6$ and $\rho_c = 1050 kg/m^3$, $v_{c,crit} = 7.7 m/s$. The model results in Ch. 5 indicate that typical values for the chip velocity are in the range $0 - 10 mm/s$. Hence, the process is far from this critical limit. This means that the Mach numbers are typically very small in continuous digesters.

Appendix I

Model parameters and operational conditions

The model parameters and operational conditions for the Peterson digester, as used in the computations in this thesis, are given below.

Model parameters

Tables I.1, and I.2 contain the model parameters. Those referred by $(*)$ have been tuned properly so as to obtain sensible steady-state profiles. For example, with respect to the reaction kinetics, the specific activation energies for the lignin and carbohydrate reactions are chosen in accordance with the values that are referred by Christensen et al. (1982). In that study, it is reported that these are almost the same irrespective of the wood species. Then, the frequency factors are chosen so as to obtain a Kappa number in the discharged pulp of about 60 at the high production rate. Further, the exogenous temperatures in the cooking zone (the steam temperature and the cooking circulation temperature) and the effective alkali concentration in the feed are chosen so as to obtain about the same Kappa number in the discharged pulp at the low production rate.

The diffusion rate coefficient for the alkali is described as (c.f. Gustafson et al. (1983)):

$$\begin{aligned} D_{EA} &= 0.16\sqrt{T_c + 273.16}e^{-2452.4/(T_c+273.16)} \\ &\cdot(-2.0\alpha_{lig} + 0.13(\rho_{EA,el}/32.0)^{0.55} + 0.58) \end{aligned} \tag{I.1}$$

The constant, 0.16, is calculated by requiring the diffusivities from Eq. (I.1) and that by Christensen et al. (1982) to be equal at $T_c = 170^oC$, Kappa number 20, and $\rho_{EA,el} = 12.0g/l$. The range of validity for the respective influences from the temperature, yield, and alkali concentration in Eq. (I.1) is $T_c = [100 - 150^oC]$ (McKibbins, 1960), yield $= [65 - 100\%]$ (Bäckström, 1960), i.e. $\alpha_{lig} \approx [0.2 - 0.3]$,

and pH = $[2-14]$ (Hägglund, 1959), i.e. $\rho_{EA,el} \approx [0-40g/l]$ according to the computation below.

Note that the values $\rho_{ODW} = 397.0kg/m^3$ ODW and $\rho_{lig} = \rho_{carb} = 1500.0kg/m^3$ correspond to a volume fraction of solids in the feed chips of 0.26.

Computation of pH and specific weight of effective alkali

The effective alkali (EA) is defined as $NaOH + \frac{1}{2}Na_2S$. Although both $NaOH$ and Na_2S take part in the cooking reactions, it can be shown that $NaOH$ provides the prime driving force (Smook, 1989). Since Na_2S hydrolyses in solution by:

$$Na_2S + H_2O \rightleftharpoons NaOH + NaSH \tag{I.2}$$

it follows that only one-half of the Na_2S is really effective in the reaction kinetics.

EA is measured as g/l $NaOH$ which has a molar weight of $40.0g/mol$ $(22.99 + 1.008 + 16.00)$. If we assume that $1mol$ $NaOH$ gives $1mol$ OH^-, this means that x$mol[OH]/l$ = x$(EA[g/l]/40.0[g/mol])mol[OH]/l$, and hence:

$$pH = 14 + log_{10}(\frac{EA[g/l]}{40.0}) \tag{I.3}$$

However, this is a conservative result since the sulphide, Na_2S, contributes to the OH^- concentration as well. Typically, pH is in the range $12-14$ for kraft cooks.

The specific weight of effective alkali is defined as (see any tables of the elements):

$$\rho_{EA} = \frac{m_{Na} + m_{O^-} + m_{H^+}}{V_{Na} + V_{O^-} + V_{H^+}} \tag{I.4}$$

where

$$\begin{aligned} V_{Na} &= \frac{m_{Na}[g/mol]}{\rho_{Na}[g/cm^3]} = \frac{22.99}{0.97} = 23.70cm^3/mol \\ V_{O^-} &= \frac{m_{O^-}[g/mol]}{\rho_{O^-}[g/cm^3]} = \frac{16.00}{1.14} = 14.035cm^3/mol \\ V_{H^+} &= \frac{m_{H^+}[g/mol]}{\rho_{H^+}[g/cm^3]} = \frac{1.008}{0.071} = 14.197cm^3/mol \end{aligned}$$

giving

$$\rho_{EA} \approx 770.2kg/m^3 \tag{I.5}$$

Operational conditions

Two typical operational conditions for a digester, low (LPR) and high (HPR) production rate, for production of liner grades from softwood, are listed in Table I.3. The cooking circulation and the lower wash circulation are included as liquor circulations. The influence from the bottom scraper is omitted as there has not been found any data in the literature to determine the relationship to the chip plug velocity (see Eq. (3.173)).

Symbol	Value	Reference
A	$15.9m^2$	(Øgård, 1980)
A_1	$1.0(kg/(m^3s))^{-1}$	$(*)$
A_2	$3.5(kg/(m^3s))^{-1}$	$(*)$
b_{lig}	$0.15kg$ alkali $/kg$ lignin	$(*)$
b_{carb}	$0.25kg$ alkali $/kg$ carb.	$(*)$
c_κ	0.153	(Christensen et al., 1982)
$C_{p,w}$	$1.47kJ/(kg^oC)$	(Smith and Williams, 1974)
$C_{p,liq}$	$4.19kJ/(kg^oC)$	(Smith and Williams, 1974)
D_c	$1.0 \cdot 10^{-3}m^2/s$	$(*)$
D_l	$1.0 \cdot 10^{-3}m^2/s$	$(*)$
$D_{cond,i}$	$15.0s^{-1}$	$(*)$
E_1	$38kJ/mol$	(Christensen et al., 1982)
E_2	$42kJ/mol$	(Christensen et al., 1982)
h_t	$38.5m$	$(*)$
h_s	$48.0m$	(Øgård, 1980)
Δh_r	$581.5kJ/kg$	(Smith and Williams, 1974)
$k_{d,ds}$	0.1	(Van Heiningen, 1993)
k_{cz}	$0.12J/(ms^oC)$	(Ineropera and De Witt, 1990)
k_{lz}	$0.68J/(ms^oC)$	(Ineropera and De Witt, 1990)
k_{cl}	$1.0 \cdot 10^4J/(m^3s^oC)$	(Härkönen, 1984)
k_{cw}	$2.0J/(m^3s^oC)$	(Härkönen, 1984)
k_{lw}	$2.0J/(m^3s^oC)$	(Härkönen, 1984)
k_{cs}	$1.0 \cdot 10^4J/(m^3s^oC)$	$(*)$
k_{ls}	$1.0 \cdot 10^4J/(m^3s^oC)$	$(*)$
k_{rpm}	$648.2(m^3/s)/rpm$	(Peterson, 1994)
k_{ts}	$0.011m^{-1}$	$(*)$
R_1	$4.6 \cdot 10^3kg/(m^3s)$	(Härkönen, 1984)
R_2	$3.9 \cdot 10^6kg/m^4$	(Härkönen, 1984)
V_{outlet}	$0.5m^3$	$(*)$
α^0_{carb}	$0.35kg$ carb. $/kgODW$	(Christensen et al., 1982)
$\epsilon_{c,in}$	$0.356m^3/m^3$ mass	$(*)$
ρ_{ODW}	$397.0kg/m^3$ ODW	(Härkönen, 1984), (Johnsson, 1971)
ρ_{lig}, ρ_{carb}, ρ_{ds}	$1500.0kg/m^3$	(Härkönen, 1984)
ρ_w	$1000kg/m^3$	
μ	0.01	(Härkönen, 1984)

Table I.1: Model parameters

Description	**Symbol**	**Value**
Reference length (digester cross-section diameter)	d	$4.5m$
Reference chip pressure	$p_{c,0}$	$34.0kPa$
Reference liquor pressure	$p_{l,0}$	$685.0kPa$
Reference concentration for effective alkali	$\rho_{EA,0}$	$30.0kg/m^3$
Reference concentration for dissolved solids	$\rho_{ds,0}$	$192.0kg/m^3$
Reference density for the chips	$\rho_{c,0}$	$1150.0kg/m^3$
Reference density for the free liquor	$\rho_{l,0}$	$1050.0kg/m^3$
Reference velocity for both phases	v_0	$6.0mm/s$
Reference temperature for both phases	T_0	200^oC
Characteristic time variable	$t_0 = d/v_0$	$750.0s$

Table I.2: Characteristic quantities

Operating point	LPR	HPR
Blow flow	$2500l/min$	$3800l/min$
Chip meter speed	$15.6rpm$	$21.3rpm$
Liquor to wood ratio	3.0	3.0
Steam pressure	$685kPa$	$685kPa$
Effective alkali feed (transport circulation)	$23.0g/l$	$25.0g/l$
Extraction (black liquor) flow	$2927l/min$	$4015l/min$
Side nozzle flow	$1850l/min$	$2800l/min$
Bottom nozzle flow	$850l/min$	$1300l/min$
Nominal chip level	41.5 metres	41.5 metres
Nominal liquor level	39.5 metres	39.5 metres
Transport circulation temperature	137^oC	137^oC
Steam temperature	165^oC	175^oC
Cooking circulation temperature	160^oC	170^oC
Lower wash circulation temperature	90^oC	90^oC
Wash water inlet temperature	90^oC	90^oC
Ambient temperature	20^oC	20^oC

Table I.3: Operational conditions for a steam/liquor phase digester for production of kraft softwood pulp